Piggybacking on the cholera toxin: Using cholera toxin B chain for the targeted delivery of proteins to motor neurones

Matthew Royce Balmforth

Submitted in accordance with requirements for the degree of Doctor of Philosophy

The University of Leeds

School of Molecular and Cellular Biology

December 2017

The candidate confirms that the work submitted is her own, except where work which has formed part of jointly-authored publications has been included. The contribution of the candidate and the other authors to this work has been explicitly indicated below. The candidate confirms that appropriate credit has been given within the thesis where reference has been made to the work of others.

Acknowledgments

I have a huge number of people to thank who I've largely depended on for the success of the following body of work. Firstly, I'd like to thank Dan Williamson, Darren Machin, Jessica Haigh, and Gemma Wildsmith for their mentorship. My PhD would have gone a lot slower without those four people. Of course, lab 1.49 wouldn't have been the enjoyable place to work it has been over the past few months if not for Kristian, Ryan and Jack. Their boundless enthusiasm for squash always keeps me in good spirits. Many people have left the lab since I started – they are not forgotten! Chadamas, Dan, James Ross, James Warren, and Darren will always be at the forefront of my memories of my PhD. Those memories would not be complete without the pub trips and shenanigans that ensued, and for that, I'd like to thank my partner in crime, Kat Horner.

Thanks to my family for enduring 4 years of studentship, particularly to my brother Nick for keeping me company over the phone on the well-trodden route from chemistry to biology.

I owe a massive thank you to my supervisors Prof Bruce Turnbull, Dr Mike Webb, and Prof Jim Deuchars. Mike has always been on hand to troubleshoot *any* problems I've encountered, as well as tirelessly hosting us year after year at his house for Christmas dinners. I'd especially like to thank Bruce for his honest opinions, for the marathon brainstorming sessions in his office, and for investing so much time into his students.

Abbreviations

ADP	Adenosine diphosphate
ALBA	Affimer lectin binding assay
ALS	Amyotrophic lateral sclerosis
AMP	Adenosine monophosphate
ATP	Adenosine triphosphate
B	Boiled
BBB	Blood brain barrier
BoNT	Botulinum neurotoxin
BSA	Bovine serum albumin
BSTG	BioScreening Technology Group
CD	Catalytic domain
CDS	Coding DNA sequence
CFG	Consortium for Functional Glycomics
CMA	Chaperone-mediated autophagy
CNS	Central nervous system
CNT	Clostridial neurotoxins
CPP	Cell-penetrating peptide
CT	Cholera toxin
CTA1	Cholera toxin A1 subunit
CTA2	Cholera toxin A2 subunit
CTB	Cholera toxin B subunit
DAD	Diode array detector
DNA	Deoxyribonucleic acid
DTT	Dithiothreitol
EDTA	Ethylenediaminetetraacetic acid
ELISA	Enzyme-linked immunosorbent assay
ER	Endoplasmic reticulum
ESMS	Electrospray mass spectrometry
FPLC	Fast protein liquid chromatography
FRET	Förster resonance energy transfer
GFP	Green fluorescent protein
GPI	Glycosylphosphatidylinositol
GST	Glutathione S-transferase
HC	Heavy chain
HIV	Human Immunodeficiency virus
HRP	Horse radish peroxidase
IG	Intergenic
IPTG	Isopropyl β-D-1-thiogalactopyranoside
ITC	Isothermal titration calorimetry
Ka	Association constant

Kd	Dissociation constant
KLD	Kinase-ligase-DpnI mix
Koff	Dissociation rate constant
Kon	Association rate constant
LB	Lysogeny broth
LC	Light chain
LED	Light emitting diode
LIC	Ligation independent cloning
LT	Heat-labile enterotoxin
LTBh	Heat-labile enterotoxin B subunit
MBP	Maltose-binding protein
MRI	Magnetic resonance imager
MWCO	Molecular weight cut-off
NGF	Neurotropic growth factor
NHS	N-hydroxysuccinimide
Ni-NTA	Nickel nitrilotriacetic acid
NSF	N-ethylmaleimide-sensitive factor
OD	Optical density
OTS-1	Oligonucleotide transporter-1
PAGE	Polyacrylamide gel electrophoresis
PBS	Phosphate buffered saline
PCR	Polymerase chain reaction
PDB	Protein Data Bank
PDI	Protein disulfide isomerase
PEG	Polyethylene glycol
PFA	Paraformaldehyde
PS	Packaging signal
PT	Pertussis toxin
RBD	Receptor binding domain
RNA	Ribonucleic acid
RU	Response units
SDS	Sodium dodecyl sulfate
SNAP25	Synaptosomal-associated protein 25
SNARE	Soluble NSF attachment protein
SPR	Surface plasmon resonance
ST	Shiga toxin
Syb	Synaptobrevin
Syx	Syntaxin-1
$t_{1/2}$	Residency half-life
TAE	Tris-acetate EDTA
TAxI	Targeted Axonal Import
TBS	Tris buffered saline
TCEP	Tris(2-carboxyethyl)phosphine

TD	Translocation domain
TE	Tris-EDTA
TEMED	Tetramethylethylenediamine
TeNT	Tetanus neurotoxin
TEV	Tobacco Etch Virus
THC	Tetanus heavy chain
TMB	Tetramethylbenzidine
TMBox	Tetramethylbenzidine diimine
t_r	Residency time
UB	Unboiled
UV	Ultra-violet

Abstract

A significant unmet need exists for the delivery of biologics to the central nervous system for the treatment and understanding of neurodegenerative diseases. Naturally occurring toxoids such as the non-toxic B subunit of the cholera toxin have been considered as tools to meet this need. However, due to the complexity of tethering macromolecular drugs to toxins, and the inherent dangers of working with large quantities of recombinant toxin, no such route has been successfully exploited. Developing a method where toxoid and drug can be assembled immediately prior to administration could therefore be extremely useful.

Using phage-display, two cholera toxin-binding antibody mimetics (Affimers) were identified that non-covalently associate with the non-GM1 binding face of the cholera toxin B subunit (CTB). The two unique interactions were characterised using a range of techniques to dissect the Affimer-CTB assembly process. Internalisation of the complex was demonstrated in tissue culture, and the system was used to deliver GFP to mammalian cells. Finally, the complex was shown to be successfully internalised into the motor neurones of the brainstem in a mouse model.

A second route to modular assembly of a protein delivery system was also explored. By using a high affinity peptide staple, a cholergenoid-botulinum toxin chimera was produced that could be assembled *in vitro* and used to deliver the functional catalytic domain of botulinum neurotoxin to cultured neuronal cells.

Table of Contents

1. Introduction

1.1. An Overview

Improved methods for the identification and delivery of protein-based therapeutics have resulted in a shift in focus from small molecules to macromolecular drugs, such as antibodies, which now represent the major class of new pharmaceuticals.[1,2] Indeed, in 2016, four out of the five best selling drugs were biologics, with all four of these being antibodies or antibody-like proteins.[3]

Due to their large size and complexity, antibodies, and biologics more broadly, for therapeutic purposes are raised almost exclusively against extracellular targets, despite the wealth of drug targets localised intracellularly.[4] The niche of targeting intracellular proteins has been filled for the most part by small molecule drugs due to their ability to penetrate the plasma membrane.[5] The delivery of biologics into a cell thus still remains a major barrier to accessing the vast array of intracellular targets. There is therefore a need to develop methods capable of cellular penetration to deliver macromolecular payloads into cells.

Strategies have been developed to facilitate protein transduction into cells. These techniques include the viral-mediated delivery of genes coding for the biologic, or the conjugation of biologics to peptide carriers, such as cell-penetrating peptides (CPP). CPPs vary in sequence and size, but share the qualities of being highly charged with interspacing hydrophobic regions, which together are sufficient to give CPPs the ability to cross the cell membrane. Thompson *et al.* demonstrated that the rate of cellular uptake of cationic GFP variants was proportional to the net positive charge of the protein.[4]

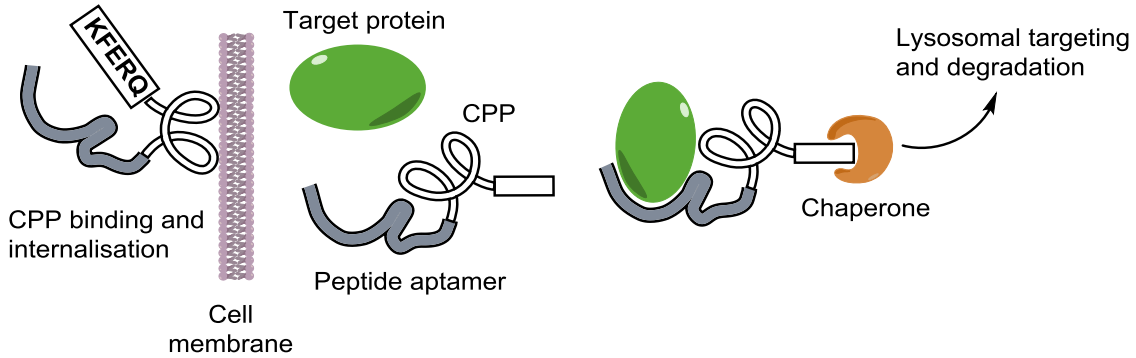

Figure 1.1. Method of protein knockdown using a CPP fused to a peptide aptamer and a KFERQ degradation signal sequence. The CPP binds to the cell membrane, resulting in cellular internalization. Upon reaching the cytoplasm, the peptide aptamer binds to its target protein. Cytoplasmic chaperones recognise the KFERQ signal sequence, and target the complex to the lysosome for degradation.[6]

Based on the knowledge that charged hydrophobic peptides are able to cross the plasma membrane, a 21-residue CPP (KETWWETWWTEWSQPKKKRKV) consisting of a hydrophobic membrane-tethering domain (orange), a spacer region (blue), and a lysine-rich domain derived from simian virus 40 (green) was designed.[7] This CPP, termed Pep-1, was used in conjunction with a human immunodeficiency virus type 1 (HIV-1) derived CPP (TAT) to deliver peptide aptamers to cells. The research group used the two CPPs to demonstrate that *in vivo*, protein knockdown can be achieved by systemic administration of the peptide-based drug.[6] The CPPs were conjugated to various peptide aptamers tagged with the chaperone-mediated autophagy (CMA) targeting motif, KFERQ. Following CPP-mediated endocytosis, target proteins would be bound by the aptamer, resulting in recognition of KFERQ, and degradation of the complex by the CMA machinery (Figure 1.1). CPPs thus provide a reliable method to deliver cargo to a cell. However, their mechanism of cellular entry remains undefined, and CPPs appear to be promiscuous with regards to the cell type they target.[8]

In addition to the complexities of crossing the plasma membrane, a second barrier to the use of biologics intracellularly, therefore, is the issue of cell targeting. A multitude of disorders afflict the central nervous system (CNS), and treatment of those disorders requires novel strategies to target drugs to the cells of the CNS, a challenge that is complicated by the presence of the blood-brain barrier (BBB).

1.2. Crossing the Blood-Brain Barrier

The BBB is a monolayer of endothelial cells that acts as a physical barrier between the blood and the CNS (Figure 1.2). The neurones of the CNS communicate via a complex network of chemical and electrical signals that are generated by the subtle movement of ions across the neuronal membrane. The neurones depend upon a constant ionic composition of the surrounding fluid (interstitial fluid) for these exquisitely precise signals to be reproducible. The BBB therefore plays a key homeostatic role by maintaining the ionic composition of the interstitial fluid, regardless of fluctuations in the ionic make-up of the blood.[19]

One of the central challenges for delivery of therapeutics to the CNS is crossing the BBB due to Its complexity and adaptability. This issue is a major challenge for the rational design of drugs to penetrate into the CNS.[10] The BBB does however provide some opportunities for drug delivery in the form of a wide array of transporters that shuttle molecules across the protective monolayer (Figure 1.2). One such transporter, aptly

named oligonucleotide transport system-1 (OTS-1), recognises and selectively transports phosphorothioate-containing oligonucleotides across the BBB.[11] OTS-1 has been exploited in mice to deliver phosporothioate antisense oligonucleotides to the gene coding for amyloid precursor protein: a precursor to the aggregation-prone protein known as amyloid β that is implicated in Alzheimer's disease.[12] Intravenous administration of this antisense oligonucleotide was shown to reverse deficits in memory and learning caused by aggregating amyloid β.[11,13]

Other approaches to penetrate the CNS involve tethering a therapeutic to a transporter ligand, thereby acting as a 'Trojan-horse' to cross the BBB by transcytosis (through cells).[14] One well-characterised example of transcytosis across the BBB is the shuttling of iron-loaded transferrin by the transferrin receptor (Figure 1.2). Iron-bound transferrin binds to its receptor at the blood-BBB interface, triggering receptor-mediated endocytosis of the complex into cells.[15] The iron is released following a pH drop following internalisation into endosomes, and the complex is recycled to the cell surface.[15,16]

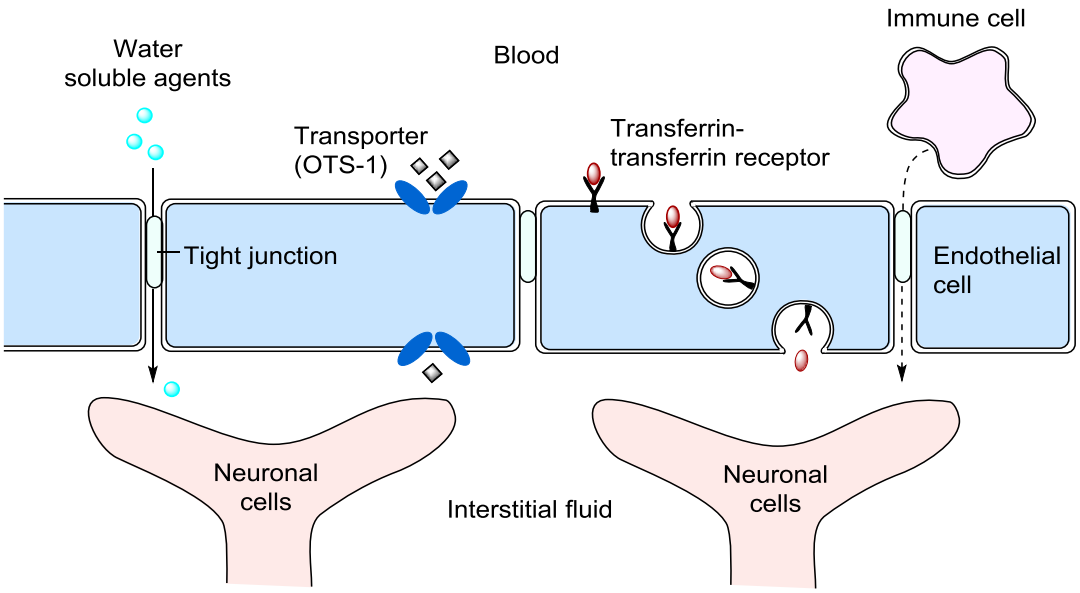

Figure 1.2. Graphic depicting the blood-brain barrier. A monolayer of endothelial cells separated by 'tight junctions' (a densely packed network of proteins that limit the passage of molecules across the BBB), surround the CNS and form a physical barrier between the blood and the interstitial fluid of the CNS. Specific transporters and receptors allow the transcytosis (cell-crossing) of certain molecules, including phosphorothioate oligonucleotides and iron-loaded transferrin. During inflammation, certain cells of the immune system can dock to the BBB, and pass across via transient openings of the tight junctions.[17]

The high concentration of transferrin receptor (TfR) at the BBB has been exploited extensively as a route to CNS penetration.[14,15,18] Particularly, isolation of an anti-TfR antibody (OX26) that prompts endocytosis upon TfR-binding has resulted in numerous

studies delivering macromolecular cargo through formation of antibody-drug conjugates.[15,19–22] Biotinylated peptide nucleic acids conjugated to streptavidin-OX26 were observed to be taken up into the brain in therapeutically significant quantities when administered systemically.[23] Similarly, functionalised nanoparticles were shown to be taken up into the CNS when tethered to OX26, and elicited an analgesic effect in mice when loaded with loperamide, an opioid receptor agonist that does not cross the BBB alone.[18]

Targeting of the low-density lipoprotein receptor, expressed at the surface of the BBB, has also been investigated for delivery of proteins to the CNS.[24–26] Spencer and Verma demonstrate that glucocerebrosidase, a lysosomal enzyme defective in Gaucher's disease, can be delivered to neurones when fused to apolipoprotein B.[27,28] The protein was expressed endogenously by using a non-replicating lentiviral system to insert a gene coding for the fusion protein into the cells of the liver and spleen.[29]

The BBB not only permits the transport of certain ligands, but also allows certain white blood cells to cross from the blood to the interstitial fluid following inflammation in the CNS.[30] For example, neutrophils and monocytes are recruited across the endothelial monolayer during transient openings of the so-called tight junctions in between endothelial cells.[31] As a result, immune cells have been considered as vectors for trafficking drugs into the CNS.[32] Klyachko *et al.* demonstrated that macrophages could be equipped with cellular 'backpacks'.[33] The backpacks were built up on glass slides from several distinct layers to form a 7 μm disc-shaped polymer. The polymer was loaded with catalase, a potent antioxidant, and conjugated to monocytes through incorporation of CD11b macrophage-binding antibodies to the polymer. The research group then demonstrated that these cellular backpacks were transported across the BBB in an inflamed brain mouse model. Effective release of the catalase was not demonstrated using this technique, although it clearly demonstrates how physiological processes can be exploited to deliver biologics to the CNS.

A recent publication demonstrated a novel method to identify mechanisms of circumventing the BBB.[34] Sellers *et al.* isolated a 14-residue peptide from an *in vivo* phage display screen that they termed targeted axonal import (TAxI) peptide. By injecting recombinant phage-peptide libraries into the calf muscle of mice, and harvesting phage from the murine spinal cord, TAxI was identified. This peptide sequence was shown to be transported selectively and efficiently into spinal cord motor neurones by retrograde transport following intramuscular injections by an as yet unknown mechanism. When

fused to Cre-recombinase or horse radish peroxidase, TAxI was shown to be able to deliver biologically active proteins into spinal cord motor neurones. This elegant system can thus be used to gain entry to the CNS by entering peripheral neurones and being transported to the spinal cord without the need to cross the BBB. The authors of this publication compared TAxI peptide to pathogens that are able to transduce motor neurones in a similar manner. Routes taken by pathogens and pathogen-derived toxins to gain entry to the CNS have long been considered as potential avenues for the delivery of therapeutics, since bacteria and viruses have developed a plethora of methods to penetrate the cells of the body.

1.3. Hijacking Toxins

Many bacteria cause disease through production of protein toxins that gain entry to the interior of the cell by first binding to cell surface receptors and gaining entry to the interior of the cell.[35] Many bacterial toxins use sialylated glycolipids called gangliosides (Figure 1.3) as cell surface receptors, particularly neurotoxins, since gangliosides are expressed in abundance at the surface of neuronal cells.[36–38] These protein toxins display diversity in receptor target, mechanism of internalisation and cell specificity, but generally share the common feature of being composed of a receptor binding domain and a toxic domain.[39] Removal of inactivation of the toxic domains provides a tool kit of diverse cell-penetrating proteins that may be manipulated for drug delivery.[40]

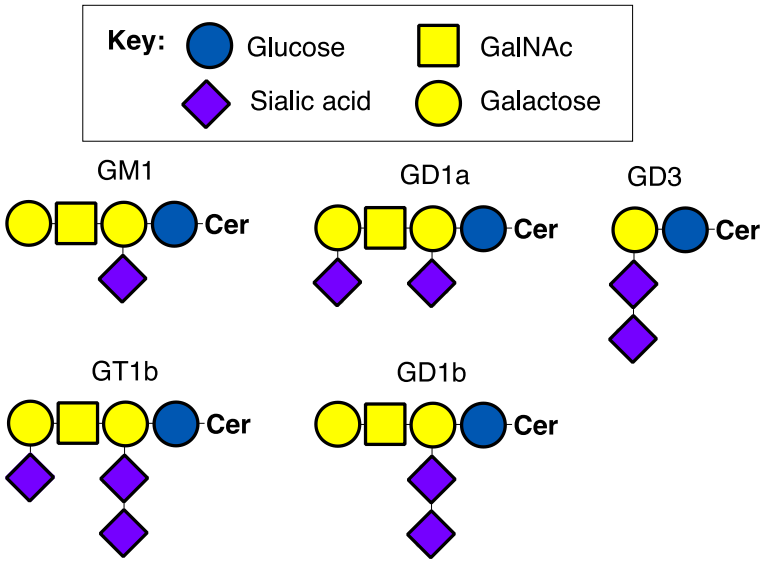

Figure 1.3. The major gangliosides of the CNS. Gangliosides GM1, GD1a, GT1b and GD1b are shown as CFG sugar symbols. Ceramide, the lipid component of gangliosides, is represented in the schematic as Cer.

1.3.1. Botulinum Toxin

Perhaps one of the best known and most potent of the bacterial toxins is botulinum neurotoxin (BoNT), which is produced by *Clostridium botulinum*.[41] Although there are seven distinct BoNT serotypes, all of them inhibit acetylcholine release at the neuromuscular junction, thus preventing muscle contraction, leading to respiratory failure and death.[42–44]

Botulinum toxin is expressed as a single 150 kDa polypeptide chain that is cleaved into two further chains, a heavy chain (HC, ~100 kDa) and a light chain (LC, ~50 kDa), connected via a disulfide bond (Figure 1.4).[41] The cleavage is directed by the human trypsin protease, producing the active form of the toxin. The light chain forms a zinc-dependent metalloprotease, whilst the heavy chain comprises a translocation domain and a receptor-binding domain.[41,45] Although the different serotypes recognise slightly different receptors, BoNT receptor binding domains are all thought to have dual receptor recognition, binding to gangliosides (GD1a or GD1b, Figure 1.3) as well as to a synaptic vesicle protein (synaptotagmin or synaptic vesicle protein 2) presented at the surface of peripheral cholinergic nerve terminals.[46–48]

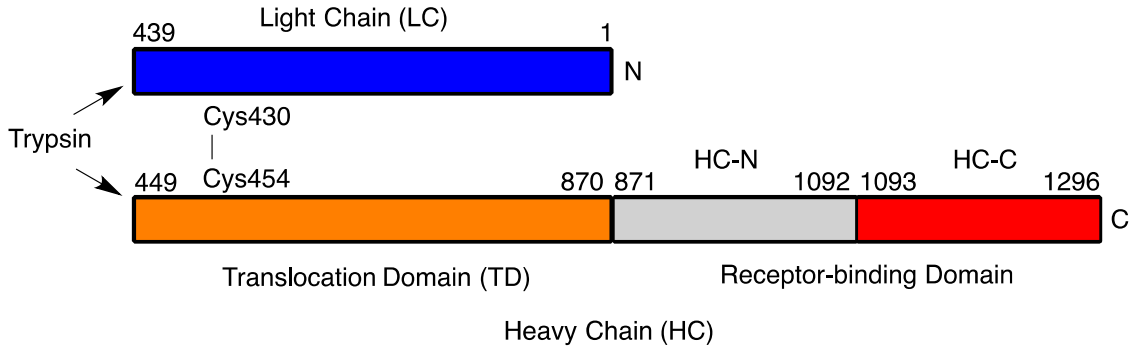

Figure 1.4. Schematic showing the arrangement of the BoNT polypeptide (~1300 amino acids). The holotoxin is expressed as a single polypeptide chain, with a single disulfide bond. The light chain (blue) is the catalytically active domain, and located at the N-terminus. The light chain is separated from the two receptor binding domains (grey and red) by a translocation domain (orange). The translocation domain and receptor binding domains together comprise the heavy chain. The polypeptide is cleaved by a host protease, leaving the light chain associated to the heavy chain by a disulfide bond.

Upon binding to its receptors, BoNT triggers endocytosis mediated by synaptic vesicle recycling, and internalisation of the holotoxin into endosomes that remain localised to the nerve terminal.[49] vATPase-mediated acidification of these endosomes is then thought to take place to drive the uptake of cytosolic neurotransmitters into the vesicles.[50,51] At this stage, the light chain is transferred to the cytosol, in a process facilitated by the translocation domain; composed of two long amphipathic α-helices.[47,52] These helices are thought to undergo conformational changes in response to vesicle

acidification, and form ion channels within the vesicle membrane, thus permitting the transport of the light chain to the cytosolic face of the membrane.[53] The process is terminated by thioredoxin reductase-thioredoxin complex, which reduces the disulfide bond releasing the catalytically active enzyme into the cytosol to carry out its toxic effect (Figure 1.5).[54–56]

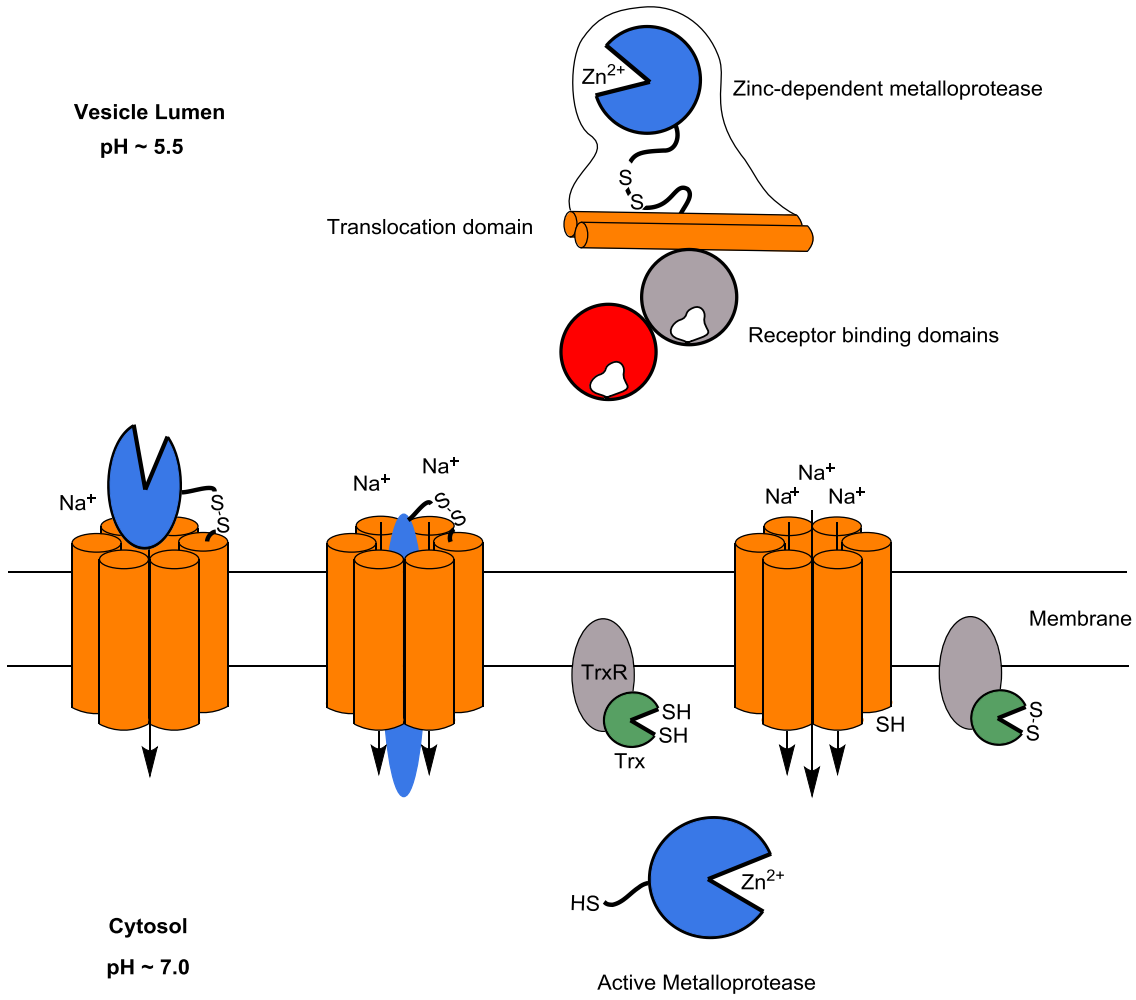

Figure 1.5. A schematic of the holotoxin in the lumen of an acidic synaptic vesicle. The translocation domain inserts into the membrane in response to changes in the pH of the lumen forming a transmembrane channel (orange cylinders). The translocation domain is postulated to associate with multiple copies of itself and form an ion channel that induces translocation of the metalloprotease into the cytosol.[53] Unfolding of the protease is required to pass through the channel, with refolding of the active protease occurring on the cytosolic face of the membrane.[57] The process is completed by reduction of the disulfide bond by the thioredoxin reductase-thioredoxin complex, releasing the active protease into the cytosol.[56] Modified from Pirazzini *et al.*[58]

Acetylcholine is a neurotransmitter that is released by motor neurones at the neuromuscular junction to induce muscular contraction. The release of acetylcholine occurs by fusion of neurotransmitter-containing vesicles with the plasma membrane at the synapse (exocytosis). Fusion is mediated by the soluble N-ethylmaleimide-sensitive

factor attachment protein receptor (SNARE) complex; a superfamily of small helical proteins that mediate vesicle fusion in all mammalian cells.[59–61]

Exocytosis at nerve terminals is facilitated by the spontaneous assembly of multiple SNARE proteins. SNARE proteins all share a common coiled-coil motif, comprising a 60-70 residue sequence.[62,63] Four SNARE motifs are required for exocytosis to take place:[64] proteins syntaxin-1 and synaptobrevin contribute one each, with SNAP-25 contributing two SNARE motifs (Figure 1.6).[65] Synaptobrevin is a relatively simple protein containing the SNARE motif and a short C-terminal transmembrane domain that anchors it into synaptic vesicles.[66] Syntaxin-1 is much larger, containing a C-terminal transmembrane for anchoring it to the plasma membrane of the neuronal terminal, as well as a more extensive region that forms interactions with other proteins.[67,68] SNAP25 is composed simply of a parallel helix-loop-helix, with SNARE motifs flanking the loop, with a pamitoylation site in the loop for membrane tethering.[69–71] As neurotransmitter-laden vesicles approach the nerve terminal, synaptobrevin, syntaxin-1, SNAP-25 associate tightly, forming an extremely stable parallel four-helix bundle that brings the two membranes into close enough proximity for membrane fusion to occur (Figure 1.6).[59,72] Interestingly, studies using liposomes reconstituted with SNARE proteins showed that formation of the SNARE coiled-coil complex is sufficient to drive membrane fusion.[73,74]

The BoNT family proteases bind to this receptor complex, with different serotypes targeting different components of the SNARE complex.[44,54] For instance, BoNT-A cleaves SNAP-25, removing nine amino acids from the C-terminus, whilst BoNT-B and BoNT-C cleave synaptobrevin from the vesicle membrane.[42,75,76] Cleavage of any of the components of the SNARE complex render it non-functional, inhibiting vesicle fusion and release of acetylcholine into the synapse.[77] The blockade of neurotransmitter release results in flaccid paralysis, preventing motor neurone-mediated contraction of the muscle.[78]

The BoNT-A serotype of the neurotoxin is used clinically in an unmodified form to treat a range of neuromuscular disorders, as well as being used as a pharmaco-cosmetic.[79] The commercial success of BoNT-A is due in part to its preferential internalisation into peripheral neurones, particularly at hyperactive nerve terminals, and its limited spreading when administered at low dose.[54] In cases of peripheral syndromes resulting from hyperactive cholinergic nerves, such as head, neck and limb dystonias and spasms, BoNT-A administration has become the first line treatment.[80] BoNTs have also been

shown to target sensory neurones responsible for pain perception, as well as motor neurones, making them a potential tool for pain management.[81]

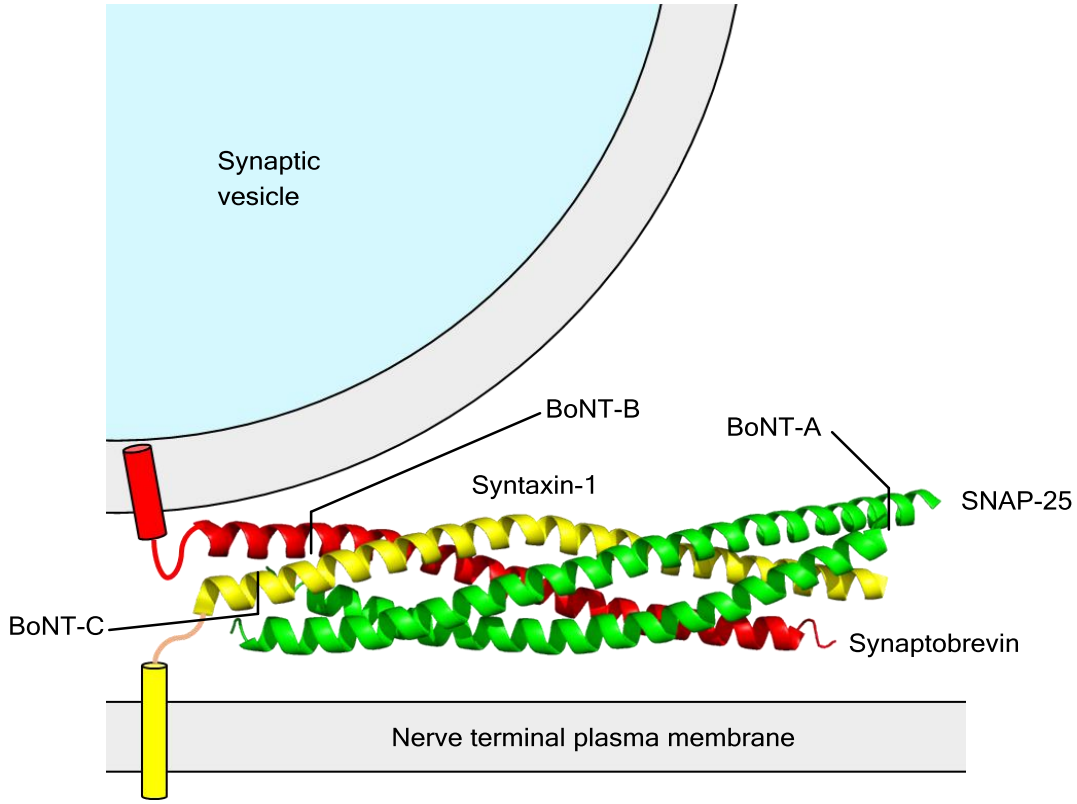

Figure 1.6. Schematic showing assembly of the four-helix bundle SNARE complex driving vesicle fusion with the nerve terminal plasma membrane. Synaptobrevin (red) is associated to the synaptic vesicle via a transmembrane receptor, and interacts with syntaxin-1, a terminal plasma membrane-associated helix. The complex is stabilised by the binding of SNAP-25 (green), a helix-loop-helix protein, resulting in vesicle fusion. BoNTs cleave members of the SNARE complex, with BoNT-B and BoNT-C serotypes both cleaving their substrates from their transmembrane domains. BoNT-A cleaves SNAP-25, preventing formation of stable SNARE complex.

BoNTs represent attractive vectors for the delivery of biomolecules to motor neurones, although engineering of BoNTs for this purpose has been limited in the literature. Bade *et al*. demonstrated that full-length BoNT-D fusion proteins could be produced, with protein-based cargoes fused to the enzymatically active light chain. The delivery system was used to deliver functional dihydrofolate reductase, GFP, and luciferase into the cytosol of neurones.[57] However, unfolding of the protein cargo at acidic pH was essential for the translocation to function. Ho *et al*. attempted to address issues with safety, low yield, and the unfolding requirement of the BoNT-D fusion proteins by removing the protease light chain, and fusing GFP to the binding domain and translocation domain as a model cargo. The group showed that the delivery system was readily taken into neurones, although cytosolic penetration was not evidenced.[82] Proteolytic activity of the

light chain can easily be eliminated through mutagenesis. BoNTs therefore show some promise as vectors for protein delivery, despite their limited exploitation.[83]

1.3.2. Tetanus Toxin

Tetanus toxins (TeNT) are members of the clostridial family of neurotoxins, and share many structural and mechanistic features with BoNT (Figure 1.7).[84,85] Like all members of the clostridial neurotoxins (CNTs), TeNT is expressed as a 150 kDa polypeptide, which is cleaved post-translationally by trypsin to an active form composed of a light and heavy chain tethered by a disulfide bridge.[86] Similarly, TeNT light chain forms a zinc-dependent metalloprotease that cleaves components of the SNARE complex.[84,87] The TeNT receptor binding site is complex, and thought to be composed of two carbohydrate binding sites that form interactions with GM1 and GD3 gangliosides.[88]

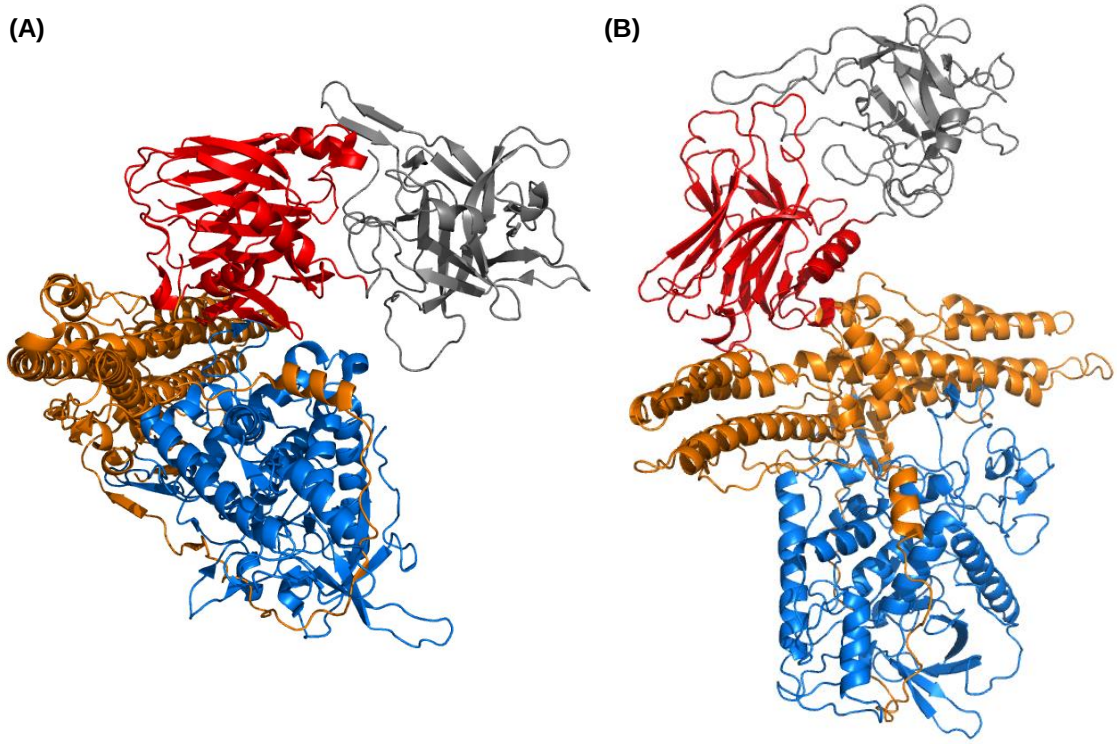

Figure 1.7. Crystal structures of **(A)** TeNT (pdb accession code: 5N0B)[55] and **(B)** BoNT-A (pdb accession code: 3BTA)[47] showing the similar structural architectures. Receptor binding domains of the heavy chain are shown at the top of the structures in red and grey, attached to the α-helical translocation domain (orange). The light chain metalloprotease is shown in blue.

A range of protein receptors are also thought to interact with TeNT binding domain, including a GPI-anchored protein and SV2.[49,89] The difference in receptor type between the two CNTs results in a different mechanism of internalisation, with TeNT undergoing retrograde endocytosis towards the cell body in a Rab5-dependent mechanism.[55] Interestingly, TeNT is transported trans-synaptically from peripheral motor neurones into

the neurones of the spinal cord.[90–92] Once in this subset of neurones, TeNT light chain is translocated into the cytosol where it carries out its toxic effect. Unlike BoNT, TeNT causes toxicity by inhibiting the release of the neurotransmitters glycine and γ-aminobutyric acid, resulting in permanent muscle contraction, otherwise known as spastic paralysis.[93] Like BoNT-B, toxicity is caused by cleavage of synaptobrevin from synaptic vesicles.[94,95]

TeNT has been more extensively studied than BoNT as a carrier for delivery of biomolecules, and it has been demonstrated that targeting of TeNT heavy chain (THC) fusion proteins to the CNS is readily achievable. Indeed, THC has been used extensively as a carrier for conjugate vaccines.[96,97] Intramuscular administration of superoxide dismutase or β-galactosidase fused to THC resulted in detection of the enzymes in the motor neurones of the brain, and were shown to follow the same route as TeNT, travelling by trans-synaptic retrograde axonal transport.[98] Replacement of the TeNT light chain with the human lysosomal enzyme N-acetylhexosaminidase A proved an effective enzyme replacement strategy, with the aminidase effectively taken up into the lysosomes of neurones.[99]

Administration of THC protein chimeras into the abdominal cavity of mice also resulted in uptake of the fusions into the CNS. THC has also been shown to be able to transport large nanoparticles of up to 250 nm in size into cultured neuronal cells in a manner consistent with transport of protein fusions.[100] Whilst this has not been demonstrated *in vivo*, viruses of a similar size are known to undergo retrograde transport into neurones, indicating that transport of large particles by THC *in vivo* is likely possible.[101] TeNT can thus be readily engineered to act as a delivery system for carrying biologics into the CNS. TeNT is regarded more as a research tool, however, due to its immunogenicity, and as result of population-wide vaccinations.[14]

To address the issue of immunogenicity, phage-peptide libraries have been screened for binding to gangliosides to identify peptides with properties analogous to THC, but lacking immunogenicity. Two research groups independently identified the same ganglioside-binding peptide, termed Tet1, that was shown to efficiently penetrate neurones and be transported trans-synaptically into the higher order neurones of the CNS.[102,103] Tet1 was shown to be able to target polymersomes and nucleic acids to specific nerves when administered intramuscularly, and the CNS more broadly when administered intravenously.[104,105] Tet1 thus shows potential as a therapeutic carrier, although a release mechanism for the cargo has yet to be designed.

1.3.3. AB_5 toxins

AB_5 toxins are a family of bacterial virulence factors that share a common architecture, and are responsible for causing a range of diseases. The best-known members of this family are the cholera toxins (CT) and heat-labile enterotoxins (LT), which cause life-threatening diarrhea; Shiga toxin (ST), which causes dysentery and colitis; and pertussis toxin (PT), the disease causative agent of whooping cough.[106,107] Together, the bacteria that produce these toxins establish infections in humans that lead to over one million deaths per year.[108]

AB_5 toxins are structurally related (Figure 1.8), composed of a single A subunit, non-covalently associated to a pentameric B_5 subunit.[109,110] The A subunits are composed of an A1 domain, tethered via a disulfide bond to an A2 linker polypeptide that non-covalently anchors the catalytic unit to the B_5 pentamer.[111,112] The A1 subunit is catalytically active, and responsible for modulation of a range of cellular activities that eventually lead to the disease state.[113] The B_5 subunit, meanwhile, mediates entry into the cell through binding to gangliosides presented at the cell surface, resulting in retrograde transport of the holotoxin.[106] The catalytic domains vary between members of the AB_5 toxins, and despite the common structural architecture, there is variation in the receptor they target, even within the CT and LT subgroup.[114] CT and LT-I bind GM1 ganglioside, whilst LT-IIa binds GD1b, and LT-IIb targets GD1a and other less-complex gangliosides at a lower affinity.[115–117]

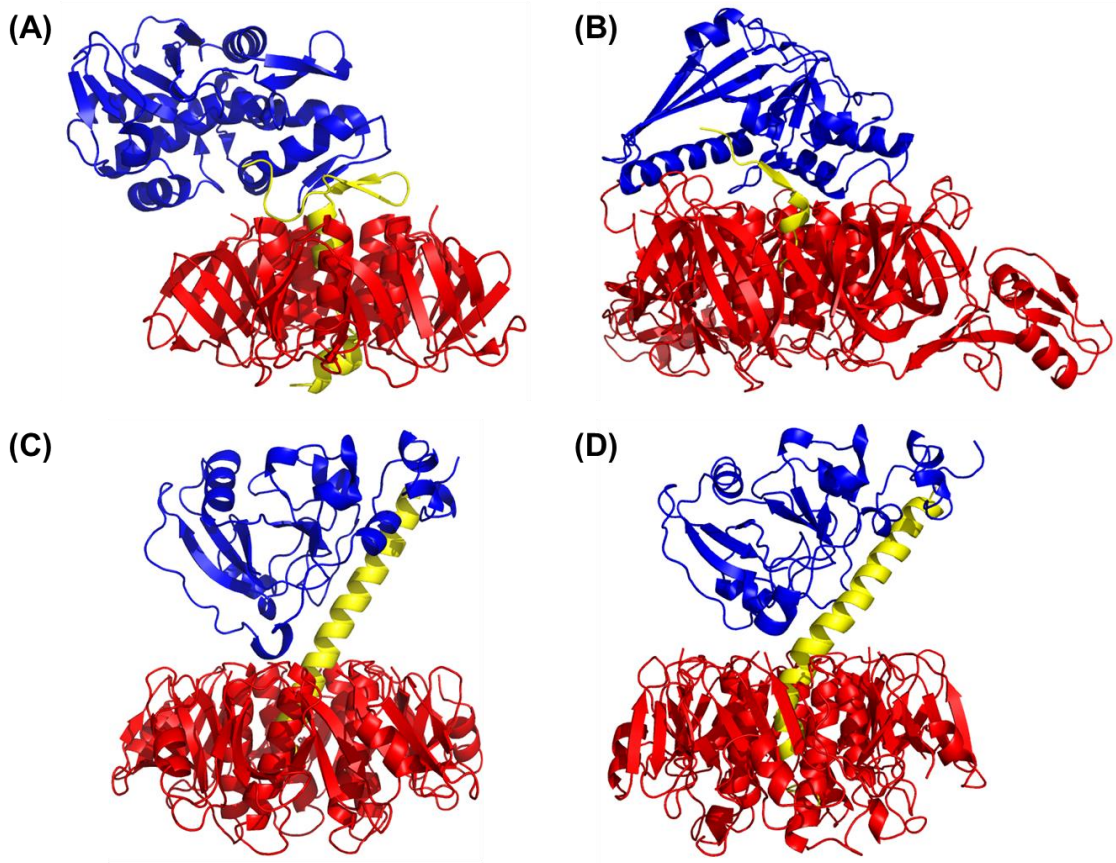

Figure 1.8. Comparison of AB_5 toxins, with catalytically active domains shown in blue, A2 peptide shown in yellow, and pentameric B_5 subunits shown in red. **(A)** shiga toxin (pdb accession code: 1R4P)[118] **(B)** pertussis toxin (pdb accession code: 1PRT)[119] **(C)** heat-labile enterotoxin IIb (pdb accession code: 1TII)[120] **(D)** cholera toxin (pdb accession code: 1XTC).[121]

Given the variety of gangliosides that can be targeted by this toxin family, exploitation of these proteins as carriers of biomolecules has been surprisingly limited. One of the few examples in the literature to manipulate these toxins in this fashion was carried out by the Barbieri research group. They designed constructs that replaced the A1 domain of LT-IIa with a protein cargo. LT-IIa binds to ganglioside GD1b.[117] During infections caused by enterotoxigenic *E. coli*, this binding results in endocytosis of the holotoxin into the cells of the gut. The endocytosed vesicles are then trafficked by retrograde transport to the endoplasmic reticulum, where the A1 domain is retrotranslocated into the cytosol and carries out its toxic effect. To exemplify the novel system, the group delivered β-galactosidase and a camelid antibody into the cytosol of neurones.[122] The camelid antibody delivered inhibited SNAP-25 cleavage by BoNT-A, demonstrating successful translocation into the cytosol.

Recently, a novel AB_5 toxin has been has been isolated and characterised from a clinical strain of *E. coli* named ExcAB. The B subunit shares structural and functional homology,

although only 63% sequence homology, with the cholera and heat-labile toxins, and binding to GM1 ganglioside with high affinity. Interestingly, however, the A subunit shares no sequence or functional homology with any of the known AB_5 toxins, instead folding into a zinc-dependent protease.[123]

The B subunits of these proteins can also be expressed in isolation, and are extremely stable, with variation in the stability profile of different B subunits. For instance, the CT B subunit is a thermostable protein, with a melting temperature of 76°C, whilst the LT B subunit is stable across a wide pH range (pH 2.0 – 11.0).[124–126] Additionally, numerous studies involving the labelling of these subunits with conjugates such as horse radish peroxidase have been carried out to demonstrate effective labelling of neurones.[127–129] The AB_5 toxin family thus presents a series of versatile protein complexes for reengineering to carry biomolecules into neurones.

1.4. The Cholera Toxin

The cholera toxin is a catalytically-active hexameric lectin produced by the marine bacterium *Vibrio cholerae*.[130,131] *V. cholerae* establishes infections in the gut, producing large quantities of the toxin which penetrates intestinal cells, eventually causing severe watery diarrhoea and dehydration.

1.4.1. Structure and formation of the toxin

The cholera toxin is an ~85 kDa protein complex.[132,133] The A subunit is expressed as a single 28 kDa polypeptide that folds into a globular protein with a protruding extended α-helical rod around which the ~11.5 kDa protomers of the B subunit homopentamer assemble and non-covalently associate (Figure 1.9).[134,135] The protruding rod thus acts as an anchor, sitting in the central cavity of the pentameric B subunit.[121]

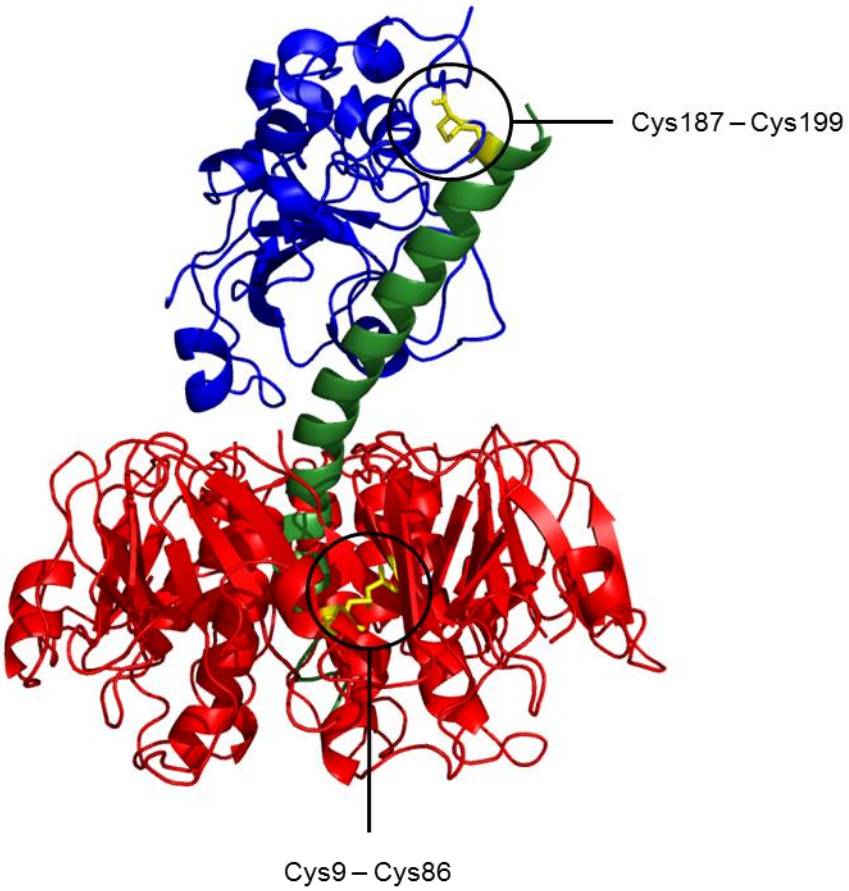

Figure 1.9. Crystal structure of the cleaved cholera holotoxin (1XTC). The toxic A1 domain (blue) is tethered to the A2 polypeptide (green) via a disulfide bond (cys187 – cys199, yellow, circled). The A2 linker sits in the central cavity of the homopentameric B_5 subunit (red). Each protomer of the B subunit is stabilised by an internal disulfide bond (cys9 – cys86, circled).

Of importance is the disulfide bond that sits between the helical anchor, and the globular protein of the A subunit (Cys187 and Cys199). In order for disulfide bonds to form in bacteria, polypeptides must be transported to the periplasm, where thiol-disulfide oxidoreductase (DsbA) catalyses the oxidation to form the disulfide.[136–138] An intramolecular disulfide bond is also formed upon folding of each B-protomer (Cys9 and Cys86), and serves to stabilise the B-protomer tertiary structure, and thus the quaternary structure of the homopentamer, since each protomer associates through inter-protomer interactions and are intimately entwined.[134,139] CTB protomers consist of an α-helix that lines the central cavity, and two adjoining anti-parallel β-sheets that twist to make parallel β-sheet interactions in the centre of the pentamer. Two β-sheets from neighbouring protomers form interactions with each other in an anti-parallel manner to form an almost contiguous β-sheet core in a ring surrounding the central α-helices (Figure 1.11B).[121]

Although the homopentamer will assemble in the absence of the A subunit, formation of the AB_5 complex is favoured due to hydrophobic interactions between the extended α-

helix and the central cavity of CTB.[140–142] The AB_5 complex forms by B-pentamer assembly around the A subunit. Crucially, dissociation of the A subunit from CTB is unidirectional, and it cannot reassociate with CTB if it becomes detached. Thus, coexpression of CTB with the A subunit is a prerequisite for assembly of the holotoxin.[143]

Assembly of the B_5 pentamer is accelerated in the presence of the A2 subunit, indicating that the A2 subunit plays a functional role in holotoxin assembly.[134] Dissection of the assembly pathway revealed that the C-terminal 20 residues of the A2 subunit interact with several protomer units prior to pentamer assembly, resulting in the A2 subunit plugging the central cavity of the B_5 pentamer.[135] Following crystallisation of the toxin, it was noticed that the cavity was composed of a ring of hydrophobic amino acids, composed of residues I74, L77 and T78, likely to be important for AB_5 toxin assembly (Figure 1.10).[120,144] Mutation of these residues to aspartate inhibited holotoxin formation, and in the case of L77, inhibited pentamer formation.[145] This mutational study demonstrates the functionality of the hydrophobic region in pentamer and holotoxin assembly.

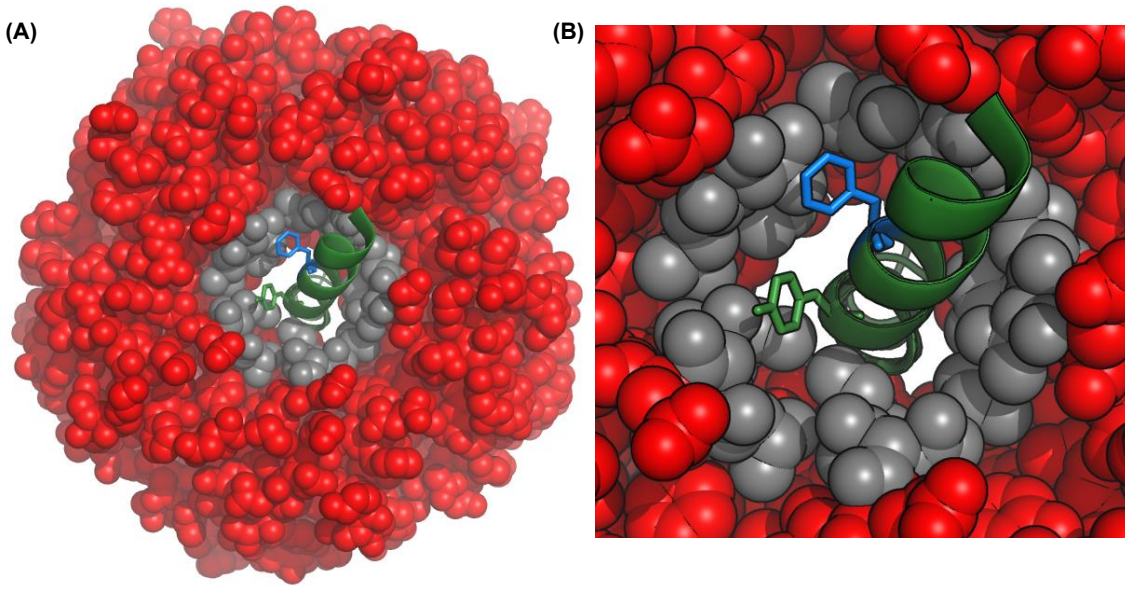

Figure 1.10. Crystal structure of the cholera toxin B subunit (red and grey) and truncated A2 peptide (green). Hydrophobic patch formed by I74, L77 and T78 CTB residues shown in grey. F223 of A2 peptide shown in blue, Y226 of A2 peptide shown in green.

Hovey *et al*. attempted to use this hydrophobic patch to rationally design pore-plugging compounds to inhibit assembly of the holotoxin. The starting point for the drug design was based on the interaction of the hydrophobic ring with residues F223 and Y226.[140] *In silico* design of compounds that mimicked the A2 subunit led to identification of a pore-binding compound that bound in the central cavity, but that the researchers concluded

was too low affinity to be an effective assembly inhibitor. Nonetheless, the research demonstrates that the non-GM1 binding face of CTB can be targeted to identify binding molecules.

The face of CTB distal to the A-subunit contains five carbohydrate binding pockets that recognise and bind to ganglioside GM1 (GM1) with exceptionally high affinity (Figure 1.11).[144,146] The association between CTB and its cognate ligand is one of the highest affinity naturally occurring protein-carbohydrate interactions known, with a dissociation constant in the nanomolar range for each binding pocket. Carbohydrate-protein interactions are more typically weak, with affinities in the millimolar to micromolar range;[147] however, the binding interaction of CTB to GM1 is much stronger, as the GM1 galactose and sialic acid moieties are pre-organised for interaction with the GM1 binding site in a so-called 'two-fingered grip' mechanism, where the sialic acid acts as a thumb, and Galβ(1—3)GalNAc acts as a forefinger. The complex is stabilised by an extensive hydrogen-bonding network, and a key tryptophan residue (W88) forms a crucial hydrophobic stacking interaction with the terminal galactose (Figure 1.11C).[148] Mutation of this residue completely ablates binding of CTB to GM1.[149,150] In addition to the high affinity of each binding site for GM1, the five pentameric B subunits provide multivalency to the system by binding up to five surface-bound ligands, thus amplifying the strength of the interaction to give an avidity in the sub-nanomolar range.[148,151,152]

CTB binds to GM1 with positive cooperativity, enhancing the avidity of the interaction.[146,153,154] In fact, the association constant has been shown to double for an unbound binding pocket binding to GM1 when the adjacent pocket is occupied.[155] Positive cooperativity and multivalency of the binding interaction have been exploited to develop extremely potent pentavalent cholera toxin inhibitors, with IC_{50} values in the picomolar range.[156,157] However, despite this cooperativity, GM1-binding induces only very minor conformational changes that result in further stabilisation of the pentameric structure of CTB.[144] Nonetheless, Chung *et al.* successfully identified single-chain fragment variable antibodies that bind specifically to the LT B_5 subunit (LTB), but not to GM1-captured LTB.[158] The researchers concluded that this was not due to steric hindrance of GM1 in the binding site, suggesting instead that the antibody recognised an epitope available in the unbound form of LTB, but not in the GM1-captured form. LTB-binding monoclonal antibodies were also identified that bound to the GM1-captured and the unbound form of LTB with high affinity.[124]

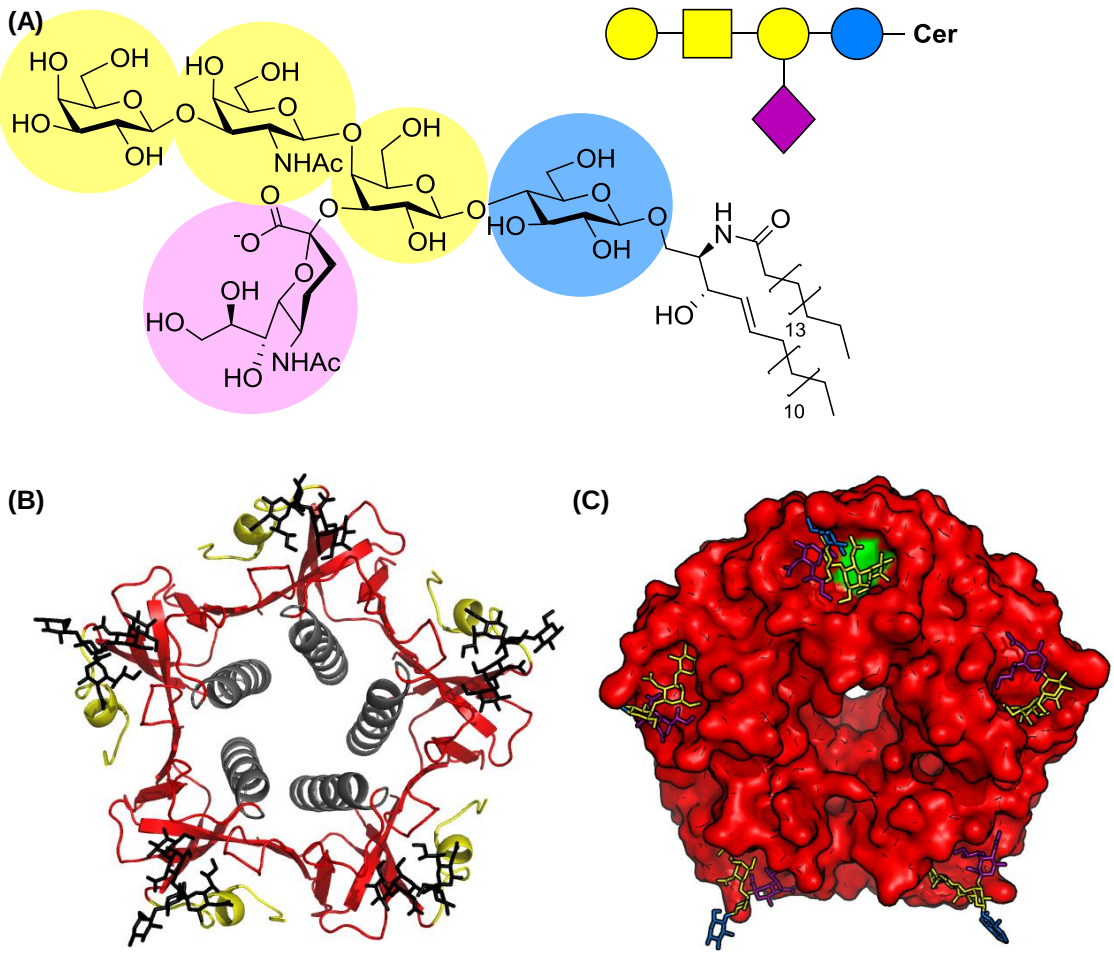

Figure 1.11. (A) Chemical structure and CGF representation of the CTB receptor GM1 ganglioside. The pentasaccharide (Gal(β1-3)GalNAc(β1-4){Neu5Ac(α2-3)}Gal(β1-4)Glc(β1-ceramide)) is presented on the surface of cells through attachment to a sphingolipid. **(B)** Ribbon diagram of CTB shown bound to its cognate receptor, GM1 pentasaccharide (black). The contiguous β-sheet ring is shown in red, with the central α-helices forming the cavity shown in grey. **(C)** Crystal structure of CTB shown bound to GM1 pentasaccharide (black). In one of the binding pockets W88 is shown in green forming interactions with the terminal galactose moiety. Sialic acid (cyan) forms interactions at the periphery of the binding pocket, giving rise to the two-fingered grip mechanism.

1.4.2. Mechanism of toxicity

Once fully assembled, the holotoxin is exported from the bacterium, where the A-subunit is cleaved by trypsin, leaving the globular domain (A1) now tethered to the α-helical anchor only by a single disulfide bond.[159] The B_5 subunit (CTB) binds to GM1 presented at the intestinal cell surface, resulting in invagination of the plasma membrane, and internalisation of the holotoxin into endocytic compartments that travel via a retrograde pathway that is independent of subunits A1 and A2 (Figure 1.12).[106,151] The toxin is then trafficked to the endoplasmic reticulum (ER), via the *trans*-Golgi network, and is retained there by an ER-retention motif (KDEL) on the C-terminus of the A2 α-helix.[160]

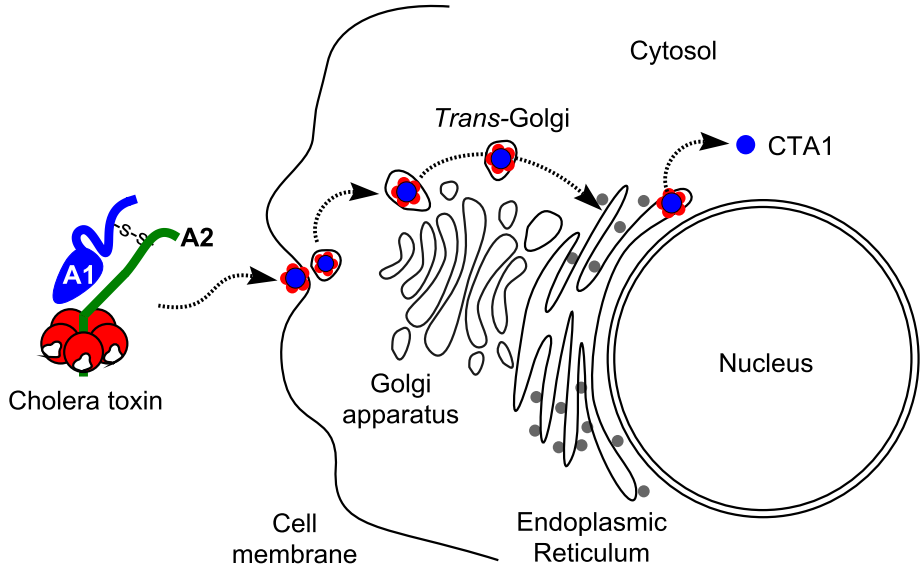

Figure 1.12. Schematic of showing internalisation and endocytosis of the cholera holotoxin. GM1-binding stimulates endocytosis of the complex into endocytic vesicles that are trafficked by retrograde transport to the endoplasmic reticulum via a compartment of the Golgi apparatus known as the *trans*-Golgi network. Once in the ER, reduction of the disulfide bond releases the A1 subunit (CTA1), which is exported into the cytosol by retrotranslocation across the membrane. Once in the cytosol, CTA1 refolds to carry out its mechanism of action.

Once in the ER, the disulfide bond is reduced by protein disulfide isomerase. PDI-mediated disulfide reduction results in dissociation of the A1 subunit from the rest of the toxin, which subsequently adopts a disordered conformation.[161] Since unfolded proteins can result in protein aggregation and cell death, cells have developed mechanisms for coping with this threat in the shape of chaperones that recognise unfolded proteins and target them for cytosolic proteasomal degradation. Unfortunately, this essential house-keeping process has been hijacked by CT. The partial unfolding of the A1 subunit results in recognition by ER chaperones and retrotranslocation of the subunit into the cytosol through the Sec61 translocon.[39,162,163] The A1 subunit refolds into a catalytically active conformation once in the cytosol, evading ubiquitination and subsequent degradation, instead ADP-ribosylating adenylate cyclase, resulting in its constitutive activation. Adenylate cyclase forms cyclic-AMP when in an active state, which in turn activates a chloride transporter.[164] It is this secretion of chloride ions that causes the water loss, and hence diarrhoea, that is characteristic of infection by *Vibrio cholerae.*

1.4.3. CTB as a neuronal tracer

The endocytic pathway that transports cholera toxin to the ER is non-toxic to the cell and thus can be used to deliver proteins safely into mammalian cells.[165] As discussed previously, GM1 coats the synaptic endings and neuromuscular junctions of neurones,

which has led to extensive use of CTB as a neuronal tracer.[98,99] Specifically, CTB conjugated to a variety of fluorophores, chemicals and proteins, has been shown to be useful in the labelling of subsets of neurones. Llewellyn-Smith *et al*. first demonstrated that CTB-conjugated gold nanoparticles could be used for retrograde neuronal tracing in the CNS.[168] Subsequently, CTB has been shown to promote the uptake of quantum dots and carbon dots when chemically conjugated.[169,170] More recently, CTB conjugated gadolinium was used as an MRI-contrast agent *in vivo*.[171] Alisky *et al*. demonstrated that administration of CTB systemically resulted in widespread labelling of motor and sensory neurones, and that labelling could be more localised when administered intramuscularly.[172]

1.5. Antibody Mimetics

Progress in display technologies, together with advances in the identification of novel scaffolds for development of antibody mimetics, promises to revolutionise the field of therapeutic discovery, leading to a new class of antibody-like proteins with improved properties to support the biopharmaceutical landscape.[173,174]

A range of artificial binding proteins currently exist that present peptide loops for binding in a manner similar to antibodies, whilst overcoming some of the latter's limitations.[175] These limitations stem from the complexity of antibodies; the network of disulfide bonds, assembly of multiple subunits, and glycosylation can make antibody production in bacteria problematic.[176] Stably transfected mammalian cell lines are often used as an alternative to bacterial expression. As such, antibodies are expensive to produce.[177] Antibody selection is also traditionally carried out in animals, adding ethical barriers to their isolation and production. Raising antibodies in animals is a time-consuming process, often taking as long as three months to identify, compared to as little as one week for the isolation of mimetics using display technologies.[178–180]

Artificial binding proteins are structurally unrelated proteins that include DARPins, Repebodies, and Kunitz domains, although to date, in excess of 50 novel protein scaffolds have been reported.[173,175,181–183] Artificial binding proteins have been designed to mimic antibody-like binding via the randomisation of the amino acids involved in binding.[184,185] Large libraries are readily produced, and rapidly assayed for binding by molecular selection methods such as ribosome, yeast, bacterial or phage display.[186] In addition to bypassing the traditional process for antibody selection, binding scaffolds have been engineered for stability and solubility; are suitable for expression on the

industrial scale in microbial systems; and are typically small (less than 200 amino acids).[173,186,187] These traits make artificial binding proteins extremely useful tools that have the potential to replace antibodies in numerous applications. Indeed, there are currently 10 non-antibody binding domains in clinical trials, one of which has been approved for use in therapy.[181] Ecallantide, a 60 residue protein derived from Kunitz domain scaffold, binds with pM affinity to a plasma protein (kallikrein), blocking a critical binding site and hence inhibiting bradykinin production in the body. This function makes Ecallantide an effective treatment for hereditary angioedema, and in 2009 this protein was approved as the first non-antibody binding scaffold to be used in clinical therapy.[188,189]

Other antibody scaffolds in clinical trials include an Affibody that binds with picomolar affinity to IL-17, a molecule implicated in psoriasis.[190] IL-17 is dimeric, and so the Affibody was engineered as a dimer with a linker region sufficiently long to allow the Affibody dimer to bind to both IL-17 sites simultaneously. The resultant Affibody dimer (ABY-035) binds IL-17 with sub-picomolar affinity, and has just completed phase I clinical trials for the treatment of psoriasis. As well as showing potential in therapy, these protein scaffolds hold promise in the commercial sector. Affibodies are already available as alternatives to antibodies for Western blotting, ELISA, and immunohistochemistry.[181]

1.6. Affimers

One such artificial binding protein scaffold, termed Affimer, and developed in Leeds, is based on the consensus sequence of phytocystatin, a class of lysosomal cysteine protease inhibitors found in plants. The concept of designing a scaffold based on a consensus sequence draws from the idea that conserved residues are important in maintaining structure, and hence stability. This approach has been effectively used to enhance thermostability of proteins including antibodies and enzymes.[191,192] The Affimer protein scaffold was generated following the alignment of 57 phytocystatin sequences, and resulted in the generation of an extremely thermostable scaffold with a melting temperature of 101°C. A high degree of thermostability usually reflects an intrinsic stability within the protein, allowing Affimers to potentially have more diverse applications that may require harsher conditions than most proteins can tolerate.[193]

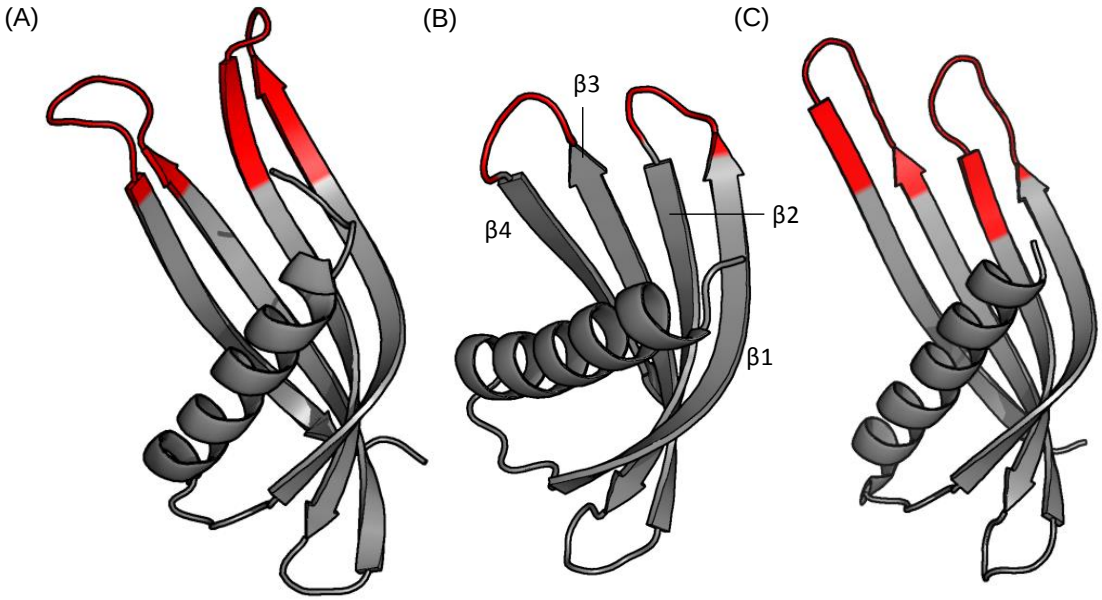

Figure 1.13. Crystal structures of three Affimers showing the common cystatin fold, comprising an α-helix in the 'palm' of a β-sheet, with variable residues shown in red. (A) Affimer raised against ubiquitin linkage K33 (pdb accession code: 5OHM). (B) Affimer scaffold (pdb accession code: 4N6T). β-strands are labelled 1 - 4. (C) Affimer raised against p300 (5A0O)

The consensus protein is small (80 residues), monomeric, and displays high stability and solubility, all of which are desirable characteristics for a peptide presenting scaffold. The Affimer scaffold consists of an α-helix and a β-sheet composed of four anti-parallel strands. The β-sheet curves, forming a half-closed palm around the α-helix (Figure 1.13). The linker regions that connect β-strand one and two, and β-strand three and four are responsible for binding and inhibiting lysosomal cysteine proteases (Figure 1.13).[194] These two inhibitory sequences from the protein were each replaced with a randomised group of nine amino acids, and used to generate a library containing approximately $1x10^{10}$ different Affimer variant coding sequences. The library was generated by overlap extension PCR amplification, which allowed manipulation of the triplet codons in the binding loops such that no cysteine or stop codons were introduced. The coding sequences were then incorporated into a phage library via fusion to the bacteriophage pIII minor coat protein, to develop a system allowing specific, high affinity binders to be pulled down against a target using phage display (*1.7. Phage Display*).[193]

The Affimer technology is novel, and yet has already been shown to have broad applications.[195] An Affimer was identified that binds to the chemokine interleukin-8, a marker of inflammation, and shown to be effective in an electrical biosensor, where analysed blood samples can be rapidly assayed for presence of the chemokine.[196] The

Affimer-biosensor was sensitive to as little as 90 fg mL^{-1} of blood, well below the clinical levels of 5 pg mL^{-1}, and thereby demonstrating the clinical significance of the device. Affimers isolated against the tumour-associated receptor VEGFR2 were shown to be effective immunohistochemical agents, staining tissue with comparable sensitivity to the commercially available antibody.[195] The same Affimers were also shown to block growth factor-dependent VEGFR2 signalling, demonstrating their applicability as research reagents.

Affimers have also been used *in vivo* as tumour-labelling reagents.[195] Affimers raised against tenascin C, an extracellular matrix protein that is often upregulated in cancers, were shown to reach and bind tumours when administered into the circulatory system. The administered Affimers were shown to have a much shorter circulatory time than Tenascin C-specific antibodies, which are larger than the glomerular filtration cut-off, and therefore remain circulating for longer. This long half-life poses problems in the clinic, since background levels of circulating labelled antibody remain high for several days. The anti-Tenascin C Affimers, however, were cleared much more readily, facilitating imaging of labelled tumours after 24 hours. These results demonstrate the applicability of Affimers to *in vivo* systems.

Affimers are identified using M13 bacteriophage display, which will be described in the following section.

1.7. Phage Display

Phage display is an *in vitro* technique that permits the identification of polypeptides with desirable qualities, such as binding, from a large library. The concept was first put forward in 1985,[197] and has since been developed into a field routinely used by the pharmaceutical and biotechnology industries, as well as in research. The premise of phage display rests on the fusion of polypeptides to the coat proteins of filamentous phage, such as M13.

1.7.1 The Life Cycle of Filamentous Phage

Filamentous phage comprise a family of non-lytic ssDNA viruses that infect Gram-negative bacteria. The circular genome is encapsulated by multiple copies of the major coat protein into a long tube of variable length, with five copies of the infectious minor coat proteins presented at the proximal face (pIII/pVI)(Figure 1.14). Phage entry into the bacterial cell is facilitated by a two-way docking mechanism.[198] The pIII minor coat

protein associates with the bacterial F pilus,[199] which results in the translocation, depolymerisation and deposition of the phage into the cytoplasm via a second pIII-mediated interaction, this time with the C-terminal domain of the host periplasmic membrane protein, TolA (Figure 1.15)[198,200]

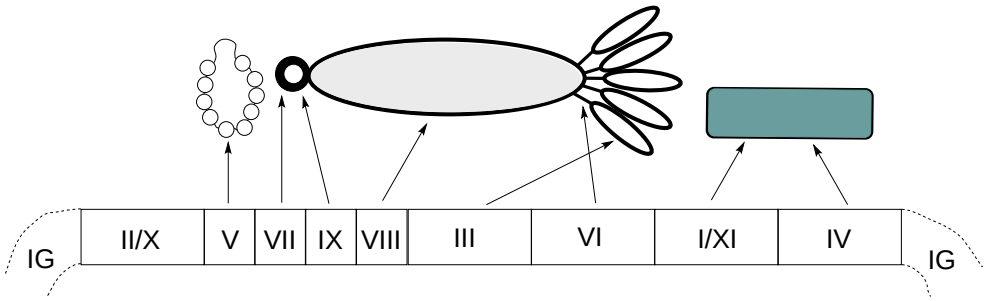

Figure 1.14. M13 phage genes and gene products. The intergenic region (IG) contains the packaging signal, as well as two origins of replication.

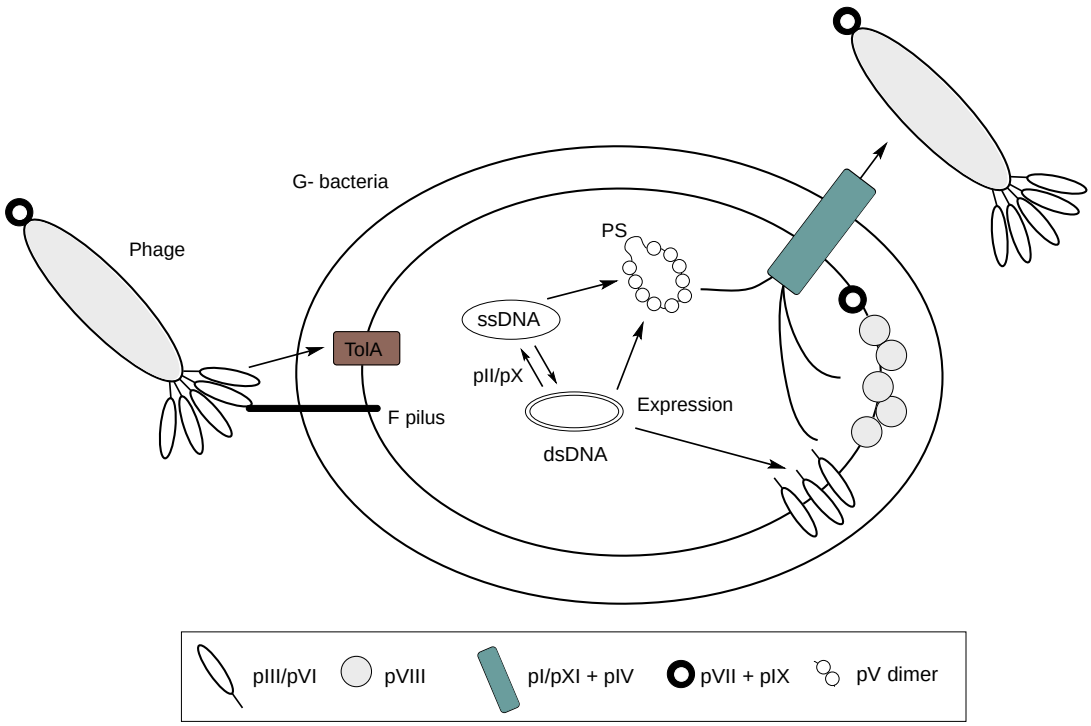

Figure 1.15. Life cycle of M13 bacteriophage – infection, replication and assembly. pIII association with the F pilus of Gram negative bacterium results in recruitment of the coreceptor TolA, and translocation of the phage particle. pII and pX are critical in ensuring replication of the ssDNA by the host to form dsDNA, as well as further ssDNA. The phage genome is transcribed, and proteins required for phage assembly and secretion are expressed. pV dimer binds to ssDNA, collapsing it for packaging, whilst leaving the packaging signal (PS) exposed, which interacts with the assembly machinery. The major and minor coat proteins (pIII, pVI, pVIII) are inserted into the inner membrane along with pVII and pIX. pI/pXI and pIX form a transport complex spanning the inner and outer membranes through which the phage components pass through and assemble.

Upon reaching the cytoplasm, the ssDNA genome is converted into dsDNA by host polymerases. This replicative form of the genome is then transcribed and translated into the M13 components.

*Gene II en*codes the endonuclease and topoisomerase pII, which binds the dsDNA in the intergenic region (IG), and nicks the positive sense strand, stimulating replication of the genome by bacterial polymerases.[197,201] *Gene VIII* encodes the 50-residue major coat protein pVIII, which forms the hollow tube around the genome by self-assembling with thousands of copies of itself. Once expressed, pVIII is anchored into the inner membrane of the periplasm by a hydrophobic transmembrane helix prior to virion assembly.[202,203] The blunt end (distal face) of the structure is composed of the proteins pVII and pIX. Although their function is currently unknown, their expression is critical for phage viability, and there are indications that the two proteins may be involved in initiation of assembly.[204] Despite their uncharacterised function, phage display has been successfully carried out by presenting polypeptides using a pVII/pIX fusion system.[205]

pVI and pIII, meanwhile, required for infection and release from the cell membrane, are expressed from *gene VI* and *gene III*. They are expressed as pro-proteins before being processed by signal sequence cleavage, and then inserted into the membrane with the pVI C-termini in the cytoplasm. pIII, a 406 residue protein, is the most typically used domain for phage display, as it can tolerate large polypeptide fusions, such as antibody fragments, and phage display libraries can be manipulated so that just one copy of the polypeptide is presented per phage (monovalent display). It is worth noting that the phage-encoded proteins involved in assembly (pVII, pIX, pVIII, pIII, pVI, pI, pXI, pIV) act as integral membrane proteins within bacteria.[206] pI/pXI and pIV assemble to form a multimeric outer membrane channel that permits non-lytic escape of the phage from the bacterium.

Gene V encodes pV, a dimeric protein that coats ssDNA to form the pro-virion, prior to packaging. Importantly, the packaging signal (PS) is not coated with pV, so that it can interact with pVII and pIX for phage assembly.[207]

1.7.2. Genetics of Affimer Phage Display

The BioScreening Technology Group (University of Leeds) have used the well characterised pIII fusion display system for presenting Affimers onto M13 bacteriophage particles. Specifically, the coding sequences for the Affimer scaffold containing the

randomised loops were fused to the 5' end of a truncated *gene III*, to produce an Affimer-pIII fusion protein, and incorporated into a phagemid vector containing an f1 origin of replication for ssDNA production, and a plasmid origin (pBR322) for dsDNA production. This phagemid vector allows the production of ssDNA, and the expression of the Affimer fused to a truncated pIII, separated by an amber stop codon (TAG).

The intervening amber stop codon was introduced to permit expression of Affimer domains separately from pIII in non-amber-suppressing *E. coli* strains such as BL21 or JM83, whilst allowing read through of the amber stop codon in an amber-suppressing strain, such as ER2738. Importantly, the Affimer-pIII sequence is preceded by a DsbA signal sequence (DsbASS) that permits trafficking of the fusion protein to the periplasm for incorporation into the phage particle.[208]

A helper phage is required to produce infectious phage. M13KO7 helper phage is added to *E. coli* harbouring the pBSTG phagemid. This helper phage contains the genes encoding the proteins required for assembly and infectivity, as well as a kanamycin resistance gene for selection.[201] This helper phage has a defective origin of replication, however, that leads to inefficient packaging of the phage genome, and preferentially packages the phagemid vector (Figure 1.16).[201] There is therefore competition between the M13 K07 wild-type pIII protein, and the recombinant Affimer-pIII fusion. However, the Affimer-pIII CDS is under control of a weak transcriptional promoter (lac promoter), resulting in fewer copies of Affimer-pIII being expressed. As a result, approximately 10% of the packaged particles will only contain one copy of the pIII fusion, whilst the remaining 90% will contain the wild-type pIII.[206] This competition results in monovalent display of the Affimer scaffold, permitting selection based purely on affinity, and thus avoiding avidity effects from having multiple Affimers expressed on the same phage particle. Additionally, the N-terminal domain of pIII is responsible for F pilus binding, thus making regulation of the number of Affimers presented on the surface of the phage necessary for formation of infectious phage particles.[209]

Once infectious virions have formed, pI, pIX, and pXI facilitate their export from the bacterium, releasing the phage-Affimer particles in a non-lytic manner into the surrounding medium for use in a phage display screen.

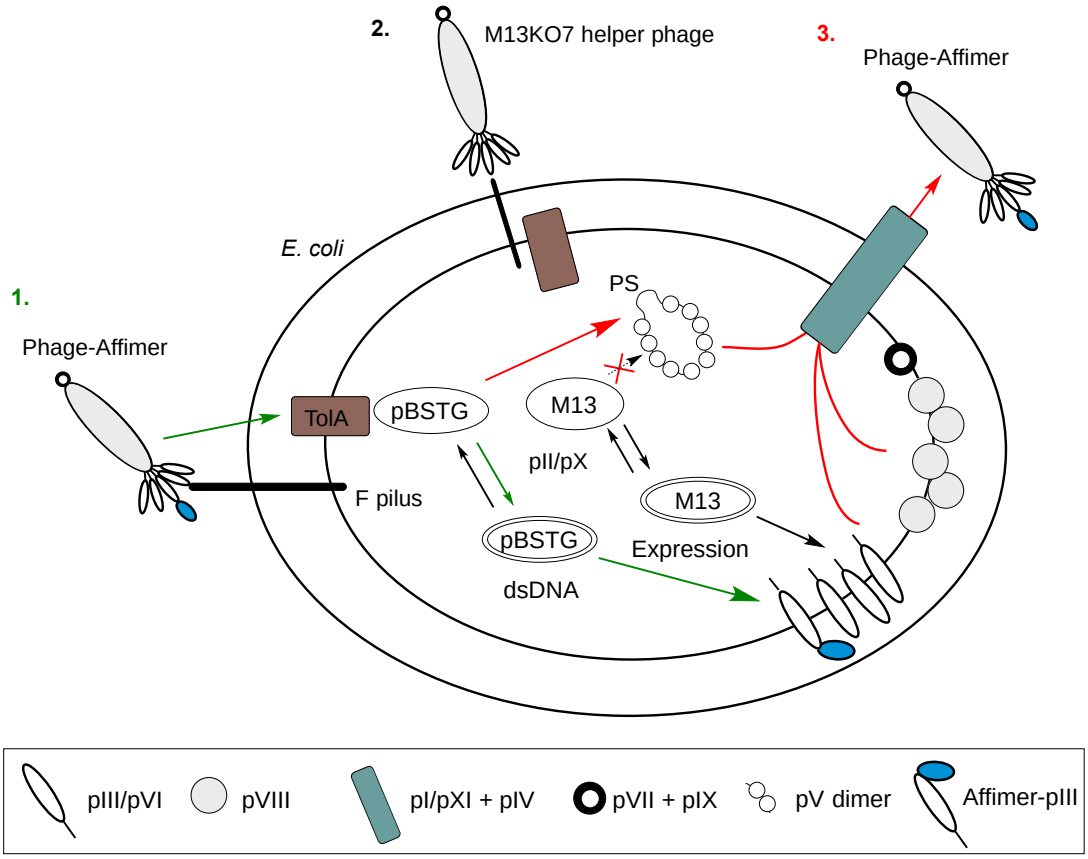

Figure 1.16. Propagating phage-Affimers following infection of E. coli with phage-Affimer particles. In **1.**, infectious phage-Affimer particles dock via interactions with the F pilus and TolA receptor. The pBSTG single-stranded DNA coding for the Affimer-pIII fusion is injected into the cell by the phage, and is converted to dsDNA by the host machinery. The DNA is transcribed, and translated (under a weak promoter) into Affimer-pIII fusions, which insert in the inner membrane of the periplasm. **2.** In order for phage to be fully formed and exported out of the bacterial cell, a helper phage is required. M13KO7 helper phage docks to the cell, and transfers its single-stranded DNA genome, that harbours a defective origin of replication. The M13KO7 DNA is converted to dsDNA, which is subsequently transcribed, and translated (under a strong promoter) into the proteins required for phage assembly. **3.** pII and pX convert pBSTG into ssDNA for packaging into virions. The defective origin of replication leads to preferential packaging of the pBSTG phagemid vector, and phage-Affimer particles are released.

1.8. Developing a CTB-based neuronal delivery platform

The ability of CTB to transport a range of cargoes into neuronal cells has been successfully demonstrated.[167,170,171,210] We postulated that CTB could thus be used safely to deliver biologics to motor neurones. Existing methods rely on chemical modification of CTB to attach a cargo. Whilst this strategy has been used successfully to deliver HRP to neurones, not all biologics are amenable to chemical modification, and the strategy usually lacks precision, since chemical labelling strategies target surface exposed lysine and cysteine residues.[211]

The Barbieri group succeeded in replacing the A1 domain of LT-IIa with a biologic, and demonstrated its functionality *in vivo*.[122] Whilst an elegant strategy, implementing it as a more general approach to deliver biologics poses some issues. Since coexpression of both the A subunit and the B subunit components is required for assembly of their delivery system, this negates the delivery of more complex proteins that cannot be expressed in bacteria. Furthermore, expression of the two components together requires the handling of biologically active protein in large quantities, adding a layer of complexity in terms of safety. These issues are equally present with the ganglioside-binding peptides Tet1 and TAxI.

A two-component system could be developed that would allow a protein cargo to self-assemble with a drug delivery vehicle (Figure 1.17). Developing such a system would have several advantages. Firstly, it would remove the need for coexpression of the cargo and delivery vehicle, allowing more complex cargos to be expressed in optimised systems. Secondly, a two-component system would allow a potent biologic to be linked to the delivery vehicle only when required for use, thus addressing safety issues with production of the complex. Finally, such a system could be tailored to disassemble once at the target site, allowing release of the cargo from the delivery component.

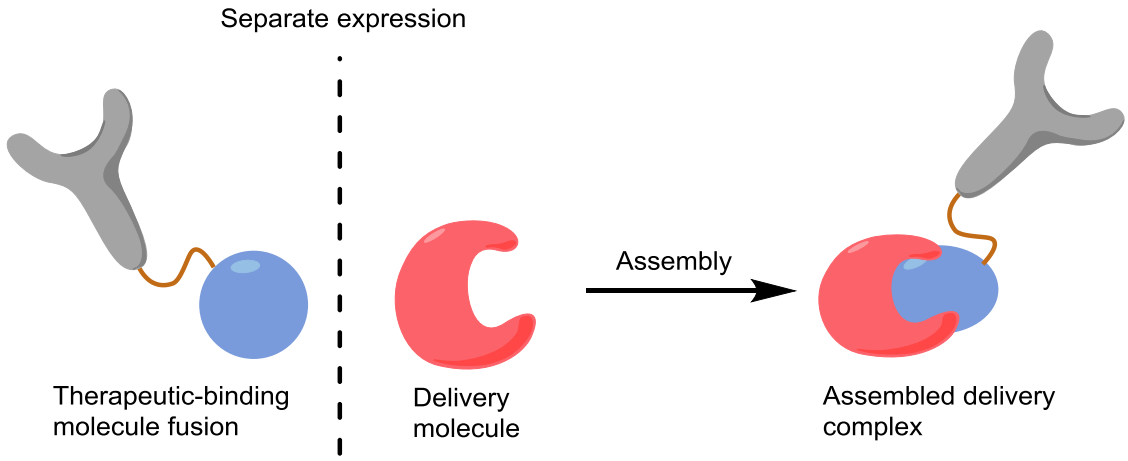

Figure 1.17. Schematic showing the concept of a two-component delivery system. A delivery molecule that can induce receptor-mediated endocytosis is combined with a binding molecule that recognises the delivery molecule, but does not interfere with its ability to be endocytosed. The binding molecule is conjugated to a therapeutic, such as an antibody. The therapeutic-binding molecule fusion and delivery molecule assemble, and can be delivered to a target cell. Development of a two-component system allows expression of both components separately, introducing a safety feature, as well as allowing optimisation of protein production for both delivery molecule and therapeutic.

One way to achieve assembly would be to identify a protein that binds to the delivery vehicle. The binding protein could be fused to the cargo, permitting association to the delivery vehicle through the binding interaction. We considered using phage display to identify antibody mimetics that bind specifically to CTB. Affimers are proven versatile binding molecules with wide ranging applications from use in biosensors to tumour-binding *in vivo*. Affimers were thus considered as a suitable tool to mediate the modular assembly of a two-component protein delivery system.

1.9. Project Objectives

The development of the delivery system was broken down into four key objectives. Accomplishing these objectives was central to establishment of the novel drug delivery tool.

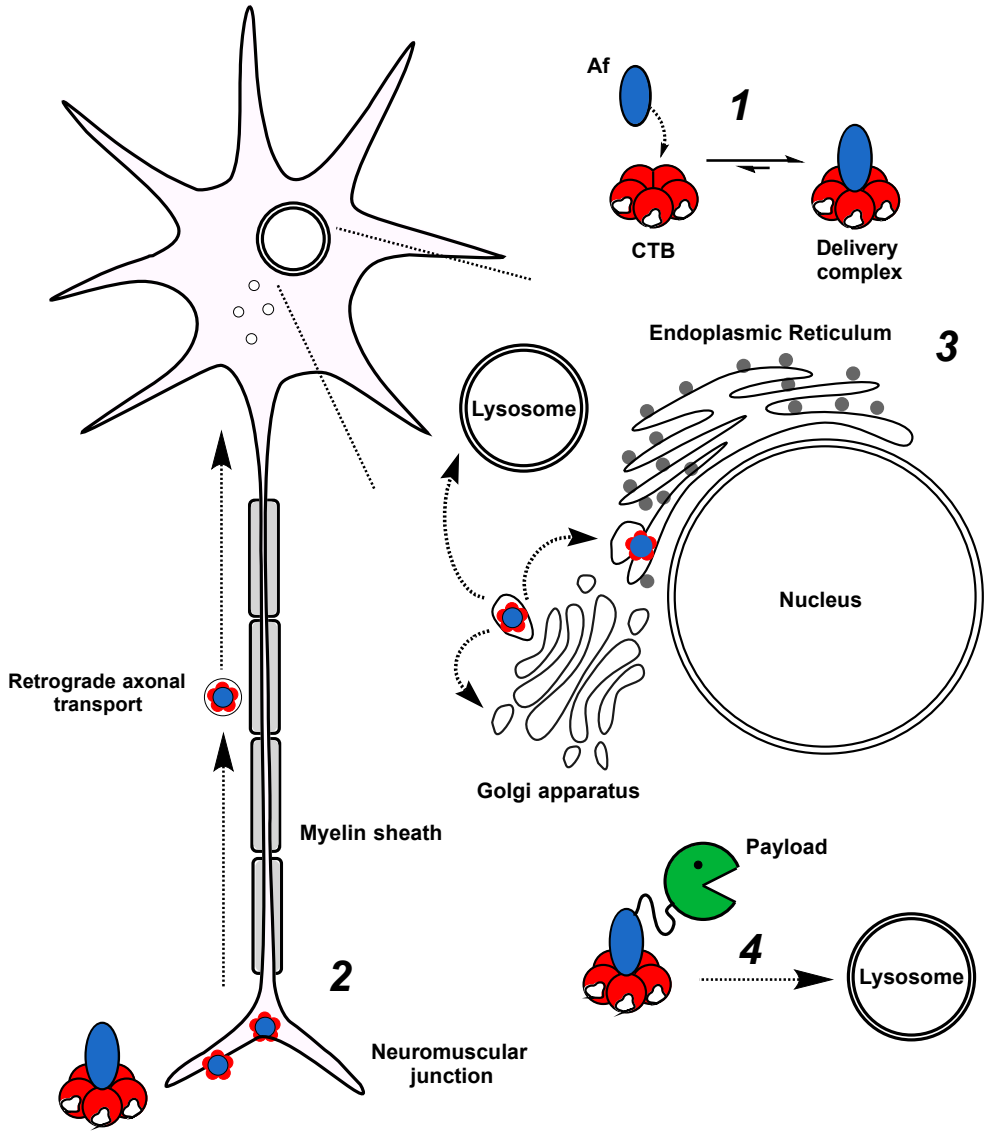

Figure 1.18. Summary of objectives.
In *objective 1*, a self-assembling complex comprising CTB (red) and an Affimer (blue) will be formed and characterised. In *objective 2*, this complex will be assessed in tissue culture, and then *in vivo* for its ability to be taken up by motor neurones. *Objective 3* investigates targeting of the complex to various subcellular compartments. The complex will be used to deliver a payload (green) to the lysosome in *objective 4*

Objective 1. Binding Affimers that target the non-GM1-binding face of CTB were to be identified by phage display in a first step to obtaining a non-covalently associated complex for protein delivery. The complex was to be characterised using a variety of biophysical techniques to measure affinity and kinetics of the binding interaction.

Objective 2. The ability of CTB to direct the binding protein to cells was to be evaluated. Constructs were to be initially tested in a cultured cell system, before testing the ability of the complex to be internalised into motor neurones *in vivo*.

Objective 3. Fluorescent proteins were to be conjugated to the binding Affimer, and used to investigate the subcellular localisation of the cargo.

Objective 4. A payload was to be tethered to the complex and administered *in vivo* as a proof of principle to demonstrate the potential for the complex to be used as a platform for delivery of proteins to motor neurones.

2. Identifying CTB-binding Affimers

As one of the central objectives of this project, identification of CTB-binding Affimers was a critical step for the formation of a CTB-Affimer complex. The main challenge would be isolating Affimers that interact specifically with the non-GM1-binding face of CTB, and characterising the manner in which these binding proteins interact with their target. In this chapter, I address how these challenges were met by describing how phage display was used to identify Affimers; how a novel assay was developed to evaluate and rank the isolated binders; and by describing the biophysical experiments carried out to understand the CTB-Affimer interactions. First, however, I describe the important process of making and modifying the CTB pentamer.

2.1. CTB Expression and Modification

2.1.1. CTB expression and crude purification

As one of the essential building blocks for this project, the expression and purification of the CTB pentamer was carried out as a crucial first step. A detailed protocol for this protein prep is outlined in *5.4.2. CTB Expression from Vibrio sp. 60*. *Vibrio sp.* 60 cells harbouring the pATA13 plasmid[212] (*7.1.1. pATA13*) were used to overexpress CTB. *Vibrio sp.* 60 is a marine bacterium that has been exploited extensively to produce CTB, and indeed other related B_5 and AB_5 toxins, due its expression efficiency, and its ability to export pentameric bacterial toxins into the extracellular growth medium.[213,214] However, the pATA13 plasmid has proved somewhat stubborn to engineer, and *Vibrio sp.* 60 is typically transformed with genetic material by the more costly method of electroporation or by triparental-mating; protein expression from this *Vibrio* strain was therefore limited to wild-type El Tor CTB and LTBh (*7.2.1. CTB/LTB protein sequences*), as stocks of these transformed bacteria were readily available. Yields of CTB obtained from *Vibrio sp. 60* were typically 30 mg L^{-1}, compared to 10 mg L^{-1} when expressed in *E. coli*.

Once expressed, the medium was isolated from the cell pellet, and the proteins were precipitated by saturating the solution with ammonium sulfate. The resulting precipitate was resuspended and applied to a nickel affinity column. This fortuitous binding to nickel resin is due principally to the five surface-exposed H13 residues present on the binding face of CTB. However, the five exposed H13 residues have a much lower affinity for nickel than a hexahistidine purification tag, and as such, a lower concentration of

imidazole must be used to wash the resin once the protein has bound. The less stringent wash results in more impurities eluting with the CTB, necessitating a further purification step by gel filtration chromatography.

2.1.2. Purification of CTB by gel filtration chromatography

Gel filtration chromatography was used to further purify CTB. A HiLoad 16/60 Superdex 75 gel filtration column was equilibrated with a phosphate buffer, and the concentrated eluate was applied to the column. Figure 2.1 shows the resultant chromatogram, with a large peak observable at a retention volume of 64 mL, corresponding to CTB.

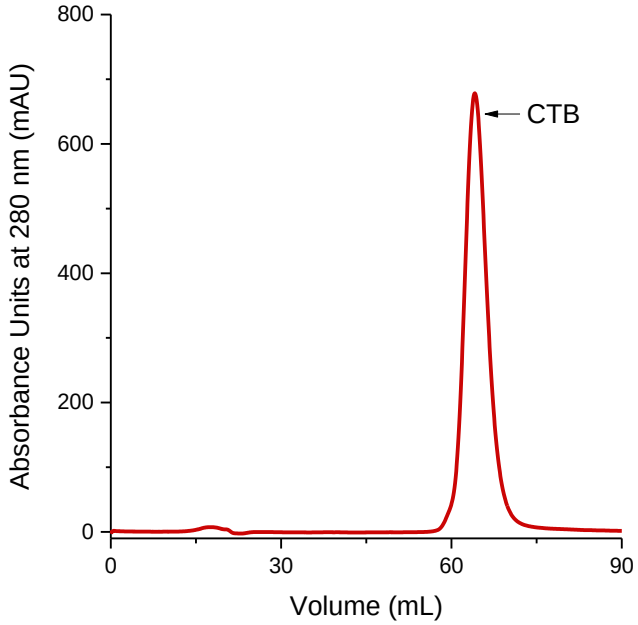

Figure 2.1. Size exclusion chromatogram generated following application of a CTB-containing sample to a HiLoad 16/60 Superdex 75 gel filtration column. A peak at a retention volume of 65 mL (arrow) indicates purification of a single protein species.

To verify isolation and purification of CTB by gel filtration chromatography, the fractions corresponding to the peak were analysed by SDS-PAGE (Figure 2.2).

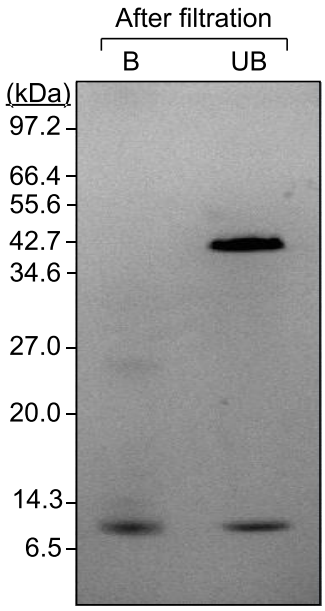

Figure 2.2. SDS-PAGE analysis of CTB fractions purified by gel filtration chromatography either boiled (B), or unboiled (UB). CTB (UB) migrates as a partially stable pentamer on the gel, with an apparent mass of ~40 kDa. Boiling CTB (B) causes the protamers to dissociate and migrate further down the gel, showing an apparent mass of ~12 kDa.

Whilst most proteins denature during SDS-PAGE, the stability of the CTB pentamer permits it to partially retain its quaternary structure during electrophoresis as long as it has not been boiled prior to loading on the gel. Figure 2.2 shows a typical post-purification analysis of boiled and unboiled samples of CTB by SDS-PAGE. Comparing the bands to the protein marker reveals an apparent mass for the pentamer of approximately 40 kDa, 18 kDa lower than the expected value (58 kDa). This is due to the compact nature of the pentamer; since the protein is not fully unfolded, it migrates faster through the polyacrylamide matrix. Upon boiling, the pentamer dissociates into a monomeric form, the apparent mass of which agrees with the expected mass of approximately 12 kDa.

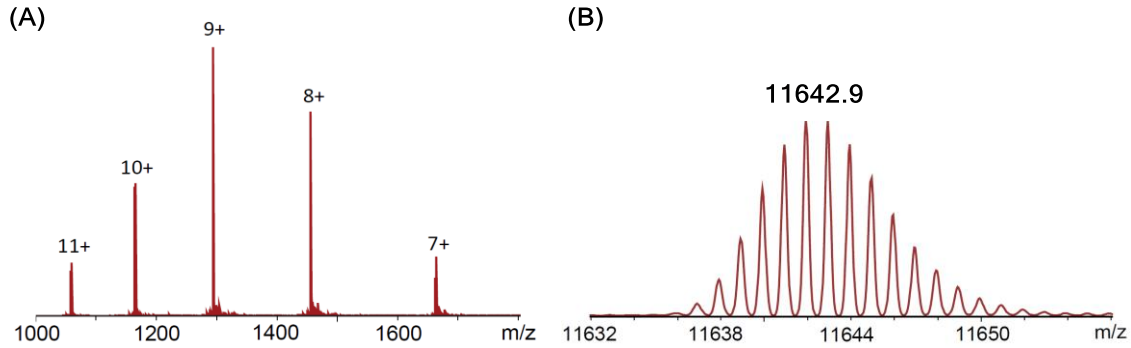

Figure 2.3. (A) Mass spectrum following analysis of the CTB B-subunit by ESMS under denaturing conditions showing a range of charge states for the CTB protamers. **(B)** Deconvolution of this mass spectrum gives a mass of 11642.9 Da (expected 11643.4).

Electrospray mass spectrometry (ESMS) was used as an additional quality control technique to confirm that the purified protein was indeed wild-type El Tor CTB. Peaks corresponding to the different charge states of monomeric CTB were readily observed (Figure 2.3), which were deconvoluted to establish a molecular weight of 11642.9 Da. The expected molecular weight was 11643.4 Da, aligning with the measured value, and thus confirming the presence of CTB in the purified samples.

2.1.2. CTB oxidation and modification

Identification of Affimers relies on being able to screen a library of phage-Affimer particles against an immobilised target. This is typically achieved by biotinylating the target protein, so that it can be robustly immobilised onto a streptavidin-coated surface ready for screening.

Biotinylation of proteins can be achieved through a variety of chemical methods, with one of the more popular techniques involving the use of biotin N-hydroxy succinimide ester (NHS-ester) (Figure 2.4). This chemical reaction is popular since it can be carried out under physiological conditions, in aqueous solvent, and reacts with any protein containing primary amines, such as those presented on the side chains of lysine residues. Analysing the amino acid sequence of CTB reveals that the protein contains nine lysine residues per pentamer, and thus would be a suitable candidate for this type of chemical modification.

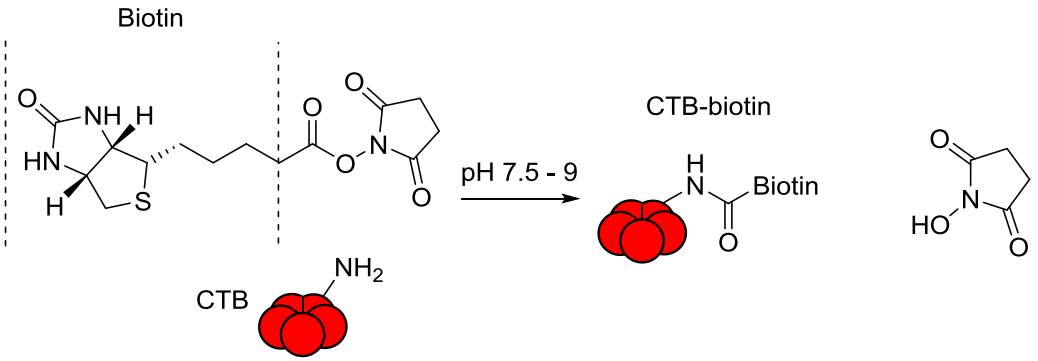

Figure 2.4. CTB can be chemically biotinylated at physiological pH through reaction of a lysine primary amine with a biotin functionalised with an NHS-ester.

CTB has two distinct faces; a binding face (the bottom) required for carbohydrate-binding and subsequent docking to the plasma membrane, and a non-binding face (the top) distal to the plasma membrane during docking. For the system to be functional, Affimers would be required to associate with the non-binding face of the pentamer, since binding to the bottom face would most likely interfere with docking to GM1 on the plasma membrane,

thereby inhibiting endocytosis. The lysine residues in CTB are distributed across the protein, and thus biotinylation would result in distribution of biotin molecules across the two faces, resulting in the isolation of Affimers recognising CTB in a range of orientations. These undesirable Affimers would have required filtering out further down the pipeline. Therefore a more elegant, site specific approach was devised to limit the range of orientations of CTB presented during phage display.

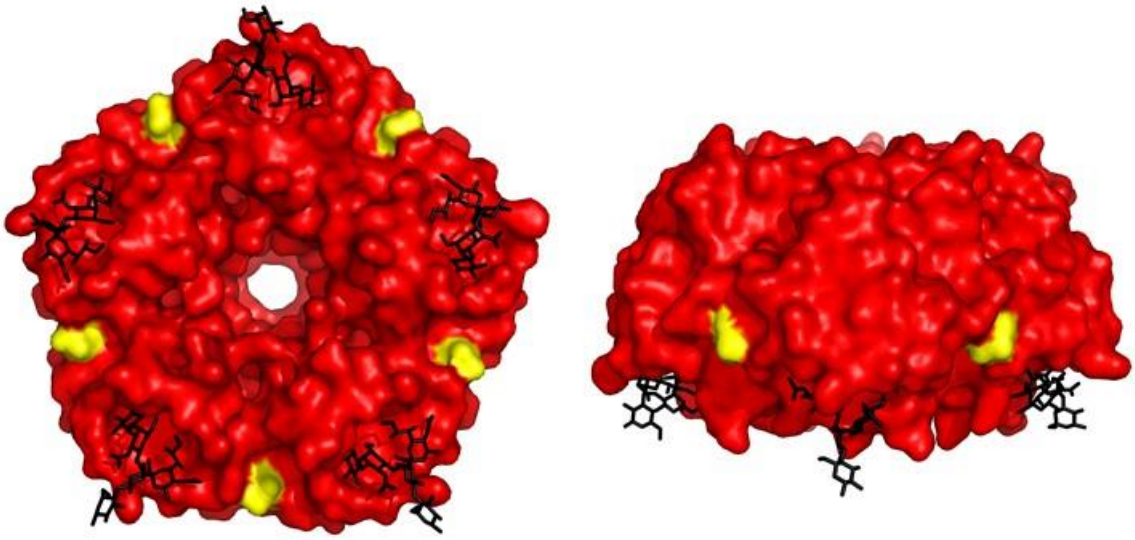

Figure 2.5. Surface representation of the three-dimensional crystal structure of CTB, shown bound to GM1os (black), with the N-termini (yellow) intersecting the GM1-binding sites. Crystal structure downloaded from the PDB, code 3CHB.[215]

The N-termini of the CTB protomers point down towards the binding face, and are located directly between the carbohydrate-binding sites (Figure 2.5). Site-specific modification at this position would therefore provide a route to orienting the CTB protein on a surface to exclude the GM1-binding face from phage particles. Chen *et al.* demonstrated that peptide extensions could be introduced onto the N-termini of CTB by oxidising the amino alcohol group of the N-terminal threonine residue to an aldehyde, and subsequently reacting the aldehyde with an aminooxy-functionalised peptide, to form an oxime linkage.[216] However, in order for the oxime ligation to proceed, the pH was lowered significantly, resulting in dissociation of the CTB pentamer, and necessitating a refolding step at a later stage. Dirksen and colleagues identified a catalyst that accelerates oxime ligations at pH 7, thereby circumventing the need for a refolding step.[217] Branson et al. have demonstrated that aniline catalysis can be applied to modification of CTB under neutral conditions where the pentamer is stable.[156] Addition of aniline to the reaction leads to formation of an intermediate iminium ion that readily forms an oxime at pH 7.0.

Site-specific biotinylation was therefore possible by using the mild oxidising agent sodium periodate, followed by the addition of aminooxy biotin and aniline (Figure 2.6).

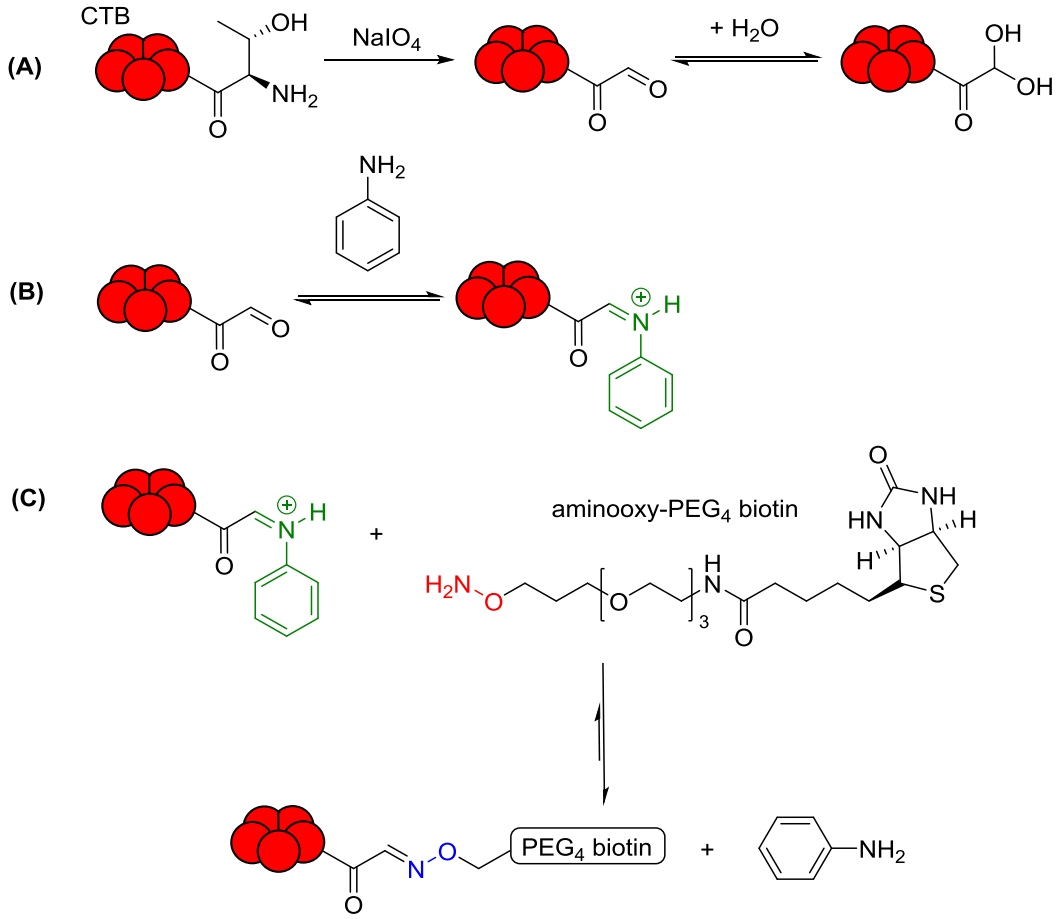

Figure 2.6. Chemical biotinylation of CTB. **(A)** Oxidation of an N-terminal threonine with sodium periodate forms a terminal aldehyde functional group that interconverts between the aldehyde and the diol. **(B)** The aldehyde reacts with aniline to form an intermediate iminium ion (green). **(C)** The iminium ion is rapidly displaced by the aminooxy (red) functionalised moiety, in this case PEG_4 biotin, to form an oxime linkage (blue).

Oxidation was carried out at a relatively high concentration of CTB (100 µM pentamer concentration) using five equivalents of sodium periodate. The reaction was monitored by ESMS, and found to proceed to completion within 30 minutes, with an observed mass loss of 27 Da. Aldehydes are transient in aqueous solution, since they are prone to hydration. The 27 Da mass loss was therefore attributed to observation of the hydrated form of the protein rather than the aldehyde form (Figure 2.6A).

In some cases, chemical modification of proteins in this manner can result in cyclisation of the peptide forming an inert product. Cyclisation is thought to occur when a proline precedes the oxidised residue, resulting in a kinking of the peptide chain, and promoting the side reaction through effects of proximity (Figure 2.7).[218] However, provided that the

oxidised protein is used immediately in subsequent oxime ligations, cyclisation can be averted.

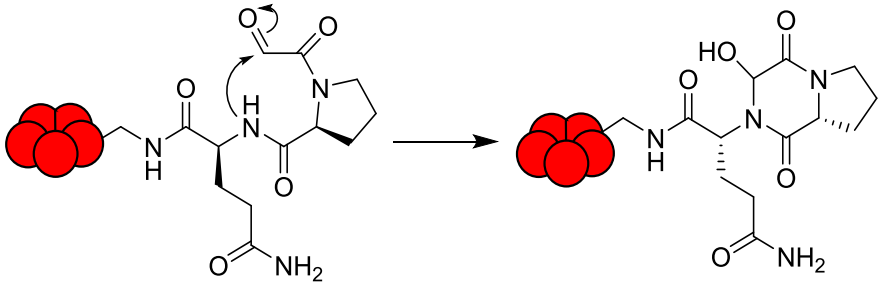

Figure 2.7. Cyclisation reaction at the N-terminus of oxidised CTB. Following oxidation of the N-terminal threonine residue of CTB, a cyclisation reaction is known to take place. The prolyl residue at position two results in a kinking of the polypeptide chain, bringing the terminal aldehyde into proximity of the amide nitrogen of the glutamine residue at position three, and leading to nucleophilic attack and cyclisation.

Oxidised CTB was then separated from excess periodate and acetaldehyde using a PD10 desalting column. The oxidised CTB was combined with aminooxy PEG_4 biotin and the aniline catalyst, and left overnight to react. The reaction was purified by gel filtration chromatography (Figure 2.8A), and samples of unmodified, oxidised, and biotinylated CTB were analysed by SDS-PAGE to ensure that the pentameric structure had been retained (Figure 2.8B).

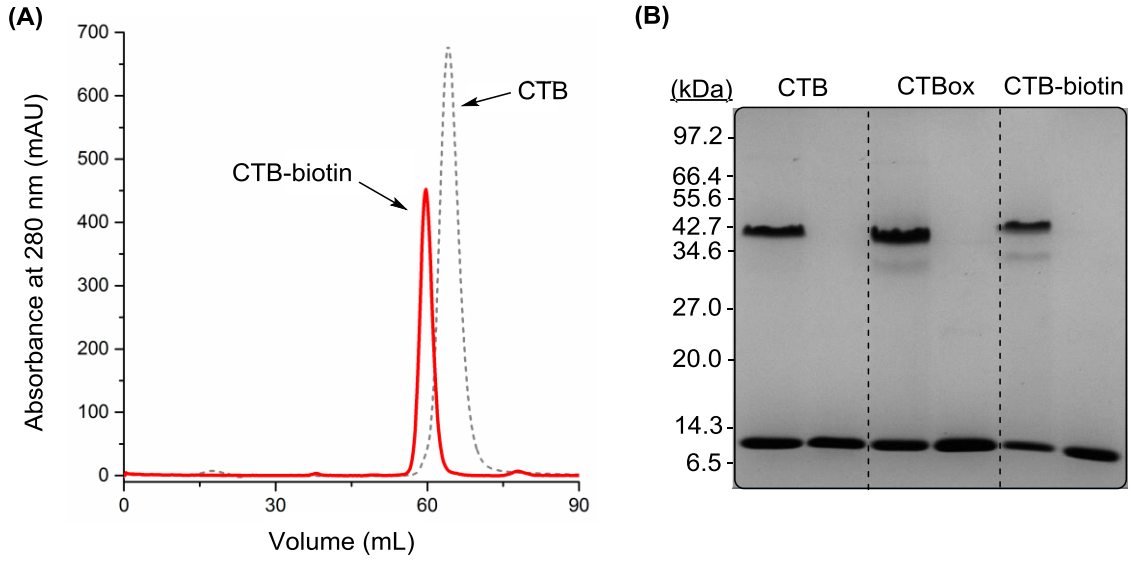

Figure 2.8. Analysis of CTB-biotin. **A)** Size exclusion chromatogram showing purification of CTB-biotin by gel filtration, and the shift in retention volume compared to CTB. **B)** Analysis and comparison of unboiled and boiled samples of CTB, oxidised CTB, and CTB-biotin by SDS-PAGE.

ESMS was used to confirm protein labelling (Figure 2.9). The mass of CTB-biotin was calculated as 12014.6 Da. The major product detected by ESMS was measured to be 12014.1 Da, thus demonstrating that CTB had been successfully modified.

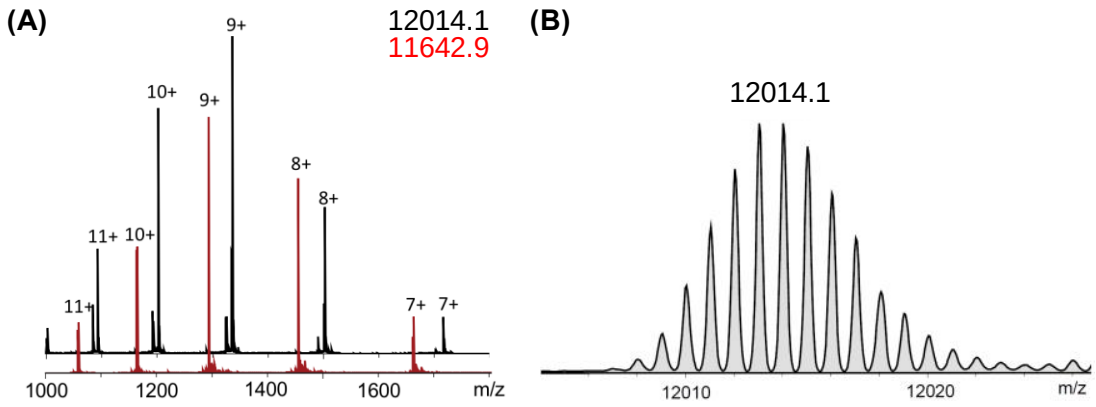

Figure 2.9. ESMS analysis of CTB-biotin following purification by gel filtration. **(A)** A clear shift in the mass to charge ratio (m/z) from unmodified CTB to CTB-biotin indicates an increase in mass. **(B)** Deconvolution of the spectrum allowed identification of a single species at 12014.1 Da, attributed to CTB-biotin (calculated mass, 12014.6 Da)

Following the successful biotinylation and purification of CTB, the chemically modified protein was used for phage display.

2.2. Phage Display

An in-depth explanation of the theory behind phage display is presented in *1.7. Phage Display*. To summarise the Affimer selection process briefly, a target is immobilised to a solid support, and then exposed to a library of recombinant bacteriophage, each expressing a unique Affimer on the surface of their minor coat proteins. Non-binding phage particles are removed, whilst binding variants are eluted under harsh dissociating conditions, and used to infect *E. coli* bacteria. Phage-Affimer particles are propagated for subsequent rounds of phage display by culturing infected bacteria. A helper phage is then added to allow phage-Affimer particles to assemble and be released into the surrounding medium. This iterative process enriches the pool of target-binding phage-Affimers, which can then be isolated and characterised.

2.2.1. Pre-panning the phage-Affimer library

With biotinylated CTB (CTB-biotin) in hand, the first rounds of phage display could be carried out. Commercially acquired streptavidin-coated 96 well plates were used for immobilisation of CTB-biotin. The wells were initially ‘blocked’ using a casein-based blocking buffer to reduce non-specific binding of the bacteriophage to the streptavidin-coated plastic. Once blocked, the naïve phage library was exposed to one of the wells in a process termed ‘pre-panning’. This process was introduced to remove from the library phage-Affimer particles that bind to some component of the plastic, casein, or

streptavidin. Implementing this process reduces the number of false positives, and enhances the enrichment of protein-specific Affimers. Pre-panning was repeated three to five times to maximise reduction in false positives prior to being exposed to the target protein.

The highly specific and high affinity interaction formed between biotin and streptavidin allows CTB-biotin to become bound to the surface simply by addition of the biotinylated protein.

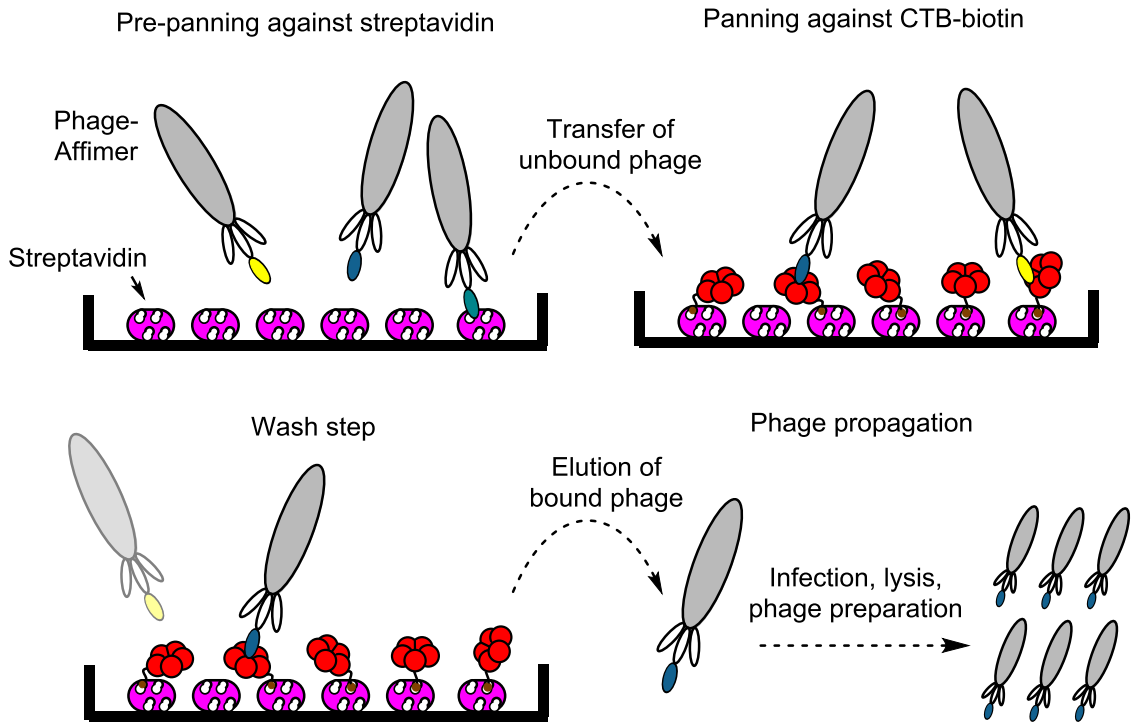

Figure 2.10. Screening against CTB-biotin to isolate target binders. The phage library is initially incubated in streptavidin-coated wells in a process termed pre-panning to remove Affimers that bind to streptavidin or another component of the well. Unbound phage are then 'panned' against a streptavidin-coated well containing immobilised CTB-biotin. The well is washed extensively to remove weakly associated material, before disruption of Affimer-target interactions with a strongly acidic buffer. The solution is neutralised, and transferred immediately to a bacterial culture for infection. After propagation of the phage in the bacteria, a helper phage is added to form lytic phage, which can then be used in further panning rounds.

2.2.2. Phage panning, propagation and extraction

The surface-bound CTB was then presented to the pre-panned phage library. After an hour of this exposure, non-binding and weakly bound phage were removed by carrying out 27 washing steps. High affinity binders were eluted from the wells by addition of acidic glycine (pH 2.2). To restore full function of the bacteriophage, the dissociated

material was combined with a neutralising solution, and then transferred to a bacterial culture for infection.

Following infection the bacteria were cultured on an ampicillin-containing agar plate. The engineered bacteriophage lack the requisite machinery for assembly and secretion, resulting in retention of the phagemid DNA within the bacterial colonies.

To carry out further rounds of panning, the phage were extracted from the bacteria by addition of M13 helper phage (M13KO7) and kanamycin. Addition of complementary parts provided by helper phage results in assembly of the bacteriophage, and secretion of the phage in a non-lytic manner into the surrounding medium. The phage could then be recovered by precipitation from the medium for use in subsequent rounds of panning. Importantly, the phage from a particular panning round or screen could be stored indefinitely at -80°C.

In subsequent rounds of panning, different methods of presentation were used to vary the background exposed to the phage library. In the first round, streptavidin-containing wells were used, but neutravidin-coated surfaces, and streptavidin-coated magnetic beads were also used in later rounds. The theory was that varying the method of presentation would reduce the likelihood of obtaining so-called 'background-binders'; that is, Affimers that adhere to a component of the plastic, the blocking reagent, or to the streptavidin.

2.2.3. Competitive selection

Competitive selection is typically employed to ensure that a set of Affimers *do not* bind to a particular protein, for instance, to a homologue of the target. By adding the unbiotinylated homologue *in excess* into the solution containing the target and the phage, any phage binding to regions of shared homology should preferentially bind the homologue in solution, and could therefore be removed from the screen.

A similar strategy could also be employed to remove low affinity Affimers from a screen. Here, unbiotinylated target protein is added in excess into the solution containing the bound phage. High affinity interactions typically have very slow dissociation rates. It was postulated, therefore, that the highest affinity binders would remain associated to the surface-bound target, while weaker-binding phage would dissociate and rebind to the unbiotinylated protein in solution (Figure 2.11).

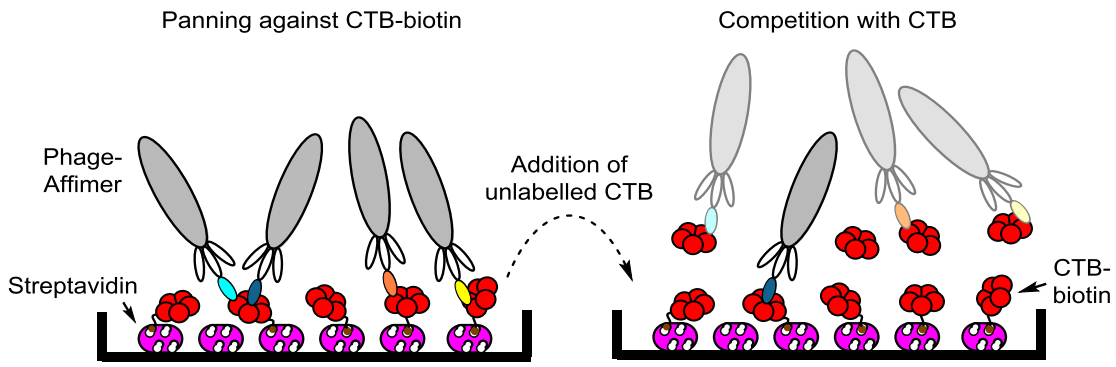

Figure 2.11. The process of competitive selection. During the panning round, soluble unbiotinylated CTB is added into the well as a competitor to the immobilised CTB-biotin. Phage-Affimers that dissociate from the CTB-biotin will bind the soluble CTB, leaving only the slowest dissociating Affimers behind for propagation.

Competitive selection was used to identify high affinity CTB-binding Affimers. The first two rounds of panning were carried out as described above. Phage prepared for long-term storage from the first and second panning rounds were designated the labels PR1 and PR2. In the third round, CTB-biotin was immobilised to a neutravidin-coated well. The phage from PR2 was then carried through for a third panning round (PR3). In PR3 the phage was incubated in the absence of target protein. The phage was then split equally between the CTB-containing well, and a blocked, but otherwise empty, control well. After a short incubation period, the solution was removed, and the wells were washed extensively to remove non-specifically bound material. Unmodified CTB was then added to both wells, at a concentration of 10 µM. This concentration was chosen arbitrarily, but was assumed to represent an excess compared to the surface-bound CTB-biotin. The CTB solution was left overnight, before removal and elution of the phage, as described previously.

The eluted phage from the wells, both from the control well and the CTB-biotin-positive well, was transferred to separate cultures of *E. coli* ER2738 cells, and plated out onto agar-ampicillin plates. However, as an initial measure of phage enrichment against the target, the cultures were spread over several plates, spanning a range of volumes increasing ten-fold from 0.1 - 100 µl. The final plates were prepared as before, with the remaining cells resuspended following centrifugation, and plated out for preparation of the phage. The following day, the number of colonies between the control plates and CTB-biotin plates were compared. A clear enrichment was observed, with 50 colonies present on CTB-biotin plates for every single colony observed on the negative control plates (data not shown). This enrichment suggests that the phage-Affimer library had been successfully enriched against the protein target, and therefore should contain selective and specific CTB-biotin-binding Affimers.

2.2.4. Detection of phage through an enzyme-linked immunosorbent assay

An enzyme-linked immunosorbent assay (ELISA) was employed to screen for the binding of the isolated phage-Affimer particles to CTB. Single colonies were picked from the plates, and cultured to prepare phage. In the previous step, the eluted phage were added to a large excess of ER2738 cells meaning that the chance of having multiple phage-Affimer particles infecting the same bacterium was unlikely. It was therefore reasonable to assume that each single colony harboured the DNA of a single Affimer sequence and would produce a homogenous population of phage-Affimer particles. Phage production was stimulated by addition of M13 helper phage leading to formation of infectious recombinant bacteriophage that were isolated from bacteria by centrifugation, leaving behind a supernatant containing phage-Affimer particles for direct use in the ELISA.

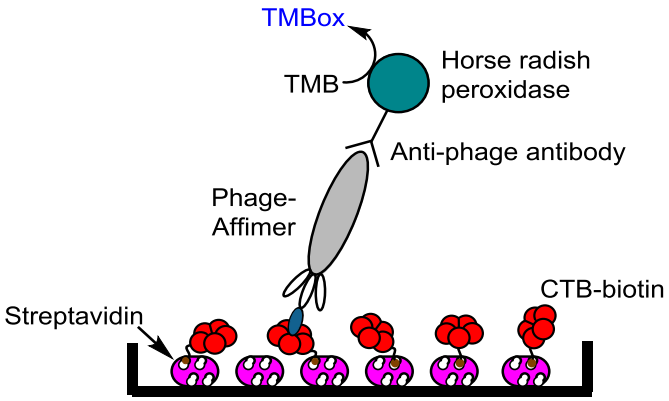

Figure 2.12. A phage ELISA for detection of phage-Affimers. Unique phage-Affimer populations are tested against CTB-biotin bound to streptavidin-coated wells. The wells are then washed extensively. Surface-bound phage remaining are detected through the use of an anti-phage antibody horse radish peroxidase conjugate. A solution of tetramethyl benzidine (TMB) and hydrogen peroxide are added, producing a blue product, tetramethyl benzidine diimine (TMBox), in the presence of the peroxidase that can be detected at 620 nm using a plate reader.

Figure 2.12 shows a cartoon representation of how an ELISA was set up to gain preliminary information on the binding of phage-Affimer particles to a target. Clear plastic plates coated with streptavidin were used to bind the biotinylated target onto the surface. Supernatant containing phage-Affimer particles were then added to wells harbouring the target, and wells that serve as negative controls with no immobilised target. The wells were washed extensively to remove any weakly associated material, and an anti-phage antibody (anti-Fd-bacteriophage) conjugated to horse radish peroxidase (HRP) was added to bind to any remaining bound phage. The plate was washed again, and the presence of a peroxidase was detected through addition of tetramethyl-benzidine (TMB) and hydrogen peroxide. The peroxidase catalyses the oxidation of TMB to tetramethylbenzidine diimine (TMBox), a coloured product, in the presence of hydrogen

peroxide (Figure 2.13). The coloured product absorbs at 620 nm, and was thus detected through use of a spectrophotometer.

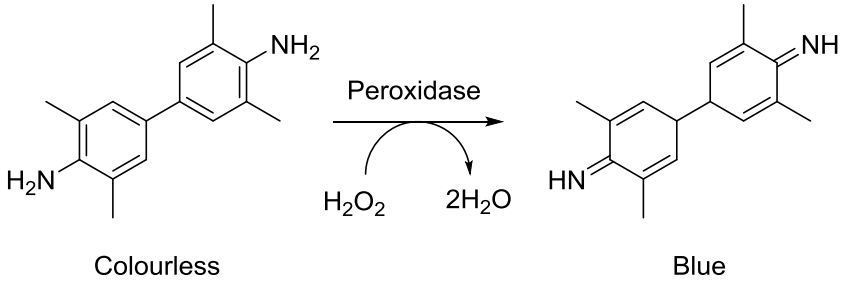

Figure 2.13. The conversion of the colourless tetramethyl benzidine to the blue tetramethyl benzidine diimine in the presence of hydrogen peroxide and a peroxidase.

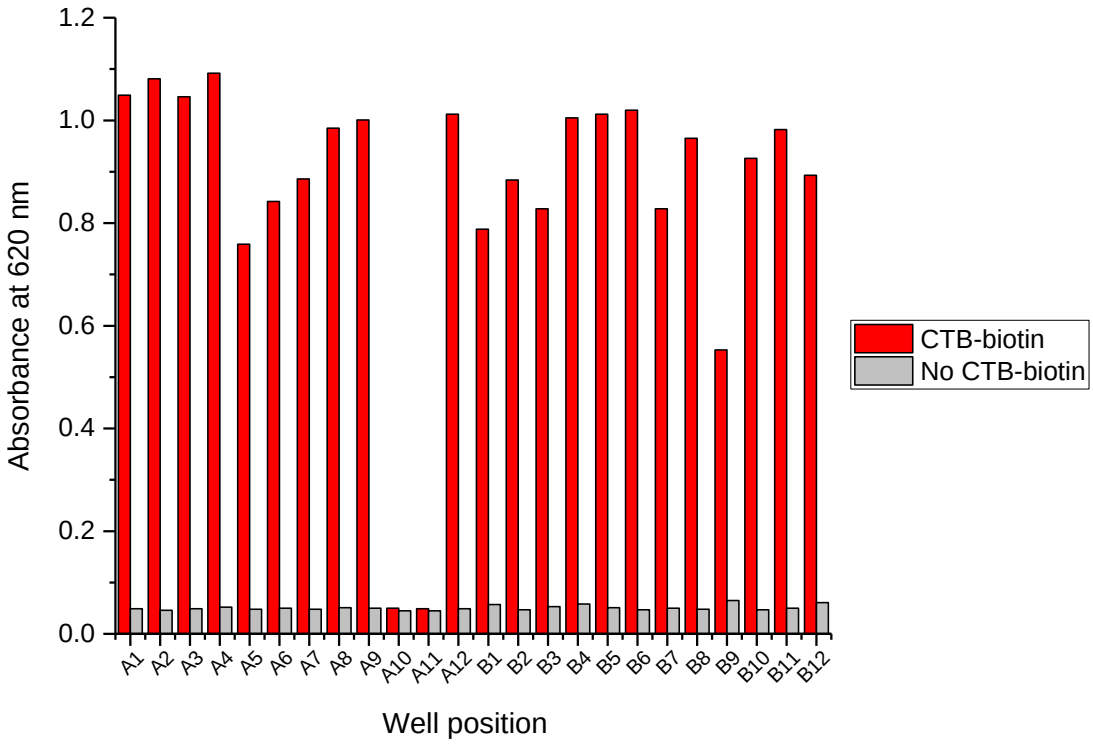

Figure 2.14. Analysis by phage ELISA of Affimers isolated following panning against CTB-biotin. A single species of Affimer is tested against either CTB-biotin bound to streptavidin, or streptavidin alone. In the advent of a binding event, a chromophore is produced resulting in an increase in absorbance at 620 nm. This change in absorbance is plotted in a bar chart against the well position of the tested Affimer to facilitate identification. 24 Affimers were tested, with 22 producing a large increase in the absorbance in the presence of CTB-biotin, and two (A10 and A11) producing no increase in absorbance.

The data are represented as a bar chart in Figure 2.14. The supernatant from 22 out of the 24 wells gave a positive result, demonstrating that all but two (A10 and A11) of the isolated phage bind selectively to CTB-biotin. The screen appeared to have been successful, and the DNA of the binding phage was therefore sequenced.

Sequencing of the Affimer coding sequence returned two unique pairs of Affimer variable loops from the 22 isolated, as shown in Table 2.1. The full Affimer primary sequence can be found in the

7.2.3. Affimer protein sequences.

Affimer	Variable loop 1								Variable loop 2									Seq rep
1A1	P	V	G	V	Q	M	N	K	K	N	K	L	L	S	Y	F	M	x19
1A2	V	P	N	G	P	I	W	V	P	K	Y	F	Q	M	Y	R	R	x3

Table 2.1. The primary sequence of the two Affimers isolated from the competitive selection screen. Amino acids are colour-coded according to their side chain (see appendix). Affimer 1A1 was represented 19 times out of the 22 sequenced Affimers, whilst 1A1 comprised three out of the 22. No conserved sequence was observed.

The majority (19/22) of the Affimers analysed were composed of the variable loop primary sequence assigned ‘1A1’, whilst the remaining three shared the other common sequence, assigned ‘1A2’. Comparing 1A1 and 1A2 reveals no significant similarities, except for the lack of acidic residues in either Affimer, and the presence of the -YF- amino acid pair in the second variable loop, although the position of the pair in the loop is different.

The lack of diversity of the pool of sequenced Affimers was unsurprising, since the stringent process of competitive selection was expected to remove all but the highest affinity binding proteins. With the data from the phage ELISA, and the sequencing revealing a reduced diversity of Affimers, it was concluded that the phage display screen had been successful, and that two high affinity CTB-binding Affimers had been isolated. The next step in the process was to validate the results of the phage ELISA, and to characterise the Affimers 1A1 and 1A2.

2.2.5. Validating the binding of 1A1 and 1A2 to CTB

Two unique Affimers had been identified from the competitive selection process. This small number of proteins allowed the low-throughput and material consuming, but information-rich technique of isothermal titration calorimetry (ITC) to be employed. However, due to its sensitivity, this technique would also require purified protein. The pBSTG plasmid was suitable for phage display and DNA production, but not suited for large-scale protein expression due to the lack of T7 promoter, and high copy number origin of replication that would have resulted in poor protein yields. In the context of

phage display, this poor yield is insignificant, since only a single unique phage-Affimer particle is required for representation in the library.

The Affimer coding sequences were subcloned using the high throughput method of ligation-independent cloning from the pBSTG plasmid into pET28a, a destination vector designed for protein expression. The subcloned DNA was transformed into BL21-Gold DE3 cells, which were used to inoculate medium for the expression of the Affimer proteins. BL21-Gold DE3 cells allowed for high quality plasmid DNA to be recovered, as well as carrying a gene coding for the T7 RNA polymerase, a prerequisite for expression using pET vectors. Using the pET28a plasmid additionally allowed the Affimers to be subcloned with a C-terminal hexahistidine tag, thus allowing purification with Ni-NTA agarose, a nickel-charged affinity resin. Protein eluted from the resin was analysed by SDS-PAGE to confirm successful expression and purity (Figure 2.15).

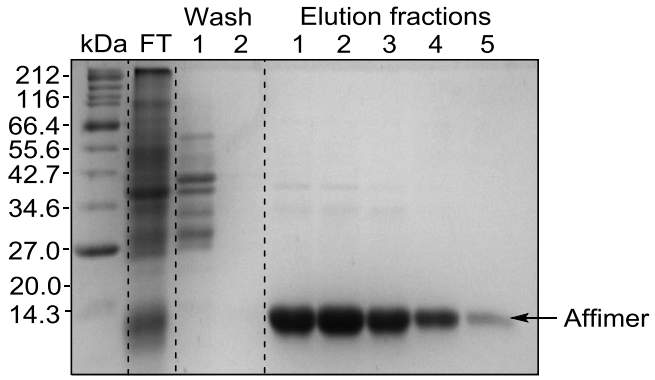

Figure 2.15. SDS-PAGE analysis of fractions collected from the purification of Affimer 1A1 by nickel affinity chromatography. A crude protein-containing solution is applied to the column, and the flow through (FT) is collected. Analysis shows a range of proteins of varying sizes comprising the FT. Two wash steps are carried out using a low concentration of imidazole (20 mM) to remove non-specifically bound material. Finally, a high concentration of imidazole (300 mM) is applied to displace proteins containing multiple consecutive histidine residues. A single band of protein corresponding to the purified Affimer can be seen (marked with arrow, ~14 kDa).

Unbound material was analysed in lane labelled FT with the subsequent two lanes containing non-specifically bound protein eluted with a moderate concentration of imidazole (50 mM). The last five lanes contain material eluted under high imidazole concentration (300 mM). The presence of a single dense band at approximately 14 kDa indicated successful Affimer expression and purification.

2.2.5.1. Isothermal titration calorimetry (ITC)

ITC is a biophysical technique used to quantify the binding affinity of a molecular interaction by measuring the heat change upon mixing two interacting species. An

introduction to how the technique works can be found in *6.6.1. Isothermal Titration Calorimetry*. Purified Affimers 1A1, 1A2, and CTB were dialysed extensively against a phosphate buffer to ensure that there was no buffer mismatch. CTB (120 µM pentamer concentration) was titrated into either 1A1 or 1A2 (12 µM). A ten-fold excess in concentration of titrated protein is usually required to saturate available protein binding sites in the cell. It was assumed that only one Affimer would bind per pentamer of CTB, provided the Affimer bound to the top face, since steric hindrance would prevent multiple binding proteins from associating. However, no binding was observed for either Affimer (Figure 2.16).

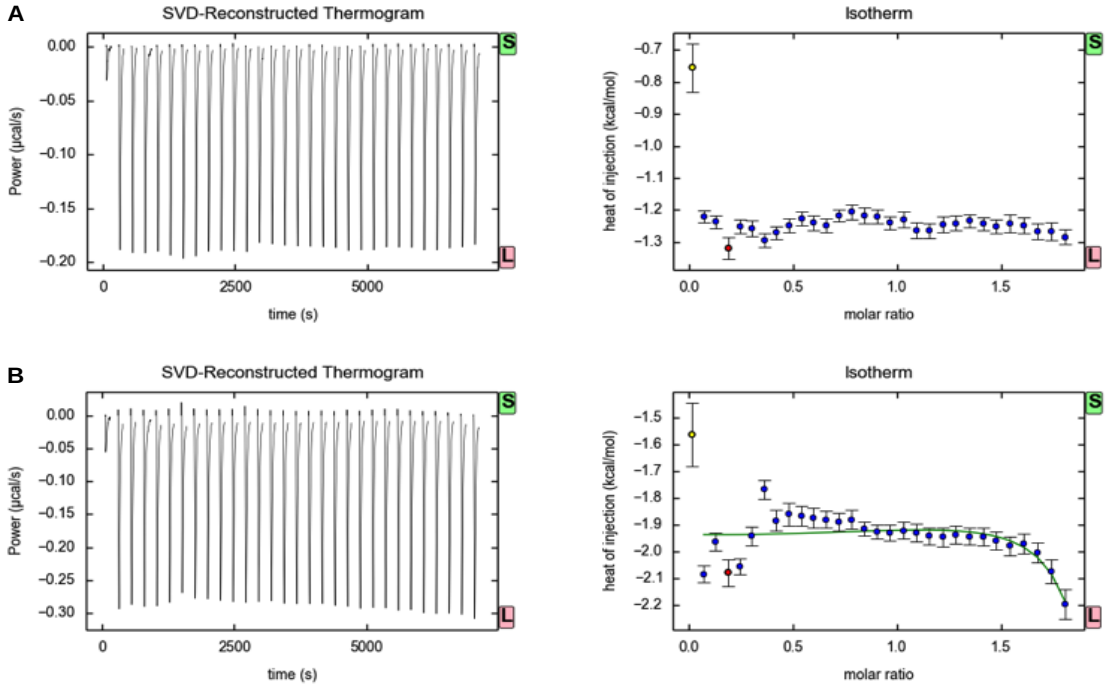

Figure 2.16. Analysis of the interaction between CTB and Affimers 1A1 **(A)** and 1A2 **(B)** by ITC. Titrating Affimer into CTB across 30 injections produced no change in peak size, indicating that no specific binding interaction was taking place. The change in power observed for each injection is caused by the heat of dilution of the titrant. The area of the peaks from the thermogram can be integrated to produce an isotherm (right).

By integrating the value of each peak, a binding isotherm can be generated. In this particular case, the isotherm produced a flat line, thus indicating that there was no observable interaction. The discrepancy between the ITC data and the data obtained from the phage ELISA was surprising. Since ITC is considered the gold standard in measuring affinity of interactions, it was concluded that neither Affimer recognised CTB in any capacity.

Screening against CTB-biotin, and using the unbiotinylated protein as a competitor could have resulted in all CTB-binding Affimers being ‘stripped’ from the screen, leaving only Affimers that recognised the biotin linker, or the protein and linker together. It was decided that competitive selection was not a practical approach to use in identifying CTB-binding Affimers, and that the screen should be repeated without adding competitor protein.

2.2.6. Screening against an unmodified target

To achieve this, the phage stored from the second panning round of the previous screen were used in a third round of panning (PR3b) against CTB-biotin immobilised to neutravidin-coated wells (Figure 2.17). No competitor protein was added in this round, but the remainder of the procedure was carried out as described earlier.

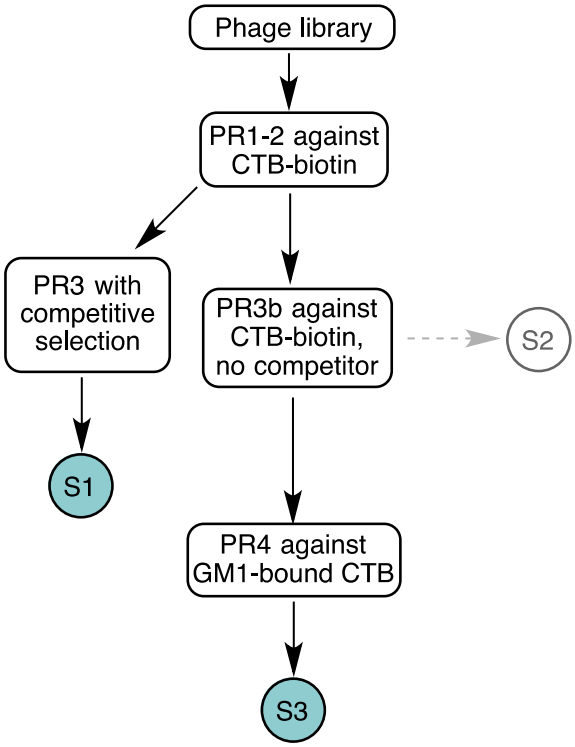

Figure 2.17. Flow diagram explaining the phage display screens carried out against CTB. The naïve phage library was presented to CTB-biotin in two sequential panning rounds (PR1 and PR2). In the first screen (S1), the phage from PR2 were carried forward and incubated with CTB-biotin in the presence of a soluble CTB competitor. In PR3b the phage from PR1 and PR2 were incubated with CTB-biotin in the absence of a competitor. Affimers identified from PR3b were sequenced, but not further characterised (S2), and not discussed in this report. Phage from PR3b were subjected to a fourth panning round (PR4) and incubated with GM1-bound CTB. The phage identified from PR4 thus made up screen 3 (S3). Affimer names quoted in this report start with the screen number from which they were identified in, and finish with the code for the well (from a 96 well plate) they were detected in by phage ELISA. Affimer 3C6, for instance, was identified in screen 3, and was detected by phage ELISA in well C6.

When immobilised to the plastic surface, CTB-biotin probably does not have all five of its biotin moieties coordinated by the adsorbed streptavidin. Streptavidin has four potential biotin binding sites, although two of these would be masked on adsorption to the polystyrene wells, as the binding sites of the tetramer lie on opposite faces.[219,220] Additionally, the biotin binding sites are ~2 nm apart on the same face,[219] compared to the 2.6 nm distance between the N-termini of CTB;[148] thus, one streptavidin tetramer is likely to coordinate only one biotin of CTB-biotin, although the 2.7 nm linker may provide some scope for binding of a second biotin moiety.

Given the possibility that a streptavidin tetramer may only be binding a single biotin on CTB-biotin, the top face of CTB may not be exposed exclusively. Indeed, the length of the linker could allow the bottom face to be fully presented in some cases. It was therefore decided to include a fourth round of phage panning against wild-type CTB bound to GM1. As discussed previously, CTB has a high affinity for GM1 oligosaccharide (K_d = 40 nM).[146] If GM1 could be presented on the surface of a well, then CTB could be immobilised to the well surface without the need for a biotinylation step or a streptavidin-coated plate. Furthermore, immobilisation of CTB in this manner would present the top face of CTB to the phage library, whilst occluding the GM1-binding face (Figure 2.18).

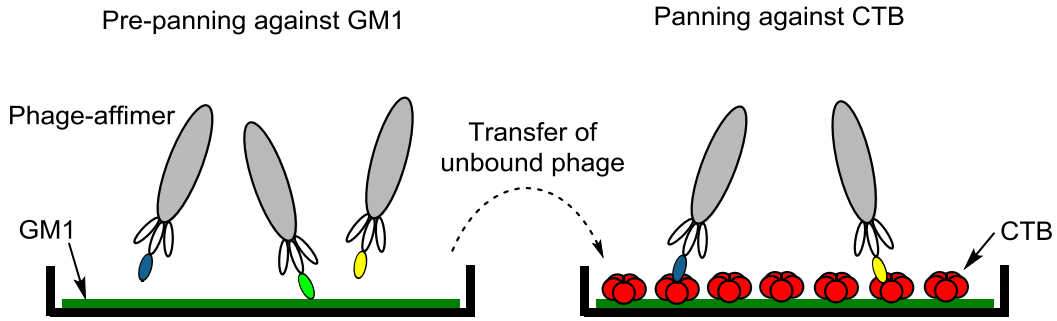

Figure 2.18. Modified phage display against wild-type CTB immobilised to GM1. Wells coated with GM1 ganglioside are presented to the phage library to pull out non-specific binders. Unbound phage are then transferred and panned against wells containing CTB bound to GM1.

A method exists, as outlined by Svennerholm and Holmgren,[221] to adsorb the greasy hydrocarbon chain of GM1 to a polystyrene surface, thus presenting the carbohydrate moiety for CTB binding. A modified version of this protocol was used, in which GM1 dissolved in methanol was transferred onto treated polystyrene plates.[149] Plates were then blocked to occupy any remaining sites for adsorption, after which CTB was immobilised simply by addition of the protein to the well, and following a short incubation, the wells were washed to remove unbound protein. 50 pmol CTB was added to GM1-coated wells, and the fourth and final panning round was carried out (PR4), with the phage from PR3b prepanned against wells containing only GM1. Half the phage was

transferred from the final prepanning well to a well containing simply GM1 to serve as a negative control, with the other half added to a well containing CTB bound to GM1. At this stage, it was expected that any phage recognising CTB-biotin specifically, or its GM1-binding face, would not be taken forward and would simply be discarded during the wash step. Phage from both the negative control and the CTB-containing well were eluted and used to infect ER2738 cells. Approximately 100-fold fewer colonies were observed on agar streaked with the negative control-infected ER2738 cells compared to those infected with phage exposed to CTB, indicating that the library had been enriched significantly with Affimers that bound to CTB.

2.2.7. Investigating binding to CTB by phage ELISA

48 colonies were selected from the plates to assess their binding by phage ELISA. Since the final panning round had been carried out against unmodified CTB, the ELISA was modified to test the binding of phage-Affimer particles to GM1-bound CTB. At least six of the phage tested appeared to display binding in the absence of CTB (A4, A10, B8, C11, D5 and D8) (Figure 2.19).

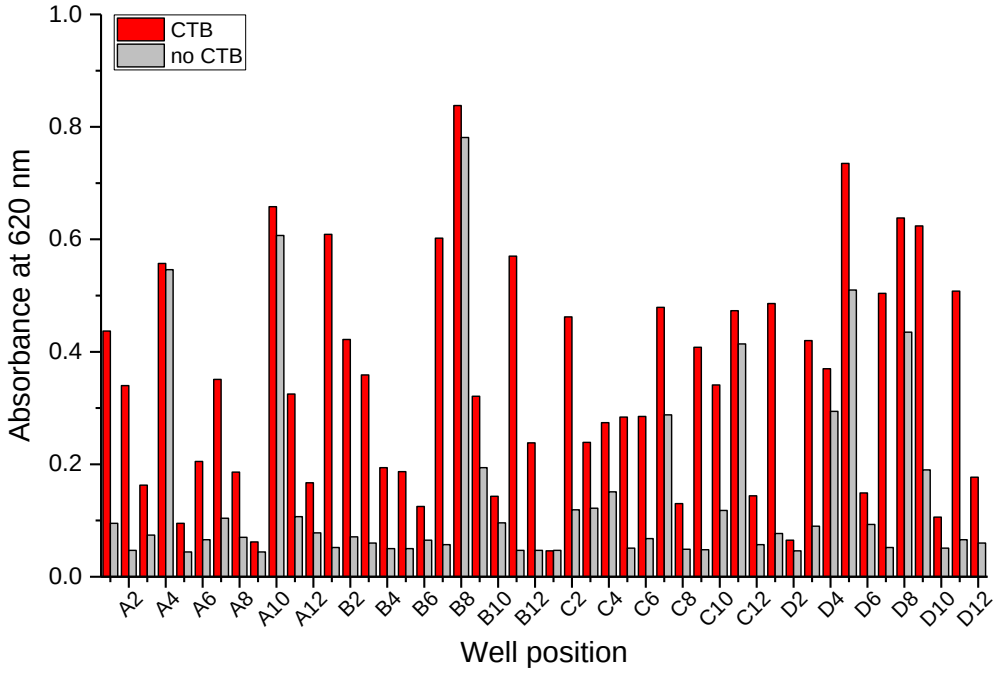

Figure 2.19. Analysis by phage ELISA of 48 Affimers isolated following panning against wild-type CTB (screen 3). A single species of Affimer is tested against either CTB bound to GM1 (red bars), or GM1 alone (grey bars). Absorbance at 620 nm is plotted in a bar chart against the well position of the tested Affimer to facilitate identification.

Identification of six CTB non-selective phage-Affimers suggested that the library of phage had perhaps not been enriched as significantly as initially thought. However, most of the phage clearly demonstrated selectivity for GM1-bound CTB. In order to reduce the number of phage to a manageable number for sequencing, any phage giving an absorbance signal in CTB-coated wells less than 0.25 absorbance units (AU_{620}) were discarded. Similarly, any phage giving an AU_{620} greater than 0.2 in the negative (Figure 2.20).

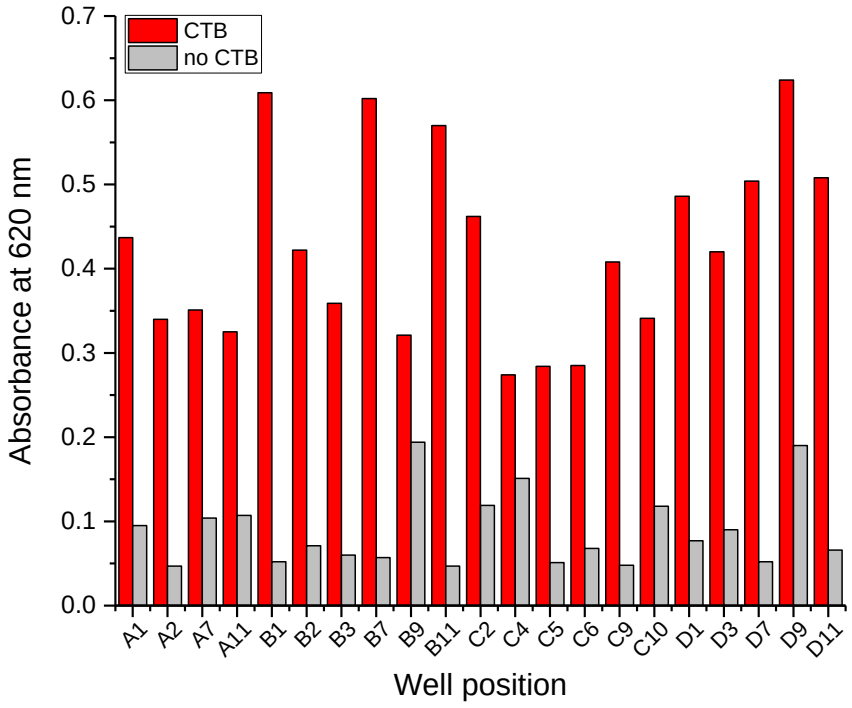

Figure 2.20. Application of two thresholds to the 48 selected phage from screen 3 to remove non-selective binders. Results of the phage ELISA (Figure 2.19) following removal of Affimers producing a change in absorbance in the absence of CTB greater than 0.2 absorbance units, and removal of Affimers producing a change in absorbance of less than 0.25 absorbance units.

Sequencing these 21 plasmids indicated that 20 unique Affimers had been isolated (*7.2.3.3. Sequence of binding loops of Affimers from Screen 3*), with little sequence homology observed between the variable loops, although 23% of the amino acids in the second loop were aromatic. The sequencing data seemed to indicate that the phage library following four rounds of panning was still very diverse, with only one of the Affimer sequences being detected twice. Reflecting on the way that the phage display was carried out, it is possible that the concentration of target protein, both CTB-biotin and CTB, were too high in each panning round, and thus introduced low stringency. Too high a concentration would result in a large amount of target being immobilised, which would

reduce competition for binding. The result would be a more diverse library with a larger representation of weaker binders that would have otherwise been competed out of the library in a more stringent screen.

Thinking back to the project objectives, the desired goal was to identify a CTB-binding Affimer that could be taken into motor neurones, and reach different compartments, and therefore targets, once inside the cell. A mechanism for the Affimer to release CTB once endocytosed would give more of a free range of the cell, since CTB would remain tightly associated to the plasma membrane. A high affinity Affimer would thus remain tightly associated to the CTB, and by extension, the plasma membrane. A lower affinity interaction would not necessarily be undesirable, since it could provide a simple route to dissociation from CTB once inside the neurone. The challenge would be striking the balance between association of the Affimer with CTB sufficiently long to be internalised into a cell, versus its dissociation from CTB once inside. A more diverse pool of Affimers with a range of affinities and dissociation rates could be advantageous.

2.3. Separating the Wheat from the Chaff

Using phage display to identify CTB-binding Affimers had resulted in the isolation of 20 unique binding proteins. Unlike the competitive selection screen, the four non-competitive panning rounds had yielded a much more diverse library of phage-Affimers. As such, a higher throughput method than ITC had to be established to assess their binding to CTB.

2.3.1. Developing a pulldown assay to validate binding

A pull-down experiment was designed to validate the results of the phage ELISA. Figure 2.21 shows a cartoon representation of this experiment, in which CTB-biotin would be immobilised to streptavidin-coated resin. A solution of purified Affimer would then be added to the resin, allowed to bind, and then washed to remove unbound protein. Bound protein would be removed from the resin using a strongly acidic eluent, and the eluate could then be analysed by SDS-PAGE to validate the Affimer-CTB interaction. To test this experiment, an Affimer was selected at random from the pool of 20.

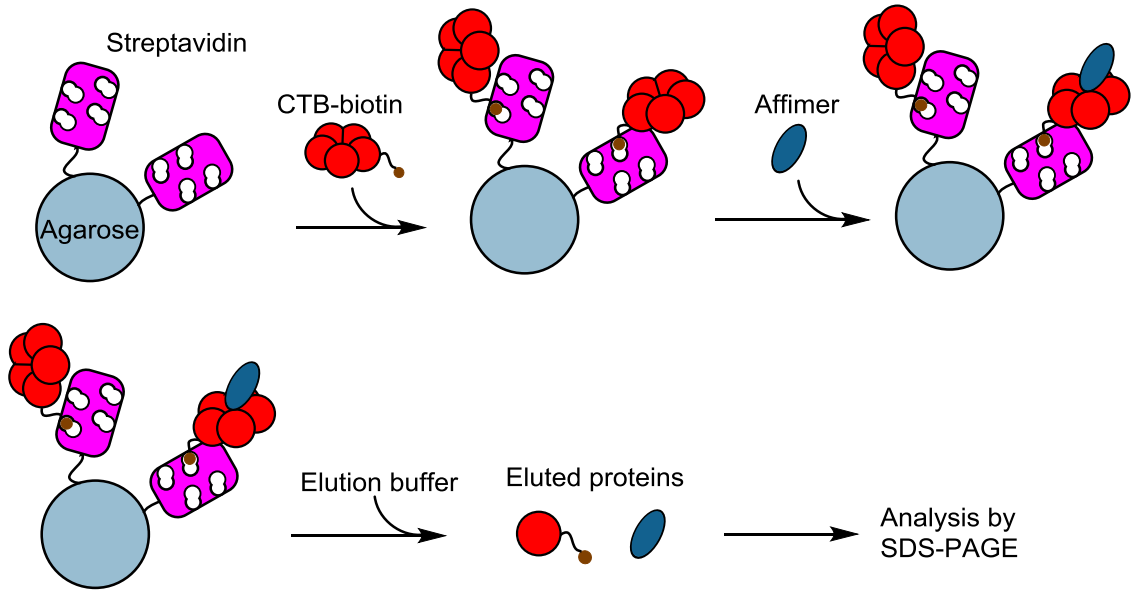

Figure 2.21. Approach to demonstrate Affimers binding to CTB using a streptavidin pulldown assay. CTB-biotin is captured on streptavidin-coated agarose prior to addition of the Affimer. After washing the agarose, a strongly acidic buffer is added to disrupt the biotin-streptavidin interaction, releasing the CTB and any bound Affimer. Strong acid also causes the CTB pentamer to dissociate into monomers. The eluted proteins are then analysed by SDS-PAGE.

The Affimer-gIII truncated gene contains an amber stop codon, TAG, separating the Affimer coding sequence from the start of the truncated gIII gene. The strain of ER2738 *E. coli* cells used in for Affimer phage display introduces a glutamine instead of terminating the amino acid sequence (Figure 2.22). Expression from the pBSTG plasmid results in the production of a hexahistidine tag at the C-terminus of the Affimer. It is therefore possible to produce protein using a non-suppressing strain of bacteria, albeit in small quantities, as the plasmid lacks a strong transcriptional promoter. The DsbA signal sequence targets the Affimer to the periplasm, necessitating a periplasmic extraction to purify the protein.

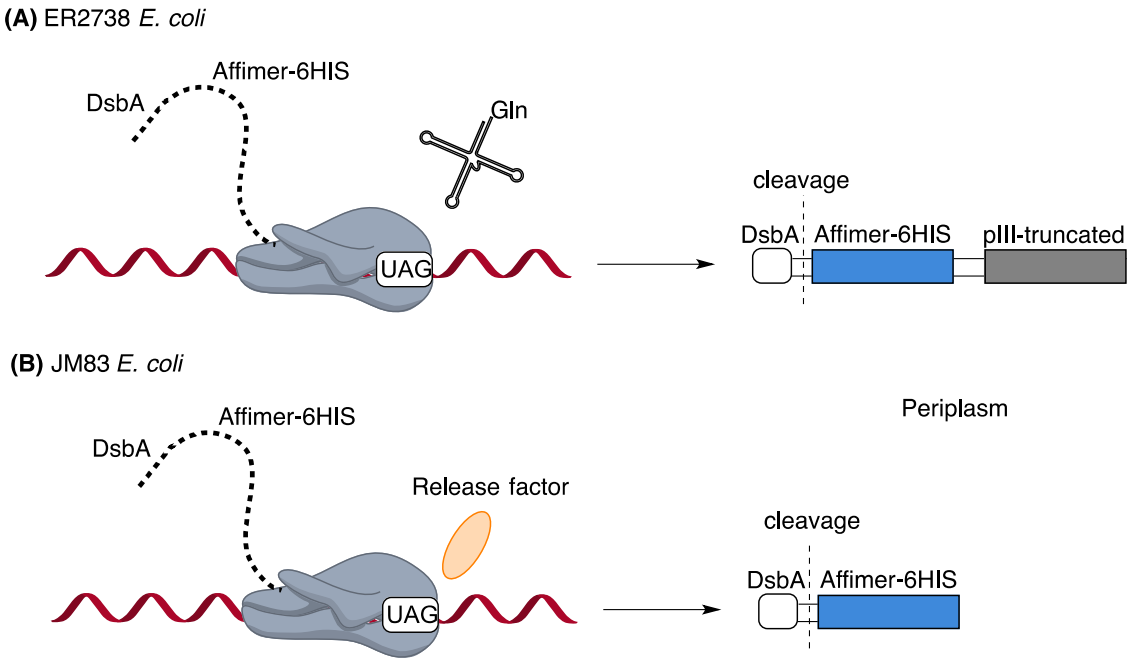

Figure 2.22. (A) Expression of Affimer-pIII fusion protein in the amber-codon suppressing ER2738 *E. coli*. The amber UAG codon separating the Affimer-hexahistidine (Affimer-6HIS) coding RNA sequence is recognised by a tRNA that incorporates Gln, resulting in read-through of the RNA sequence, and production of an Affimer-6HIS-pIII fusion protein. The DsbA signal sequence results in transport of the nascent polypeptide chain to the periplasm, where the signal sequence is cleaved. **(B)** Expression of Affimer protein in non-amber suppressing JM83 *E. coli*. Translation is terminated following binding of release factors to UAG stop codon. The polypeptide is trafficked to the periplasm, where the DsbA sequence is cleaved.

Affimer 3C9 was extracted by sucrose shock from the periplasm of transformed and induced *E. coli* cells (JM83) (*6.4.6. Periplasmic Extraction of Proteins Using Sucrose Shock*). The Affimer was then purified by Ni-NTA affinity chromatography. CTB-biotin was then immobilised to streptavidin resin, and the newly purified protein was added to streptavidin beads treated either with CTB-biotin, or buffer, to serve as a control. The flow through was collected, as were the five subsequent washes, for analysis alongside the eluate. These fractions were analysed by SDS-PAGE as shown in Figure 2.23. 3C9 was detected in the flow through and the first wash fractions for both the CTB-biotin-treated streptavidin and the control, after which no additional protein was observed. 3C9 was also detected following elution of CTB-biotin from the streptavidin beads, but not in the absence of CTB-biotin. It was surmised therefore that Affimer 3C9 does indeed bind to biotinylated CTB. This observation is perhaps not surprising, since the first three panning rounds of this screen were carried out against CTB-biotin.

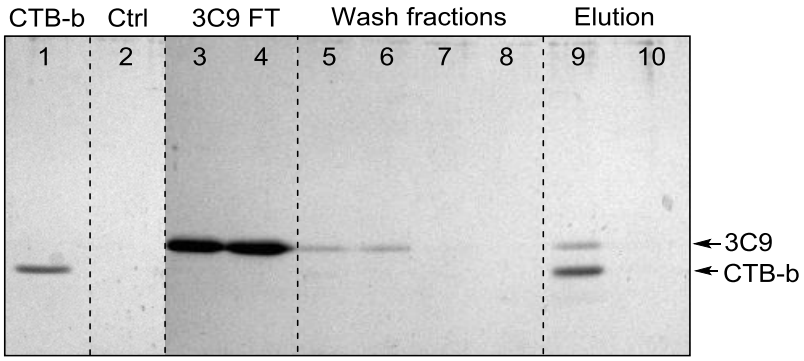

Figure 2.23. SDS-PAGE analysis of a 3C9-CTB-biotin streptavidin pulldown assay. Flow through (FT) of CTB-biotin or buffer were analysed in lanes CTB-b and Ctrl respectively (lanes 1 and 2). Fractions following application of 3C9 (3C9 FT, lanes 3 and 4), wash buffer (wash fractions, lanes 5 - 8) and elution buffer (elution, lanes 9 and 10) were also analysed.

A complementary pull-down strategy was implemented to evaluate binding of the Affimers to unmodified CTB. In this case the polyhistidine tag on the Affimer would be used to immobilise the Affimer on Ni-NTA resin to provide a solid-phase receptor for CTB. However, El Tor CTB has an endogenous ability to bind to nickel affinity resin, due to a surface exposed residue, H13 (Figure 2.24). This residue would need to be mutated to prevent direct binding to Ni-NTA resin.

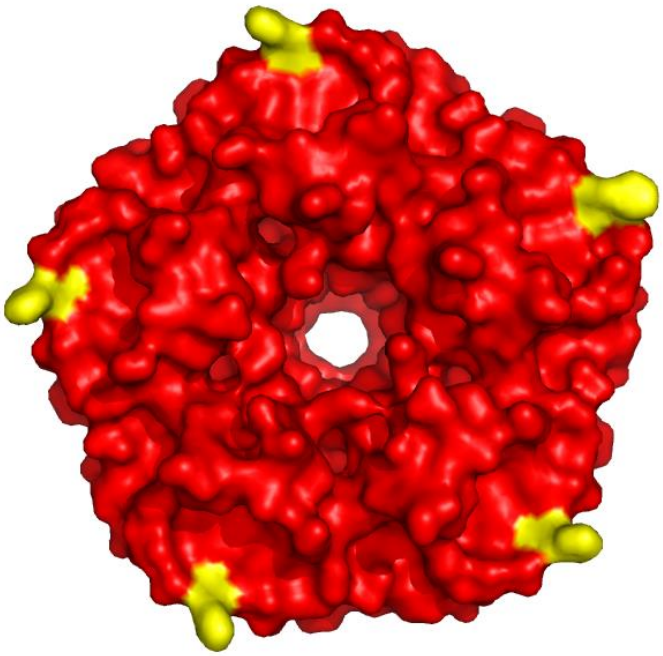

Figure 2.24. A surface representation of the crystal structure of CTB (3CHB), with histidine residue 13 shown in yellow.

A variant of *E. coli* heat labile enterotoxin B5 subunit isolated from a porcine host shares 82% sequence identity with CTB, but carries an arginine residue at position 13 (*7.2.1. CTB/LTB protein sequences*). An H13R CTB variant could therefore be produced for use in a Ni-NTA-based pulldown assay (Figure 2.25).

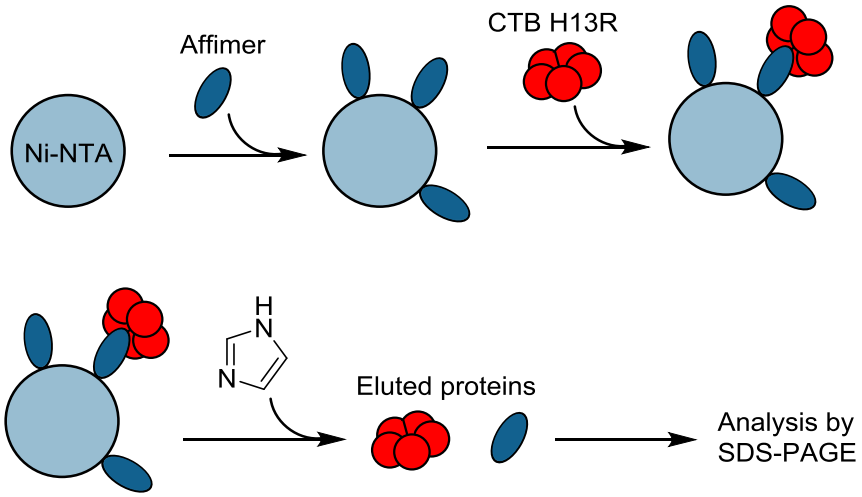

Figure 2.25. Approach to demonstrate that Affimers bind to unbiotinylated CTB. Affimers are complexed to Ni-NTA agarose through a histidine tag. CTB H13R is added to the complexed Affimer, and washed with a low concentration of imidazole to remove weakly associated material. Complexed proteins are then eluted using a high concentration of imidazole, which can then be analysed by SDS-PAGE.

Site-directed mutagenesis was performed to introduce the H13R mutation on the pSAB2.2 plasmid (see

7.1.4. pSAB2.2 for sequence), a vector created in-house for the expression and manipulation of CTB DNA coding sequences in *E. coli*. The mutant was then expressed, and purified by lactose affinity chromatography (Figure 2.26), since its ability to bind nickel resin had been ablated by introduction of the mutation. CTB has a weak affinity for lactose, a disaccharide composed of galactose and glucose, since the terminal galactose residue of GM1 forms the majority of the interactions with the carbohydrate binding site of CTB.[222]

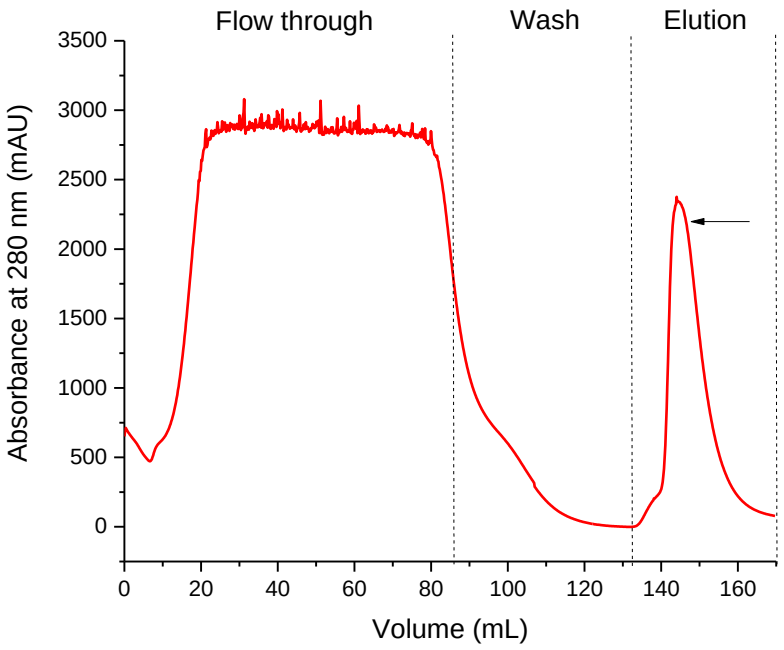

Figure 2.26. Purification of CTB H13R by lactose affinity chromatography. A concentrated solution of medium containing the protein in question is applied to a column containing lactose resin under flow. The flow through from the column is analysed by a detector, and the absorbance at 280 nm is plotted as a function of volume. The flow through can be observed as a flat line at ~3000 mAU, the saturation limit for the detector. Once the medium is applied, a wash step is introduced, and the absorbance decreases. Once at zero, an elution step begins, using a lactose-containing buffer to elute the bound lectin. The arrow denotes the peak corresponding to purified protein.

The pulldown experiment was carried out by binding Affimer 3C9 to nickel resin, followed by the H13R mutant. A negative control was also carried out, in which the H13R mutant was added to the nickel resin in the absence of 3C9. Fractions analysed by SDS-PAGE are presented in Figure 2.27.

Very little 3C9 can be detected in lane 1 – 4, indicating efficient binding of the Affimer to the nickel resin. The contrast in amount of H13R CTB detected in the flow through fractions of the resin treated with 3C9 (lane 5) compared to the negative control (lane 6) seemed to suggest that the mutated CTB was interacting with 3C9. When eluted (lane

9), both 3C9 and CTB can be detected, again appearing to confirm binding of 3C9 to CTB. Some H13R can be observed in the negative control elution (lane 10), although to a much lesser extent than the elution of 3C9 and CTB. Introducing the mutation may have knocked out the primary histidine involved in nickel-binding, but other surface exposed histidine residues, such as H94, provide CTB with additional capacity to bind nickel.

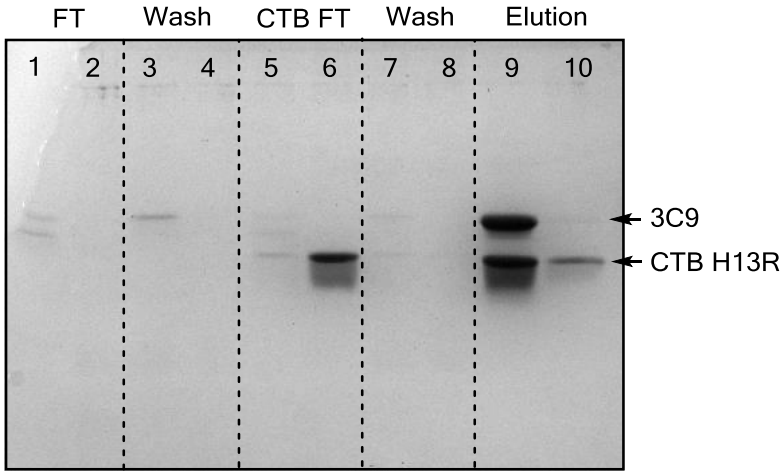

Figure 2.27. SDS-PAGE analysis of a Ni-NTA 3C9-CTB pulldown assay. Ni-NTA agarose was treated with 3C9 or buffer only, and the flow through from each was collected and analysed (lane 1 and lane 2 respectively). The treated agarose was then washed with 20 mM imidazole, and the flow through analysed (lanes 3 and 4). CTB was then applied to the agarose, and the flow through analysed (lanes 5 and 6). Subsequent washes were analysed in lanes 7 and 8. Finally, bound proteins were eluted with 300 mM imidazole, and analysed in lanes 9 and 10.

Confirming binding of Affimers to CTB via pulldown was not as high throughput as initially hoped, and is a qualitative technique, providing no route to rank the Affimers in terms of binding capacity. An alternative method was therefore considered.

2.3.2. Ranking the binders using an Affimer-lectin binding assay

A plate-based assay was developed to assess binding of Affimers to CTB. Drawing on inspiration from the phage ELISA, a plate-based assay was developed by detecting Affimers adhered to GM1-bound CTB. Since Affimer-recognising antibodies were not available, the Affimers were labelled with biotin to facilitate their detection using a streptavidin-HRP conjugate and TMB (Figure 2.28).

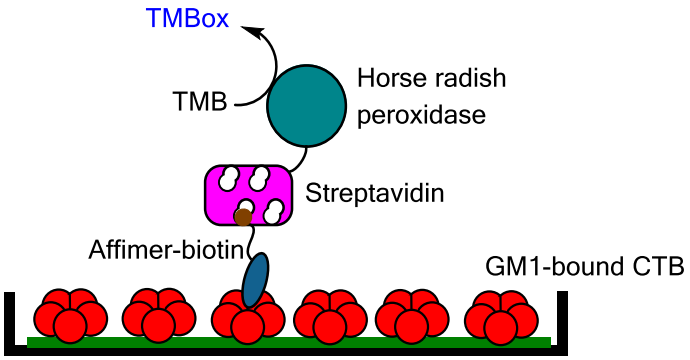

Figure 2.28. The setup for an Affimer-lectin binding assay. Biotinylated Affimer is tested against GM1-bound CTB. Bound Affimer is detected through the use of a streptavidin-horse radish peroxidase conjugate. A solution of TMB is added that is converted to a blue product (TMBox) in the event of binding.

The University of Leeds Bio-Screening Technology Group (BSTG) has previously developed a reliable strategy for expressing Affimers with a C-terminal residue. Since the primers provided by BSTG were not compatible with pET28a, all 20 Affimers were subcloned into pET11a to incorporate a cysteine at the Affimer C-terminus. The cysteine allowed modification of the Affimer with a biotin via reaction of a maleimide functional group with the cysteine thiol (biotin-PEG2-maleimide, Figure 2.30A). Crucially, the Affimer C-terminus is distal to the binding loops, and so the biotin would be presented facing away from the plate surface and would be accessible for binding to streptavidin-HRP.

Once subcloned successfully, the Affimers were expressed on a small scale, purified by nickel affinity chromatography, and analysed by SDS-PAGE (Figure 2.29, *7.2.2.4. Various figures*). The purified proteins were dialysed into a phosphate buffer containing TCEP for reaction with biotin-PEG2-maleimide. At this stage, three of the 20 Affimers appeared to aggregate (3A7, 3B7, 3C5), and would not stabilise at a high enough concentration for labelling. These three proteins were therefore not taken any further for characterisation.

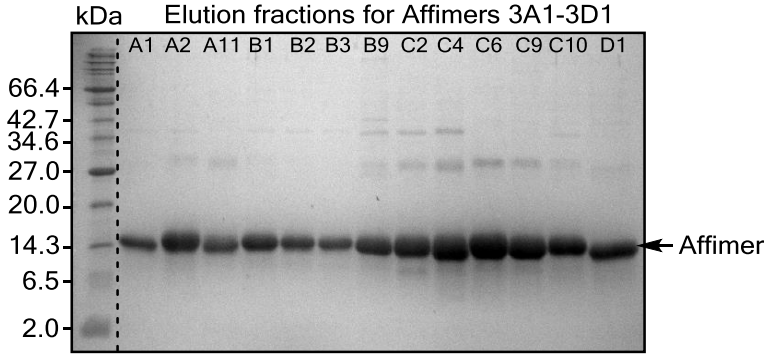

Figure 2.29. SDS-PAGE analysis of 13 Affimers identified from S3, purified by Ni-NTA chromatography (see *7.2.2.4. Various figures* for remaining four). Each Affimer migrates at approximately 14.3 kDa.

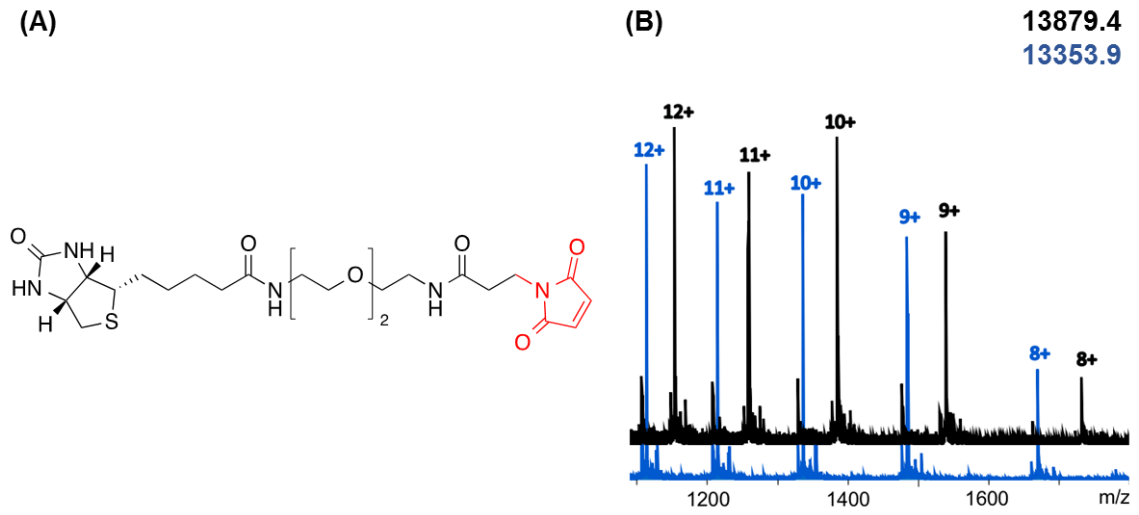

Figure 2.30. (A) Chemical structure of biotin-PEG2-maleimide. The maleimide functional group is shown in red. **(B)** Example mass spectrum of an Affimer (3C6) unmodified (blue) and biotinylated (black) to demonstrate successful protein modification. Calculated mass for 3C6 = 13355.01 Da, measured mass = 13353.9. Calculated mass for 3C6-biotin = 13880.24 Da, measured mass = 13879.4 Da.

The remaining 17 Affimers were labelled with biotin-PEG2-maleimide (Figure 2.30A). Labelling was verified by ESMS (Figure 2.30B). The biotinylated Affimers were then subjected to an Affimer-lectin binding assay (ALBA), in which Affimers were incubated with either GM1-bound CTB or GM1 alone.

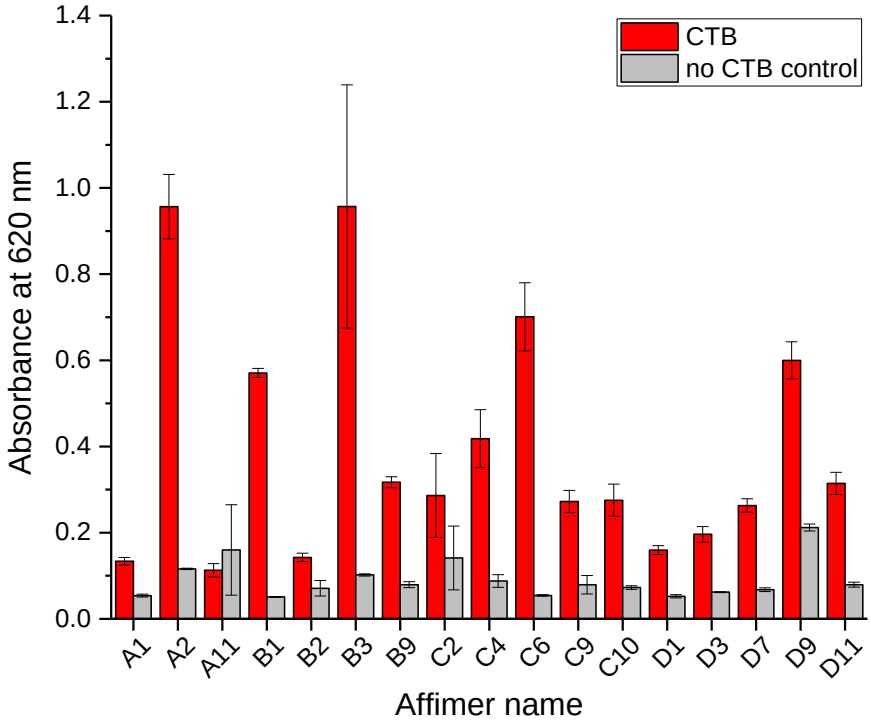

Figure 2.31. Analysis of CTB-binding Affimers from screen 3 using an Affimer-lectin binding assay. For each Affimer, the red bar represents the change in absorbance at 620 nm when Affimers were incubated with GM1-bound CTB, whilst the grey bar is the corresponding control experiment performed in the absence of CTB. Error bars represent the standard error of three technical replicates.

The assay provided a robust method to rank the binders in terms of their binding capability (Figure 2.31). Surprisingly, these data do not correlate with the data obtained from the phage ELISA (Figure 2.33). Several Affimers (3A1, 3A11, 3B2, 3D1 and 3D3) were detected very poorly by the ALBA, but seemed to perform well in the phage ELISA (Figure 2.32).

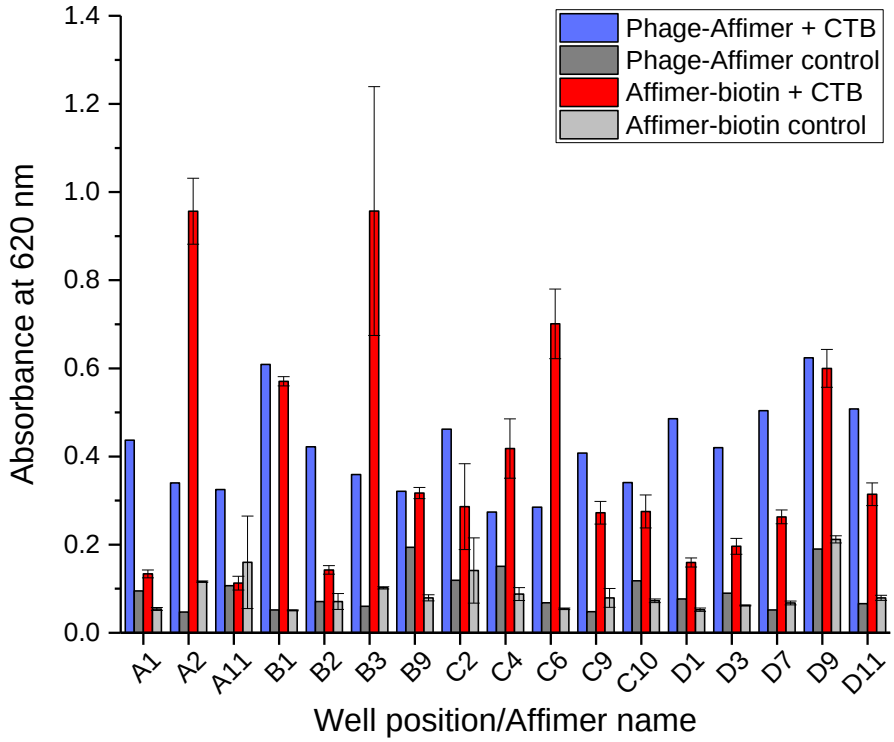

Figure 2.32. Comparison of data on Affimers obtained from screen 3 from the phage ELISA (blue and dark grey) and ALBA (red and light grey) experiments. Error bars show the standard error of three technical replicates for ALBA experiments.

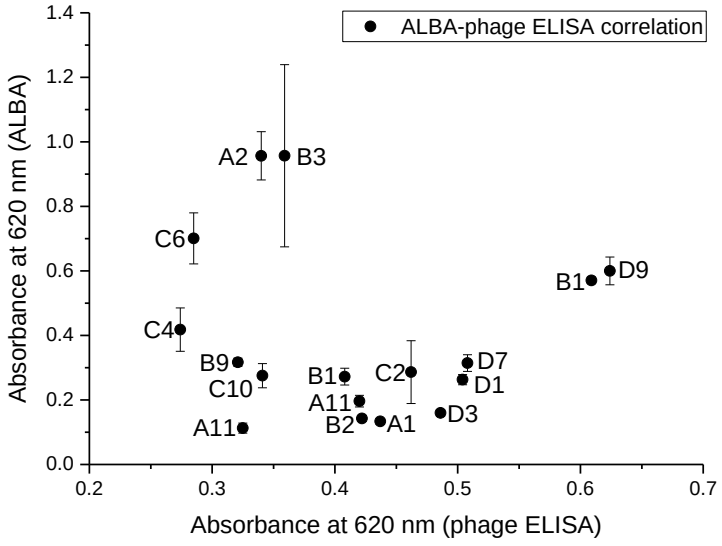

Figure 2.33. A linear correlation plot for phage ELISA and ALBA experiments. Absorbance at 620 nm for the ALBA (y-axis) is plotted against absorbance at 620 nm for the phage ELISA (x-axis) to generate a linear correlation plot. A lack of linearity indicates poor correlation between phage ELISA measurements and ALBA measurements for the same Affimers.

Despite the many similarities between these two assays, there are some important differences. One of the key drawbacks of using phage ELISA as a method for assessing binding is the unknown factor of concentration. Phage are prepared from a solution of bacteria, but the exact amount of phage that is produced is difficult to quantify. The OD of the phage-producing bacteria is assumed to be consistent across the different cultures, but there may be scope for variation, and the concentration is therefore likely to change across the different phage-Affimer populations. By contrast, the concentration of Affimer used for the ALBA is more easily quantified.

The HRP substrate TMB was exchanged for the more sensitive and stable substrate Amplex Red. Amplex Red is a reagent that is oxidised in the presence of peroxidase to the fluorescent product resorufin (Figure 2.34).

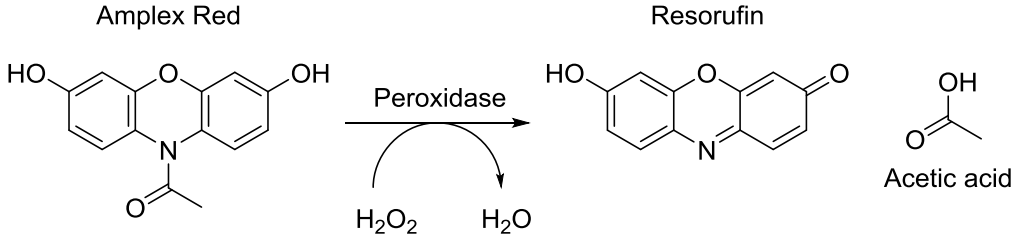

Figure 2.34. Conversion of Amplex Red to resorufin in the presence of a peroxidase enzyme and hydrogen peroxide.

To ensure that the assay was comparable between the two substrates, the assay was repeated with Amplex Red, and aligned, with the data presented in a bar chart in Figure 2.35. ALBAs using TMB and Amplex Red were compared in a linear correlation plot (Figure 2.36). The data points correlated in a linear fashion, indicating that the results obtained from either substrate were comparable.

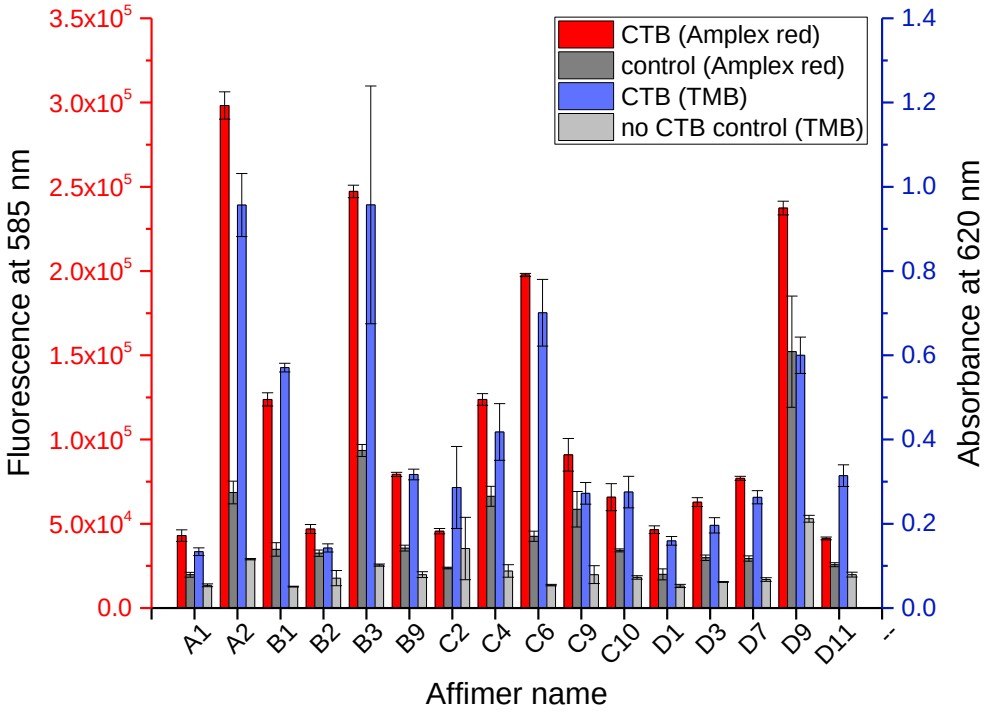

Figure 2.35. Comparison of data gathered from ALBA experiments using either TMB (blue) or Amplex Red (red) as peroxidase substrates. Data from the ALBA using Amplex Red is plotted on the left-hand y-axis (fluorescence at 585 nm), while data from the ALBA using TMB is plotted on the right-hand y-axis.

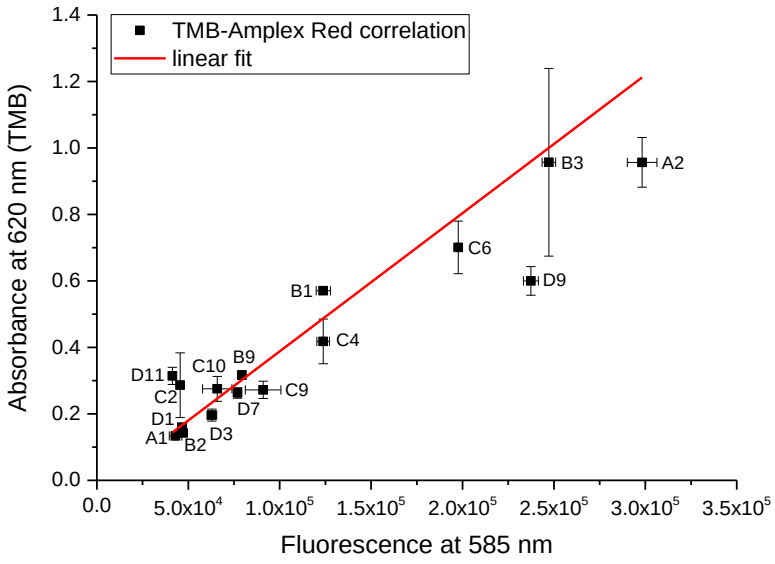

Figure 2.36. A linear correlation plot for data obtained from ALBA experiments using Amplex Red and TMB HRP substrates. Absorbance at 620 nm (y-axis) is plotted against fluorescence at 585 nm (x-axis). A straight line has been fitted to the data points.

The results compared well, although the value obtained from wells tested with Affimer 3D9 in the absence of CTB was noticed to be much higher than the average. Looking back at previous data, 3D9 consistently returned the highest value in negative controls. Detection of Affimer in the absence of target could indicate non-specific association with one, or several, components of the well (polystyrene, casein, GM1). 3D9 was therefore not taken forward for further characterisation.

The number of CTB-binding proteins was reduced from 17 to five by picking the five Affimers that returned the highest values in the ALBA. The Affimers that remained were 3A2, 3B1, 3B3, 3C4, and 3C6 (Figure 2.37).

	Variable loop 1								
3A2	Q	H	E	R	S	H	W	V	D
B1	P	P	D	S	T	E	Q	Q	R
B3	E	F	S	S	S	R	R	V	K
C4	V	D	Q	K	P	P	A	R	M
C6	M	D	L	N	A	G	L	P	R

Variable loop 2								
H	N	Q	F	F	D	Y	F	I
K	W	P	G	K	F	N	K	Y
G	L	S	T	I	G	K	I	L
K	N	F	W	F	P	S	Q	N
Q	G	L	K	K	L	K	F	T

Figure 2.37. Primary sequences of the variable loops of the five Affimers selected from ALBA experiments. Colour scheme corresponds to grouping of amino acid sidechains (*7.2.3.3. Sequence of binding loops of Affimers from Screen 3*)

2.3.3. Demonstrating selectivity using ALBA

Human heat labile enterotoxin (LTh) is an AB_5 toxin produced by enterotoxigenic *E. coli* isolated from a human host, and is closely related to CT in terms of structure and function.[165,223] The B_5 subunit of LTh (LTBh) shares 83% sequence identity with CTB (*7.2.1. CTB/LTB protein sequences*), making their three-dimensional structures virtually indistinguishable (Figure 2.38). Importantly, since the GM1-binding sites of CTB and LTBh are identical,[224] LTBh can also form high affinity interactions with GM1 ganglioside receptors.

Vibrio sp 60 cells transformed with plasmid PMMB68[225] for the expression of LTBh were available in-house. It was therefore possible to use LTBh in an ALBA to elucidate whether the five isolated Affimers could distinguish between LTBh and CTB pentamers.[1] This assay was carried out as described earlier, keeping CTB and LTB concentrations identical.

[1] The primary sequence of LTBh differs from porcine LTB at four positions, notably at position 13, where LTBh possesses a histidine. LTBh can therefore be purified by nickel affinity chromatography or lactose affinity chromatography.

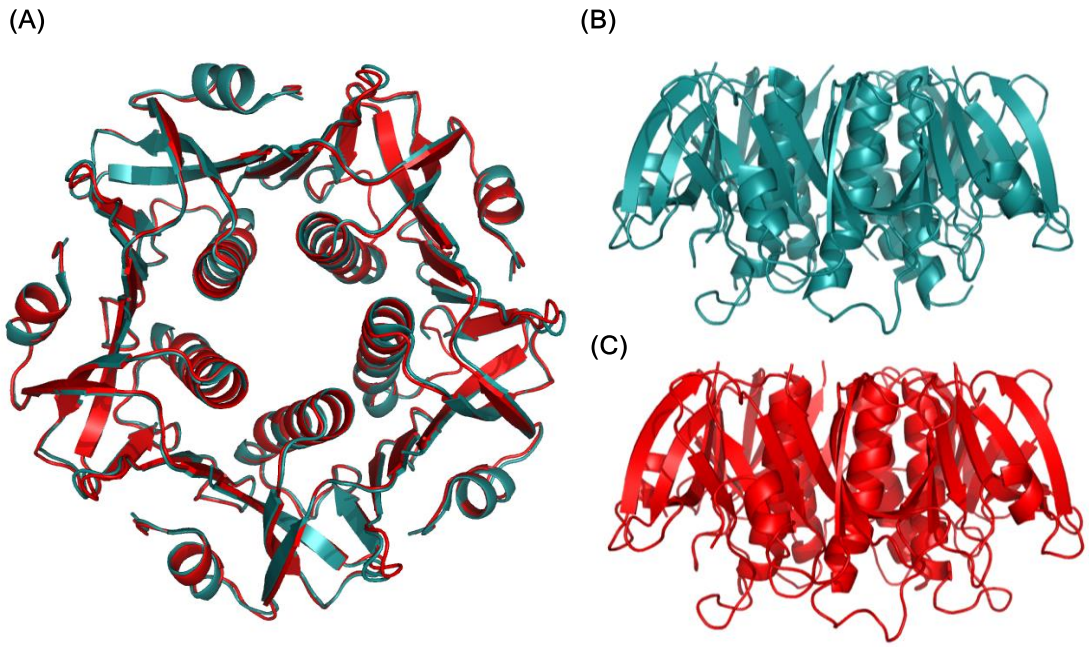

Figure 2.38. CTB and LTB are structurally similar. **(A)** Overlay of CTB (3CHB) and LTB (2O2L) crystal structures. **(B)** Side on view of LTB (top) and **(C)** side on view of CTB (bottom).

3B1, 3B3 and 3C6 appear not to discriminate between the two toxoids (Figure 2.39). Affimer 3A2, however, appeared to demonstrate exquisite selectivity, binding exclusively to CTB in this assay. 3C4 also seemed to distinguish between the two pentamers, however, the Affimer did not seem to perform well in this assay, and was not included in further analyses.

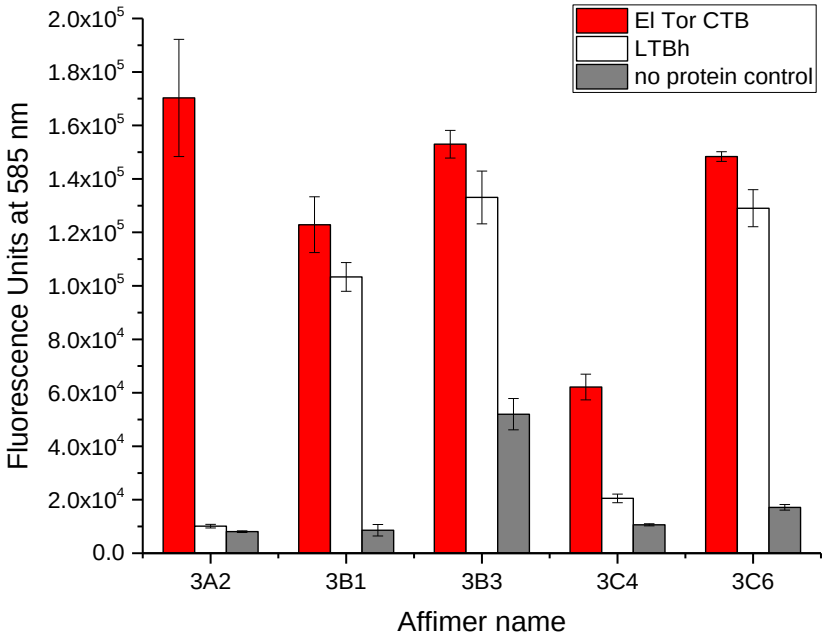

Figure 2.39. CTB-binding Affimers demonstrate variable selectivity for binding to CTB. Results of an ALBA using Amplex Red testing Affimers 3A2, 3B1, 3B3, 3C4 and 3C6 against GM1 bound CTB (red), GM1 bound LTB (white), or GM1 alone (grey).

Interestingly, of the 17 residues that differ between CTB and LTBh, only five of these are surface exposed on the top face of the B_5 subunit (Figure 2.40).

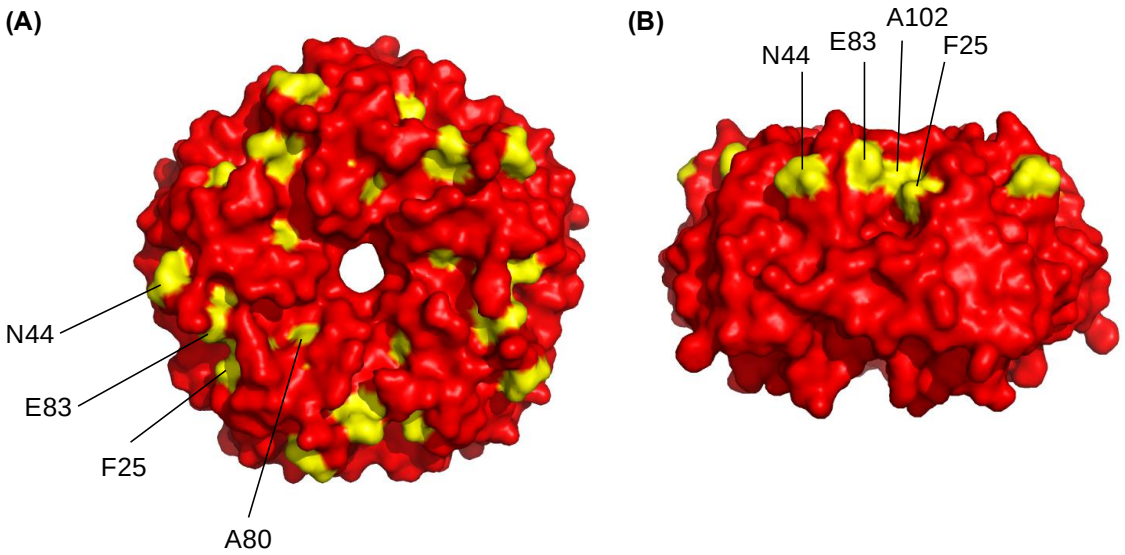

Figure 2.40. (A) A surface representation of the top face of CTB. There are five surface exposed residues per protomer that differ between the top faces of CTB and LTB. These residues have been highlighted in yellow. **(B)** A side on view of CTB with surface exposed residues differing to LTB coloured in yellow.

As Affimer 3A2 can distinguish between CTB and LTB, it is a reasonable hypothesis that these are the most likely residues to be forming interactions with the Affimer variable

loop(s). Of these five residues in CTB, three (F25, E83, A102) form a cluster at the interface of two CTB protamers, revealing a possible binding site for 3A2. To validate this hypothesis, mutagenesis was performed on pSAB2.2 to make five CTB/LTBh hybrids, each carrying mutations at one of the surface exposed amino acids (Table 2.2).

Residue Position	El Tor CTB	LTBh	Mutation introduced into CTB
25	F	L	F25L
44	N	S	N44S
80	A	T	A80T
83	E	D	E83D
102	A	E	A102E

Table 2.2. The position and type of the five surface exposed residues that differ between the non-binding face of CTB and LTB, and the mutation made to CTB to form a CTB-LTB hybrid.

During protein expression, B_5 toxoids are exported out of the cell and into the surrounding medium.[138] This feature allowed the protein-containing medium to be applied directly to GM1-coated plates for immobilisation of the CTB/LTB hybrids. Affimer 3A2 was detected in the CTB-containing control well, as well as in four out of the five wells treated with CTB/LTB hybrids (Figure 2.41).

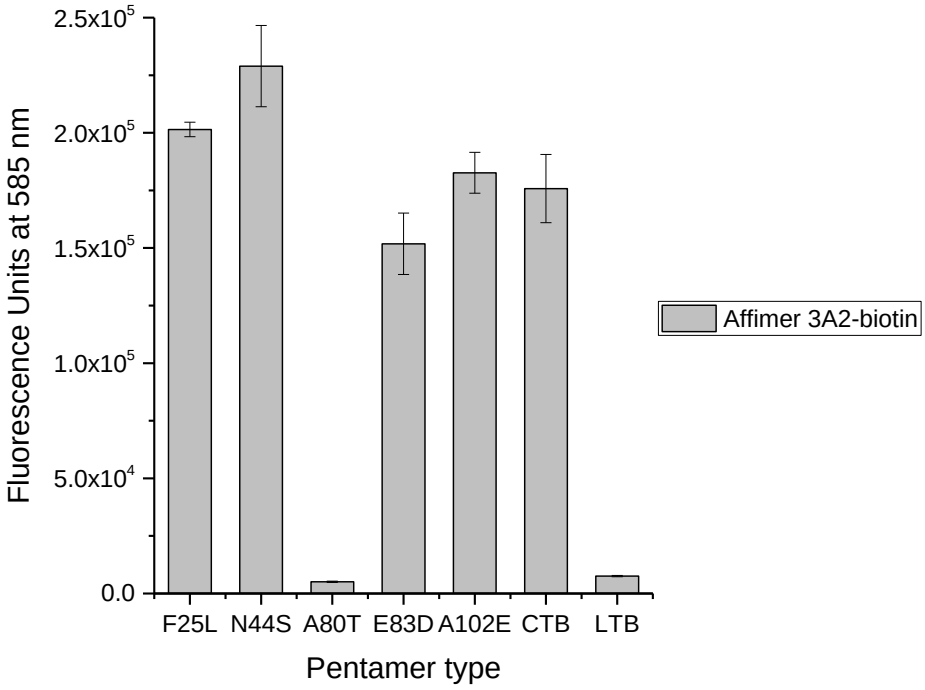

Figure 2.41. Bar chart assessing fluorescence at 585 nm (y-axis) detected following testing of 3A2-biotin against a series of five CTB-LTB hybrids (F25L, N44S, A80T, E83D, A102E, LTB and CTB).

Variation of the signal intensity observed for different CTB-LTB hybrids (Figure 2.41) was to be expected, as the concentration of protein in the medium used in this assay was unknown. No binding was observed in control wells treated with LTB, which was consistent with previous findings. Furthermore, no binding was detected for the mutant A80T, suggesting that this could be the residue in LTB responsible for interfering with Affimer 3A2 binding. To confirm that CTB A80T had indeed been expressed, the assay was then repeated using purified protein, which confirmed that introduction of this mutation prevents detection of Affimer 3A2 by ALBA (Figure 2.42).

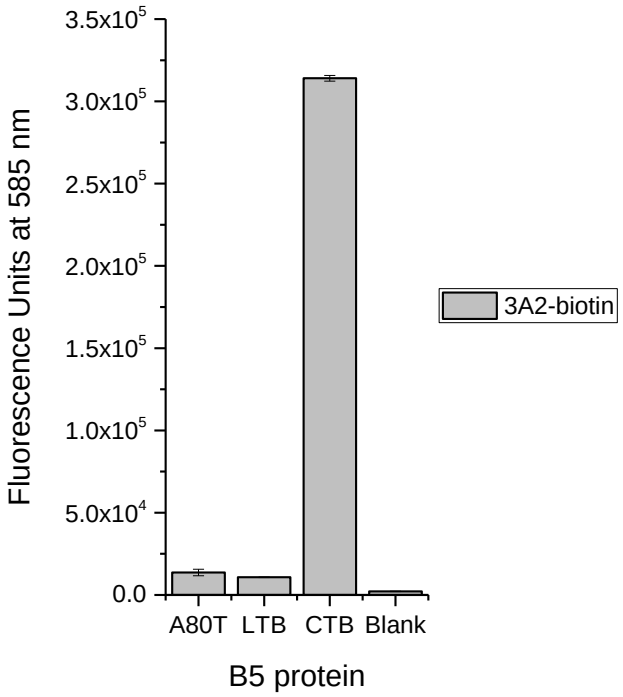

Figure 2.42. Bar chart showing fluorescence at 585 nm as a response to 3A2-biotin detection to purified A80T, LTB, or CTB.

To verify that this mutation was necessary and sufficient to prevent 3A2 binding, the reverse mutation was introduced into LTBh. Since LTBh was only available in a pATA plasmid, the synthetic gene for LTBh T80A gene was purchased. The DNA was digested using restriction enzymes SphI and HindIII, and ligated into pSAB2.2, similarly digested. The protein was expressed in *E. coli* and purified, but was obtained in much lower yield than expected. The synthetic DNA sequence for the LTBh T80A gene had been codon optimised, rather than using the known DNA sequence for LTBh. Overlaying the sequences revealed that the two sequences shared only 73% nucleotide identity, despite coding for the same protein (*7.2.1. CTB/LTB protein sequences*). Since LTBh is an *E. coli* protein, it is possible that the codon optimised sequence may have interfered with

protein production at the translational level, resulting in a reduced yield. Introducing high frequency usage codons is known to interfere with translation by altering so-called translational pause sites.[226]

Introduction of the T80A mutation in LTBh rescued Affimer 3A2 binding and detection in the ALBA (Figure 2.43), confirming A80 as a critical residue in CTB to allow Affimer 3A2 to bind.

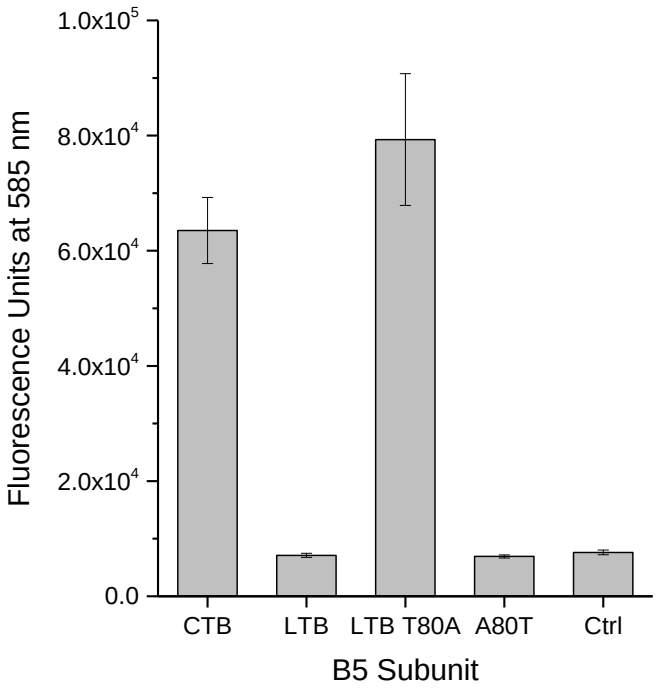

Figure 2.43. Testing the binding of 3A2-biotin to LTB T80A. A significant increase in fluorescence at 585 nm was detected in wells treated with CTB and LTB T80A, but not for LTB and CTB A80T.

Alanine 80 is close to the central cavity of CTB (Figure 2.44), lying in a channel at the interface of two protamers. If one of the Affimer loops does bind in this channel, then the bulkier threonine sidechain of LTB could be obstructing 3A2 from binding. In the absence of atomic crystallographic data, identification of this residue as essential for 3A2 binding provides structural information that suggests that the screening method was successful in isolating Affimers that can associate with the top face of CTB.

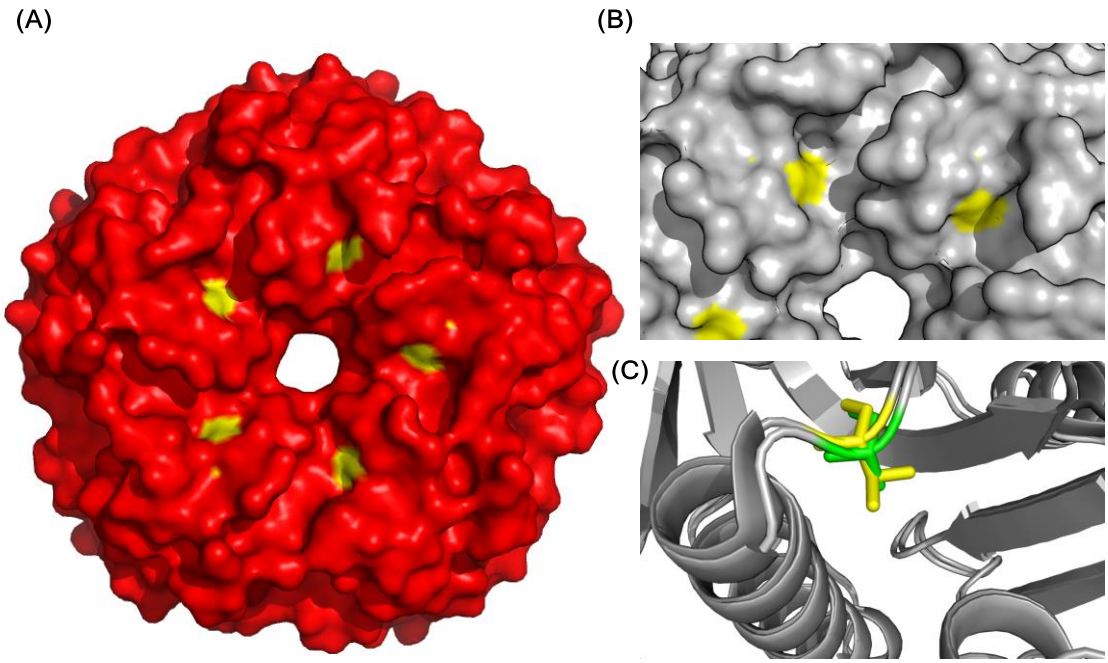

Figure 2.44. (A) Surface representation of the non-binding face of CTB, with residue A80 coloured in yellow. **(B)** A close up image of the hypothesised 3A2 binding groove, showing A80 in yellow. **(C)** A close up of an overlay of CTB and LTB with A80 shown in green, and T80 shown in yellow.

2.4. Biophysical Characterisation: Quantifying Affimer-CTB binding interactions

A series of four CTB-binding Affimers had now been identified. A novel binding assay had permitted assessment of the binding properties of the Affimers in a qualitative manner, and had revealed some structural information for the Affimer 3A2-CTB complex. To understand the true nature of the Affimer-CTB interactions, however, more quantitative data would need to be obtained. Of particular importance for the formation of a stable Affimer-CTB complex would be the derivation of association or dissociation constants, which would give a measure of how tightly the complex associates, and derivation of the association and dissociation rate constants, which would provide information on the residency time of the complex. ITC can be used to calculate binding constants and stoichiometry, whilst surface plasmon resonance (SPR) can be used to measure kinetic parameters. In the first instance, however, gel filtration was used to assess complex stability and stoichiometry.

2.4.1. Demonstrating complex formation by gel filtration chromatography

As demonstrated previously, gel filtration can be used to separate proteins of different shape and size by passing a solution through a column containing a bed of porous beads.

Proteins of similar shape and mass should have comparable retention volumes. Protein solutions can therefore be examined by gel filtration on an analytical scale, and compared to a calibration curve to get an approximation of protein mass. Thus, by calibrating the column with standards of known mass, and analysing both CTB and Affimers by analytical gel filtration, the complex could also be analysed to obtain information on stoichiometry of the interaction.

A Superdex 75 Increase 10/300 GL gel filtration column was used for analysis of complex formation, since this column has an upper limit on the mass of proteins that can be accurately separated of 75 kDa. In order to use gel filtration chromatography to extrapolate an estimate of molecular mass (M_r) from the elution volume of a particular protein, a series of low molecular weight standards of known M_r were obtained. These were combined, separated by gel filtration (Figure 2.45), and their retention volumes (V_e), assumed to be the point at maximal absorbance, were measured.

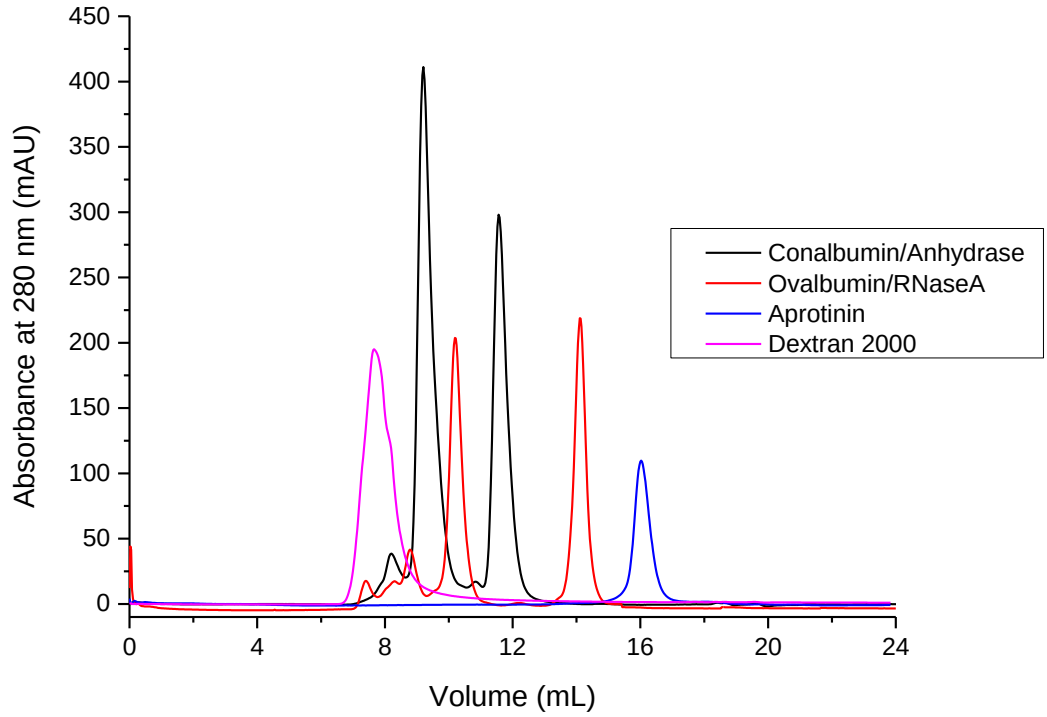

Figure 2.45. Analysis of the elution volumes of six macromolecules by gel filtration chromatography on a Superdex 75 Increase 10/300 GL gel filtration column. The absorbance at 280 nm is plotted as a function of elution volume to produce a chromatogram. Four traces are overlaid: Dextran 2000 (~ 2 MDa) (pink), a mixture of conalbumin (75 kDa) and carbonic anhydrase (29 kDa) (black), a mixture of ovalbumin (44 kDa) and RNase A (13.7 kDa) (red), and aprotinin (blue).

Dextran Blue is a polymer of high molecular mass (~2 MDa). This polymer was included in the calibration test since it would pass through the column via the shortest route, as it

would be too large to enter any of the resin pores. Measuring the V_e of Dextran Blue would thus provide a measure of the column void volume (V_o). The recorded retention volumes for the calibrants were used to calculate a gel phase distribution coefficient (K_{av}) using Equation 2.1, where V_c is the geometric column volume, calculated as $V_C = \pi r^2 l$, where l is equal to the column length. Plotting the K_{av} for each standard against the logarithmic of the molecular weight allowed the derivation of a linear function (**Figure 2.46**).

$$K_{av} = \frac{V_e - V_O}{V_C - V_O}$$

Equation 2.1. Calculation of the gel phase distribution coefficient using the retention volume (V_e), void volume (V_o), and column volume (V_c).

Protein standards	Elution volume (mL)	M_r (Da)	K_{av}
Conalbumin	9.2	75000	0.09
Ovalbumin	10.1	44000	0.15
Carbonic anhydrase	11.6	29000	0.25
Ribonucelase A	14.1	13700	0.40
Aprotinin	16	6500	0.52
Dextran2000	7.7	2000000	-

Table 2.3. Elution volume, relative molecular mass (M_r) in Da, and gel phase distribution coefficient (K_{av}) for each protein standard used to calibrate the analytical Superdex 75 Increase 10/300 GL column.

Retention volumes, and thus values for K_{av}, for proteins and protein complexes of unknown mass could be measured, and the equation of the calibration line could be used to calculate an apparent M_r.

This method was used with variable results. Purified CTB eluted at 11.3 mL (Table 2.4), giving an apparent M_r 16 kDa less than expected (32 kDa). This observation was thought to be due to the compact nature of CTB. CTB is a tightly ordered protein, with few unstructured, and therefore more mobile, regions. Addition of a 2.7 nm long flexible linker to the N-terminus of CTB is sufficient to significantly speed up its passage through the column (Figure 2.8A). Affimers 3A2 and 3C6 were also analysed by gel filtration (Figure 2.47), with apparent masses that were closer to their expected M_r (Table 2.4).

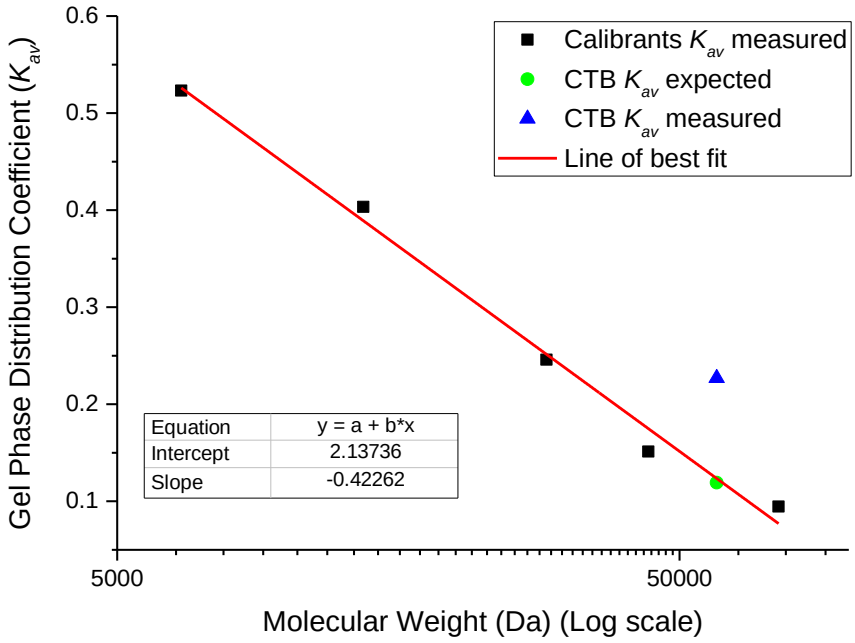

Figure 2.46. Linear fit (red) of gel phase distribution coefficient, a ratio of elution volume to the void and column volume for each calibrant, and the molecular weight for each calibrant shown on a log scale. The green data point corresponds to the expected distribution coefficient for CTB, whilst the blue data point corresponds to the measured distribution coefficient for CTB.

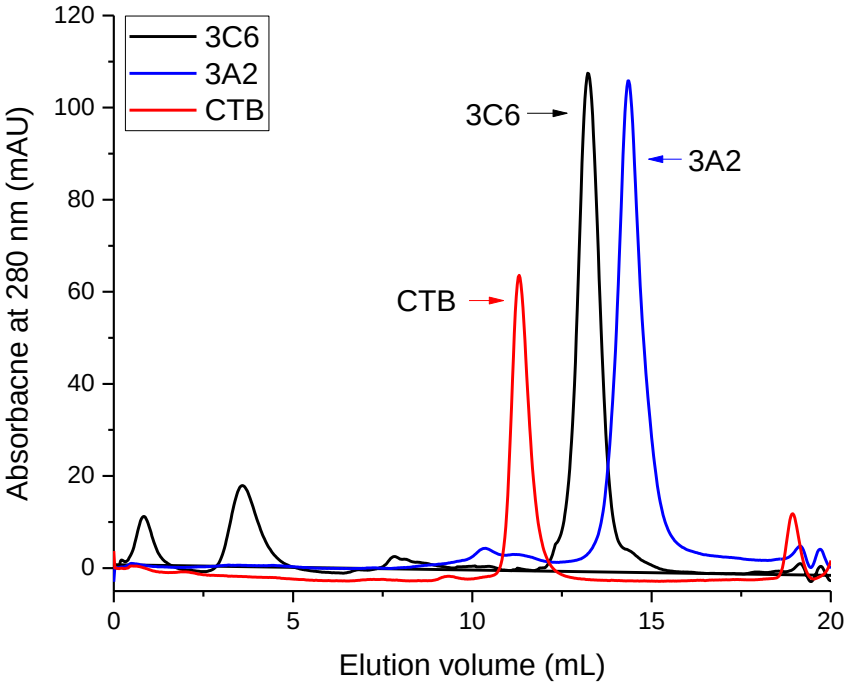

Figure 2.47. Overlaid chromatograms following analysis of 3A2 (blue), 3C6 (black), and CTB (red) by gel filtration chromatography using a Superdex 75 Increase 10/300 GL gel filtration column.

Sample protein	Elution Volume (mL)	K_{av}	M_r (app) (Da)	M_r (Da)
CTB	11.30	0.23	32300	58225
3A2	14.36	0.42	11300	13729
3C6	13.24	0.35	16600	13355

Table 2.4. The elution volume, gel phase distribution coefficient, apparent relative molecular mass (M_r (app)) and calculated relative molecular mass (M_r) in Da for CTB, and Affimers 3A2 and 3C6.

The disparity between the M_r (app) for 3C6 and 3A2 could indicate a difference in the conformation of variable loops. It is possible that Affimer 3A2 adopts a more compact shape than Affimer 3C6, perhaps due to the larger number of hydrophobic residues present in the second variable loop of 3A2, whilst the variable loops of 3C6 may project further away from the core scaffold. With the individual constituents of the complex analysed, the next step was to combine them and analyse their propensity to form complexes.

Since CTB is a homopentamer, it has five repeating epitopes that can be recognised by the two variable loops of a given CTB-binding Affimer. The closer that these five epitopes are to the central cavity of the B5 subunit, the more likely it is that issues such as steric hindrance will come into play, allowing only a single Affimer to bind to each pentamer. By the same logic, the closer these epitopes are to the periphery of the pentamer, the more likely it will be that multiple Affimers could associate to the same molecule of CTB (Figure 2.48).

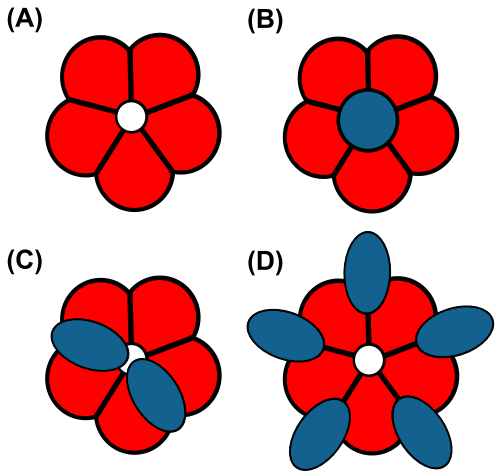

Figure 2.48. (A) Cartoon representation of the non-binding face of CTB. **(B)** Scenario where the epitopes for CTB recognition are close to the central cavity of CTB, resulting in one Affimer being able to bind per pentamer. **(C)** The Affimer binding sites are located in the centre of each protomer, allowing two Affimers to bind per pentamer. **(D)** Affimer binding sites are located on the periphery of the non-binding face of CTB, allowing five Affimers to associate per CTB pentamer.

Complexes composed of five, two, and one Affimer(s) per molecule of CTB were thus thought to be possible. Given the proximity of alanine residue 80 to the central pore of CTB, Affimer 3A2 was postulated to have a stoichiometry of 1:1 (Affimer :CTB pentamer).

Since CTB elutes from the gel filtration column with a larger elution volume than expected relative to its mass, Affimer-CTB complex formation was analysed using the Superdex 75 Increase 10/300 GL gel filtration column. One, two, and three molar equivalents of Affimer were combined with CTB, incubated for an hour, and applied to the column (Figure 2.49). If the stoichiometry was greater than 1:1, then a shift in the peak for retention volume was expected. In both cases, no shift was observed (Figure 2.49/*7.2.2.4. Various figures*), indicating that the stoichiometry for both Affimers was likely to be 1:1.

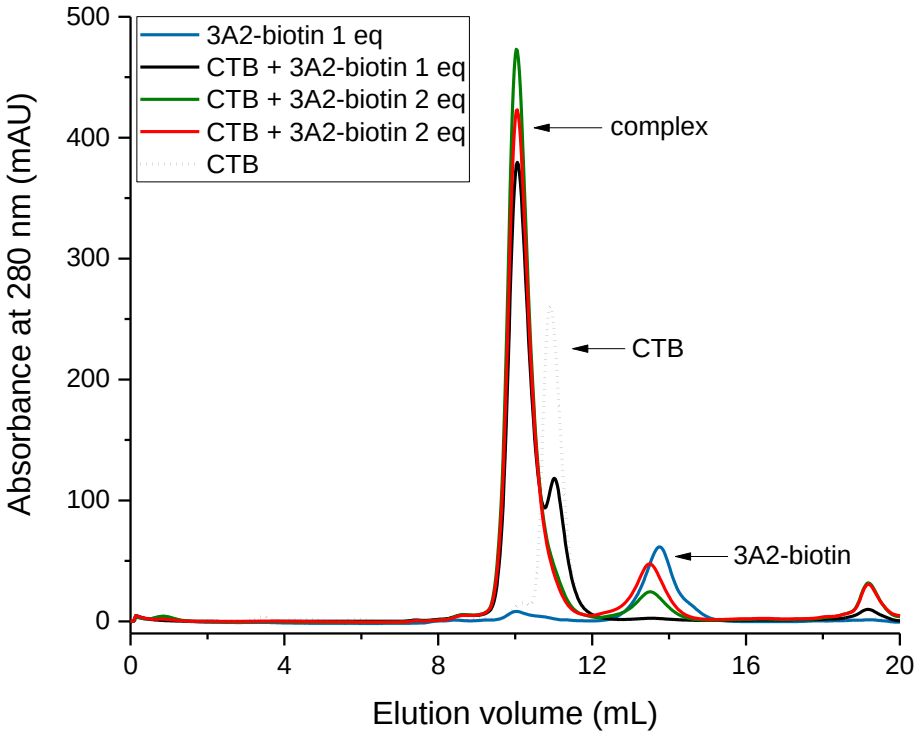

Figure 2.49. Chromatogram following analysis of varying amounts of 3A2-biotin and CTB by gel filtration chromatography using a Superdex 75 Increase 10/300 GL gel filtration column. 3A2-biotin was initially analysed alone (blue). CTB was then combined with one equivalent of 3A2-biotin (black) and analysed, followed by two equivalents (red) and three equivalents (green) of 3A2-biotin with CTB.

The fractions corresponding to the observed peaks were analysed by SDS-PAGE (Figure 2.50) to confirm the presence of CTB and Affimer. The detection of both proteins, and the observation of a shift in the retention volume peak on addition of Affimers to CTB

indicated that complex formation was occurring, and that the complex was stable under the conditions of gel filtration. The stoichiometry also appears to be reflected in the ratio of Affimer to CTB pentamer band intensity observed in the SDS-PAGE gel (Figure 2.50), with the intensity of 3A2-biotin being considerably less than the intensity of CTB.

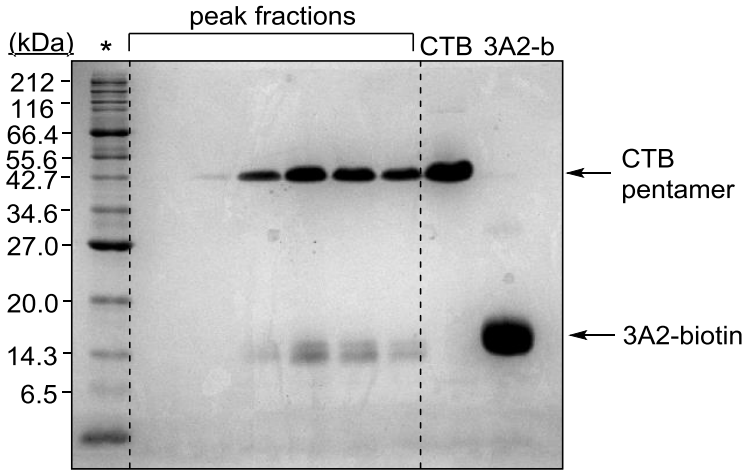

Figure 2.50. SDS-PAGE analysis of the gel filtration fractions under the peak corresponding to 3A2-CTB complex formation (Figure 2.49). CTB and 3A2-biotin (3A2-b) are shown for comparison. In peak fractions 3-6, bands corresponding to CTB pentamer and 3A2-biotin were observed.

The gel phase distribution coefficient was calculated for both complexes, and used to establish the apparent M_r of the two complexes (Table 2.5). Subtracting the apparent M_r for CTB from the values calculated for 3A2:CTB and 3C6:CTB leaves apparent masses of 17 kDa and 15 kDa, further verifying the theory that the stoichiometry for both interactions is most probably 1:1 (Affimer:CTB pentamer).

Sample protein	Elution Volume (mL)	K_{av}	M_r app (Da)	Calculated M_r from molecular formula (Da)
A2-biotin	13.7	0.38	14200	14467
C6-biotin	12.7	0.32	20000	13880
CTB	11.30	0.23	32300	58225
A2-biotin:CTB complex	10.05	0.15	49600	72692
C6-biotin:CTB complex	10.16	0.16	47700	72105

Table 2.5. The elution volume, gel phase distribution coefficient (K_{av}), apparent molecular weight (M_r app), and calculated molecular weight (M_r) for biotinylated Affimers 3A2 and 3C6, CTB, and the corresponding protein complexes, 3A2-biotin:CTB and 3C6-biotin:CTB.

2.4.2. Measuring affinity and thermodynamics

For a given binding interaction between a ligand and receptor, an equilibrium will be reached between free ligand and receptor, and the ligand-receptor complex. The strength, or affinity, of this interaction can be described by the binding constants K_a and K_d, described by the ratio of unbound to complexed material (Figure 2.51).

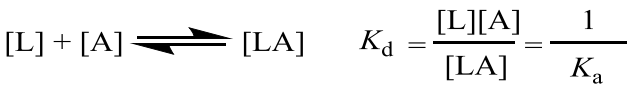

Figure 2.51. Interaction between a ligand, L, and receptor, or analyte, A, to form a ligand-analyte complex, LA. The relationship between the dissociation constant, K_d, and the ratio of the concentrations of free ligand and analyte to the concentration of complex, and the association constant.

These constants are connected intrinsically to the change in Gibbs energy (ΔG^0) of the interaction. Since ΔG^0 comprises contributions from both entropy (ΔS^0) and enthalpy (ΔH^0), defined by the thermodynamic equation $\Delta G^o = \Delta H^o - T\Delta S^o$, the recognition event must be connected to changes in the structure and dynamics of both binding partners. In order for binding to take place spontaneously, ΔG^0 must be negative, but can be driven by enthalpy, entropy, or a combination of the two. Therefore, to understand the nature of the driving forces underlying the recognition and interaction between two binding partners, the thermodynamic parameters should be understood.

Enthalpic contributions to ΔG are associated with specific types of non-covalent interactions, such as electrostatics, hydrogen bonding, and van der Waals interactions. These forces are usually associated with the specificity of the interaction.[227] Entropic contributions, meanwhile, are representative more of the dynamics of the interaction, for instance changes to the flexibility and motion of the components upon binding. It is difficult to measure entropy directly. ΔS^0 must therefore be calculated from measurements of ΔH^0 and K_d, using the thermodynamic equation shown above, together with the equation $\Delta G^o = RTlnK_d$, where T is the temperature in degrees Kelvin, and R is the gas constant. ΔH^0 and K_d can be measured accurately in a single experiment using the technique isothermal titration calorimetry (ITC).

2.4.2.1. Examining the Affimer-CTB interaction by ITC

To define the thermodynamic parameters for the Affimer-CTB interaction, and to supplement the evidence for the binding stoichiometry, protein titration experiments were carried using ITC. How the instrument functions is described in detail in the *6.6.1. Isothermal Titration Calorimetry*.

To obtain thermodynamic information for Affimers 3A2 and 3C6, experiments were set up under the assumption that the stoichiometric ratio of Affimer to CTB pentamer was 1:1. Addition of two molar equivalents of a ligand to a receptor is sufficient to saturate all the available binding sites, provided that both components are at a concentration at least 10 times higher than the dissociation constant for the interaction. CTB was titrated into

the calorimeter cell containing either 3A2 or 3C6, and the trace showing the change in heat was plotted and analysed using Microcal Origin software.

An exothermic heat change was observed for both Affimers (Figure 2.52). Table 2.6 and Table 2.7 display the list of measured and calculated thermodynamic parameters for both Affimer-CTB interactions. For Affimer 3C6, a K_d of 97 nM was measured, and a binding stoichiometry (n) of 1.05 was inferred from the fitted curve, in line with the data obtained by gel filtration. For Affimer 3A2, a K_d of 1.1 µM was measured, and the binding stoichiometry was measured as 1.15:1, also in line with gel filtration experiments. The slight error in measurement of stoichiometry was likely a result of inaccuracies stemming from the calculation of protein concentration.

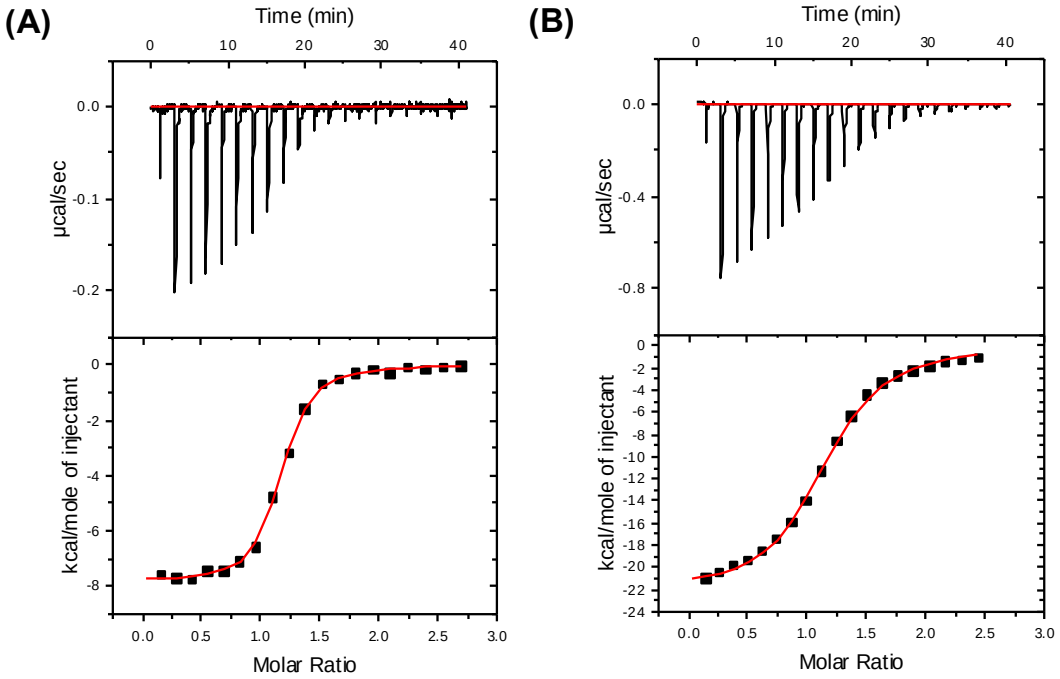

Figure 2.52. (A) Thermogram and binding isotherm generated following the titration of 100 µM CTB into 10 µM 3C6 at 35ºC by ITC. The data are fitted with a one-site binding model using Microcal Origin software following baseline subtraction using CTB into buffer titrations. **(B)** Thermogram and resultant Wiseman binding isotherm following high concentration titrations of 200 µM CTB into 17 µM 3A2 at 35ºC by ITC. The data are fitted with a one-site binding model using Microcal Origin software following baseline subtraction using CTB into buffer titrations.

#	Temp (K)	ΔH^0 (kcal/mol)	ΔG^0 (kcal/mol)	K_d (nM)	$T\Delta S^0$ (kcal/mol)	*n*
1	308	-6.80 ± 0.08	-10.24 ± 0.13	55 ± 12	3.44 ± 0.21	0.98 ± 0.007
2	308	-7.86 ± 0.06	-9.67 ± 0.06	139 ± 13	1.81 ± 0.12	1.13 ± 0.006
Average	-	-7.33 ± 0.14	-9.95 ± 0.19	97 ± 30	2.62 ± 0.33	1.05 ± 0.013

Table 2.6. Data table showing the thermodynamic parameters (enthalpy (ΔH), Gibb's energy (ΔG), enthalpy (TΔS)), as well as the stoichiometry (*n*), measured and calculated for two CTB titrations into Affimer 3C6 by ITC, as well as the average across the two experiments (for ITC data for both experiments see *7.3.1. Titration of CTB into Affimer 3C6*). All repeats are true biological replicates, using different protein stocks and buffers, and taking place on different days.

#	Temp (K)	ΔH^0 (kcal/mol)	ΔG^0 (kcal/mol)	K_d (μM)	$T\Delta S^0$ (kcal/mol)	*n*
1	308	-22.06 ± 0.17	-8.47 ± 0.56	1.00 ± 0.05	-13.59 ± 0.73	1.15 ± 0.01
2	308	-22.69 ± 0.16	-8.43 ± 0.58	1.06 ± 0.04	-14.26 ± 0.74	1.12 ± 0.01
3	308	-24.37 ± 0.55	-8.30 ± 0.52	1.32 ± 0.13	-16.07 ± 1.07	1.19 ± 0.02
Avg.	-	-23.04 ± 0.87	-8.40 ± 1.65	1.13 ± 0.21	-14.64 ± 2.52	1.15 ± 0.03

Table 2.7. Data table showing the thermodynamic parameters (enthalpy (ΔH), Gibb's energy (ΔG), enthalpy (TΔS)), as well as the stoichiometry (*n*), measured and calculated for three CTB titrations into Affimer 3A2 by ITC, as well as the average across the three experiments (for ITC data for all three experiments see *7.3.2. Titration of CTB into Affimer 3A2*). All repeats are true biological replicates, using different protein stocks and buffers, and taking place on different days.

The K_d for Affimer 3A2 was measured as 1.1 μM, a surprisingly low affinity in the context of the ALBA, where Affimer 3A2 consistently produced a higher signal than Affimer 3C6. To assess whether Affimer 3A2 binds more tightly to GM1-bound CTB than the free protein, titrations of GM1os-bound CTB into 3A2 were carried out. No significant difference in thermodynamics were measured for binding of CTB to either Affimer 3A2 or 3C6 (Figure 2.53) in the presence of GM1os. CTB binding GM1 therefore does not appear to dramatically affect binding of Affimers 3A2 and 3C6 to CTB.

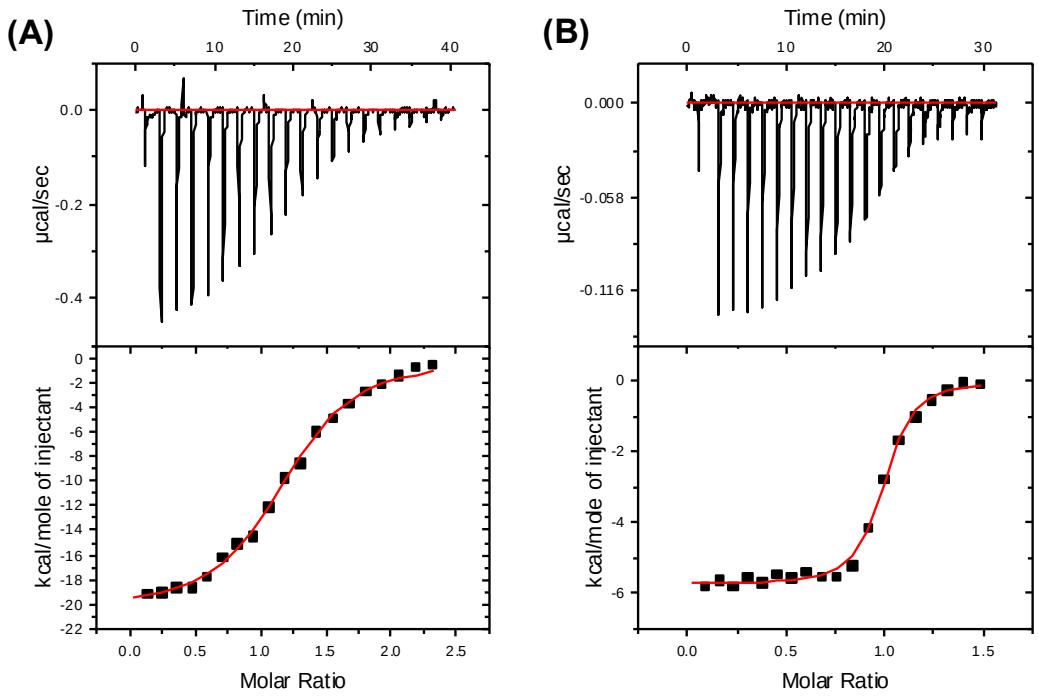

Figure 2.53. Thermogram and resultant binding isotherm following titration of **(A)** GM1-bound CTB (130 µM) into a solution of 3A2 (13 µM) and GM1 at 35ºC **(B)** GM1-bound CTB (130 µM) into a solution of GM1 (750 µM) and 3C6 (20 µM) at 35ºC. The data are fitted with a one-site binding model using Microcal Origin software following GM1-bound CTB titrations into GM1-containing buffer.

Affimer	Temp (K)	ΔH^0 (kcal/mol)	ΔG^0 (kcal/mol)	K_d (nM)	$T\Delta S^0$ (kcal/mol)	*n*
3A2	308	-20.45 ± 0.28	-11.86 ± 0.52	820 ± 70	-11.86 ± 0.80	1.20 ± 0.01
3C6	308	-5.76 ± 0.06	-10.06 ± 0.09	72 ± 11	4.31 ± 0.15	0.97 ± 0.01

Table 2.8. Data table showing the thermodynamic parameters measured and calculated for GM1-bound CTB titrations into Affimer 3A2 or 3C6.

These two Affimers have very different thermodynamic signatures. The 3A2-CTB interaction is an enthalpically driven process, whilst the contributions of enthalpy to binding of 3C6 to CTB are much smaller. Additionally, the entropies differ between the two binding interactions, with 3A2-CTB being entropically unfavourable, whilst 3C6-CTB binding is entropically favourable. However, despite these differences in enthalpy and entropy, the binding stoichiometry for both interactions is one-to-one, suggesting that binding of both Affimers to CTB takes place near the central cavity of the CTB pentamer.

Affimer 3A2 had a longer retention time than Affimer 3C6 when analysed by gel filtration chromatography (Figure 2.47), indicating that Affimer 3A2 is more compact than Affimer 3C6. However, both Affimer-CTB complexes had similar elution profiles (Table 2.5) suggesting that the hydrodynamic radii of the complexes are comparable. The

dissimilarity in hydrodynamic radius of the two Affimers may account for the differences in thermodynamics observed for the two interactions; the variable loops of Affimer 3C6 may be pre-organised for binding, whilst the variable loops of Affimer 3A2 may need to adopt a binding conformation in order to interact with CTB.

2.4.3. Measuring binding kinetics

Whilst establishing binding constants for the Affimer-CTB interaction provides key information for characterisation of the complex, it only reveals half the story. A binding interaction between multiple components is a dynamic process, eventually reaching an equilibrium of associated and dissociated material (Figure 2.54).

Figure 2.54. The relationship between the dissociation and association rates, and the concentration of free ligand and analyte, and complexed ligand and analyte.

Deriving the rate of this dissociation and association, i.e. how rapidly a molecule will bind to a partner, and for how long on average it will remain associated, is not possible from K_a and K_d, as these binding constants are ratios of the association (k_{on}) and dissociation (k_{off}) rates (Equation 2.2).

$$K_a = \frac{[LA]}{[L][A]} = \frac{k_{on}}{k_{off}} = \frac{1}{K_d}$$

Equation 2.2. The relationship between the association and dissociation constants, K_a and K_d, the concentration of free ligand and analyte and ligand-analyte complex, and the association and dissociation rates (k_{on} and k_{off}).

Since the binding constants are ratios, two interactions may have similar affinities, but differ wildly in their kinetic parameters. Therefore, for an interaction with a low affinity, it is possible that a high activation barrier (a slow k_{on}) could result in slow binding, but may also result in slow dissociation, resulting in a long-lived interaction. The rate of dissociation thus dictates the residency time for a ligand bound to its receptor.

For the Affimer-CTB interaction, residency time (t_r) (Equation 2.3) is of fundamental importance. Once administered *in vivo*, the complex needs to remain associated sufficiently long for the CTB to bind, and be subsequently internalised. Dissociation prior to internalisation would preclude delivery of the Affimer into the target cells. It was therefore desirable to determine the kinetic parameters of the CTB-Affimer complexes.

$$t_r = \frac{1}{k_{off}}$$

Equation 2.3. Calculation of the residence time (t_r) from the dissociation rate (k_{off}).

2.4.3.1. Examining the binding kinetics of the 3A2-CTB interaction

One way to measure kinetic parameters is by exploiting a phenomenon known as surface plasmon resonance (SPR). SPR systems typically use sensor chip-based binding assays under flow conditions to determine parameters for kinetics and affinity for biomolecular interactions.

Since biotinylated Affimer and CTB were already available, streptavidin sensor chips were used to investigate the binding kinetics of the interaction. For a given change in mass concentration on a microchip surface, the change in refractive index is effectively the same for all proteins. 3A2-biotin was therefore initially immobilised to the sensor chip, since binding of CTB to fixed Affimer would result in a larger change in refractive index than the converse, thus increasing the signal to noise ratio. Biotinylated samples were immobilised to the streptavidin sensor chips by injecting at a very low concentration (20 pM).

A minimal amount (25 RU) of 3A2-biotin was initially immobilised, with a first 'test' experiment, injecting 2 µM CTB across the chip, showing that association and dissociation could be measured (Figure 2.55).

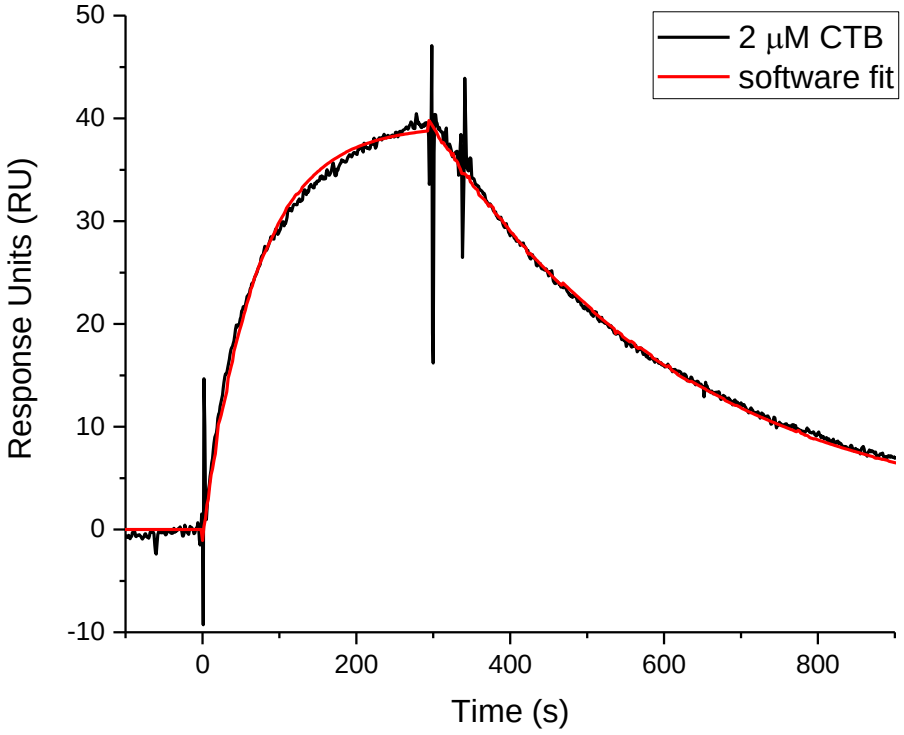

Figure 2.55. SPR sensorgram generated following the titration of 2 μM CTB across a streptavidin-coated dextran sensor chip with 25 RU 3A2-biotin captured to the surface. The data (black) were fitted with a one-to-one binding model (red) using BIAcore evaluation software.

A one-to-one binding model was fitted to the data using BIAcore software providing preliminary data on the affinity and kinetics (Table 2.9).

k_{on} (M^{-1} s^{-1})	k_{off} (ms^{-1})	R_{max} (RU)	[CTB] μM	K_a (M^{-1})	K_d nM
5830 ± 91	2.99 ± 0.02	50.9 ± 0.27	2	$1.95 \times 10^6 \pm 4.54 \times 10^4$	513 ± 12

Table 2.9. Preliminary association and dissociation rates and constants measured from the titration of 2 μM CTB across 25 RU of streptavidin-bound 3A2-biotin.

As the preliminary data was quite noisy, a larger quantity of 3A2 (577 RU) was immobilised to give smoother data (**Figure 2.56**). Nine titrations of CTB were carried out across the functionalised chip, and the resultant sensorgrams were globally fitted to a one-to-one binding model to derive the rate constants. A K_d of 1.72 μM was calculated from the rate constants, since $K_d = k_{off}/k_{on}$. The binding model does not perfectly fit the data, suggesting that the binding process is more complex than can be described by a one-to-one binding model. However, the value obtained for K_d was in line with the data obtained by ITC.

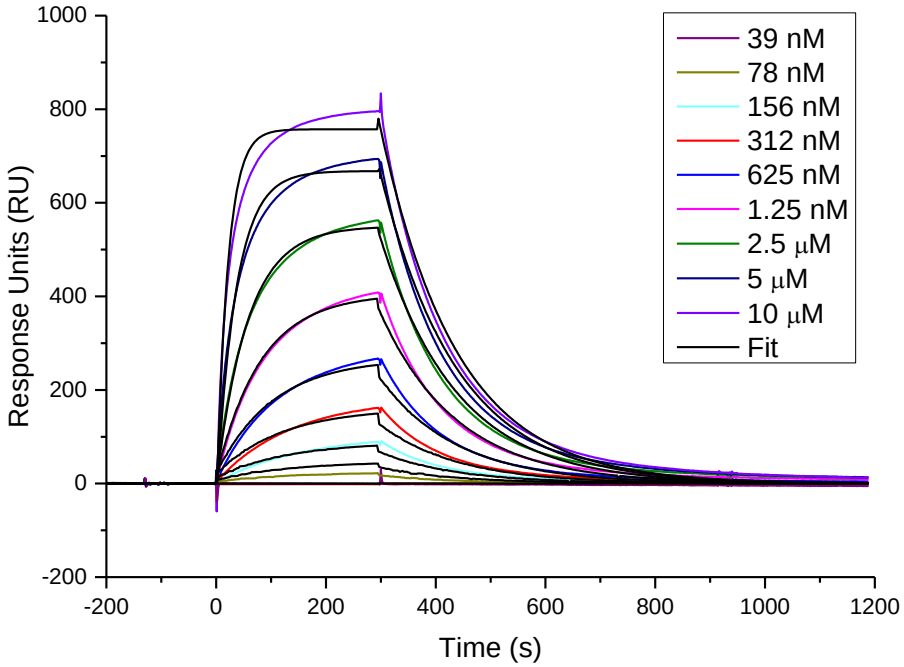

Figure 2.56. Sensorgram generated following the titration of a range of concentrations from 39 nM to 10 μM CTB across a streptavidin-coated chip with 577 response units of 3A2-biotin captured on the surface.

	k_{on} (M^{-1} s^{-1})	k_{off} (ms^{-1})	R_{max} (RU)	K_a (M^{-1})	K_d (μM)
577 RU	4140 ± 15	7.12 ± 0.01	918 ± 1.6	5.65 x 10^5 ± 3.10 x 10^3	1.72 ± 0.01

Table 2.10. Data table showing the association and dissociation rates and constants measured after titration of CTB across chips coated with 25 RU or 577 RU of 3A2-biotin.

The K_d can also be calculated from the equilibrium binding data, as K_d is equivalent to the concentration of analyte required to reach half the R_{max} (the number of RU corresponding to saturation of the surface-bound ligand) (Equation 2.4).

$$RU = \frac{R_{max}[A]}{K_d + [A]}$$

Equation 2.4. Using the response units at equilibrium, and the concentration of analyte to calculate the maximum response units (R_{max}) and the dissociation constant (K_d).

R_{eq} for the nine titrations of CTB against 3A2-biotin (577 RU) were plotted against the analyte concentration, and a one site bind model was fitted using Equation 2.4 in Origin (Figure 2.57). The K_d of 1.52 μM agrees broadly with the calculation of K_d from the rate constants, despite some uncertainty arising from the difficulty in fitting a single rate equation to all nine titrations. These affinity calculations by SPR also agree with data

obtained by ITC, demonstrating that Affimer 3A2 has a binding affinity for CTB in the range of 1-2 µM.

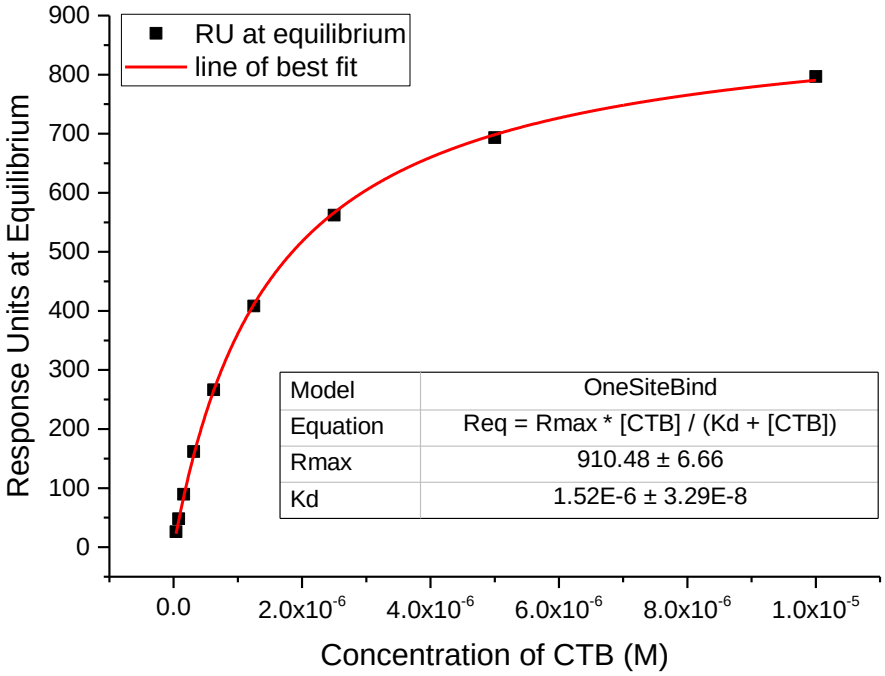

Figure 2.57. Graph plotting the response units measured at equilibrium, the plateau of the association curve, against the concentration of CTB (M). Fitting a one site bind model to the data allows calculation of the dissociation constant.

Rate constants for the 3C6-CTB interaction were unable to be measured by SPR. The association and dissociation phases occurred in vertical steps (data not shown), perhaps suggesting that binding and dissociation were occurring too rapidly to be measured by SPR.

The measurement of the dissociation rate allows calculation of parameters concerning the life-time of the Affimer-CTB complex, such as the complex half-life ($t_{1/2}$), which is the duration required for half the molecules of receptor-bound ligand to dissociate, and the complex residence time (t_r), which is the average duration that a ligand occupies a receptor.[228]

As discussed earlier, the residence time is of particular importance in pharmacology to the efficacy of a drug *in vivo*. In an *in vitro* binding experiment, an equilibrium is formed between receptor and ligand, where the concentration of the complex remains constant. In an *in vivo* system, however, mass transport of solutes in the circulatory system results in depletion of dilution and separation of unbound ligand, taking the system away from

equilibrium conditions. Since the ligand is only effective when bound, a slow dissociation and thus longer residence time is desirable.

Measurement of the kinetics of the 3A2-CTB interaction allowed calculation of t_r and $t_{1/2}$. These two parameters are related to the dissociation rate and to each other by Equation 2.3 and the two following equations:

$$t_{1/2} = \frac{ln2}{k_{off}}$$

Equation 2.5. Calculation of the half-life of the complex ($t_{1/2}$) from the dissociation rate (k_{off}).

$$t_{1/2} = ln2 \times t_r$$

Equation 2.6. Relationship between the complex half-life ($t_{1/2}$) and the residence time (t_r).

The half-life of the complex is therefore approximately 0.693*t_r. The calculated parameters are show in in Table 2.11 using the measured rate constants. The residence time was calculated as 140 s, suggesting that the 3A2-CTB interaction is short-lived, with 50% of molecules dissociating after 97 seconds.

	k_{on} (M^{-1} s^{-1})	k_{off} (ms^{-1})	t_r (s)	$t_{1/2}$ (s)	K_d (μM)
577 RU	4140 ± 15	7.12 ± 0.01	140 ± 0.25	97 ± 0.18	1.72 ± 0.01

Table 2.11. Data table showing the association and dissociation rates measured from titrations of CTB across a chip coated with 577 RU 3A2-biotin. Residence times and complex half-lives have been calculated.

A residence time so short would make delivery of 3A2 into neurones by intravenous administration unlikely to succeed. Nevertheless, administration of the complex at a concentration above K_d directly into a tissue, where it is less subjected to movement by the circulatory system, could be more successful, and is discussed in detail in the next chapter.

2.5. Chapter Conclusion

In this chapter, I have described how CTB-binding Affimers were identified by phage display, and how *in vitro* experiments were carried out to characterise the binding of these Affimers to CTB. Initially, a competitive selection process was employed in an attempt to select high affinity binders. However, this selection turned out to be too stringent. Although two unique Affimers were identified in the screen, no binding to CTB was observed when the purified proteins were tested by ITC.

A new approach was undertaken for a second screen, wherein the phage library was presented CTB adhered to GM1. The second screen resulted in isolation of a much wider range of Affimers. A novel Affimer lectin binding assay was developed to identify the best hits from the second screen. This plate-based assay allowed determination of the best binders from the screen, as well as providing some insight into the selectivity of these Affimers for CTB. From the screen, two Affimers were selected, 3A2 and 3C6. Successful complex formation was demonstrated by gel filtration chromatography, and dissociation constants of 1.1 µM for 3A2-CTB, and 100 nM for 3C6-CTB were measured by ITC. SPR experiments were carried out for Affimer 3A2, allowing measurement of k_{on} and k_{off} rates for the 3A2:CTB interaction. The K_d calculations by SPR corroborated the measurements by ITC (1.5 µM). Test experiments were carried out to investigate the binding of 3C6 to CTB. However, the kinetics appeared to be very fast, making it difficult to assess binding and obtain kinetic data.

The Affimers identified have fast k_{on} and k_{off} rates, and are relatively weak in affinity for their target. Whilst this could be beneficial for release once inside a cell, higher affinity interactions with longer residence times would be more favourable for delivery into the cells. Ultimately, higher affinity Affimers could have been obtained from the phage library. The concentration of CTB immobilised for phage display was probably too high for all four panning rounds, which could have led to little discrimination between higher and lower affinity Affimers. Simply reducing the amount of CTB presented to the phage library may have been sufficient to identify binders with more favourable binding properties. Nonetheless, Affimers 3A2 and 3C6 were carried forward for *ex vivo* and *in vivo* characterisation as it was judged that the affinities and residence times would be sufficient for administration by direct injection into a target muscle.

3. From the Test Tube to the Cell

Having identified two CTB-binding Affimers, the next phase of the development of this novel tool was to demonstrate its efficacy *in vivo*. In this chapter, I describe how the Affimer-CTB complex was assembled and delivered into cells, in tissue culture and *in vivo*, and how the system was modified to transport a macromolecular cargo.

3.1. Delivery of the Complex to Cultured Cells

3.1.1. Detecting the complex

In order to validate the use of the complex in tissue culture, a method for detection of both the CTB and the Affimer had to be found. Anti-CTB antibodies are available commercially, thus facilitating the detection of CTB by immunohistochemistry, but no equivalent antibody currently exists that is selective for the Affimer scaffold. A range of detection methods were considered, such as using an anti-His tag antibody, or incorporating an epitope such as a FLAG tag, and using a corresponding antibody for detection. Initially, it was decided that chemical labelling of the Affimer with a fluorescent dye would be the best first approach, since it would allow for direct detection of the Affimer in cells.

A range of commercial fluorophores are now available for protein labelling, such as fluorescein, rhodamine, ATTO dyes, and Alexa Fluor dyes. A fluorophore was sought that was water soluble, bright, and with a minimal tendency to photobleach. Fluorescein and rhodamine are cheap fluorophores, but are known to be prone to photobleaching, whilst the ATTO dyes are more photostable, but less water soluble. Alexa Fluor dyes are expensive, but show good photostability and solubility, and were therefore selected to label Affimers 3A2 and 3C6.

The C-terminal cysteine residue provided an opportunity to label the proteins by reacting the thiol with a maleimide-derivatised Alexa Fluor (Alexa Fluor 555 C2 maleimide). Affimers were labelled, and purified by gel filtration chromatography. Successful labelling was verified by detection of a peak in absorbance at 555 nm (the excitation maximum for Alexa Fluor 555 that coincided with the peak in absorbance at 280 nm for the Affimers eluting at 12 – 14 mL (Figure 3.1) from a Superdex 75 Increase 10/300 gel filtration column.

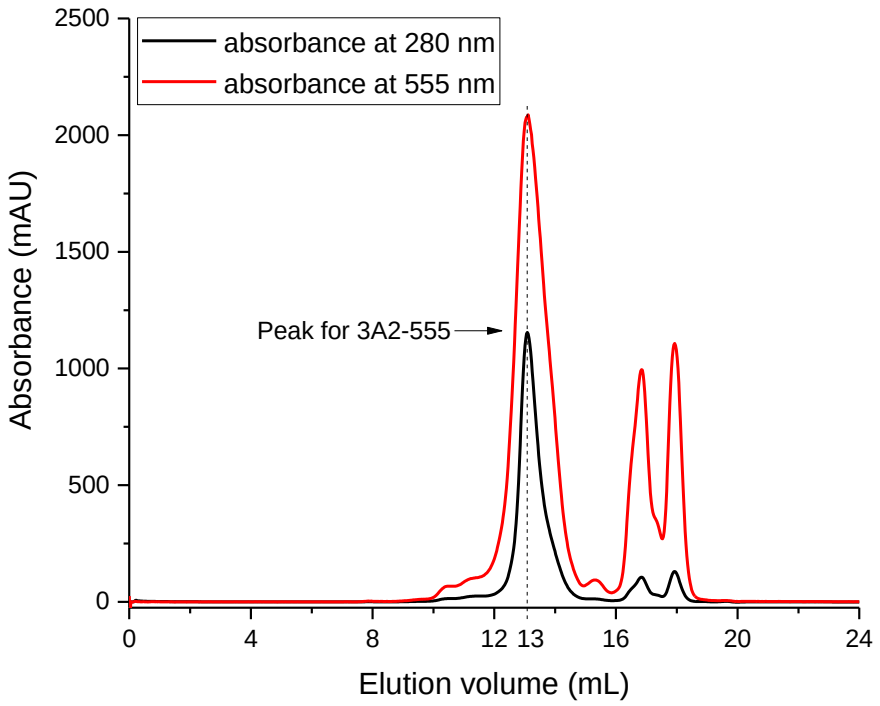

Figure 3.1. Gel filtration chromatogram generated following purification of a labelling reaction containing Affimer 3A2 and Alexa Fluor 555 C2 maleimide, with detection at 280 nm and 555 nm. Black arrow denotes peak formed from labelled 3A2-555, eluting with a retention volume of 13 mL on a Superdex 75 10/300 gel filtration column.

To show that the labelled Affimers still bound to CTB, Affimer 3C6-555 (Affimer 3C6 labelled with Alexa Fluor 555) was combined with CTB, and applied to a gel filtration column (Figure 3.2). Observation of a peak with strong absorbance at both 280 nm and 555 nm with an elution volume of ~10 mL indicated the successful formation of 3C6-555:CTB complex. Fractions corresponding to the peak were taken for analysis by SDS-PAGE, and prior to staining with Coomassie Blue, were imaged using a UV transilluminator (Figure 3.3). Capturing an image of the gel in this manner facilitated detection of the fluorophore attached to the Affimer. Analysis of the gel shows two bands present in both boiled and unboiled lanes, with the CTB pentamer dissociating into its monomeric form upon boiling, and a fainter band present just above ~14 kDa in both lanes that fluoresces following illumination with UV light. This analysis conclusively demonstrated that CTB and 3C6-555 co-eluted.

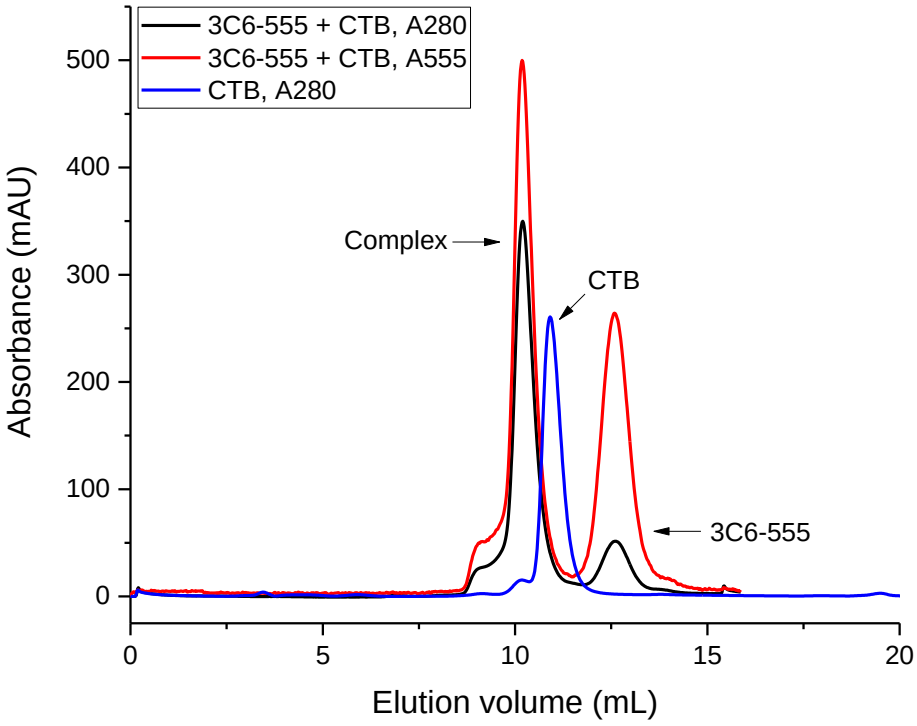

Figure 3.2. Gel filtration chromatogram generated following the purification of 3C6-555:CTB complex using a Superdex 75 10/300 GL gel filtration column, with detection at 280 nm (black) and 555 nm (red) absorbance. Arrows denote the complex formed and free unbound 3C6-555 (Affimer 3C6 labelled with Alexa Fluor 555). A chromatogram of CTB (blue) has been overlaid as a reference to show the shift in elution volume of the complex.

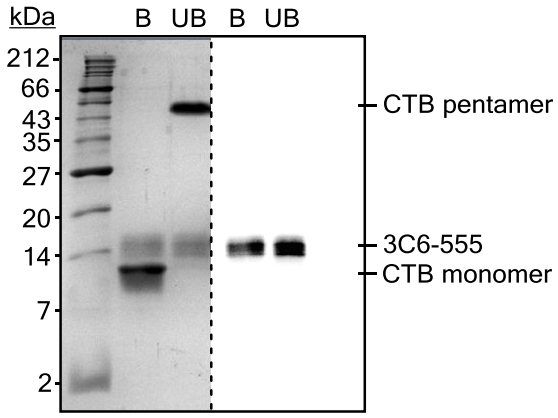

Figure 3.3. SDS-PAGE analysis of fractions corresponding to the peak formed by 3C6-555:CTB complex. Fractions were subjected to SDS-PAGE as boiled (B) or unboiled (UB) samples. Left – Coomassie-stained gel. Right – gel visualised using a UV trans-illuminator and colour-inverted for comparison to detect the Alexa Fluor 555 conjugated to the Affimer.

3.1.2. Selecting GM1-presenting mammalian cells

With a fluorescent CTB:Affimer complex at the ready, application to mammalian cells was the next step. In order for cell entry to be successful, the cell line had to express GM1 ganglioside at the surface of the plasma membrane. Two cell lines were available that matched these criteria; Human Embryonic Kidney 293 (HEK293) cells, and African Green Monkey kidney epithelial (Vero) cells. Both cell lines have been used successfully for studying the cholera toxin,[229,230] but distinguishing specific organelles in HEK293 cells is more challenging due to a large nucleus occupying much of the cell volume. Vero cells, meanwhile, have smaller nuclei relative to the size of the cell, making visual analysis of cells much more straightforward.

3.1.3. Delivering the complex to cultured cells

Vero cells were cultured and seeded onto glass coverslips for testing with the 3C6-555:CTB and 3A2-555:CTB complex. Both complexes were added to the cell medium at a final concentration of 750 nM, well above K_d for 3C6, but slightly below that for 3A2. Additional sets of cells were prepared, and treated with the fluorescently labelled Affimers alone at the same concentration, to ensure that the Affimers were not able to enter the cells in the absence of CTB. Following treatment, cells were incubated for six hours to allow complex internalisation and retrograde trafficking within the cell. Cells were processed by treatment with acetic acid to remove any protein still associated with the plasma membrane, and paraformaldehyde was added to preserve the cells in a 'fixed' state. A rabbit anti-CTB primary antibody was added to the cells, followed by a donkey anti-rabbit secondary antibody conjugated to Alexa Fluor 488. DAPI nuclear stain was added to the cells, which were then mounted onto microscope slides, and imaged by confocal microscopy (Figure 3.4).

CTB was readily detected immunohistochemically, appearing to be dispersed throughout the cells, but absent in the nucleus, and more concentrated in discrete puncta in an area directly adjacent to the nucleus. The localisation and distribution of these discrete 'clumps' of CTB are consistent with the morphology of the Golgi apparatus, with some halo formation surrounding the nucleus, more indicative of localisation to the endoplasmic reticulum (ER). CTB is known to enter recycling endosomes, and be transported to the *trans*-Golgi network from the cell surface, resulting in accumulation of CTB in the Golgi apparatus.[231,232] Preliminary analysis of complex localisation therefore appears to agree with previous observations.

The fluorescence of the Alexa Fluor 555 tethered to Affimers 3A2 and 3C6 was detected directly only in cells treated with CTB-Affimer complexes, indicating that Affimer transport into cells was CTB-dependent. The fluorescence from both labelled Affimers overlays completely with the immunolabelled CTB, although the Affimer fluorescence is less widely dispersed than CTB. The difference in methods of detection may be responsible for the apparent discrepancy in the localisation of the two proteins. Detection by immunohistochemistry results in amplification of the CTB signal, with multiple primary antibodies binding to CTB, and multiple secondary antibodies binding to the primary antibody. Detection of the fluorescently-labelled Affimer meanwhile is a direct measure of the amount of labelled protein in the cells.

These results are consistent with the reported retrograde transport pathway of CTB.[231] In the case of the cholera toxin, GM1-binding and endocytosis are mediated by CTB alone, and are not dependent on the A1 and A2 subunits (*1.4.2. Mechanism of toxicity*).[233,234] Once internalised, the toxin is trafficked to the ER via the *trans*-Golgi network.[235] The A2 subunit harbours a four residue C-terminal ER-retention signal sequence, the so-called 'KDEL sequence', resulting in the retention of the toxin in the ER through association with the membrane-associated ERD2.[236,237] ERD2 itself cycles between the *cis*-Golgi and the ER, a process that also leads to anterograde transport of the cholera toxin between the Golgi and ER.[238] Removal of the KDEL sequence does not prevent the holotoxin from penetrating the ER, but does lead to a reduced efficiency in toxin action, as less accumulates in the ER.[151,239]

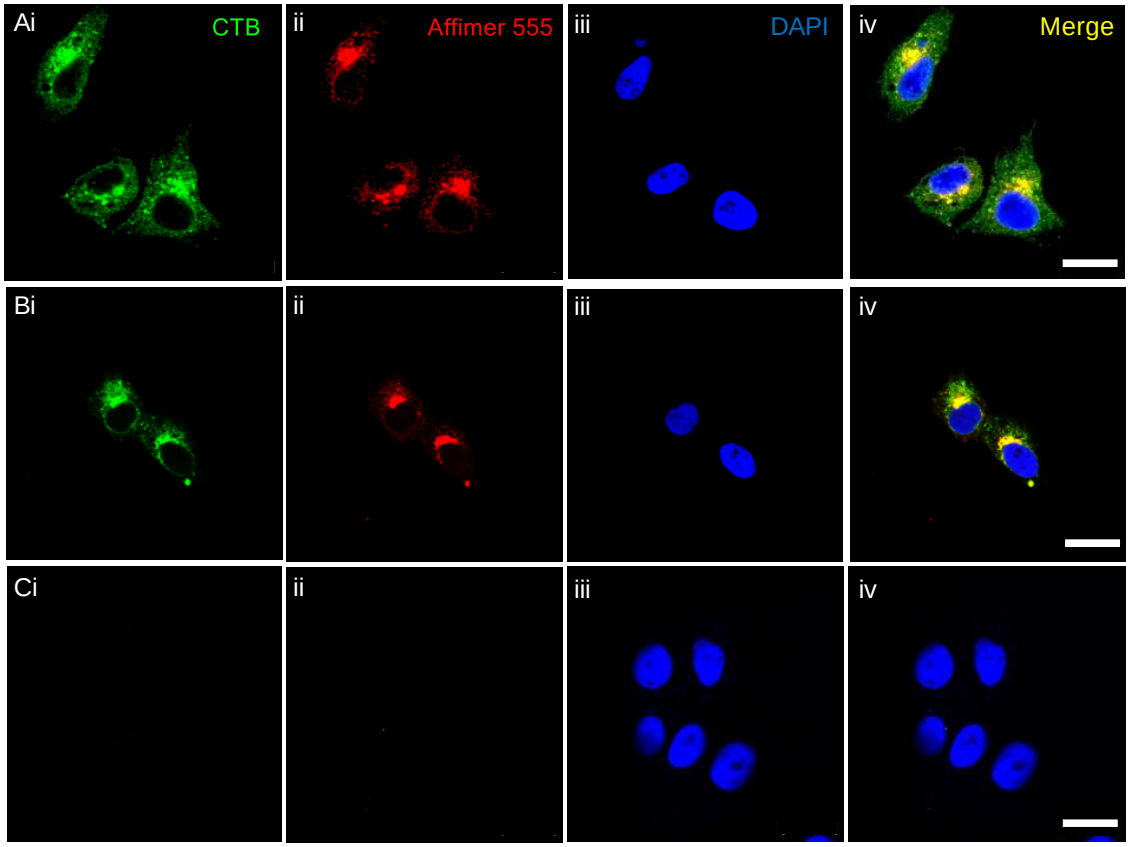

Figure 3.4. Vero cells incubated with **(A)** 3C6-555 + CTB, **(B)** 3A2-555 + CTB, **(C)** 3C6-555 only, at 750 nM, fixed after six hours, and immunolabelled for CTB (panel **i**) and DAPI (panel **iii**). Alexa Fluor 555 fluorescence is detected in panel **ii**. Scale bars are 20 µm.

Accumulation of CTB in the Golgi apparatus, with some detection of CTB in the ER, as observed in Figure 3.4 was therefore to be expected.

To investigate whether localisation of the Affimer could be modified, a KDEL sequence was inserted at the Affimer C-terminus (*7.2.3. Affimer protein sequences*). The Affimer was expressed, purified (Figure 3.5), and then labelled with Alexa-Fluor 555.

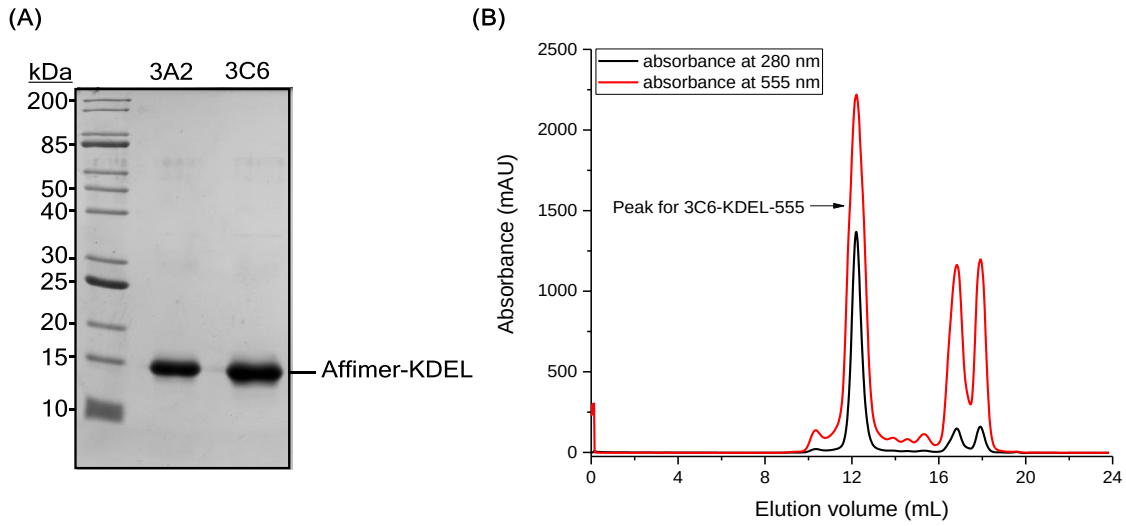

Figure 3.5. (A) SDS-PAGE analysis of purified Affimer-KDEL. **(B)** Purification of Alexa Fluor 555-labelled Affimer 3C6-KDEL using a Superdex 75 Increase 10/300 GL gel filtration column.

Affimers 3C6-KDEL-555 and 3A2-KDEL-555 were combined with CTB, and added to seeded Vero cells at 750 nM, and after six hours, were fixed, immunostained, and visualised, as before (Figure 3.6).

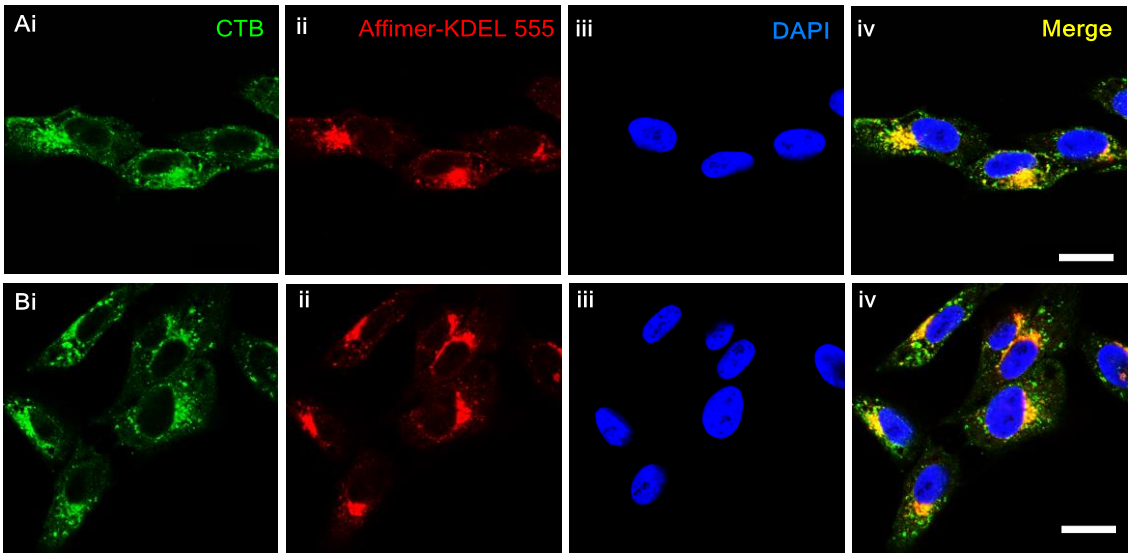

Figure 3.6. Vero cells incubated with **(A)** 3A2-KDEL-555 + CTB, **(B)** 3C6-KDEL-555 + CTB at 750 nM, fixed after six hours, and immunolabelled for CTB (panel **i**), imaged for Alexa Fluor 555 fluorescence (panel **ii**), DAPI (panel **iii**), and finally the signals were combined in panels **iv** to form a merged image. Scale bars are 20 µm.

Both CTB and Affimer-KDEL were successfully detected, but with little change in the localisation. The morphology still appears to be Golgi-like, suggesting that the KDEL sequence is not interacting with the KDEL receptor for retention in the ER. Returning to the example of the cholera toxin, the KDEL sequence of the A2 subunit faces the membrane, and is thus able to form interactions with the membrane-associated KDEL

receptor. Since both CTB-binding Affimers are thought to associate with the non-binding face of CTB, CTB-bound Affimers may be less likely to form the necessary interactions with ERD2 for ER-retention. Therefore, it is likely that the Affimers are still bound to their target once inside the cells.

3.1.4. Labelling CTB for direct detection

In order to visualise both the Affimer and CTB by direct detection, thereby making the fluorescent signal from both proteins comparable, CTB was labelled at the N-terminus with an aminooxy Alexa Fluor 488 (Figure 3.7).

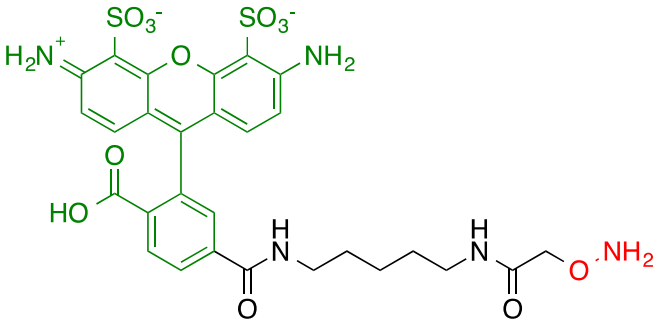

Figure 3.7. Chemical structure of aminooxy Alexa Fluor 488. Alexa Fluor 488 shown in green. Aminooxy functional group shown in red.

The pentamer was oxidised as described previously (*2.1.2. CTB oxidation and modification*), and combined with two equivalents of the fluorescent label per pentamer. After labelling, the complex was purified by gel filtration chromatography (Figure 3.8).

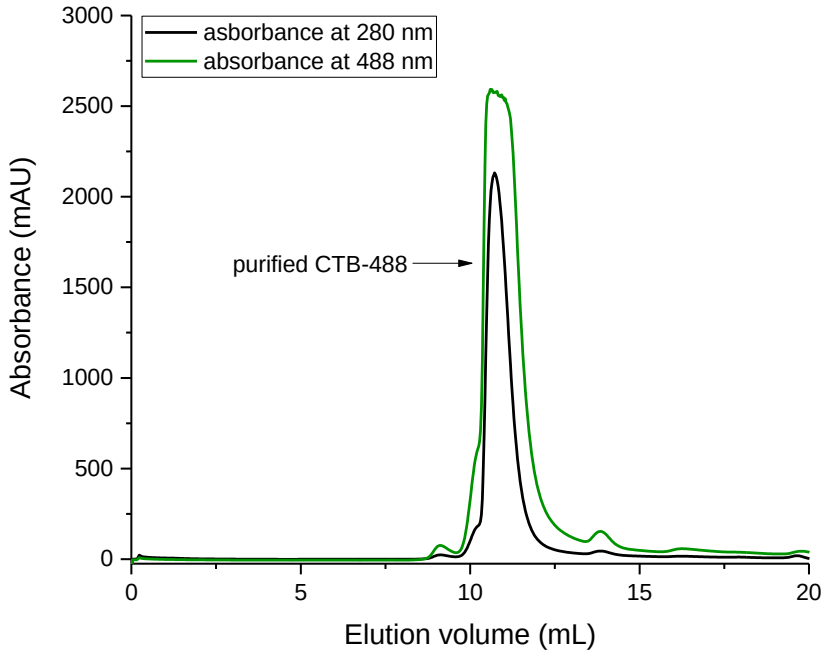

Figure 3.8. Purification of CTB-488 by gel filtration chromatography (Superdex 75 Increase 10/300 GL), with detectors set at 280 nm and 488 nm to detect elution of protein and Alexa Fluor 488.

Following purification, the number of fluorophores per CTB pentamer was calculated using the following equation provided by Thermo Fisher Scientifc:

$$Concentration\ of\ protein = (A_{280} - (A_{494} \times 0.11))/Extinction\ coefficient\ of\ protein$$

Calculation of the concentration of labelled CTB was then used to infer the number of moles of dye per mole of protein.

$$Moles\ of\ dye\ per\ mole\ of\ protein = (A_{494})/(71{,}000\ \times concentration\ \ of\ protein)$$

This calculation revealed that each pentamer on average was labelled with 3 – 4 Alexa Fluor dyes (3.66).

Now that each binding partner was labelled with a fluorophore, both proteins could be detected in tissue culture by direct detection. Additionally, however, fluorescence-based assays, such as Förster resonance energy transfer (FRET), could be possible. FRET occurs when a donor fluorophore enters an excited state, and transfers its energy non-radiatively to an acceptor fluorophore, resulting in excitation of the acceptor, and thus fluorescence at the emission wavelength of the acceptor.[240] FRET will only occur if the donor and acceptor are within a defined distance (10 – 100 Å), with the distance at which energy transfer is 50% efficient being termed the Förster radius.[241] This distance is dependent on various spectral properties of the donor and acceptor fluorophores, but

has been calculated for the FRET pair Alexa Fluor 488 and Alexa Fluor 555 as 70 Å. The FRET efficiency varies with the separation distance, as defined by the following equation:

$$E = \frac{1}{1 + (r/R_0)^6}$$

Equation 3.1. The relationship between FRET efficiency (E), the separation distance between the fluorophore pair (*r*), and the Förster radius (R_0).

By overlaying the crystal structures for an Affimer protein and CTB, and arranging the Affimer in a position in which it is likely to be orientated in the case of 3C6 and 3A2 binding to CTB, an approximate distance between the termini can thus be measured (Figure 3.9). Since neither fluorophore label contains an interspacing PEG linker, the fluorophores will be located close to the site of modification. Thus using Equation 3.1, together with an average of the measured separation distances between the termini of the complex, an approximate FRET efficiency of 66% can be calculated. This technique could thus be applied to the Affimer-CTB system to determine if the two proteins are interacting.

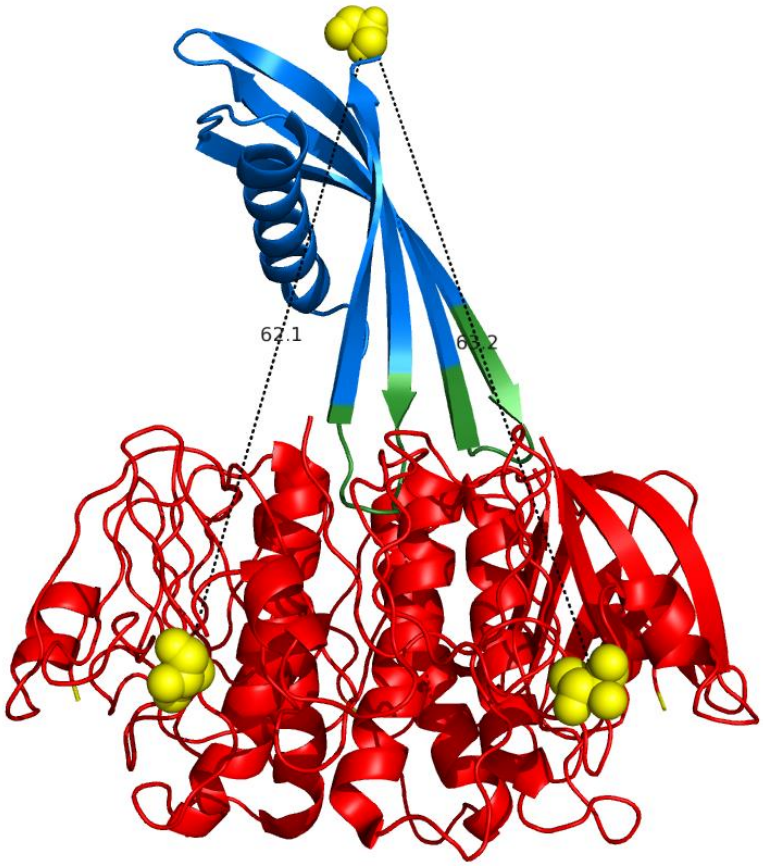

Figure 3.9. An overlay of crystal structures for CTB (red) and an Affimer protein (5A0O) (blue), with distances measured (yellow) between two of the N-termini of CTB and the C-terminus of the Affimer protein (62 Å and 63 Å).

Preliminary FRET experiments were carried out by using a fluorescence spectrophotometer to excite CTB-488 (300 – 440 nM) at 490 nm, and the emission spectrum measured. An emission maximum at 517 nm was observed to the CTB-488 (Figure 3.10 and Figure 3.11). A concentrated sample of Affimer-555 was then added to give a final concentration of 400 – 500 nM. Excitation of the sample once more at 490 nm led to a decrease in the fluorescence intensity at 517 nm as expected, corresponding to the loss in energy that is transferred to the acceptor fluorophore. This decrease in intensity at 517 nm was accompanied by a small increase in fluorescence intensity at the emission maximum for Alexa Fluor 555 (565 nm).

It had been initially planned to use FRET to assess whether the proteins are complexed in cells *ex vivo* and *in vivo*. Whilst the FRET change is measurable *in vitro*, it is unlikely to be sufficient for FRET microscopy on cells *in vivo*. The small FRET change observed suggests that the fluorophore separation distance is greater than calculated.

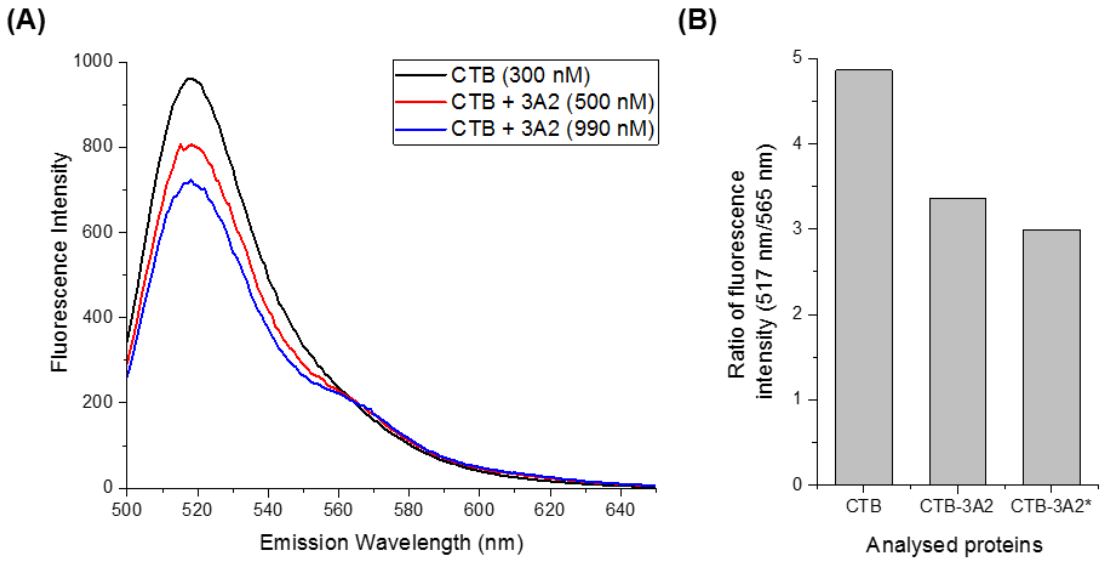

Figure 3.10. (A) Emission spectrum of 300 nM CTB-488 in the presence of either no Affimer, 500 nM 3A2-555, or 990 nM 3A2-555. **(B)** Bar chart showing the ratio of fluorescence intensity at 517 nm and 565 nm for 300 nM CTB-488 in the presence of no Affimer (CTB), 500 nM 3A2-555 (CTB-3A2), or 990 nM 3A2-555 (CTB-3A2*). All data has been adjusted factoring in the fluorescence spectra and ratio of fluorescence intensity in the absence of CTB-488 (control fluorescence subtraction).

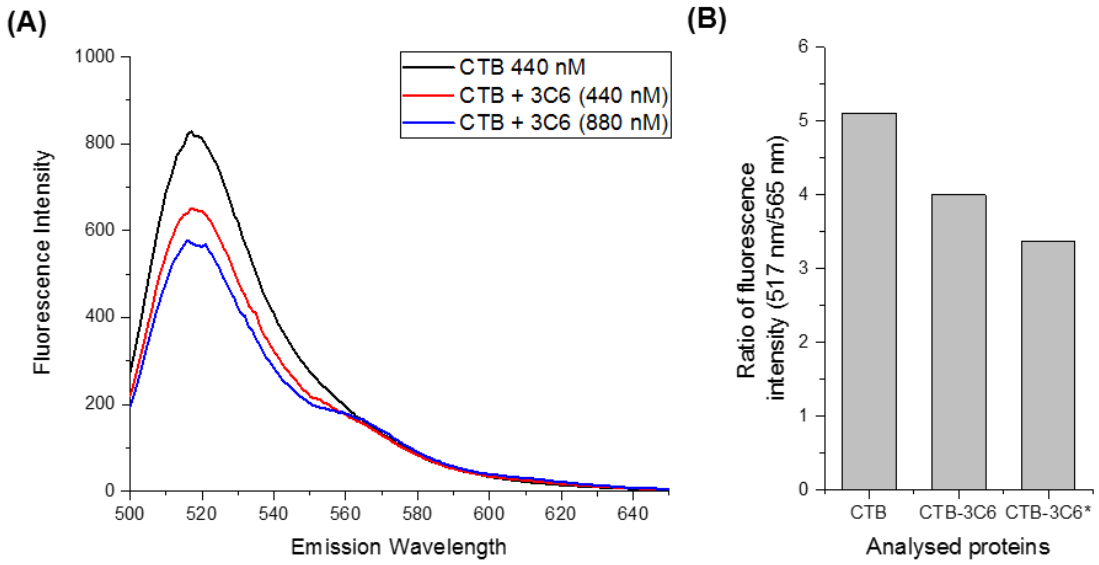

Figure 3.11. (A) Emission spectrum of 440 nM CTB-488 in the presence of either no Affimer, 440 nM 3C6-555, or 880 nM 3C6-555. **(B)** Bar chart showing the ratio of fluorescence intensity at 517 nm and 565 nm for 440 nM CTB-488 in the presence of no Affimer (CTB), 440 nM 3C6-555 (CTB-3C6), or 880 nM 3C6-555 (CTB-3A2*). All data has been adjusted factoring in the fluorescence spectra and ratio of fluorescence intensity in the absence of CTB-488 (control fluorescence subtraction).

3.1.5. Establishing a minimum concentration

Interestingly, in cell culture experiments testing 3A2-555 with CTB, internalised Affimer was still readily detected, despite the tested concentration (750 nM) being below K_d for the 3A2-CTB interaction. The Alexa Fluor dyes are particularly bright fluorophores, and therefore it is likely that only a fraction of the Affimer needs to be internalised for detection to be possible. However, determining a minimum concentration of complex required for detection of internalised Affimer, and thereby determining the limits of the system in tissue culture, would provide important information. A range of concentrations from 500 nM to 15 nM of complex were tested with both Affimers against Vero cells, and visualised after six hours (Figure 3.12). Since Alexa Fluor-labelled CTB was used (CTB-488), direct detection was possible for both of the complex components.

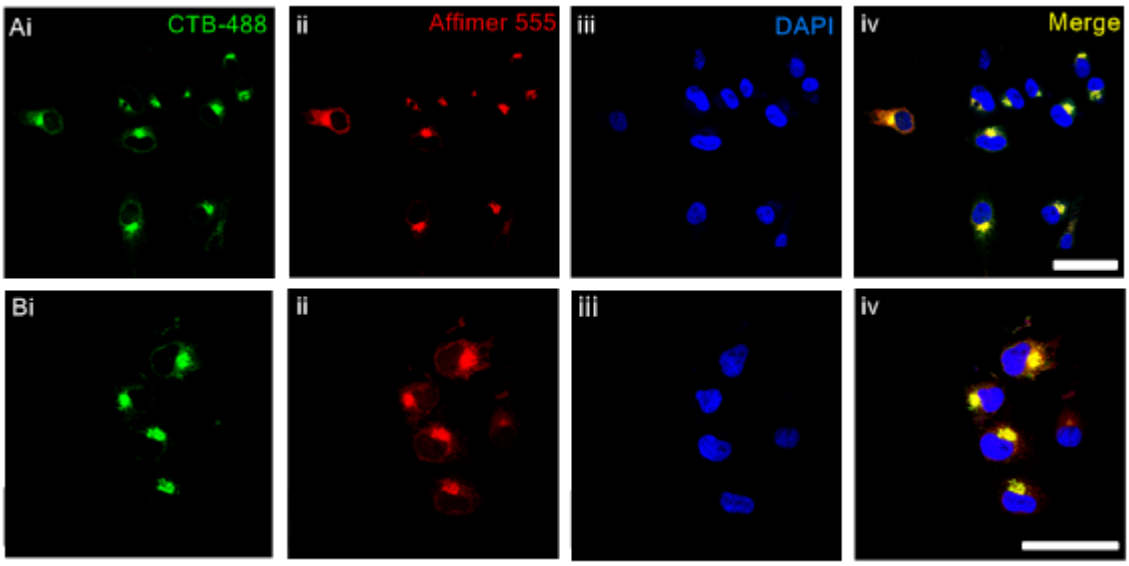

Figure 3.12. Vero cells treated with **(A)** 15 nM CTB-488 + 3C6-555 complex **(B)** 175 nM CTB-488 + 3A2-555 complex. Cell were excited at 488 nm to detect CTB-488 (panels i), 555 nm to detect Affimer-555 (panels ii), and 358 nm to detect the DAPI-stained nuclei (panels iii). The detected signals were compiled into a final merged image (panels iv). Scale bars are 50 µm.

The minimum concentration of 3A2-555-CTB complex required before a noticeable decrease in fluorescence at 580 nm was observed was 175 nM. Fluorescence was still visible at this wavelength at lower concentrations, however the intensity was visibly weaker, and was almost completely undetectable by 15 nM (Figure 3.13).

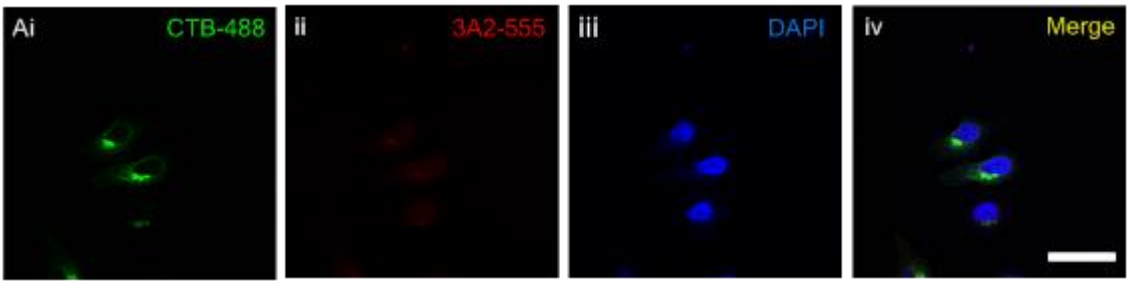

Figure 3.13. Vero cells treated with 15 nM CTB-488 + 3A2-555. Cell were excited at 488 nm to detect CTB-488 (panels i), 555 nm to detect Affimer-555 (panels ii), and 358 nm to detect the DAPI-stained nuclei (panels iii). The detected signals were compiled into a final merged image (panels iv). Scale bar is 50 µm.

For Affimer 3C6, the minimum concentration tested was 15 nM, with little fluorescence decrease observed across the dilution series. Figure 3.14 shows an 80x magnification of Vero cells treated with 15 nM 3C6-555 CTB-488 complex. The two fluorescent signals overlay perfectly, and the clumps of fluorescence are localised in an area that is consistent with the morphology of the Golgi apparatus, indicating that even at lower concentrations, the complex is likely to still be assembled.

The ability for complex internalisation to take place at low concentrations perhaps reflects the rate at which the complex is endocytosed relative to the residency time of the complex. Once inside the vesicular system the complex will be maintained at relatively high concentration, and thus is less likely to dissociate.

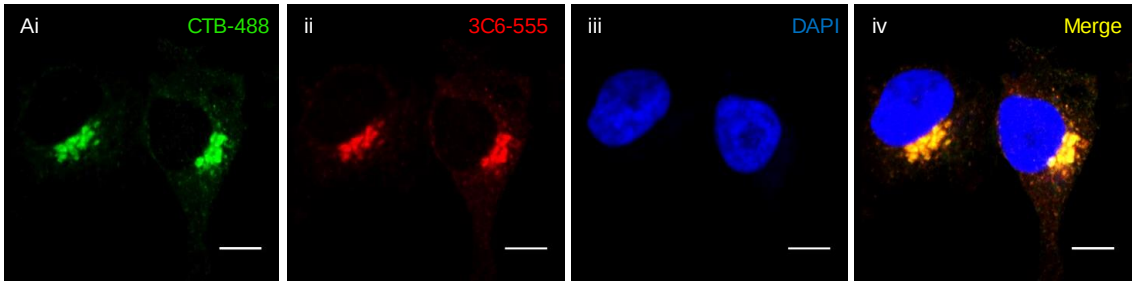

Figure 3.14. Vero cells treated with addition of CTB-488/3C6-555 complex to a final concentration of 15 nM, and stained with DAPI nuclear stain. See Figure 3.13 for panel information. Scale bars are 20 µm.

3.1.6. Delivering a cargo

Having delivered a chemical fluorophore to cells using the novel system, the next logical step was to tether a biological fluorophore to the Affimers, and test internalisation of the protein complex. Enhanced green fluorescent protein (eGFP) was thus selected as the first macromolecular cargo to be delivered by the complex.

Tethering the cargo to the Affimers by producing a fusion protein was the simplest strategy. To achieve this, Affimers were subcloned into pNIC-GFP (a vector for producing GFP fusion proteins, *appendix*), producing a fusion construct as shown in Figure 3.15.

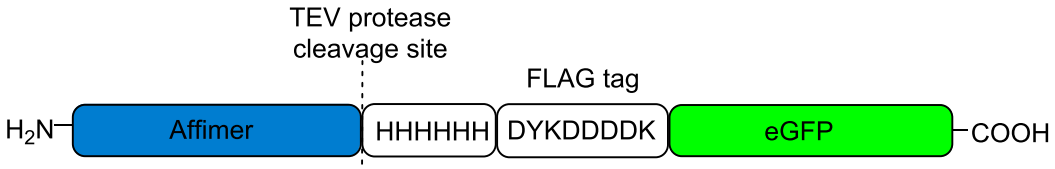

Figure 3.15. Schematic for an Affimer-GFP fusion construct. Affimer constructs are cloned into a vector containing the coding DNA sequence for eGFP preceded by a TEV protease cleavage site, a 6HIS tag, and a FLAG tag.

The peptide sequence intersecting the Affimer and eGFP subunits carried a TEV protease site, a 6HIS tag, and a FLAG tag. The TEV protease cleavage site would allow separation of the Affimer from eGFP using TEV protease leaving the Affimer without any purification tags. This tag-free Affimer could potentially be used in crystallisation studies with CTB. The 6HIS tag provided a method to purify the protein, with the entire intersecting peptide sequence acting as a linker, or buffer, to separate the Affimer from eGFP.

Both 3C6-eGFP and 3A2-eGFP were expressed, purified, and analysed by SDS-PAGE and gel filtration (Figure 3.16). A band was observed at 43 kDa, corresponding to the fusion protein, which was calculated to have a mass of 42.7 kDa. The presence of a single large peak that absorbed at 280 nm and 488 nm by gel filtration further confirmed the identity of the purified fusion protein.

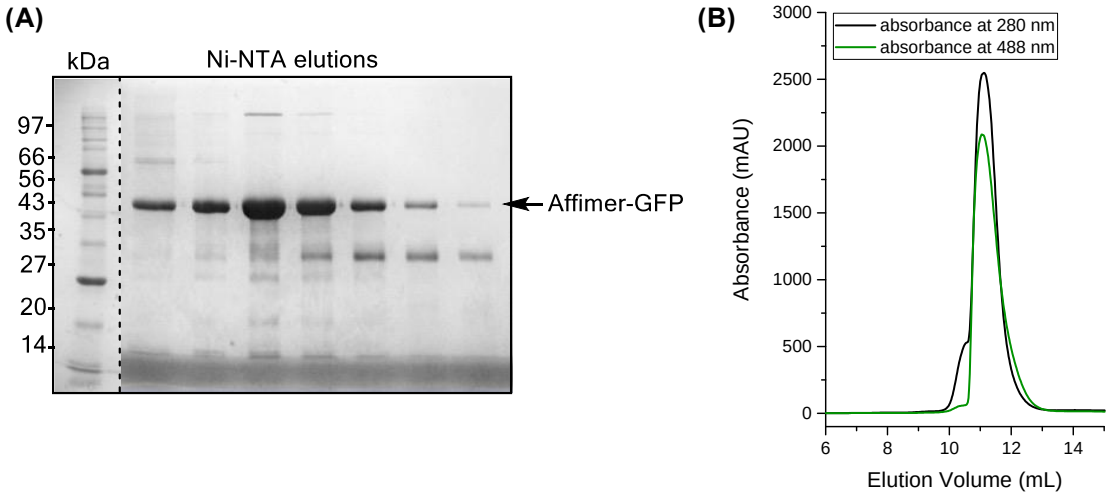

Figure 3.16. (A) SDS-PAGE analysis of 3A2-GFP fusion protein purified by Ni-NTA affinity chromatography. A band electrophoresing at ~43 kDa corresponds to purified 3A2-GFP **(B)** Purification of 3C6-GFP by gel filtration, with absorbance measurements at 280 nm and 488 nm.

Since a large protein cargo had been tethered to the Affimer, it was important to discern whether this interfered with the ability of the Affimer to bind to CTB. Gel filtration was used once more to establish whether complex formation was possible with this novel fusion protein. 3A2-eGFP was combined with CTB, and passed down a gel filtration column. A clear shift in peak elution was observed on addition of the CTB to the 3A2-eGFP, indicative of binding (Figure 3.17).

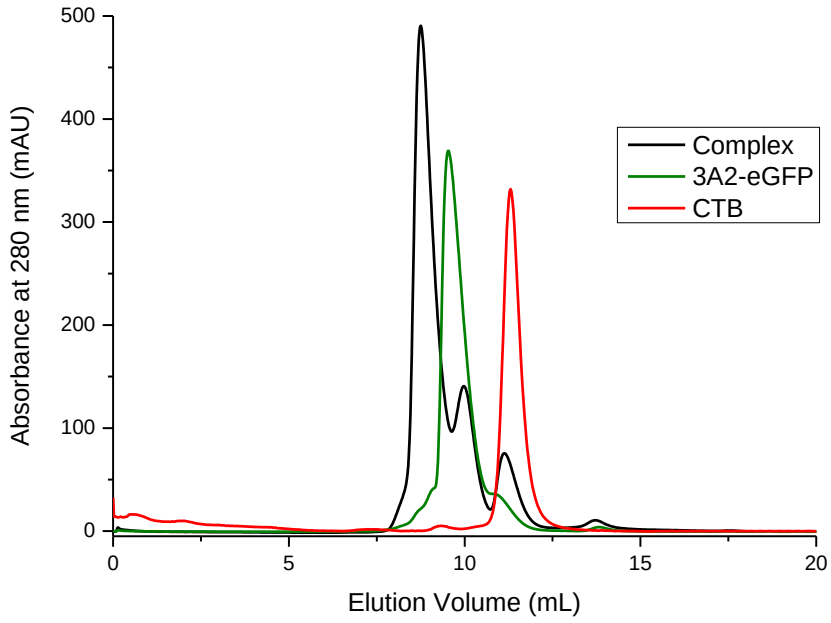

Figure 3.17. Purification of 3A2-GFP + CTB complex by gel filtration. Traces for 3A2-GFP (green) and CTB (red) are overlaid for reference.

SDS-PAGE analysis of the fractions corresponding to the major peak revealed that it was composed of both 3A2-eGFP and CTB, indicating that the complex had successfully formed (Figure 3.18).

Application of the newly formed complex to Vero cells revealed that the system could successfully transport a macromolecular cargo intracellularly (Figure 3.19). However, the fluorescence of the eGFP could not be detected directly, and required signal amplification by using an anti-GFP antibody, and a secondary antibody conjugated to Alexa Fluor 488. This difficulty in detection of GFP fluorescence was likely due to the fixing process. Using a strong fixing agent such as paraformaldehyde results in extensive crosslinking of the cellular contents, which could lead to loss of fluorescence.

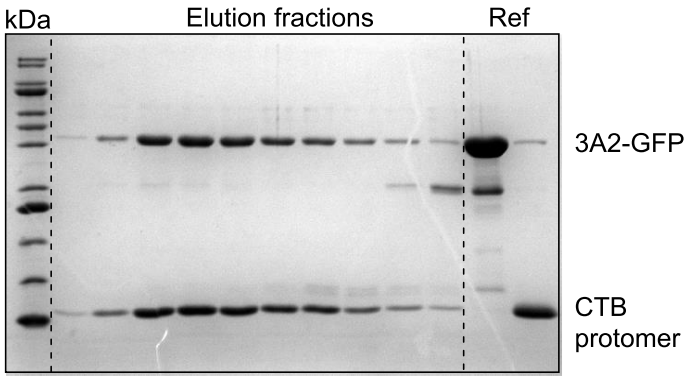

Figure 3.18. Analysis of elution fractions corresponding to the peak formed following complexation of 3A2-GFP + CTB (Figure 3.17) by SDS-PAGE, with uncomplexed 3A2-GFP and CTB included for comparison (Ref).

The GFP and CTB appear to be colocalised in a defined area of the cell, forming a cluster adjacent to the nucleus. The staining pattern is similar to the pattern observed in cells treated with CTB and Affimer-555, indicating that the protein cargo is not dramatically altering the localisation of the complex.

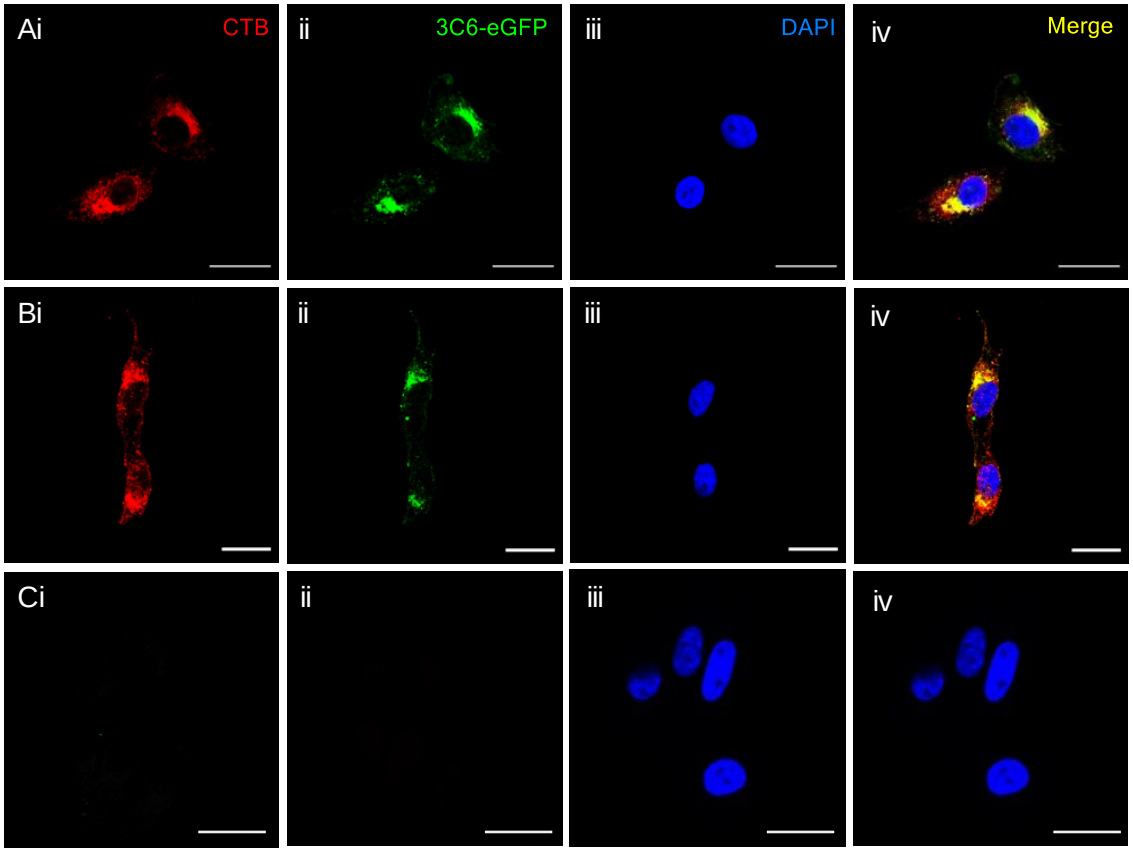

Figure 3.19. Vero cells tested with **(A)** 400 nM 3A2-eGFP + CTB **(B)** 400 nM 3C6-eGFP + CTB **(C)** 3C6-eGFP alone. Cells were immunolabelled with anti-CTB (red) (panels i) anti-GFP (green) (panels ii), DAPI stain (panels iii) and merged (panels iv). Scale bars are 20 µm.

3.2. *in vivo* delivery of the complex

3.2.1. Overview

Having effectively validated the complex in cultured cells by demonstrating that the system is able to deliver a small molecule such as an Alexa Fluor, as well a larger biological molecule such as GFP, the next step was to demonstrate function in an animal model.

As discussed previously, CTB has been used extensively as a neuronal tracer due in part to the abundance of GM1 ganglioside presented at the neuronal surface, but also due to the efficient uptake and transport of CTB into neurones in both the peripheral and central nervous systems.[36,128,172] The receptor for CTB has been found to be particularly enriched in motor neurones, although CTB uptake into sensory neurones is also well documented.[37] Hirokawa *et al.* demonstrated that CTB could be used to identify subsets of motor neurones responsible for innervation of a particular muscle.[242] Following administration of CTB into the calf muscle of rats, they showed that CTB could be detected immunohistochemically in the anterior horn of the spinal cord 72 hours after injection. CTB thus has the ability to penetrate the central nervous system following peripheral administration.

Several studies have shown that administration of CTB conjugated to HRP into the tongue of a range of animals resulted in retrograde transport of CTB into the motor neurones of the brainstem; specifically, a region known as the hypoglossal nucleus.[127,172,243] This region of the brainstem contains the cluster of cell bodies of the hypoglossal nerve which is the bundle of motor neurones responsible for innervation of the tongue. Figure 3.20 shows an immunolabelled cross-section of a brainstem of a mouse injected in the tongue (paralingually) with CTB. In the higher magnification frame the cell bodies of the neurones can be seen. Immunolabelling of CTB in the cell bodies demonstrates that CTB effectively bypasses the blood-brain barrier following peripheral injection, and undergoes retrograde transport (towards the cell body, *c.f.* anterograde transport, towards the synapse).

Administration of CTB into the abdominal cavity also results in extensive labelling of the hypoglossal nucleus, as well as other regions within the brainstem and spinal cord.[172] The latter route for administration of the CTB-Affimer complex was deemed unsuitable, since the complex would likely dissociate before neuronal uptake, or would be taken up in quantities too dilute to detect. Paralingual administration, by contrast, has two key

advantages. 1) It would allow selective labelling of the hypoglossal nucleus, localising the complex to a subset of neurones; 2) injection of the complex directly into a muscle would maximise the probability of it being endocytosed rapidly prior to dissociation and separation of the component parts.

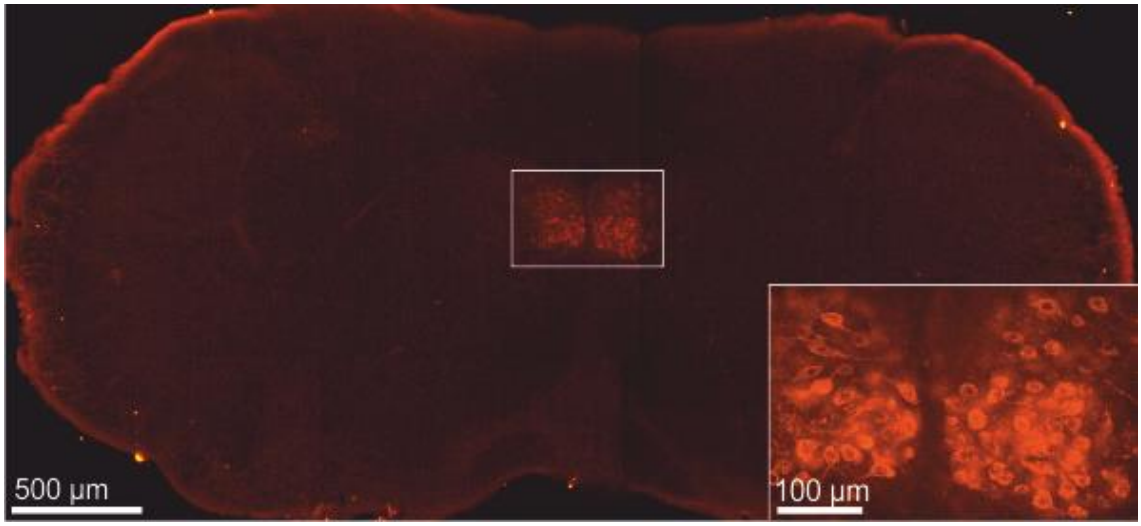

Figure 3.20. Cross-section of the brainstem of a mouse injected paralingually with 80 µg CTB and sacrificed after 72 hours, then immunolabelled with an anti-CTB antibody and a fluorescent secondary antibody to facilitate CTB detection. White box denotes the location of the hypoglossal nucleus.[2]

3.2.1. Complex preparation

A caveat of using immunohistochemistry as a labelling technique is that large quantities of protein must be administered for antibody detection to be possible. This fact, in conjunction with the small volume (2 µl) that can be easily injected into the tongues of mice, required high concentrations of complex to be used. Complexes were prepared at a concentration of 50 µM in phosphate buffer, before lyophilisation for reconstitution at a concentration of 200 µM. Reconstitution of the complex in a smaller volume would alter the concentrations of the components of the phosphate buffer, resulting in a salt (NaCl) concentration of 800 µM.

To ensure that the effects of salt and lyophilisation did not impact complex formation, Affimers 3A2 and 3C6 were concentrated to 80 µM and lyophilised. The proteins were then reconstituted in water, to a concentration of 80 µM, and the concentrations were remeasured. The lack of observed precipitation, and the lack of change in the concentration indicated that Affimers were stable following lyophilisation and redissolution. The reconstituted Affimers were then complexed with CTB, and spiked with NaCl to a final concentration of 800 mM. Following a one hour incubation, the

[2] Figure reproduced, with permission, from Dr Jessica Haigh

complexes were analysed by gel filtration (Figure 3.21 and Figure 3.22). The ability of these proteins to assemble appeared to be unaffected by the changes in salt concentration.

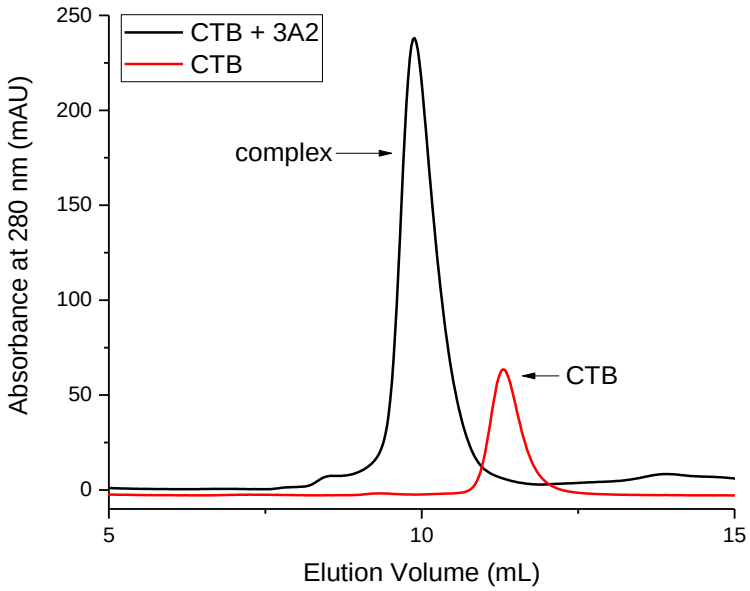

Figure 3.21. Analysis of 3A2-CTB complex integrity by gel filtration following protein lyophilisation, and in the presence of 800 mM NaCl.

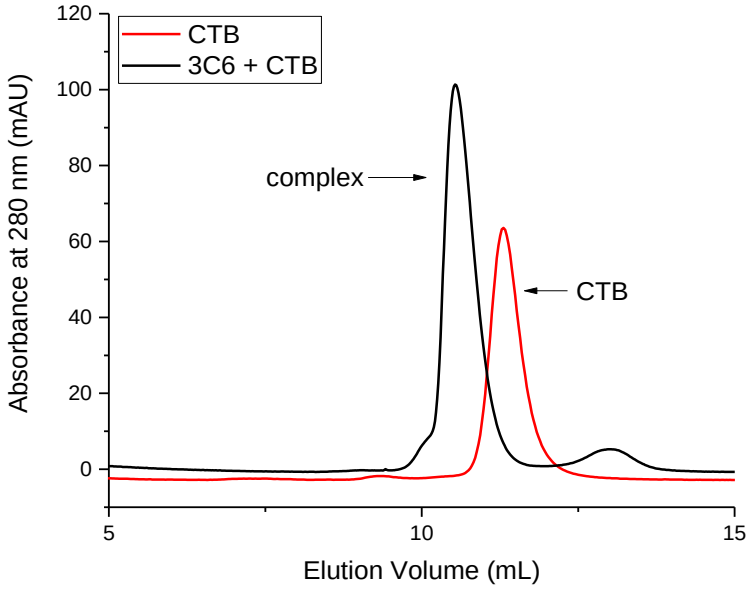

Figure 3.22. Analysis of 3C6-CTB complex integrity by gel filtration following protein lyophilisation, and in the presence of 800 mM NaCl.

After establishing that these factors would not affect complex formation, four mice (two control mice for Affimer only) were used for *in vivo* administration of Alexa Fluor-labelled Affimers complexed to CTB. Complexes were prepared to 50 µM, and reconstituted following lyophilisation to a concentration of 200 µM (~14 mg mL^{-1}). 2 µl was then injected paralingually into the mice, which were then sacrificed after 24 hours. Cross-sections of the brainstem were taken and stained for CTB. *All handling of live animals in this project was carried out by either by Professor Jim Deuchars, or Dr Jessica Haigh, who also dedicated a lot of time into helping me with animal dissections*. See *6.7.2. In Vivo Experimentation* for ethical arrangements for the animals and methodology.

Affimer 3A2-555 was readily detected when administered with CTB, but not when administered alone (Figure 3.23). CTB was readily detected, with some hypoglossal cells staining positive for CTB, for not for 3A2-555. Transport of 3A2-555 is clearly CTB-dependent, however. No fluorescence could be detected in mice injected with Affimer 3A2-555 alone (Figure 3.23Bi), indicating that none of the Affimer was internalised in the absence of CTB. 3A2-555 fluorescence was broadly dispersed throughout 3A2-positive cells, with little 3A2-CTB colocalisation observed (Figure 3.23A).

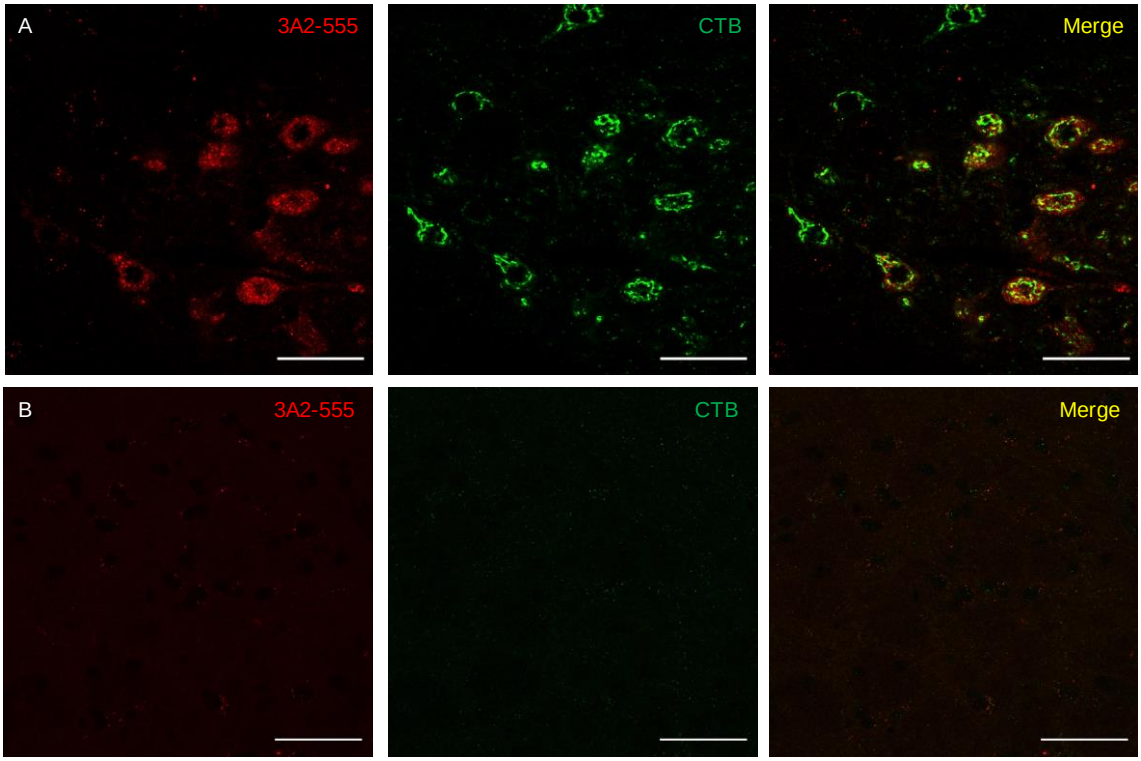

Figure 3.23. Magnified cross-sections of the brainstem focusing on the hypoglossal nucleus showing **(A)** mice injected paralingually with 3A2-555 + CTB **(B)** mice injected paralingually with 3A2-555 alone. Left hand panels show the tissue sections excited at 555 nm to detect 3A2-555, middle panels show the tissue sections excited at 488 nm to detect the immunolabelled CTB, and the right hand panels are merged images. Scale bars are 50 µm for both sets of panels.

Affimer 3C6-555 was also very clearly observed in the cells of the hypoglossal nucleus, forming discrete rings around the cell nuclei that overlaid with staining for CTB (Figure 3.24). Few CTB-positive cells did not also contain 3C6-555. In the absence of CTB, very little fluorescence was detected, indicating that 3C6-555 is not taken up in any detectable capacity into the neurones of the hypoglossal nucleus.

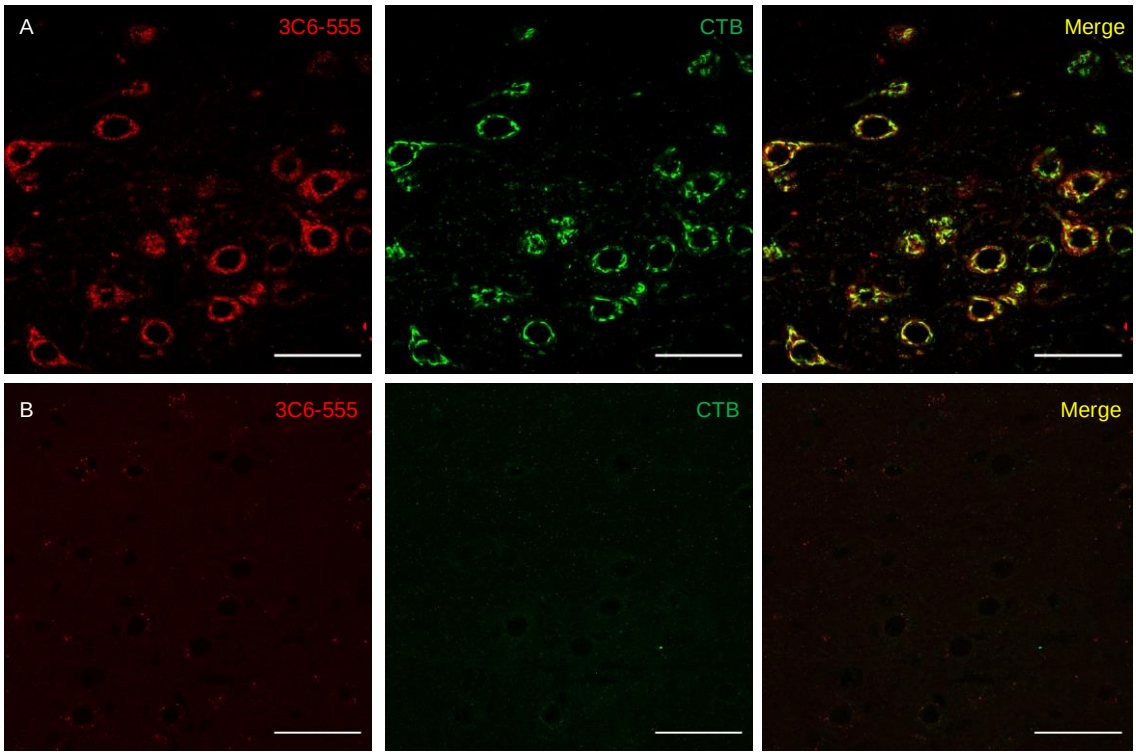

Figure 3.24. Magnified cross-sections of the brainstem focusing on the hypoglossal nucleus showing **(A)** mice injected paralingually with 3C6-555 + CTB **(B)** mice injected paralingually with 3C6-555 alone. Left hand panels show the tissue sections excited at 555 nm to detect 3A2-555, middle panels show the tissue sections excited at 488 nm to detect the immunolabelled CTB, and the right hand panels are merged images. Scale bars are 50 µm for both sets of panels.

Looking more closely at the Affimer-positive panels, the distribution of 3A2 and 3C6 are very different. 3A2 can be quite clearly seen to be distributed in small punctate spots throughout the cell, whilst distribution of 3C6 is much more ordered, with fluorescence detected as halos surrounding the cell nuclei (Figure 3.25). These halos of Affimer fluorescence overlay to a great extent with the detected CTB, indicating perhaps that 3C6 is still bound to its target once internalised, although some vesicle-like compartments positive for 3C6, but not CTB, can be seen (Figure 3.26). Fluorescence for 3A2-555 overlaid very poorly with CTB, suggesting that the complex had dissociated upon internalisation.

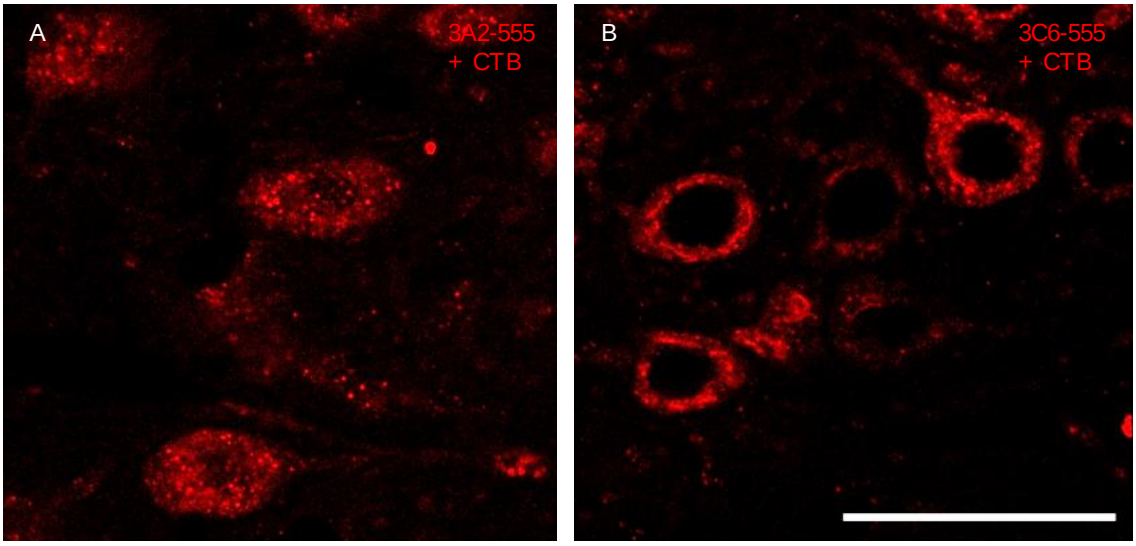

Figure 3.25. Magnification of cells of the hypoglossal nucleus in brainstem cross-sections for mice injected with (A) 3A2-555 + CTB (B) 3C6-555 + CTB showing exclusively the channel for Affimer fluorescence. Scale bars are 50 µm.

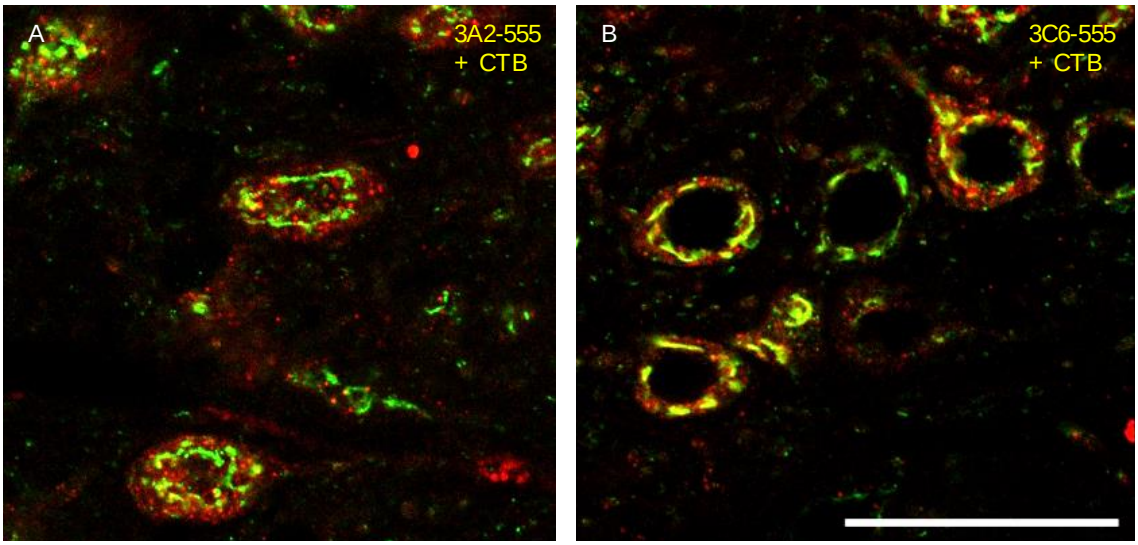

Figure 3.26. Magnification of cells of the hypoglossal nucleus in brainstem cross-sections for mice injected with (A) 3A2-555 + CTB (B) 3C6-555 + CTB, showing Affimer fluorescence overlaid with CTB labelling at 488 nm.

The CTB appears to be comparably distributed in both cases, forming discrete structures surrounding the nuclei, perhaps in the ER and Golgi, although further experiments using anti-ER and anti-Golgi antibodies would be required to confirm this.

The fluorescent vesicle-like compartments are likely to be lysosomal or endosomal vesicles targeting the Affimer for degradation. The lack of overlay between CTB labelling and Affimer fluorescence negates the possibility that these are vesicles travelling retrograde from the synapse. This observation indicates that the complex is dissociating,

or partially dissociating, inside the neurone, and the Affimer is then being sequestered inside endosomes for lysosomal degradation.

A further experiment to establish the longevity of the complex *in vivo* was carried out by administering the complex paralingually, and sacrificing the mice after one week. Few 3A2-555 positive cells were detected, with nearly all remaining fluorescence appearing clustered in punctate spots Figure 3.27A. 3C6-555, however, was readily detected in the hypoglossal nucleus, with much of 3C6-555 fluorescence overlaying with CTB fluorescence (Figure 3.27B). The dispersion of CTB in both samples appeared to be much more granulated.

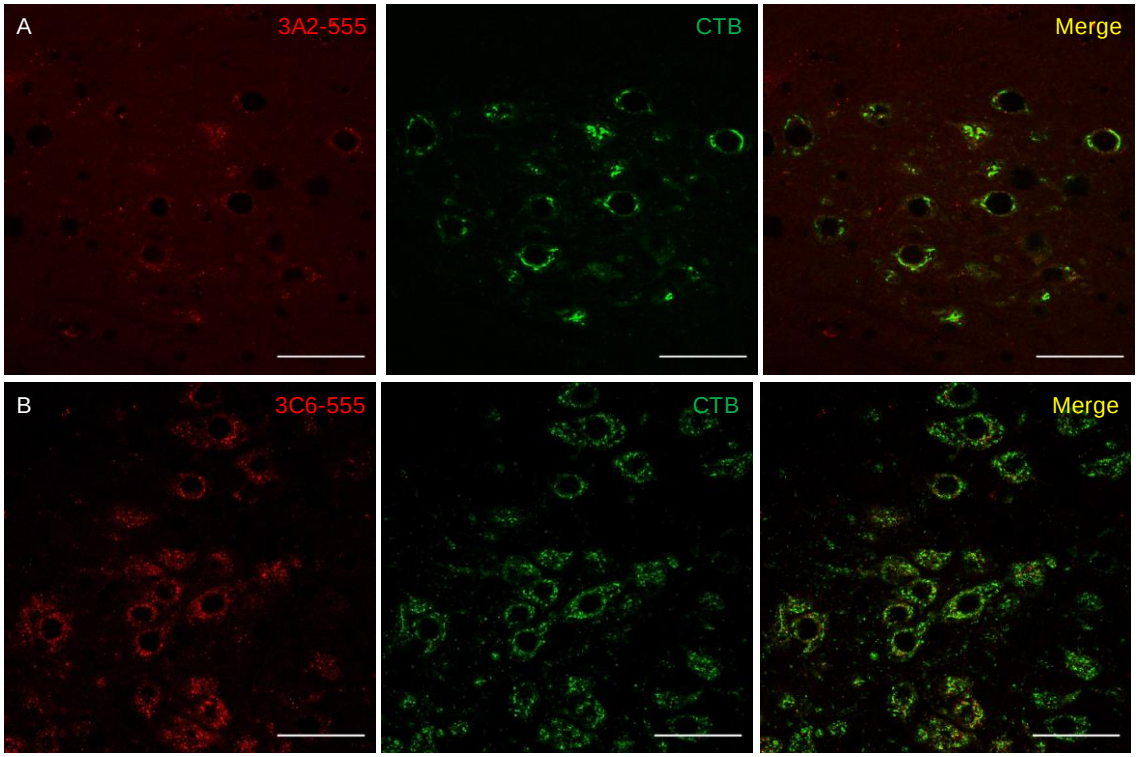

Figure 3.27. Cross-section of brainstems of mice injected paralingually with **(A)** 3A2-555 + CTB and **(B)** 3C6-555 + CTB. Mice were sacrificed one week following injections, with Affimer fluorescence detected at 555 nm (left hand panels), CTB detected by immunolabelling (middle panels), and with the images merged in the right hand panels. Scale bars are 50 µm.

3.3. Chapter Conclusions

The experiments outlined in this chapter were carried out to validate the ability of CTB to transport a CTB-binding Affimer attached to a cargo into motor neurones *in vivo*. The complex was initially tested in surface-adhered mammalian Vero cells, which express GM1 ganglioside, the receptor required for CTB endocytosis. Both the 3A2 and 3C6-CTB complexes were shown to be functional in this setting by labelling Affimers with a

fluorescent dye, and detecting them directly in cells by microscopy. The localisation of the complex after six hours appeared to be Golgi-like, and addition of an ER-retention signal sequence to the Affimers appeared to have no effect.

A minimum concentration required for observation of internalised Affimer was then established. After addition of as little as 175 nM complex to cells, 3A2-555 was still detectable after six hours. The lowest concentration of 3C6-555 tested was 15 nM, with fluorescence still clearly observable. Relating these minimum concentrations to the dissociation constants, for the two Affimer-CTB interactions, it is unsurprising that 3C6 was detected at concentrations lower than 3A2, since the K_d for the 3C6-CTB interaction is approximately 10-fold higher affinity than the 3A2-CTB interaction. Since the complex was applied to cells in a system in stationary liquid, the K_d would be assumed to be a more relevant indicator than k_{off} and k_{on} in terms of ability to enter cells, since any complex dissociating could rebind without being removed from the system. It was expected that the kinetics would play a more important role *in vivo*.

Affimer-GFP fusion proteins were then produced, and used to demonstrate that a large protein could be transported into mammalian cells in tissue culture by piggybacking onto CTB. GFP and CTB were both detected in cells and appeared to colocalise in a compartment of the Golgi apparatus. The staining was comparable to staining seen in cells treated with CTB and Alexa Fluor-labelled Affimer, suggesting that the presence of a larger protein did not drastically alter the localisation of the complex once internalised.

Both 3A2-555 and 3C6-555 were successfully transported into motor neurones by CTB, as evidenced by detection of Alexa Fluor 555 fluorescence, and detection of CTB by immunohistochemistry in the brainstems of treated mice. 3A2 appeared to be less efficiently delivered than 3C6, with fewer Affimer-positive fluorescent cells being detected for 3A2 than 3C6. Additionally, much of the 3A2 fluorescence did not overlay with CTB labelling, and was observed in vesicles that were broadly dispersed throughout the neurones. 3C6 fluorescence overlaid to a much greater degree with CTB, indicating that the complex was still intact. The higher affinity interaction therefore appeared to be more robust once internalised, whilst 3A2-CTB had more of a propensity to dissociate.

To determine conclusively whether Affimer and CTB were still in a bound state, CTB-488 + Affimer-555 could be complexed and delivered to motor neurones. FRET microscopy could then be used to image regions of the hypoglossal nucleus where FRET was taking place. Since FRET only occurs when an acceptor and donor fluorophore are within close

range to one another, this technique would reveal the extent of complexation within the tissue section. Preliminary experiments carried out using CTB-488 and Affimer-555 have already demonstrated that FRET is possible *in vitro* using this system, although the linker length may need to be optimised to achieve a larger change in FRET. Alternatively, a FRET pair with a larger Förster radius, such as Alexa Fluor 594 and Alexa Fluor 647, could be used to label the complex component proteins.

Dissociation once inside the neurone is desirable, since any tethered cargo could then be retargeted to a different cellular compartment. Some 3C6 fluorescence appeared to be localised to vesicular compartments, presumably lysosomes, although to a much lesser extent than 3A2. Importantly, lysosomal pH is 4.5 – 5.0, whilst the pH stability of Alexa Fluor 555 ranges from pH 4.0 – 10. The dye should thus remain visible once in endosomal and lysosomal compartments. One week after complex delivery, 3C6 could still be detected, whilst 3A2 was scarcely visible, indicating that the 3C6-CTB has a longer lifetime once inside neurones than 3A2-CTB. CTB labelling appeared to be more granular, and localised to vesicle-like structures, indicating that after one week, delivered CTB was beginning to be targeted for lysosomal degradation. Interestingly, much of the CTB seems to be colocalising with 3C6-555, suggesting that the complex may be still associated. 3C6-CTB could thus potentially be used to release cargos destined for organelles such as the lysosome at a slower rate than 3A2-CTB.

The lysosome itself is an attractive destination to target for research and for neurotherapies. Neuronal ceroid lipofuscinosis (NCL) is a rare genetic disorder caused by a defective copy of the gene encoding palmitoyl protein thioesterase (PPT). This enzyme catalyses the removal of palmitate fatty acyl groups from proteins during lysosomal degradation, but displays no activity in patients afflicted by NCL due to a mutation in the active site.[244,245] Delivery of a functional copy of this protein using the Affimer-CTB complex could therefore provide a therapeutic route to treat NCL.

Fewer Affimer-positive cells were detected in mice treated with 3A2-CTB than with 3C6-CTB. There are two potential explanations for this observation. The first explanation is simply that less 3A2-555 was internalised. Dissociation of the complex prior to endocytosis, and subsequent clearance of unbound Affimer by the circulatory system would lead to less of the protein being internalised, and thus less being detected. Experiments in tissue culture did show that 3C6-CTB was more readily taken up than 3A2-CTB, although this was only true at very low concentrations of complex. *In vivo* administrations of complex were carried out at 200 µM, 200-fold above K_d for the 3A2-

CTB interaction. The average 25 g mouse has a total blood volume of 1.46 mL.[246] Administered intravenously therefore, a 2 µl injection of 200 µM complex would result in a concentration of CTB and Affimer in the blood of 270 nM. At this concentration, internalisation of Affimer would be still expected. However, injections were carried out intramuscularly, and therefore the concentration would have been higher since administration was more localised. Furthermore, GM1 binding, and thus CTB endocytosis, is expected to occur rapidly *in vivo*, or at least faster than the measured dissociation rate for the 3A2-CTB interaction.

The second explanation is that more Affimer 3A2-555 has been degraded and cleared from the neurones, thus leading to a decrease in fluorescence. Once inside endocytosed vesicles, the complex presumably remains assembled, since both proteins would be confined into a limited space. Once reaching the organelles of the cell body, however, the complex would become more dilute, perhaps sufficiently dilute for the complex to dissociate and for clearance of the Affimer to commence. Detection of 3C6-555 one week after injection, but not 3A2, suggests that 3A2 is more readily cleared from the neurones than 3C6.

Both Affimers have thus been shown to be reliably transported into motor neurones by CTB, but displaying differing properties once internalised that are perhaps related to the affinity of the two interactions. Delivery of a cargo using the system has been demonstrated in mammalian cells in tissue culture, but not *in vivo*. The next phase of this project that is beyond the scope of the work prepared for this thesis would be to exemplify the novel system by delivery of GFP, or indeed other proteins, to motor neurones.

4. Developing a Cholera-Botulinum Toxin Chimera

4.1. An Introduction to BoNT-A, BiTox and the SNARE Complex

In the two previous chapters, CTB-binding Affimers were shown to be able to piggyback on CTB into motor neurones. This approach to protein delivery overcomes a safety barrier by allowing the components needed for this drug delivery system to be produced separately, and assembled directly before use, thereby minimising exposure to 'active' molecules.

The Davletov research group (University of Sheffield) have independently addressed this safety issue by developing a system that allows non-covalent assembly of the botulinum neurotoxin.[247,248] This novel method of protein assembly has been used to produce novel botulinum neurotoxins and botulinum-tetanus chimeras. In this chapter, I describe a collaborative project in which this approach was applied to generate a novel botulinum-cholera chimera capable of delivering botulinum protease to GM1-positive neurones.

4.1.1. Botulinum neurotoxin serotype A

As discussed in *1.3.1 Botulinum toxin*, botulinum neurotoxins (BoNTs) are a family of seven neurotoxin serotypes that share structural and functional similarities.[41,44,93] BoNT serotype A is the most common cause of botulism in humans, and also the most widely used BoNT serotype in medicine.[249–251] BoNT-A formulations are routinely used in the field of cosmetics, marketed under the brand name BOTOX.[79,252] Beyond cosmetics, however, BoNT-A is used to treat dystonias (muscle spasms).[251–253]

BoNT-A is expressed as a monomeric ~150 kDa protein composed of four distinct domains. The receptor binding domain (RBD) is a heterodimer, with each subunit recognising different receptors. The RBD is linked to the translocation domain (TD), a unit composed of two amphipathic α-helices that mediates translocation of a catalytically active zinc-dependent metalloprotease (CD) into the cytosol. The region tethering the catalytic domain to the translocation domain is cleaved by trypsin, leaving the two domains associated by a single conserved disulfide bond.

4.1.2. The SNARE complex

SNAP25 is a critical component of the SNARE complex, a coiled coil protein assembly (Figure 4.1) that drives synaptic vesicle fusion with the nerve terminal plasma membrane.

The components of the SNARE complex that mediate vesicle fusion are the α-helical polypeptides synaptobrevin (Syb), syntaxin-1 (Syx), and SNAP25. These protein components all share a conserved SNARE motif; a peptide sequence required for complex assembly.

Syb, Syx and SNAP25 assemble through the four SNARE motifs in a highly enthalpically favourable reaction to form an extremely stable four-helix bundle that is resistant to a range of detergents, chaotropic agents, high temperatures, and proteases, and whilst a non-covalent association, is effectively an irreversible process.[247,254,255] Indeed, the residence half-life of the SNARE complex has been estimated to be ~158 years, making the interaction one of the highest affinity protein-protein interactions known.[256] In neuronal cells, dissociation of the SNARE complex is an ATP-dependent process, requiring the efforts of the NSF ATPase.[257] Interestingly, cleavage of the C-terminal nine residues from SNAP25 by BoNT-A does not inhibit SNARE complex formation.[254] Synaptic vesicles are thought to still be recruited to the membrane following SNARE assembly, but in the absence of the C-terminal residues of SNAP25, vesicle fusion does not take place.[258,259]

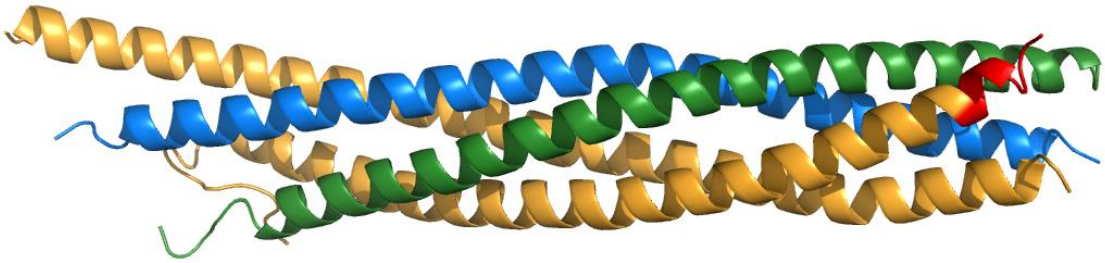

Figure 4.1. Ribbon representation of the crystal structure of the coiled coil SNARE complex. Synaptobrevin (green), syntaxin-1 (blue), and SNAP25 (orange) associate with each other to form a tightly packed coiled coil four-helix bundle. Shown in red are the nine C-terminal residues cleaved from the SNARE complex by BoNT-A catalytic domain leading to inhibition of SNARE-mediated vesicle fusion.

4.1.3. Stepwise assembly of a multimodular medicine

The Davletov research group have used this incredibly high affinity interaction as an irreversible peptide staple, creating fusion proteins of the BoNT CD-TD and BoNT RBD with either SNAP25 or Syb. When the fusion proteins were combined, stapling was induced by addition of soluble Syx, assembling a multi-component protein complex.

To generate the fusions, truncated SNARE components were selected based on the minimal core structure required for coiled coil assembly.[260]

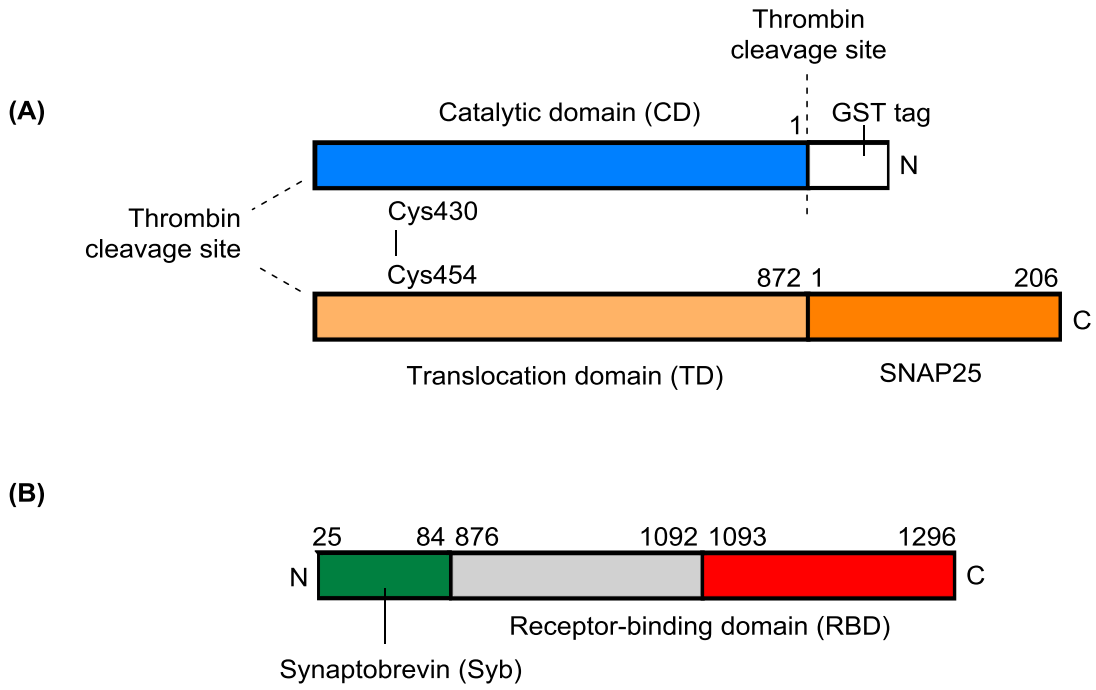

Figure 4.2. Strategy for production of BiTox. (A) The catalytic domain and translocation domain of BoNT-A are expressed as a fusion with SNAP25 (orange) at the C-terminus. The fusion protein is purified by an N-terminal GST purification tag that is cleaved off following treatment with thrombin. Thrombin also mediates cleavage between the catalytic domain and translocation domain, leaving them associated by a single disulfide bond. (B) The receptor-binding domain (grey and red) is expressed as a fusion with a truncated synaptobrevin (forest green) at the N-terminus.

They sought to reassemble BoNT-A by generating a CD-TD-SNAP25 fusion. To mimic the trypsin based cleavage of the CD from the TD, leaving the complex associated simply by a disulfide bond, the group inserted a thrombin cleavage site between the two domains (Figure 4.2). A GST purification tag was inserted into the fusion, preceding the CD, which could also be cleaved by thrombin. The fusion protein was purified, treated with thrombin, and combined with Syb-RBD and Syx. Reassembly was shown to be effective, with the stapled products shown to be stable under the denaturing conditions of SDS-PAGE, and separating into two components upon addition of a reducing agent.

The stapled product, named BiTox (Figure 4.3), when applied to cultured neurones was shown to colocalise with synaptophysin, a marker for synaptic vesicles. An EC50 for the reassembled complex was measured as ~30 pM by Western blotting, whilst the EC50 of the reassembled neurotoxin was measured as slightly less, at 100 pM. Importantly, toxicity was not observed in the absence of the stapling peptide, Syx, demonstrating that the full SNARE complex was needed for complex assembly.

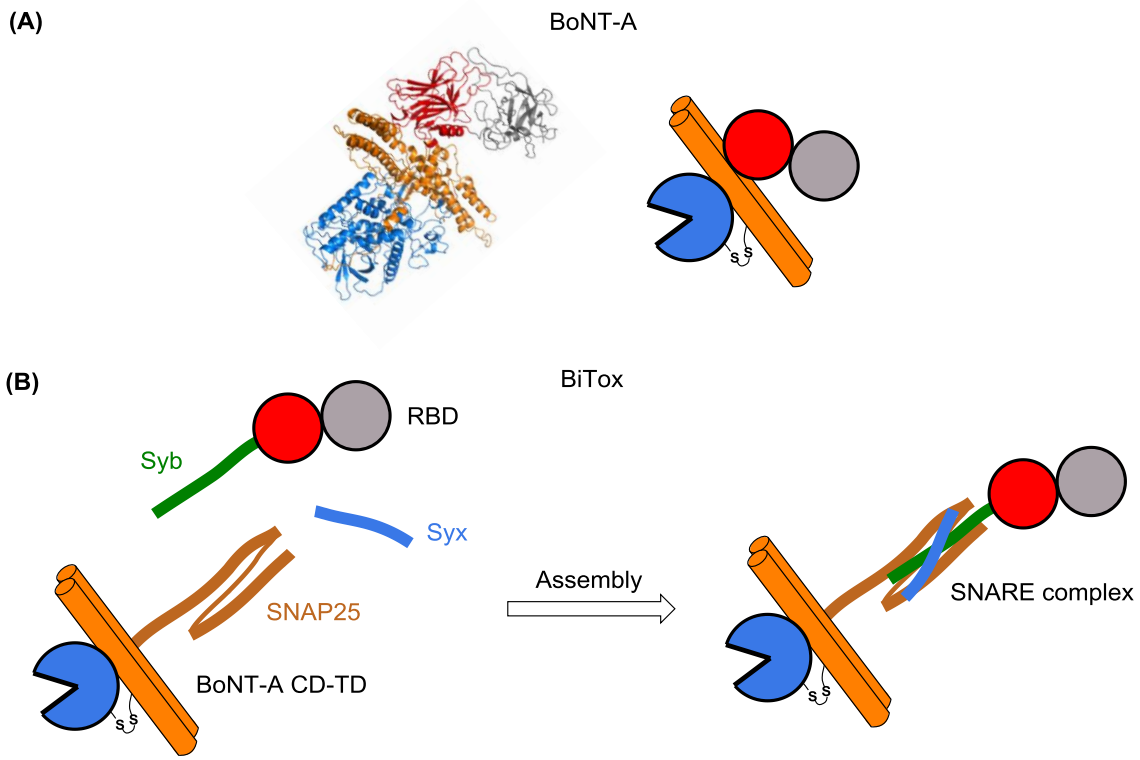

Figure 4.3. (A) A crystal structure and cartoon representation of BoNT-A. (B) Using the SNARE complex to reassemble the botulinum toxin. The BoNT-A catalytic domain (CD) is associated to a SNAP25-translocation domain (TD) fusion protein by a disulfide bond. A receptor binding domain (RBD) synaptobrevin (Syb) fusion is produced and combined with syntaxin-1 (Syx) and the CD-TD-SNAP25 fusion to produce a reassembled BoNT-A (BiTox).

Following experiments *in vivo,* the authors noted that the ability of the stapled complex to induce blockade of exocytosis at neuromuscular junctions was markedly reduced, and BiTox caused no observable paralysis, indicating that the stapled BoNT has different properties to the wild-type, including a lack of systemic toxicity.

The group further demonstrated that the RBD of tetanus toxin (TeNT) could replace the BoNT RBD in BiTox to produce a a TeNT-BoNT chimera (Tet-Bot) by stapling the RBD of TeNT to the CD-TD of BoNT (Figure 4.4).[261] Tet-Bot was shown to be effectively targeted to the neurones of the CNS following peripheral administration, and able to modulate neuronal function by cleavage of SNAP25, thereby demonstrating that the catalytic domain of BoNT could be retargeted by altering the RBD.

The ability of BiTox and Tet-Bot to retarget BoNT-A protease to modulate CNS functions without causing neuromuscular paralysis could result in application of these chimeras to medicine to treat a range of neurological disorders such as epilepsy, and have been considered as anti-nociceptives to treat chronic pain.[262] We considered whether the

targeting of BoNT-A protease could be expanded further by using CTB as a delivery vehicle (Figure 4.4).

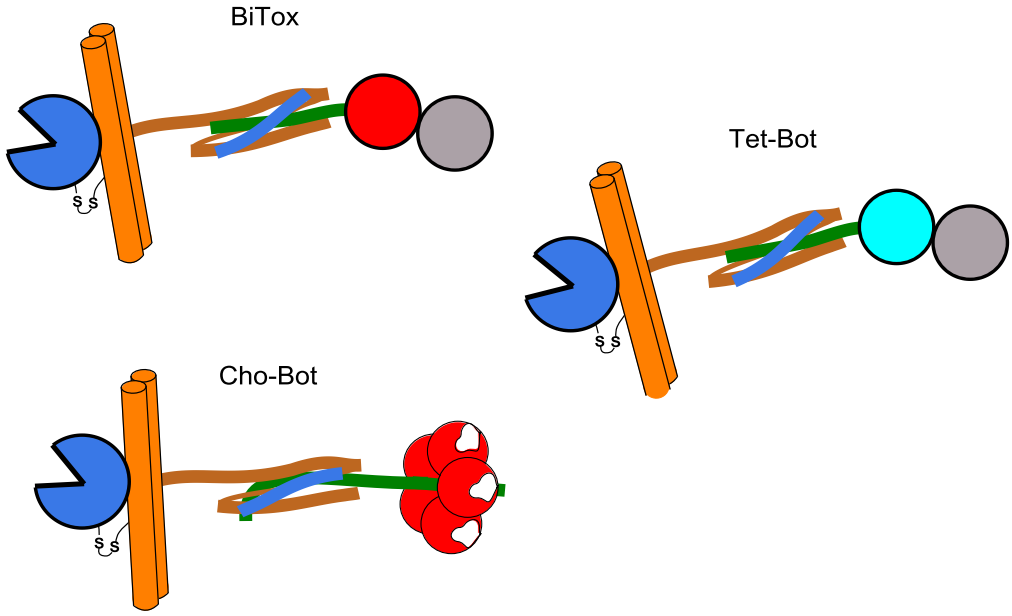

Figure 4.4. Using the SNARE complex to assemble toxin hybrids. BiTox is made from stapling the BoNT-A receptor-binding domain (RBD) to the BoNT-A catalytic and translocation domains. A tetanus-botulinum chimera (Tet-Bot) is made by stapling the TeNT RBD to the catalytic and translocation domains of BoNT-A. A cholera-botulinum chimera (Cho-Bot) could be produced by stapling a cholera toxin AB_5 protein complex to the catalytic and translocation domains of BoNT-A.

4.2. Production and Assembly of a Cholera-Botulinum Chimera

The cholera holotoxin is produced as an AB_5 protein by assembly of CTB protomers around the α-helical CTA2 subunit in the periplasm to form a hexameric lectin. The C-terminus of the CTA2 subunit effectively anchors the A subunit by interacting with the central cavity of CTB. Since the components of the SNARE complex are also alpha-helical, it was decided that the peptide staple could be incorporated onto a truncated CTA2 subunit of an AB_5 protein.

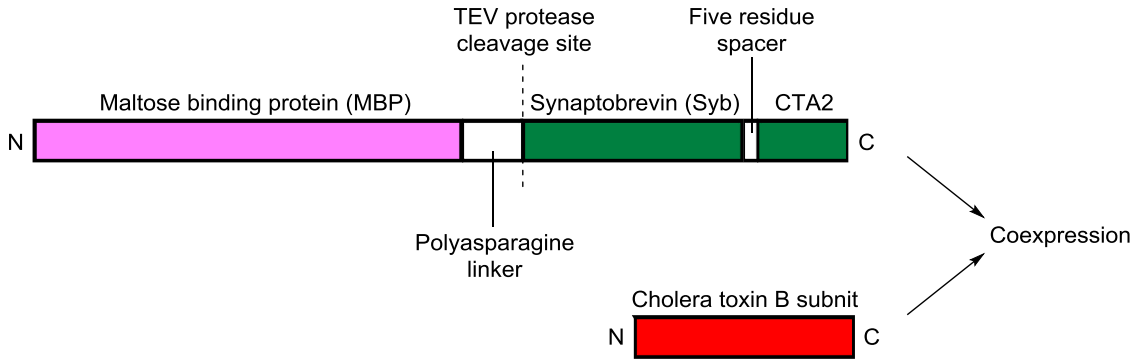

Figure 4.5. Strategy for expression of synaptobrevin-cholera AB_5. A fusion protein consisting of an N-terminal maltose binding protein (MBP) linked to synaptobrevin and a truncated CTA2 peptide is coexpressed with cholera toxin B subunit. The subsequent complex can be treated with TEV protease to cleave off the MBP, leaving synaptobrevin-CTA2 domain associated to CTB.

Assembly of Tet-Bot had been achieved by fusing Syb to the tetanus toxin RBD. We therefore decided to replicate this approach by introducing Syb onto the N-terminus of a truncated CTA2 subunit (Figure 4.5). An *E. coli* codon-optimised gene coding for the fusion was designed. A truncated form of Syb (amino acids 3-84) from *Rattus norvegicus* was selected for producing the fusion, since the truncated form had been used successfully to produce Tet-Bot. Whilst full-length Syb contains a C-terminal helical transmembrane domain, and thus fusion to a helical protein should be of little consequence to the structure of either peptide, a short five amino acid spacer was introduced in between CTA2 and Syb to separate the two helices to allow them to adopt their specific conformation. The C-terminal 25 residues of the CTA2 subunit were then incorporated at the C-terminus of the polypeptide sequence, since these residues make up all of the interactions between the CTA2 subunit and CTB.

Coexpression of this novel fusion with CTB should result in the production of a Syb-AB_5 protein complex. However, it was anticipated that uncomplexed CTB would likely also be produced, and could prove difficult to separate from assembled complexes. Therefore, to facilitate purification of the complex, an MBP-fusion tag was included at the N-terminus, separated by a polyasparagine linker and a TEV protease site to allow cleavage of the maltose affinity tag. A plasmid containing the coding DNA sequence for this fusion protein and for CTB was purchased and expressed in *E. coli* BL21 Gold cells.

MBP-Syb-AB_5 was purified using a dual purification strategy (Figure 4.6). The MBP affinity tag facilitated isolation of MBP-Syb-AB_5, native MBP, and uncomplexed MBP-CTA2 through use of an amylose column. The MBP-containing eluate could then be applied to an Ni-NTA affinity column, purifying exclusively CTB-containing protein

complexes. Applying the flow-through and elution fractions from the Ni-NTA chromatography step to an SDS-PAGE gel clearly shows uncomplexed MBP-CTA2 in the flow through, and a high molecular weight smear that dissociates into two discrete bands upon boiling in the elution fractions (Figure 4.7A). AB_5 complexes are only partially stable in the presence of the concentration of SDS used for SDS-PAGE, giving rise to the smear that is likely a combination of MBP-Syb-AB_5 complex, CTB, and MBP-Syb-CTA2. The boiled sample yielded two discrete bands corresponding to monomeric CTB and MBP-Syb-CTA2.

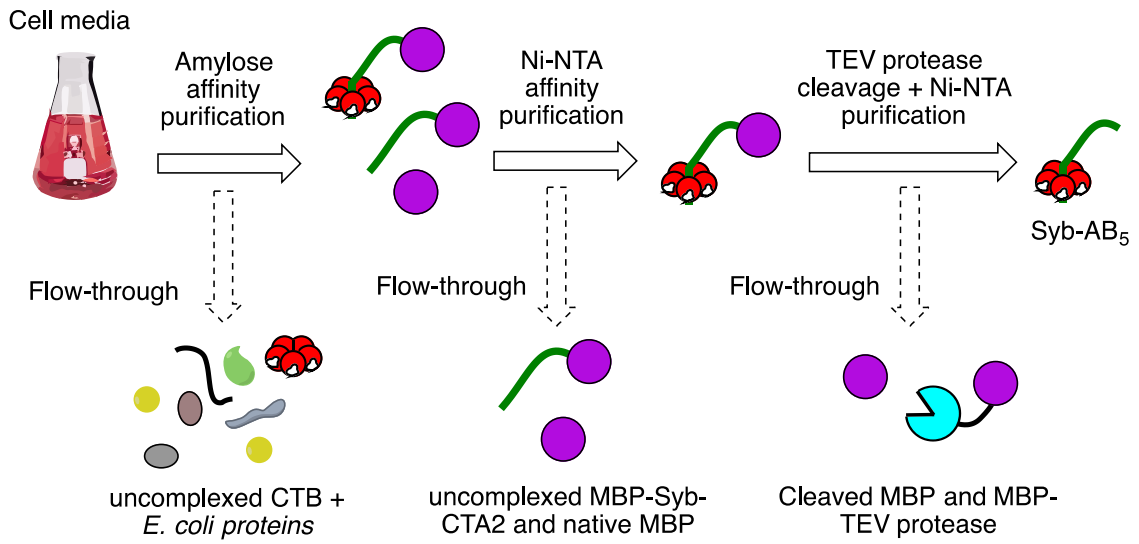

Figure 4.6. Purification strategy for Syb-AB_5. Cell medium is applied directly to an amylose column, isolating the MBP-tagged complex, uncomplexed MBP-Syb-CTA2 and native MBP. MBP is shown as a purple circle, the Syb-CTA2 subunit is shown as a green rod, and CTB is shown as a red donut. Uncomplexed CTB does not bind and is discarded with other unwanted proteins. The eluate from the amylose column is applied to a Ni-NTA affinity column, resulting in purification of MBP-Syb-AB_5 and loss of uncomplexed MBP-Syb-CTA2 as well as native MBP. The purified protein is treated with MBP-tagged TEV protease, resulting in cleavage of the MBP tag from Syb-AB_5. Purification of Syb-AB_5 is achieved through a second round of Ni-NTA affinity chromatography, resulting in loss of MBP and TEV protease, and purification of Syb-AB_5.

The purified protein was then treated with TEV protease to cleave the MBP tag, and the reaction was purified by Ni-NTA chromatography to remove the cleaved MBP and TEV protease, whilst retaining the Syb-AB_5 complex. Analysis by SDS-PAGE of boiled and unboiled Ni-NTA elution fractions demonstrated that cleavage was successful. In the unboiled sample a thick band can be observed between 42.7 kDa and 55.6 kDa that disappears upon boiling. CTB pentamer migrates to ~42 kDa when analysed by SDS-PAGE. The band is therefore likely to be a combination of Syb-AB_5 and CTB complex. A band at ~15 kDa can be seen corresponding to Syb-CTA2. A larger protein can be detected in both unboiled and boiled lanes that could correspond to MBP-TEV protease

that had not been successfully removed from the second Ni-NTA column purification step.

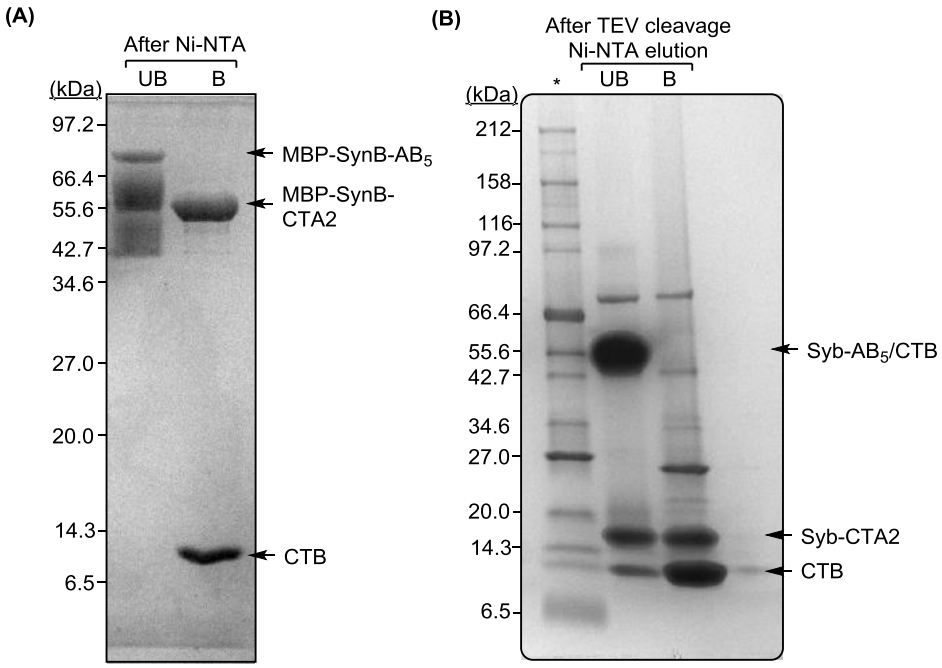

Figure 4.7. (A) SDS-PAGE (15 % acrylamide) analysis of Ni-NTA chromatography elutions following amylose purification of protein from medium. Samples were electrophoresed in a boiled (B) or unboiled state (UB). (B) SDS-PAGE (4-15 % acrylamide) analysis of Ni-NTA chromatography elution (lanes 2, 3) following cleavage with MBP-TEV.

To confirm the identity of the purified proteins, the samples were analysed by ESMS under denaturing conditions (Figure 4.8).

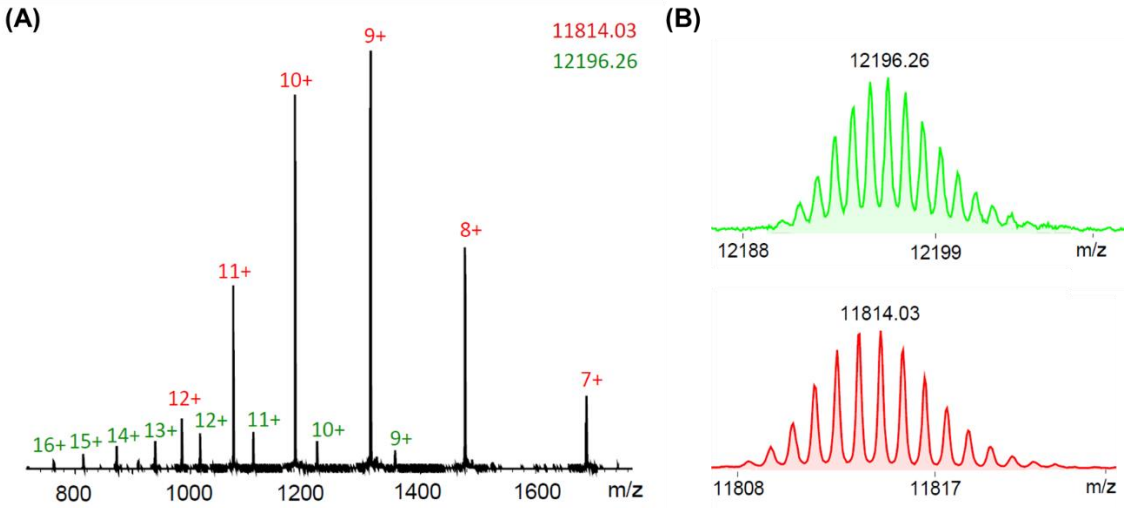

Figure 4.8. Analysis by ESMS of Ni-NTA chromatography elution fractions following MBP cleavage of MBP-Syb-AB_5 by TEV protease. (A) Ionisation spectrum for Syb-AB_5 showing ionisation peaks for CTB (red) and Syb-CTA2 (green). (B) Deconvoluted mass spectrum of Syb-CTA2 (top) and CTB (bottom). Expected mass for $(Gly)_3$ CTB: 11814.52 Da vs. observed 11814.03 Da. Expected mass for SynB-CTA2: 12196.43 Da vs. observed 12196.26 Da.

Ionisation peaks were observed that deconvoluted to give a mass of 11814.03 Da (calculated, 11814.52 Da), thus confirming the presence of CTB. Further peaks were observed that deconvoluted to 12196.26 Da (expected 12196.43 Da) confirming the presence of Syb-CTA2. No peaks for other proteins were detected, suggesting successful cleavage and purification of the AB_5 complex.

In order to assess the stability of the complex, purified Syb-AB_5 was lyophilised, re-dissolved, and analysed by gel filtration chromatography (Figure 4.9). A single peak was observed that eluted with a retention volume of 9.2 mL. When compared to a chromatogram of CTB, no overlap was observed, confirming that the Syb-CTA2 subunit remained associated with CTB. The K_{av} was derived, and compared to calibration standards (Figure 4.10). The expected mass (71 kDa) broadly agreed with the mass calculated (65 kDa) from the calibration linear fit. Interestingly, despite being only 12 kDa larger than CTB, addition of the Syb-CTA2 subunit results in the complex passing through the column much faster than CTB. CTB elutes as a 32 kDa protein relative to a calibration line, whilst Syb-AB_5 elutes as a 65 kDa protein. Addition of Syb-CTA2, a long and flexible helix, to CTB clearly significantly increases its hydrodynamic radius, resulting in a shorter duration on the gel filtration column.

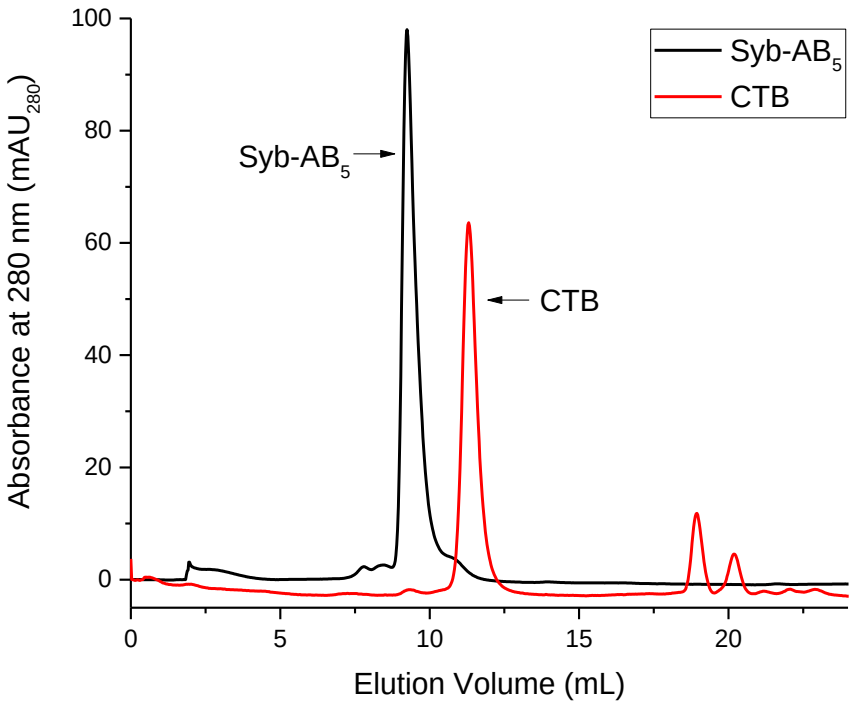

Figure 4.9. Chromatogram generated following gel filtration chromatography of SynB-AB_5 complex (black) using a Superdex 75 Increase 10/300 GL gel filtration column, overlaid with a trace of purified CTB (red), showing retention volume (mL) against absorbance at 280 nm (mAU).

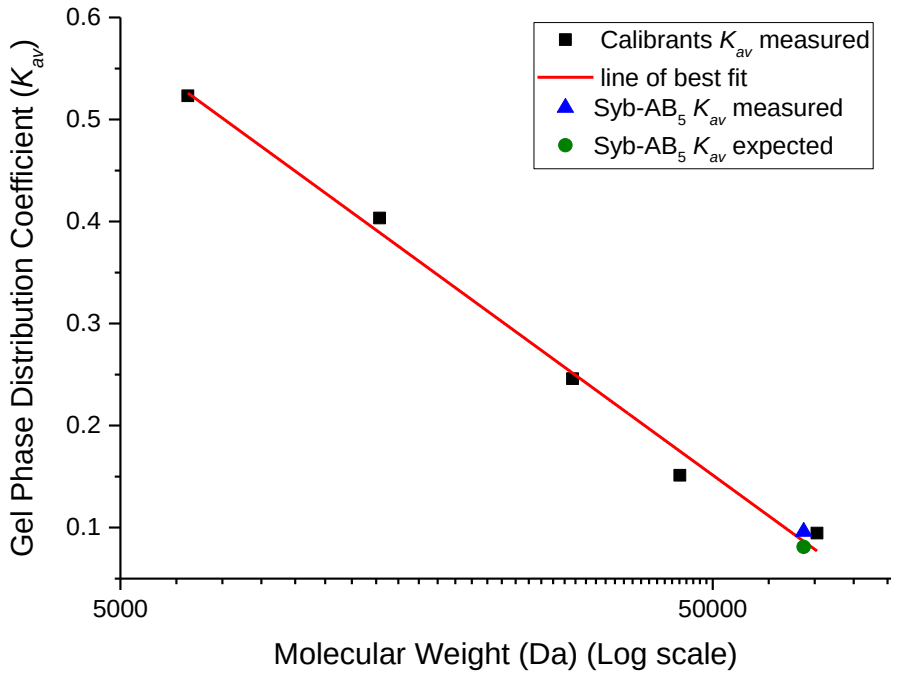

Figure 4.10. Linear fit (red) of gel phase distribution coefficient, a ratio of elution volume to the void and column volume for each calibrant, and the molecular weight for each calibrant shown on a log scale. The green data point corresponds to the expected distribution coefficient for Syb-AB$_5$, whilst the blue data point corresponds to the measured distribution coefficient for Syb-AB$_5$.

Having demonstrated that the complex was successfully expressed, cleaved, and purified, Syb-AB$_5$ was sent to the Davletov group in Sheffield for stapling to the BoNT-A CD-TD-SNAP25 fusion protein to make a chimera, that we have called Cho-Bot. The following experiments were carried out by Dr Charlotte Leese, a postdoctoral researcher in the Davletov group.

Assembly of the stapled complex was verified by SDS-PAGE in the absence of reducing agent. Boiling the sample resulted in the separation of three discrete bands on the gel. The SNARE staple is SDS-resistant at room temperature, but dissociates following boiling in SDS. The three bands were thus identified as CD-TD-SNAP25, Syb-CTA2, and monomeric CTB. In the absence of boiling, four bands can be discerned, with a small shift in the highest molecular weight band that is presumed to be assembled CD-TD-SNARE-CTA2. Pentameric and monomeric CTB can be seen (~45 kDa and ~12 kDa respectively). Although no fully stapled Cho-Bot was detected by SDS-PAGE (expected ~190 kDa), the presence of CD-TD-SNARE-CTA2 was sufficient evidence to suggest that Cho-Bot had been successfully assembled.

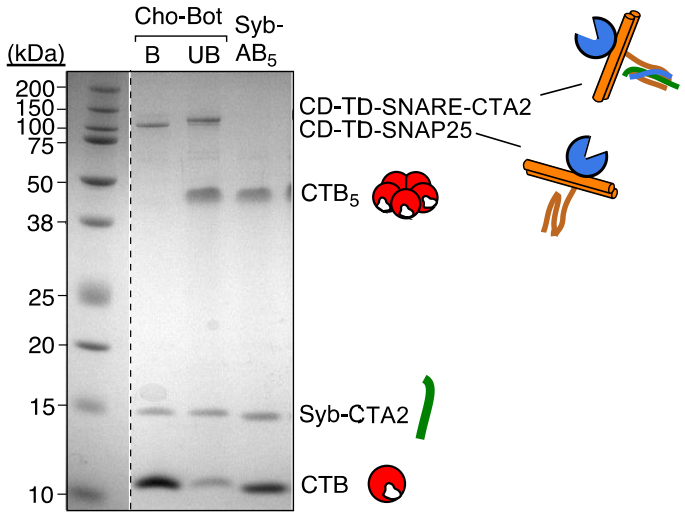

Figure 4.11. SDS-PAGE analysis of boiled and unboiled samples of CD-TD-SNAP25 + Syb-AB_5, and an unboiled sample of Syb-AB_5. Figure produced by Dr Charlotte Leese (University of Sheffield).

The assembled Cho-Bot was then tested for internalisation by treating cultured rat cortical neurones with a titration of Cho-Bot complex. After three days the cells were lysed and analysed by SDS-PAGE. Since the cleaved SNAP25 is nine amino acids shorter than the uncleaved SNAP25, the two can be separated using this technique. The resultant gel was then subjected to western blotting, using an anti-SNAP25 antibody to detect both the cleaved and uncleaved material (Figure 4.12). Band densitometry was then used to quantify the percentage of cleaved SNAP25 relative to an untreated control. This process was repeated twice, and an average was taken and plotted as a log function of the concentration of complex used (Figure 4.12). Fitting the data allowed determination of an EC_{50} for the complex of 72 pM.

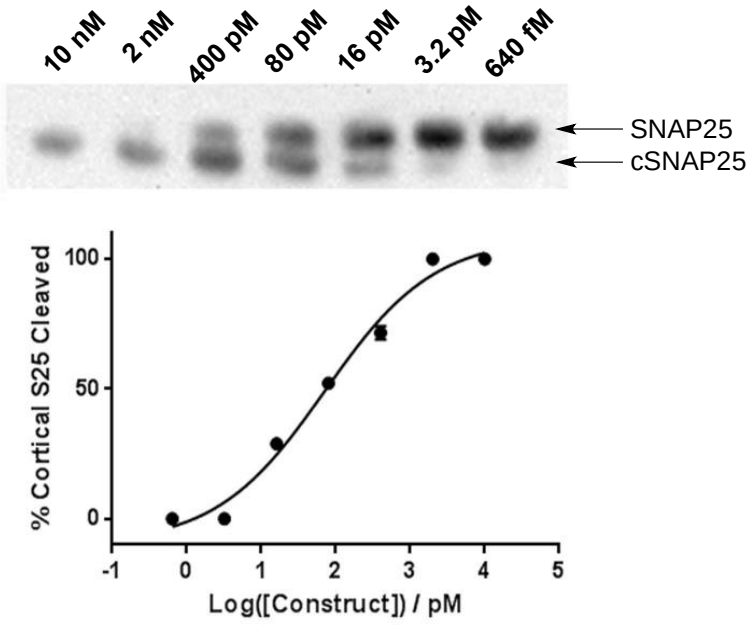

Figure 4.12. Top – western blot of lysed rat cortical neurones following treatment with a range of concentrations of Cho-Bot, and stained with an anti-SNAP25 antibody. Bottom – EC_{50} graph showing the percentage of cleaved SNAP25 in the rat cortical neurones as a log function of the concentration of Cho-Bot (log pM). Figure produced by Dr Charlotte Leese (University of Sheffield).

Detection of cleaved SNAP25 in the rat cortical neurones clearly demonstrates that the complex has been internalised, and the cargo effectively delivered. The fact that SNAP25 cleavage occurs in a concentration-dependent manner has allowed determination of an EC_{50} for the complex (72 pM), that is very similar to both BoNT-A and BiTox (30 pM and 100 pM respectively). The process must be CTB-mediated, since previous experiments have demonstrated that SNAP25 cleavage is not detected in the absence of a receptor binding domain.[247]

4.3. Concluding Remarks

A critical difference in the RBD for BoNT-A and CTB is that CTB has a single receptor, with internalisation occurring following ganglioside binding, whilst BoNT-A internalisation is dependent on two receptors. This dual receptor binding model results in BoNT-A neuronal uptake being dependent on the rate of exocytosis of the target motor neurone (*1.3.1. Botulinum Toxin*). It is for this reason that BoNT-A has been so successful in the treatment of disorders characterised by hyperactive nerve activity. The ability of CTB to be taken up into any subset of neurones expressing GM1 on their surface therefore presents many opportunities; for instance, Cho-Bot may have application in the treatment of chronic pain through the capacity of CTB to be internalised into sensory

neurones.[242,263] Moreover, whilst CTB is transported into neurones by retrograde transport, it does not undergo trans-synapsis like tetanus toxin. Cho-Bot should therefore be retained within the targeted nerve, and not be transcytosed into further connecting neurones, therefore allowing its activity to be localised to a specific area.

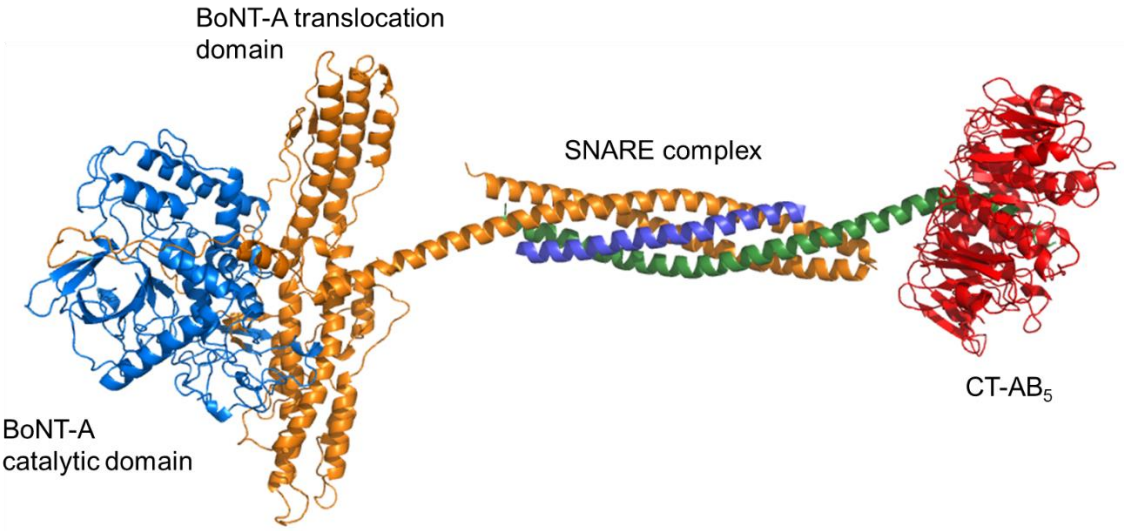

Figure 4.13. Ribbon diagram of a molecular model of Cho-Bot constructed in PyMol software using PDB accession codes 3BTA (BoNT-A), 1N7S (SNARE complex), and 1XTC (Cholera AB_5). Syb-CTA2 helix is shown in green, syx is shown in dark blue, and SNAP25/BoNT-A translocation domain is shown in orange.

These experiments have therefore shown that CTB can function as an effective delivery vehicle for BoNT-A protease into cultured neurones when combined stapled to the CD-TD complex. Experiments to validate internalisation of the complex *in vivo* are currently underway to assess the effects of retargeting the BoNT-A protease.

5. Conclusions and Future Work

5.1. A Project Summary

The aim of this project was to develop a novel modular protein delivery system that would allow the independent expression of a macromolecular cargo and a targeting protein which would self-assemble to make an active delivery system. The strategy was to identify Affimers that targeted the non-GM1-binding face of CTB to effectively 'piggyback' into motor neurones. The system would be validated in a mouse model by delivering a cargo-Affimer fusion protein complexed to CTB into motor neurones.

Objective 1. Identifying and characterising CTB-binding Affimers

Initially, Affimers were screened by phage display against biotinylated CTB. Three rounds of panning were carried out, with addition of unmodified CTB as a competitor in the third round. From this first screen two unique Affimers were identified, but they displayed no affinity for CTB that could be detected by ITC. Screening was repeated against biotinylated CTB, but this time no unmodified CTB competitor was added. An additional fourth round of panning was incorporated where the phage were incubated with CTB adhered to GM1. From this screen, 20 unique Affimers were identified.

To verify the binding of these 20 Affimers to CTB, an Affimer-lectin binding assay (ALBA) was developed. From the ALBA two Affimers were selected for further characterisation, Affimers 3A2 and 3C6, that showed different selectivity for CTB and LTB. Affimer 3C6 bound to both CTB and LTB, whilst Affimer 3A2 bound exclusively to CTB in the context of the ALBA. By producing five CTB-LTB hybrids, ALBA was used to identify a single amino acid (A80) that mediates selectivity of Affimer 3A2 for CTB.

The two Affimer-CTB interactions were then characterised by gel filtration chromatography. Experiments indicated that Affimer 3A2 is more compact than Affimer 3C6, but the complexes they form with CTB are of similar hydrodynamic radius. Analysis by gel filtration chromatography also indicated that the binding stoichiometry was one-to-one. This observation was confirmed by analysis of the binding interactions by ITC. However, the binding stoichiometry appeared to be the only similarity between the two interactions. The dissociation constants calculated for the two interactions differed by an order of magnitude; Affimer 3A2 bound CTB with a K_d of 1 µM, whilst Affimer 3C6 bound CTB with a K_d of 100 nM. Both interactions also had different thermodynamic signatures, with the 3A2-CTB interaction being an enthalpically favourable process, whilst 3C6 binding to CTB was driven more by entropic contributions.

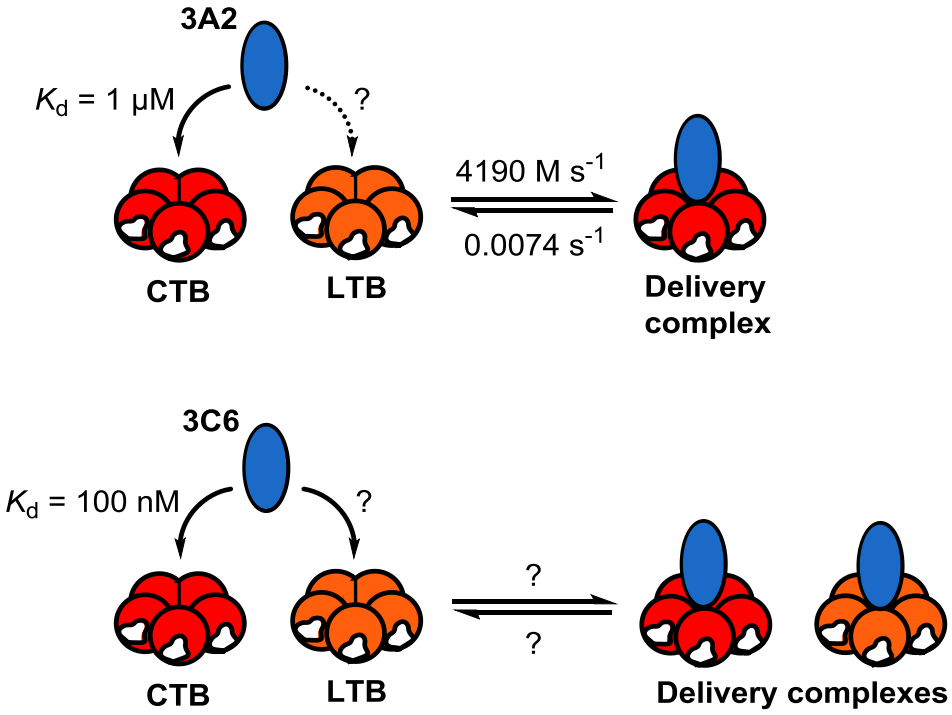

Figure 5.1. A summary of the data obtained for the interaction of Affimers 3A2 and 3C6 with CTB and LTB.

Binding of 3A2 to CTB was then assessed by SPR to determine the rate constants of the binding interaction. The association and dissociation rate constants were 4190 M s^{-1} and 0.0074 s^{-1}, respectively, allowed determination of the residency time (140 s) and half-life of the complex (95 s). The K_d value determined by SPR, derived both from the rate constants as well as from the response units at equilibrium, was in agreement with that measured by ITC. Binding of 3C6 to CTB could not be easily determined by SPR.

Objective 2. Demonstrating complex internalisation into cells

Affimers 3A2 and 3C6 were fluorescently labelled and complexed to CTB, and then added to a GM1-expressing cell line (Vero cells). Immunolabelling CTB and imaging cells by microscopy demonstrated that Affimers were readily internalised, and appeared to colocalise with CTB in a Golgi-like compartment of the cell. A minimum concentration of fluorescently-labelled complex required for detection of internalised complex was then determined. Affimer 3A2-555 was readily detected at 175 nM when combined with CTB-488, but not at lower concentrations, whilst Affimer 3C6-555:CTB-488 complex was still clearly detected at 15 nM.

Preliminary FRET experiments were carried out with Alexa Fluor-labelled CTB and Affimer. FRET was observed on addition of Affimer to CTB, but the change was not

considered large enough to use techniques such as FRET microscopy to determine whether Affimer and CTB were still associated following complex internalisation into cells.

Next, GFP-Affimer fusion proteins were expressed and shown to be internalised into cultured Vero cells when combined with CTB. GFP-labelling colocalised with CTB, both which appeared to be retained within a Golgi-like compartment of the cell.

Objective 3. Delivering the complex to motor neurones

Having demonstrated that the complex could be successfully internalised into cultured cells, Affimer-555:CTB complex was administered into the tongue of mice to deliver the complex to the hypoglossal nerve.

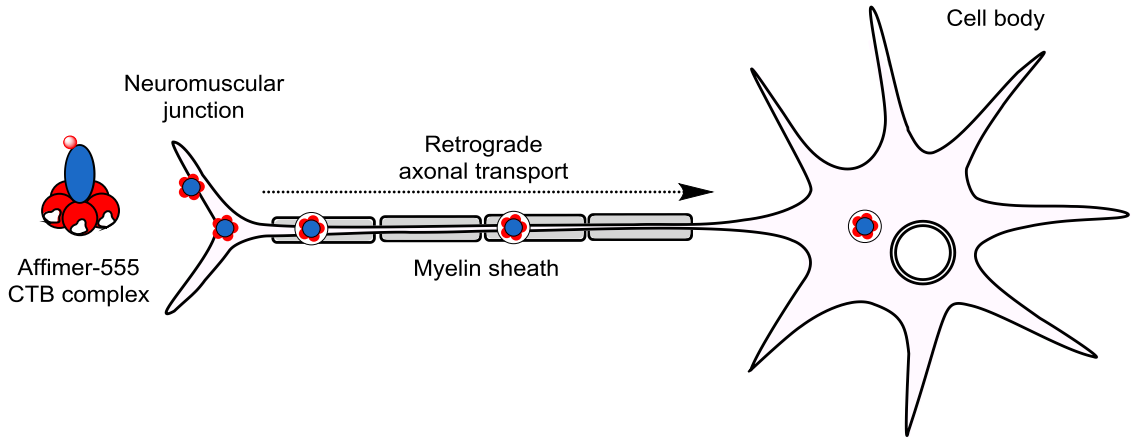

Figure 5.2. Internalisation of fluorescently-labelled Affimer (Affimer-555) complexed to CTB to motor neurones and trafficking to the cell body by retrograde axonal transport.

Fluorescence was readily detected in the cell bodies of the motor neurones of the hypoglossal nerve for both Affimer-CTB complexes after 24 hours. 3C6-555 fluorescence overlaid with immunolabelled CTB in a compartment close to the cell nuclei. 3A2 fluorescence meanwhile did not overlay with CTB and appeared to be more dispersed throughout the cell body, localised in discrete vesicular compartments presumed to be lysosomes. After one week 3A2-555 fluorescence was no longer detected whilst 3C6-555 fluorescence was still clearly visible. 3C6-555 fluorescence was still colocalised with CTB, although the proteins appeared to be localised to lysosome-like compartments.

Whilst both complexes were internalised following intramuscular injection, they had different fates once inside the neurone. Affimer 3A2 appeared to dissociate from CTB once internalised and be readily trafficked into lysosomes. However, Affimer 3C6

appeared to remain associated with CTB, and after one week the complex appeared to be trafficked into lysosomes.

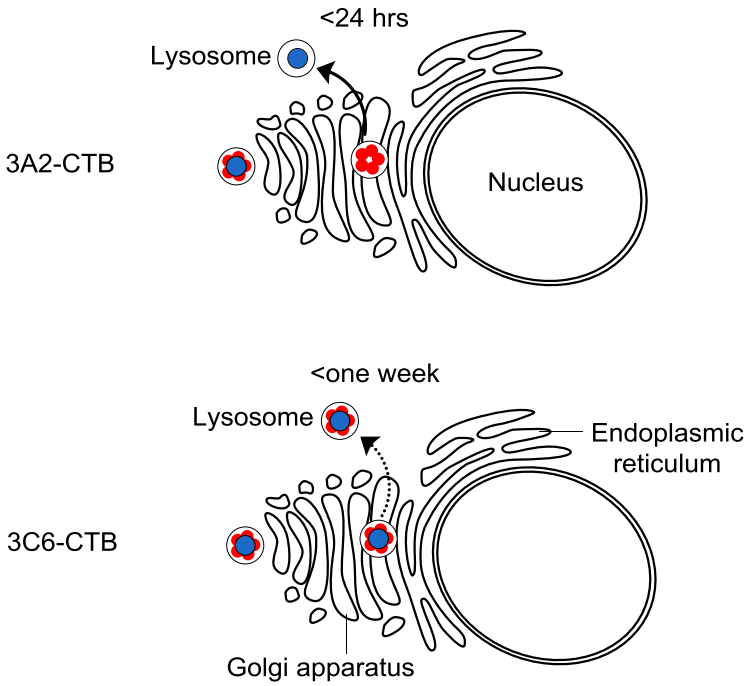

Figure 5.3. Hypothesis of the fate of the Affimer-CTB complex once internalised into motor neurones. (Top) Affimer 3A2-CTB complex is trafficked to the Golgi apparatus in the cell body. Once inside the neurone, Affimer 3A2 dissociates from CTB, and is rapidly targeted to lysosomes for degradation. (Bottom) Affimer 3C6-CTB complex is trafficked to the Golgi apparatus. The complex remains associated and is eventually targeted for lysosomal degradation.

Using the SNARE complex to achieve a modular delivery system

A collaboration with the Davletov group (University of Sheffield) allowed a second strategy for modular assembly of a protein delivery system to be explored. A novel toxin chimera was produced by using the SNARE complex to staple CTB to the translocation and catalytic machinera of botulinum toxin. A cholera-toxin AB_5-synaptobrevin fusion protein was produced by incorporating synaptobrevin to the N-terminus of a truncated variant of the CTA2 subunit. This protein was coexpressed with CTB, producing the synaptobrevin-AB_5 complex. The complex was shown to be stapled to a fusion protein of the BoNT-A catalytic domain, translocation domain, and SNAP25 when combined with the third component of the SNARE complex; syntaxin. The resultant toxin chimera was then shown to be successfully internalised into cultured neuronal cells. The catalytic domain of BoNT-A was able to cleave its intracellular target (SNAP25) as shown by Western blotting, and an EC_{50} value was calculated for the complex of 72 pM.

Experiments testing the novel complex *in vivo* are currently underway at the University of Sheffield.

The novel chimera may allow the catalytic domain of BoNT-A to be targeted to a subset of neurones that are inaccessible to the medical formulation of the toxin, thus leading to the production of a novel therapeutic.

5.2. Future Work

5.2.1. Further characterisation of Affimers 3A2 and 3C6

Biophysical characterisation of Affimers 3A2 and 3C6 has been carried out during this project. However, in order to fully characterise the system, there are some outstanding questions that should be addressed. Rate constants for binding of 3C6 to CTB need to be measured. Since the kinetics could not be readily measured by SPR, rate constants could be determined by using a stopped-flow apparatus coupled to a fluorescence spectrophotometer to measure FRET between fluorescently labelled CTB and 3C6, although the linker length and FRET pair of the fluorophores would have to be optimised.

To fully understand how the Affimers interact with CTB would require elucidation of the structure of the complex. Some structural information has already been determined. Alanine 80 in CTB is known to be important for binding of Affimer 3A2 to CTB. A Master's student (Ben Milborne) in the Turnbull lab carried out a series of experiments to identify residues in the variable loops of Affimer 3A2 that are required for binding to CTB. A series of 17 mutants were produced by mutating each residue in the Affimer 3A2 binding loops to an alanine. Affimers were then tested at three concentrations for their ability to bind to captured CTB-biotin by SPR. Ben found that 10 of the mutations did not bind at lower concentrations (1 µM), but that binding could be rescued for all but four of the mutants by increasing the concentration of analyte to 30 µM. He therefore identified four residues that appear to be critical for Affimer 3A2 binding to CTB. He also hypothesised that two of these residues (F89, F92) may be interacting with the central cavity of CTB in a manner similar to the interactions formed between F223 and Y226 (*1.4.1. Structure and formation of the toxin*) of the CTA2 subunit and the hydrophobic ring of CTB.

Obtaining a crystal structure of the Affimer-CTB complexes would thus allow Ben's hypothesis to be tested, and provide key information to understand how these proteins interact.

Tested conc.	Binding loop 1								
	Q51A	H52A	E53A	R54A	S55A	H56A	W57A	W58A	D59A
1 µM	-	+	+	-	+	-	-	+	+
6 µM	-	+	+	+	+	-	-	+	+
30 µM	-	+	+	+	+	+	-	+	+

Tested conc.	Binding loop 2								
	H85A	N86A	Q87A	F88A	F89A	D90A	Y91A	F92A	I93A
1 µM	-	n/a	+	-	-	+	-	-	-
6 µM	-	n/a	+	-	-	+	+	-	+
30 µM	+	n/a	+	+	-	+	+	-	+

Table 5.1. Binding data obtained following analysis of Affimer 3A2 binding loop alanine mutants. Affimers were tested by SPR against captured CTB-biotin at three concentrations (1 µM, 6 µM, and 30 µM). Binding is noted by a '+' sign, whilst no observed binding is denoted by a '-' sign. Highlighted in yellow are the four residues that are critical for Affimer 3A2 interaction with CTB.

A crystal structure of the complex may also provide the basis to develop constrained peptides to mimic one of the Affimer binding loops. Initially, single-loop variants of Affimers 3A2 and 3C6 could be produced, and assessed for binding to CTB. Binding loops could then be synthesised as short peptides, and constrained in a variety of ways to reproduce the presentation of the loop by the Affimer. Peptides could be presented on a scaffold in a pentavalent array, thereby acting like a five-fingered claw crane to bind CTB. Five-membered coiled coils have been observed in nature, as well as being designed de novo. CTB-binding peptides could therefore be presented on the termini of the pentameric coiled coils.[264,265] The reduced affinity from using only one of the binding loops would thus be compensated for by the enhancement in avidity.

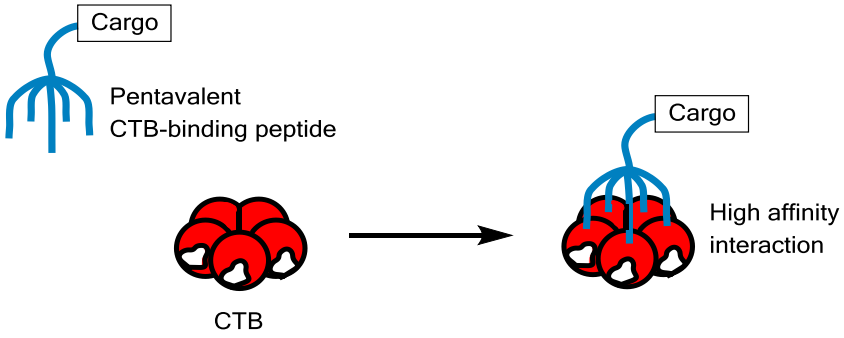

Figure 5.4. Binding of a cargo-bound pentavalent peptide to CTB.

5.2.2. Delivering a cargo using the CTB-Affimer complex

Delivering a cargo to motor neurones using the developed system is essential to demonstrate its function *in vivo*. GFP has already been shown to be readily delivered by CTB-Affimer complexes into cultured cells, and is thus the obvious candidate for delivery. Two additional constructs have also been produced and expressed as Affimer fusion proteins, but time constraints precluded their testing. These fusion proteins include Affimer-cre recombinase and Affimer-parvalbumin fusion proteins.

Cre recombinase is an enzyme that is able to excise DNA located between two specific recognition sites (loxP sites).[266] An *in vivo* reporter system is available to determine whether DNA excision has taken place, thereby providing a measurable output that is more sensitive than immunohistochemistry to determine whether the complex has been delivered. However, delivery of this cargo relies on a nuclear localisation signal sequence being sufficient to direct a protein from the endocytic machinery to the nucleus. Sellers *et al.* demonstrated that Cre-recombinase was transported to the nucleus of neurones when fused to a neuronal-targeting peptide.[34] Furthermore, Barbieri *et al.* showed that fusion proteins could be delivered to the cytosol of neurones without the requirement for a cytosolic-targeting strategy.[122] Delivery of the cargo into the cells may therefore be the sole requirement for certain proteins to be transported to their desired destination.

Parvalbumin is a calcium-binding protein expressed in certain cells of the CNS, but not in motor neurones. Studies have suggested that parvalbumin expression in motor neurones may have neuroprotective effects.[267,268] Delivery of this protein using the CTB-Affimer system may therefore have a therapeutic application.

Other model proteins to exemplify the system could include neurotrophic growth factors (NGFs). NGFs have been used in clinical trials as treatments to rescue neuronal cell death in patients afflicted with amyotrophic lateral sclerosis.[269] However, trials have failed due to the short half-life of NGFs in the blood, an inability to target the NGFs to the CNS, and side-effects following systemic administration.[270] Delivering NGFs to motor neurones in the CNS by producing an NGF-Affimer fusion complexed to CTB could circumvent the short half-life in the blood and side effects by delivering the protein directly into motor neurones.

In its current form, the CTB-Affimer protein delivery system is well suited for the delivery of proteins to the vesicular system. Certain neuronal disorders are known to be caused by defective proteins in the vesicular organelles, and the CTB-Affimer protein could thus

be employed to address some of these disorders. Cystatin C is an inhibitor of the lysosomal cysteine protease cathepsin B, and has recently been shown to have neuroprotective activity against amyotrophic lateral sclerosis (ALS).[271] Delivery of cystatin C to lysosomes may therefore provide a novel therapeutic approach to treat ALS. Fragmentation of the Golgi apparatus of motor neurones occurs during ALS, and is hypothesised to take place due to the loss of function of a chaperone called tubulin binding cofactor E.[272] Delivering this chaperone to motor neurones using the CTB-Affimer system may help to address this hypothesis, potentially resulting in restoration of the Golgi in an ALS mouse model.

5.2.3. Cytosolic delivery of proteins

A key challenge to protein delivery is escaping from the vesicular machinery and into the cytosol. Cho-Bot achieves this by using the translocation domain of BoNT-A. However, translocation into the cytosol is dependent on the presence of the catalytic domain of BoNT-A. Bade *et al.* successfully demonstrated that proteins could be fused onto the catalytic domain (CD) and translocated into the cytosol.[57] Non-toxic mutants of the CD could therefore be produced to allow delivery of inactive-CD fusion proteins into the cytosol. Various other approaches have been implemented in the literature.

Ryou et al. generated a toxin chimera by fusing the translocation domain (TD) of exotoxin A from *Pseudomonas aeruginosa* to the B subunit of shiga toxin and to GFP.[273] Following internalisation, the exotoxin A TD-GFP fusion is cleaved from shiga toxin B subunit by furin protease. The research team showed that fusion of the exotoxin A TD to GFP was sufficient for the proteins to be transported into the cytosol following internalisation of the shiga toxin B subunit.[274] A cargo-exotoxin A TD-Affimer fusion protein could be produced and combined with CTB to facilitate transport of the fusion into the cytosol of neurones.

Sudo et al. have identified a 19-residue fusogenic peptide from human sperm that acts as an effective transporter across endosomal membranes.[275] Incorporation of the fusogenic peptide along with a protein cargo and a cell-penetrating peptide (CPP) was sufficient for cytosolic delivery of the protein cargo. Whilst the mechanism of action has not been identified for entry into the cytosol, the fusogenic peptide was shown to be unable to penetrate cells in the absence of a CPP. CTB-binding Affimers could thus be decorated in the fusogenic peptide to mediate cytosolic delivery of the tethered protein cargo.

5.2.4. Identifying novel toxin-binding Affimers

Affimers 3C6 and 3A2 bound to CTB tightly enough to be internalised into motor neurones when administered into a muscle. However, if administered systemically, the residency time of the complexes would likely not be sufficiently long for the complex to be internalised into neurones. Furthermore, systemic administration would lead to wider distribution of the complex, resulting in a larger number of motor neurones being targeted.[276] Higher affinity CTB-binding Affimers could be identified to allow administration of the complex intravenously or intraperitoneally. Identification of these Affimers would require further phage-Affimer screens, but under more stringent conditions.

Whilst CTB is clearly an effective delivery vehicle, this approach to piggybacking on a toxoid to enter the CNS could be applied more broadly. Binding Affimers could be identified against a range of toxin receptor-binding domains, such as shiga toxin B_5 subunit, or the receptor-binding domain of tetanus toxin. Shiga toxin B subunit recognises ganglioside Gb3. Once in the blood stream, Gb3 binding targets the toxoid to kidney cells.[277–279] The target selectivity could thus be modulated by changing the toxin. Tetanus toxoid, meanwhile, is known to travel trans-synaptically.[87,91,92] Identification of tetanus-binding Affimers could therefore allow penetration of the complex into neurones of the CNS that are inaccessible to CTB. An array of toxoid-binding Affimers could therefore be identified to generate a toolkit for protein delivery into neurones and other target organs.

5.3. Concluding Remarks

A novel approach to the delivery of proteins to neuronal cells has been demonstrated. By piggybacking onto CTB, antibody mimetics have been successfully internalised into motor neurones. Modification of the binding scaffolds with a macromolecular cargo could lead to the use of the CTB-Affimer system as a novel research tool.

6. Materials and Methods

6.1. Standard Buffer Solutions

All common buffers were adjusted to pH 7.4, unless otherwise stated, and made up with 15 MΩ water to the required volume.

Phosphate Buffer: 50 mM NaH_2PO_4, 150 mM NaCl

Phosphate Buffered Saline (PBS): 10 mM Na_2HPO_4, 1.8 mM KH_2PO_4, 137 mM NaCl, 2.7 mM KCl

PBS-T: 50 mM NaH_2PO_4, 150 mM NaCl, 0.05% TWEEN20

Tris Buffered Saline 1X (TBS): 50 mM Tris-HCl, 150 mM NaCl

Lysis Buffer: 50 mM NaH_2PO_4, 300 mM NaCl, 1 µg mL^{-1} DNAse I, 1/100 Vol Halt 100x Protease Inhibitor

TEZ Buffer: 0.2 M Tris, 0.5 mM EDTA, 0.5 M sucrose, pH 8.0

Lactose Elution Buffer: 50 mM NaH_2PO_4, 300 mM NaCl, 300 mM lactose

Ni-NTA Wash Buffer: 20 mM imidazole, made up to desired volume with lysis buffer

Ni-NTA Elution Buffer: 500 mM imidazole, made up to desired volume with lysis buffer

Amylose Elution Buffer: 10 mM maltose in phosphate buffer

6X DNA Loading Dye: 5 mM Tris-HCl pH 8.0, 0.15% w/v Orange G (Sigma), 2.5% w/v Ficoll 400 (Sigma), 10 mM EDTA, dissolved in sterile H_2O

TAE Buffer: 40 mM Tris base, 20 mM Acetic acid, 1 mM EDTA

SDS-PAGE Running Buffer: 25 mM Tris base, 192 mM glycine, 0.1% SDS

SDS-PAGE Loading Buffer: 62.5 mM Tris HCl, 5% w/v β-mercaptoethanol, 10% w/v Glycerol, 2.5% w/v SDS, 0.002% w/v Bromophenol Blue

SPR Buffer: 50 mM NaH_2PO_4, 150 mM NaCl, 0.1% Triton-X 100

Blocking Buffer: 20% v/v 10x Casein Blocking Buffer in *PBS-T*

Cell Cleansing Buffer: 0.2 M acetic acid, 0.5 M NaCl, pH 2.8

Solubilisation Buffer: 10 mM Na_2HPO_4, 1.8 mM KH_2PO_4, 137 mM NaCl, 2.7 mM KCl, 0.1% Triton-X 100

6.2. Media

Miller's Lysogeny Broth (LB) Medium: 1.0% w/v tryptone, 0.5% w/v yeast extract, 1.0% w/v NaCl

LB Agar Antibiotic Plates: 1.5% w/v agarose, 2.5% w/v LB medium**.** The agar was supplemented with a final concentration of 100 µg/ml ampicillin or 50 µg/mL kanamycin to generate the selective medium.

2x Tryptone/Yeast Medium (2TY): 1.6% w/v Tryptone, 1.0% w/v Yeast Extract, 0.5% w/v NaCl

High Salt LB Growth Medium: 1.0% w/v Tryptone, 0.5% w/v Yeast Extract, 2.0% w/v NaCl

Cell Culture Medium: DMEM/F-12 GlutaMAX, 10% v/v foetal bovine serum, 5% v/v penicillin-streptomycin (Sigma)

6.3. DNA Manipulation

6.3.1. Polymerase Chain Reaction

Standard polymerase chain reaction (PCR) was used to amplify DNA for gel extraction, or for product analysis, to ensure that all primers resulted in a single, specific DNA fragment being produced. In all cases, New England Biolabs (NEB) enzymes and buffers were used, and all products were analysed by nucleic acid electrophoresis (see *6.3.4. Nucleic Acid Electrophoresis*). Standard PCR was set up in 50 µl reactions on ice, and contained the following:

1x Phusion High Fidelity Polymerase buffer (NEB)
500 nM Forward primer
500 nM Reverse primer
400 µM dNTP
1-25 ng DNA template
1 unit Phusion High Fidelity Polymerase (NEB)

This solution was made up to 50 µl with sterile H_2O, and the following cycling conditions were used:

95˚C	5 minutes		
95˚C	20 seconds	}	30 Cycles
T_m	20 seconds		
72˚C	45 seconds		
72˚C	5 minutes		
4˚C	Hold		

An extension time of 45 seconds was suitable for amplification of DNA segments less than 1 kb in size. A further 20 seconds was added for every additional kb of DNA to be amplified.

Primers for PCR were designed to be of length 18-30 bp, and to have a T_m of 55-65˚C. The primer melting temperature (T_m) was calculated by using the free online tool OligoCalc provided by *W. A. Kibbe*.[280]

6.3.2. PCR Product Purification

Following PCR, the product needed to be separated from contaminants such as polymerase, primers, and nucleotides. This was achieved by using a Qiagen silica spin column. The reaction mixture was combined with a high-salt buffer (Buffer QG), and applied directly to the column. After binding, the silica column was washed with an ethanol-containing buffer (Buffer PE), followed by elution of the DNA under low-salt conditions (H_2O).

6.3.3. DNA Fragmentation by Restriction Enzyme Digestion

Restriction digests were carried out using NEB restriction enzymes, using specified manufacturer's buffers. Digests for DNA analysis were set up in a final volume of 20 µl, with approximately 1 unit of enzyme per µg of DNA. Following a one hour incubation at 37˚C, the products were analysed via nucleic acid electrophoresis.

6.3.4. Nucleic Acid Electrophoresis

Separation of DNA fragments by size was achieved using agarose gel electrophoresis. 1% agarose gels were prepared for separation of fragments greater than 500 bp in length, whilst 1.5% gels were run to separate smaller DNA fragments. The gels were prepared by dissolving 30 mL agarose in TAE buffer, followed by the addition of 3 µl Invitrogen SYBR Safe DNA Gel Stain to permit visualisation of DNA fragments under UV light exposure. 6x DNA loading buffer was added to the DNA samples, before being loaded onto the gel. Gels were electrophoresed at 80 V for 30 minutes in TAE buffer in Bio-Rad Mini Sub-Cell Gel Tanks.

6.3.5. DNA Purification from Agarose Gels via Gel Extraction

DNA fragments of different size were separated and purified from agarose gels via gel extraction. Gels were visualised under a blue light transilluminator, and the gel region containing the DNA of interest was cut out using a scalpel blade. This was transferred to a microcentrifuge tube and weighed, then trimmed down to 400 mg or less so as not to

exceed the binding capacity of the column. Following this, the agarose slice was dissolved in Buffer QG, and purified as discussed in section *6.3.2. PCR Product Purification*.

6.3.6. DNA Quantification

All DNA concentrations were measured using a NanoDrop 2000 Spectrophotometer (Thermo Scientific). The instrument was typically blanked with H_2O. Absorbance at 260 nm was then measured to reveal the concentration of DNA in ng μl^{-1}.

6.3.7. DNA Ligation

For ligation reactions, destination vectors were digested with restriction enzymes, and purified from the intervening DNA fragment by gel extraction. Additionally, the vectors were treated with a phosphatase, to remove 5' phosphate groups as a measure to prevent the vector from ligating with itself. Smaller segments of DNA, digested with compatible ends, were quantified, and then ligated with the vector using NEB T4 DNA Ligase in a molar ratio of 3:1 insert to vector. The number of pmol μl^{-1} was calculated using the following equation:

$$pmol\ \mu l^{-1} = \frac{DNA\ concentration\ in\ ng\ \mu l^{-1}}{0.65\ \times\ number\ of\ bp}$$

In a typical reaction, 10x T4 Ligase Buffer was thawed on ice, and 2 µl was combined with the digested insert and vector. The solution was then made up to 19 µl with sterile H_2O, and 1 µl T4 DNA Ligase was added. Several control reactions were additionally set up, including a reaction lacking the vector, a reaction lacking the insert, and a reaction lacking both the insert and ligase. The ligation mixtures were incubated at room temperature for four hours prior to transformation. Colonies on the control plates were then compared in number against the colonies transformed with the complete ligation experiment as a preliminary measure to determine ligation efficiency and success.

6.3.8. Ligation Independent Cloning

For the cloning of an insert into a vector by ligation independent cloning (LIC), 10 µg destination vector (pNIC-CTHF, *7.1.6. pNIC-CTHF*) was digested at 50˚C with BfuAI (NEB) for two hours. BfuAI sites flank a 1 kbp region of DNA coding for the sacB gene in the destination vector. SacB confers sensitivity to sucrose, and can thus be used as a counterselectable marker. This reaction was then electrophoresed on a 1% agarose gel, and the digested vector excised using a sharp scalpel. The vector was purified from the agarose, before being treated with T4 DNA polymerase (NEB). 2.5 mM dCTP, 5 mM DTT, BSA, 600 ng digested vector, and 0.5 µl T4 DNA polymerase were combined with

NEB buffer 2, and dH_2O to a final volume of 20 µl. The reaction mixture was incubated at 22˚C for 30 minutes, followed by a 75˚C incubation for 20 minutes. This process exploits the 3'-5' exonuclease activity of T4 polymerase that acts in the absence of nucleotides. T4 polymerase 'chews back' the ends of the vector until a cytosine is reached, at which point the polymerase activity of the enzyme is activated, due to the presence of dCTP in the solution, leaving a 14 bp overhang. The insert was amplified by PCR using primers complementary to the gene of interest, but containing the following sequences at the 5' ends of the forward and reverse primers respectively:

5' – TTAAGAAGGAGATATACTATG – 3'

5' – GATTGGAAGTAGAGGTTCTCTGC – 3'

The PCR product was then purified and similarly treated with T4 DNA polymerase, but in a reaction containing 2.5 mM dGTP instead of dCTP. An overhang complementary to the destination vector overhang was generated in this process, allowing the two treated DNA segments to be combined and transformed without the requirement of a ligase. Vector and insert were mixed in a 1:3 molar ratio, and incubated for ten minutes prior to transformation.

6.3.9. Site Directed Mutagenesis

Conventional site-directed mutagenesis was carried out to change nucleotides within a plasmid in a site-specific manner. The process relies on primers with a high degree of complementarity flanking the region that is to be altered, and hence amplifying the plasmid whilst introducing the desired mutation. DpnI, an enzyme that recognises and cleaves methylated DNA, is added to digest the wild-type plasmid, leaving exclusively the amplified product for transformation. All primers were designed using *Agilent Technologies QuikChange Primer Design* program.[3] Polymerase chain reactions were set up as follows:

1x KOD Hot Start Polymerase buffer (VWR)
140 nM Forward primer
140 nM Reverse primer
1.5 µM $MgSO_4$
200 µM dNTP
50 ng DNA template
1 unit KOD Hot Start Polymerase (VWR)
ddH_2O to 50 µl

[3] https://www.genomics.agilent.com/primerDesignProgram.jsp

Cycling conditions:

95˚C	2 minutes	
95˚C	20 seconds	20 cycles
55˚C	20 seconds	
70˚C	2 min 30 sec	
72˚C	10 minutes	
4˚C	Hold	

The PCR product was combined with 1 µl DpnI, and incubated at 37˚C for two hours, before transformation into XL10 *E. coli* cells.

Insertion or deletion of nucleotides was carried out using primers complementary to the DNA flanking the region where the insertion or deletion was desired (Figure 6.5). Any nucleotides to be inserted were added on to the 3' end of the primers, and any region to be deleted was flanked by the primers, thus omitting it from amplification during PCR. As a result, a linear, double-stranded fragment of DNA was produced. This linear fragment was then treated with a cocktail of enzymes supplemented with ATP, to phosphorylate and ligate the blunt ends whilst digesting the parent DNA, thus allowing transformation exclusively of circularised, mutated plasmid. The enzyme mix (kinase, ligase and DpnI), as well as the ATP-containing buffer, was purchased as part of a kit from NEB (Q5® Site-Directed Mutagenesis Kit).

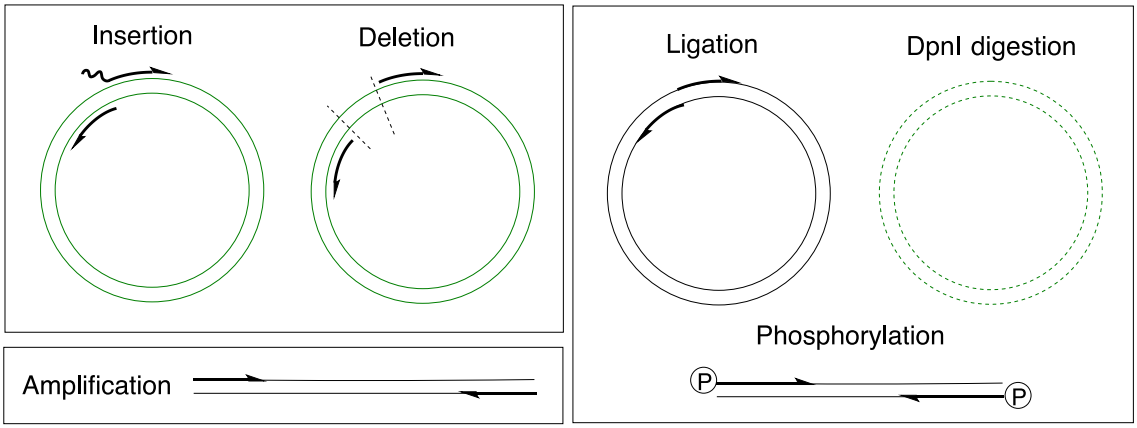

Figure 6.5. Schematic showing how PCR mutagenesis can be used to insert or delete nucleotides from a plasmid. (A) Primers are designed to flank the region to be modified. In case of deletion, flanking primers are all that is required. For insertion, one of the primers should carry the additional nucleotides to be inserted. (B) Amplification of the plasmid produces linear, double-stranded DNA. (C) A kinase, ligase and DpnI enzyme are added to the linear fragment in a one pot reaction to phosphorylate the 5’ end of the DNA, allowing ligation of the linear strands into a circularised plasmid. The DpnI degrades the hemi-methylated parent DNA, leaving only the ligated product for transformation.

In order to carry out mutagenesis in this fashion, the following reaction was set up:

12.5 µl Q5 Hot Start High-Fidelity 2X Master Mix (NEB)
500 nM Forward primer
500 nM Reverse primer
1-25 ng DNA template
ddH_2O to 25 µl

PCR cycling conditions:

98˚C	30 seconds	
98˚C	10 seconds	} 25 cycles
T_m	20 seconds	
72˚C	30 sec/kb	
72˚C	2 minutes	
4˚C	Hold	

Following the PCR, the product was used in a subsequent reaction:

PCR Product 1 µl
5 µl 2X KLD Reaction Buffer
1 µl 10X KLD Enzyme Mix
3 µl ddH_2O

The solution was incubated at room temperature for 30 minutes, and 3 µl used for a transformation into XL10 *E. coli* cells.

6.3.10. Heat-shock Transformation of XL10/BL21 Gold *Escherichia coli*

Chemically competent *E. coli* cells were transformed via heat-shock. XL10-Gold *E. coli* cells were used for plasmid production, whilst BL21 Gold DE3 cells were employed for protein expression.

10 µl of cells were combined with 1 µl of plasmid DNA in sterile H_2O, and kept on ice for 30 minutes. Following this, the cells were placed in a 42˚C water-bath for 90 seconds, and then immediately supplemented with 500 µl room-temperature LB medium, and incubated at 37˚C for 1 hour. The cells were then spun down for 4 minutes at 13000 RPM. 400 µl supernatant was then removed, and the cells were resuspended in the

remaining LB medium. 100 µl of the transformed *E.coli* cells were then plated out onto LB agar ampicillin or kanamycin plates, and incubated overnight at 37˚C.

6.3.11 Small Scale Plasmid DNA Purification

XL10 colonies were picked under sterile conditions from LB-agar plates, and added to 5 ml 2TY medium, and combined with 5 µl ampicillin or kanamycin, to ensure selective growth of the picked colonies. This pre-culture was then shaken at 160 rpm for 16 hours at 37˚C. Following this, instructions were followed as laid out in the QIAprep® Spin Miniprep Kit High-Yield Protocol.

6.4. Protein Manipulation

6.4.1. Protein Expression

BL21 DE3 *E. coli* cells, harbouring the desired plasmid, were collected under sterile conditions from a glycerol stock or from a LB-agar plate, and added to 5 ml LB medium together with 5 µl ampicillin (100 mg/mL) or kanamycin (50 mg/mL), to ensure selective growth. This pre-culture was shaken at 200 rpm for 18 hours at 37°C, before being used to inoculate 1 L LB-medium in a 2 L conical flask containing the appropriate antibiotic. Following inoculation, cultures were induced with 0.5 mM IPTG at OD_{600} 0.6, and incubated at 30°C overnight.

6.4.2. CTB Expression from *Vibrio sp. 60*

For the production of wild-type CTB, a preculture of the *Vibrio sp.60* stock was initially set up in 100 mL high salt LB growth medium, with 100 µg mL^{-1} of ampicillin. This was incubated at 30°C for 18 hours, before being used to inoculate 5 x 1 L high salt LB growth medium in 2 L conical flasks. Once the OD_{600} reached 0.6-0.8, 240 mg/L IPTG was added to the flasks to induce protein expression. Following IPTG induction, the cells were incubated at 30°C for another 24 hours, before cell pellet isolation by centrifugation at 17000 x*g* for 25 minutes. The supernatant was retained, as this contained the protein of interest, and was thus separated from the cell pellet, and purified by ammonium sulfate precipitation.

Solid ammonium sulfate was added and dissolved to a final concentration of 57% w/v. The saturated solution was then stirred for two hours using a magnetic stirrer at room temperature. The solution was then centrifuged at 18,000 x*g* for 30 minutes, and the supernatant was discarded, whilst the pellet was resuspended in 20 mL PBS. This in turn was centrifuged at 18,000 x*g* for 10 minutes to remove insoluble material, and to allow

the suspension to be filtered through a 0.8 µm Sartorius Minisart filter. Finally, the filtered suspension was separated on a lactose affinity column at 4°C, and eluted with lactose elution buffer. The eluate was dialysed 4 times against PBS.

6.4.3. Expression and Purification of CTB variants from *E. coli*

1 L LB medium in a 2 L conical flask was inoculated and induced, as stipulated in *6.4.1. Protein Expression*. The induced culture was incubated for ~20 hours, and then centrifuged at 10,000 x*g* for 10 minutes at 4°C to pellet the cells. The supernatant was retained and combined with ammonium sulfate to precipitate the protein as outlined in *5.4.2. CTB Expression from Vibrio sp. 60*. The presence of the surface exposed H13 in CTB confers affinity for Ni-NTA resin, offering an alternate purification route. This purification strategy was often employed when expressing multiple CTB variants, as purification by Ni-NTA chromatography could be set up in a higher throughput manner than lactose affinity chromatography. A less pure eluate was obtained via this route, necessitating purification by gel filtration.

6.4.4. Expression and Purification of MBP-AB_5 proteins

1 L LB medium was inoculated and induced, as stipulated in *6.4.1. Protein Expression*. Protein overexpression was induced at an OD_{600} of 0.6 with the addition IPTG (240 mg L^{-1}). The cells were incubated at 30°C for ~20 hours, before isolation of the cells by centrifugation (10,000 x*g* for 10 minutes). The cell pellet was then discarded, whilst the supernatant was retained.

The supernatant was filtered through a Sartorius Minisart 0.8 µm filter, and applied to an amylose column to retain the overexpressed MBP-AB_5. Some uncomplexed MBP-CTA_2 proteins were also retained by the amylose resin, necessitating a second purification step. The column was washed with five column volumes of phosphate buffer, before elution of the bound protein with five column volumes of amylose elution buffer. The eluted fractions were then combined with 10 mL Ni-NTA resin, and applied to a Bio-Rad Econo-Pac® Chromatography Column to isolate the MBP-AB_5 complex exclusively. The resin was washed with five column volumes of phosphate buffer before protein elution with Ni-NTA elution buffer.

6.4.5. Cell Disruption for Protein Purification

Cells were pelleted by centrifugation for 10 minutes at 10,000 x*g*. The supernatant was discarded, and the remaining cell pellet was resuspended in a lytic cocktail containing 8 mL lysis buffer, 0.8 mL BugBuster (Novagen). This suspension was incubated at room temperature on a rocker for 40 minutes for standard proteins, or 20 minutes, followed by

an additional 20 minute incubation at 50˚C, to be carried out when purifying Affimers. The lysate was then clarified by centrifugation at 10,000 x*g* for 30 minutes, followed by filtration through a 0.45 µm Sartorius filter.

6.4.6. Periplasmic Extraction of Proteins Using Sucrose Shock

Small quantities of Affimer could be produced from the pBSTG phagemid without the need for subcloning into an expression vector. Since the Affimer CDS was preceded by a periplasmic-targeting sequence, the proteins could be isolated directly from the periplasm by sucrose shock. An amber stop codon followed the Affimer CDS, requiring expression to be carried out in a non-suppressor strain of *E .coli*, such as JM83 or BL21 cells. Following inoculation, induction, and incubation of the transformed *E. coli*, the cells were pelleted, and resuspended in 200 mL L^{-1} culture of TEZ buffer by gentle agitation on a rocker for two hours. Once fully resuspended, 300 mL L^{-1} culture of 0.2 X TEZ buffer diluted in water was added, and the solution was left on a rocker at 4°C for 30 minutes. Following the incubation period, the cells were pelleted, and the supernatant retained and applied to a nickel affinity column for purification of the Affimer (*6.4.6. Purification of His-tagged Proteins*).

6.4.6. Purification of His-tagged Proteins

2 mL Ni-NTA slurry was transferred to a Bio-Rad Econo-Pac® Chromatography Column, and washed with 25 mL lysis buffer to dilute and remove the resin storage solution. The liquid was drained, and the clarified cell lysate was transferred to the column containing the resin, which was capped at both ends, and placed on a rocker for 30 minutes to facilitate binding of the His-tagged protein to the Ni-NTA resin. The lysate was drained from the column, and the settled resin was washed with 50 mL Ni-NTA wash buffer. The bound material was then eluted with 10 mL Ni-NTA elution buffer and collected in 2 mL fractions.

6.4.7. Purification of MBP-tagged Proteins

20 mL Amylose resin was transferred to a Bio-Rad Econo-Pac® Chromatography Column, and washed with 60 mL phosphate buffer to dilute and remove the resin storage solution. The solution containing the MBP-tagged protein was then applied to the column. The resin was washed with five column volumes of phosphate buffer, before elution of the bound protein with five column volumes of amylose elution buffer.

6.4.8. Concentration of Protein Samples

Following size exclusion chromatography, protein samples were concentrated using Amicon Ultra-15 Centrifugal Filter Units with cut-off range of 3 - 30 kDa. 5 mL fractions were transferred to the filter units, and centrifuged at 3,500 x*g* until the protein was

concentrated to an appropriate volume. As the protein collects on the filter, resuspension of the protein every 15 minutes using a P200 Gilson pipette was necessary.

6.4.9. Protein Quantification

All protein concentrations were measured using a NanoDrop 2000 Spectrophotometer (Thermo Scientific). The instrument was blanked with either the protein buffer, or the flow through from the centrifugal filter units. Absorbance at 280 nm of a 2 µl sample was measured, and using the molar extinction coefficient provided by ProtParam protein sequence analysis, along with the protein mass, the concentration was calculated. A feature of the NanoDrop 2000 allows the concentration of protein and fluorescent label to be measured simultaneously, thus revealing the percentage of labelled protein in the sample.

6.4.10. Dialysis

Dialysis was frequently employed to remove small molecules such as imidazole or urea from a protein solution. 5 cm Thermo Scientific SnakeSkin Pleated Dialysis Tubing 3500 MWCO was placed in buffer, and left for 5 minutes to hydrate. One end of the dialysis tubing was folded over and clipped shut using a tubing clip. The solution to be dialysed was then placed within the tubing, and sealed inside with a second tubing clip, ensuring that no bubbles were present. The tubing was then placed inside 1 L buffer with a magnetic follower inside, and left at 4 °C for 4 hours, before replacing the buffer and repeating the process.

6.4.11. Purification by Gel Filtration Chromatography

Following elution from affinity columns, protein solutions were further purified by gel filtration chromatography. This process can be used to separate proteins on the basis of their shape and size. A sample is applied at a fixed flow rate to a column containing a porous resin composed of cross-linked carbohydrates, such as dextran and agarose. Once the sample enters the resin, the smaller molecules become trapped in the pores, and thus have a longer retention time than the larger molecules, which bypass the pores due to their larger size, and take a shorter route through the resin. This process is sufficiently high resolution to separate proteins from contaminants and small molecules, such as imidazole, and from other proteins, although the resolution for a given mass range will vary dependent on the type of resin used. A detector measuring absorbance at a range of wavelengths analyses the column flow-through, plotting absorbance as a function of retention volume. The resultant chromatogram can then be used to identify the protein-containing fractions, which can be collected and analysed.

All columns were stored in 20% ethanol, and all solutions to be applied directly to size exclusion columns were filtered through a 0.2 µm Sartorius Minisart filter. Columns were equilibrated initially with water, to displace the ethanol, followed by 1.5 column volumes of an appropriate protein buffer. When displacing the ethanol, flow rates were set at half the standard flow rate to prevent exceeding the pressure limit of the column.

For large-scale purification of proteins, a HiLoad™ 16/60 Superdex™ 75 prep-grade column (GE Healthcare) was attached to an Äkta Purifier FPLC system, and flowed at a rate of 1 mL min^{-1}. Protein samples ranging from 500 µl to 5 mL in volume, and between 10 kDa and 80 kDa in mass, were loaded onto this prep-grade column.

For analytical scale purification of proteins, a Superdex™ 75 Increase 10/300 column was attached to the FPLC system, and flowed at a rate of 0.5 mL min^{-1}. Volumes ranging from 50 µl to 1 mL were loaded onto the analytical column, with a mass range of 10 – 80 kDa.

Proteins samples for purification or analysis were injected manually into the injection loop of the FPLC system. The loop was then flushed with buffer (1.5 x the loop volume) in an automated process to apply the loop contents to the resin. Fractions were collected once the void volume of the column had been reached, and were analysed by a detector measuring absorbance at 280 nm, or 488/555 nm if purifying fluorescently-labelled proteins.

6.4.12. Denaturing SDS Polyacrylamide Gel Electrophoresis

To separate proteins on the basis of their mass, 10 µl of the protein samples were boiled for 10 minutes in 10 µl SDS-PAGE loading buffer. The boiling results in denaturation, whilst the presence of the β-mercaptoethanol reduces any potential disulfide bonds within the protein. The SDS then coats the polypeptide chain in a negative charge, allowing the protein to migrate solely on the basis of its mass.

A resolving polyacrylamide gel was then set up using the recipe in Table 6.2. Directly following addition of TEMED, the solution was poured into a fixed BioRad 0.75 mm spacer plate, and left to set with a layer of isopropanol on the surface to prevent dehydration of the gel. Once the gel had set, the isopropanol was removed with a paper towel, the top of the gel was washed with sterile water, and a 1 mL solution of loading gel was added, followed by a 0.75 mm BioRad comb. Once the loading gel had set, the comb was carefully removed, and the gel was transferred to a BioRad electrophoresis

tank. The inside of the tank, where the gel was fixed, was filled with SDS-PAGE running buffer to ensure that no leaking was taking place. Finally, the surrounding section of the tank was half-filled with running buffer, the samples were loaded into the wells using a Gilson pipette, and the gel was electrophoresed at 180 V for 45 minutes.

	12% Resolving Gel	15% Resolving Gel	Stacking Gel
dH_2O	2.1 mL	1.725 mL	657.5 µl
40% Bisacrylamide	1.5 mL	1.875 mL	127.5 µl
1.5 M Tris-HCl pH8.8	1.3 mL	1.3 mL	-
1.0 M Tris-HCl pH6.8	-	-	195 µl
10% SDS	50 µl	50 µl	10 µl
10% APS	50 µl	50 µl	10 µl
TEMED	2 µl	2 µl	1 µl

Table 6.1. Recipes for 12% and 15% SDS-PAGE gels. Higher percentage gels were used to separate proteins of similar masses.

6.4.13. Mass Spectrometry

Protein samples were diluted to 30-50 µM, and 20 µl of the diluted solution was transferred to a 500 µl tapered glass vial. The sample was analysed by a Bruker HCT-Ultra mass spectrometer via electrospray ionisation.

6.4.14. Protein labelling

6.4.14.1. Labelling Affimers with Alexa Fluor 555 C2 maleimide

Affimers carrying a C-terminal cysteine residue were concentrated to 150 µM in TCEP phosphate buffer (50 mM phosphate, 150 mM NaCl, 0.5 mM TCEP, pH 7.2). 400 µl Affimer was combined with 0.94 mg Alexa Fluor 555 C2 maleimide (aliquoted and lyophilised) (equal to five molar equivalents). Samples were incubated at room temperature for four hours in foil, before purification using a PD-10 desalting column, concentration to 250 µl, and a final purification by gel filtration using an analytical Superdex 75 increase column. Concentration of labelled Affimer was calculated using an equation provided by Thermo Fisher Scientific:

$$[Affimer]M = \frac{(A_{280} - (A_{555} * 0.08)) * dilution\ factor}{\mathcal{E}\ cm^{-1}\ M^{-1}}$$

6.4.14.2. Labelling CTB with aminooxy Alexa Fluor 488

CTB was labelled with aminooxy Alexa Fluor 488 by oxidising the N-terminal threonine, and combining the subsequent oxidised CTB with two molar equivalents of the lyophilised fluorophore. CTB (500 µM [protamer concentration], in phosphate buffer

only), L-methionine (10 equivalents), and $NaIO_4$ (5 equivalents) in phosphate buffer, were incubated together at room temperature out of light for 45 minutes, before buffer exchanging into phosphate buffer (**pH 6.8**) using a PD10 desalting column. The 1 mL eluate was then concentrated to 0.5 mL (~500 µM), and added to 0.4 mg lyophilised fluorophore (2 molar equivalents) and 4.5 µl aniline (neat). To reduce the number of fluorophores per pentamer, the amount of fluorophore can be reduced to 0.4 molar equivalents. After a 20 hour incubation, the protein was purified using a G25 desalting column, concentrated to 0.5 mL, and purified by gel filtration.

6.5. Phage Display

Phage display provides a robust method for the identification of binding molecules from a large library of potential binders. These binders are expressed as fusions on the surface of the phage coat proteins, and the sequence of the binding molecule is usually intrinsically linked to the DNA of the phage carrying the fusion. In order for these libraries of phage-binder to be created, established, and proven to be functional, a considerable amount of work and time must be invested. Furthermore, use of such phage libraries requires specialist equipment and dedicated facilities to use the tool successfully, and to prevent the spread of phage infections. The work carried out in this project would not have been possible without the foundations built by the Bio Screening Technology Group that allowed me to use a phage-dedicated facility and have access to the phage-Affimer library.

6.5.1 Preparation of ligand-coated plates

6.5.1.1. Streptavidin plate preparation

Streptavidin-coated plates were prepared by coating Nunc MaxiSorp flat-bottom 96 well plates with 100 µl 100 nM streptavidin diluted in PBS. The plate was sealed, and incubated at 37°C overnight to adsorb the protein to the plate surface. The following day, the 96-well plate was washed with PBS-T, and then blocked with blocking buffer overnight at 37°C. The commercial blocking buffer is casein-based, and blocks sites in the wells not occupied by streptavidin to prevent non-specific binding. After the incubation, the plate was washed once more with PBS-T prior to use.

6.5.1.2. GM1 plate preparation

GM1-coated plates were prepared by coating Nunc MaxiSorp flat-bottom 96 well plates with 100 µl 1.3 µM solution of GM1 ganglioside in methanol. The methanol was allowed to evaporate, thereby adsorbing the ganglioside to the plates. The GM1 plates were blocked overnight by incubating them at 37°C with a casein-based blocking buffer. The

following day, the plate was washed once with 300 µl PBS-T on a plate washer immediately before use.

6.5.2. Panning the phage library using streptavidin-coated strips

In the first step, streptavidin-coated plastic wells were prepared for pre-panning the phage-Affimer library. 300 µl blocking buffer was added to four wells of a Pierce streptavidin-coated 8-well strip (Thermo Scientific). The strip was sealed, and incubated overnight at 37°C. Three of the wells were to be used for pre-panning the library, with the final well required for panning the phage against the biotinylated target protein. A colony of ER2738 cells was transferred into 5 mL 2TY supplemented with 12 µg mL^{-1} tetraycline (2TY tet) for overnight growth.

The wells were washed three times with PBS-T using a plate washer. 100 µl blocking buffer and 20 µl of CTB-biotin (1.5 µM or 100 µg mL^{-1}) were added to the fourth well, for capture of the target to the streptavidin, whilst 100 µl blocking buffer only was added to the first three pre-panning wells. The strips were sealed once more, and incubated for two hours at room temperature on a vibrating platform shaker. Buffer from the first pre-pan well was removed, and was replaced with 100 µl blocking buffer and 5 µl of the phage library. The phage was then mixed and incubated in the well on a vibrating platform for 40 minutes. The buffer from the second pre-pan well was removed, and the solution from the first pre-pan well was transferred. The transferred phage was incubated for 40 minutes once more, and the same process was repeated for the third pre-pan well. This process was employed to remove phage-Affimer particles that bind to a component of the well, such as the bound streptavidin, or to other adsorbed proteins such as casein. The wells containing the target protein were washed six times, before adding the phage from the pre-pan wells. A two-hour incubation at room temperature followed on the vibrating platform shaker to allow the transferred phage to bind to the immobilised target.

6.5.3. Phage elution and propagation

A fresh culture of ER2738 *E. coli* cells was grown to an OD_{600} of approximately 0.6 by diluting the overnight culture 1/15 into 8 mL 2TY, and incubating the solution at 37°C for one hour.

Whilst the culture was growing, the panning well was washed 27 times with PBS-T. The phage was then eluted by adding 100 µl of 0.2 M glycine, pH 2.2, and incubating the solution for ten minutes at room temperature before neutralisation with 15 µl of 1M Tris-HCl, pH 9.1. The resulting solution was transferred immediately to the fresh 8 ml culture of the ER2738 *E. coli* cells. To ensure that all bound material had been successfully

eluted, 100 µl of triethylamine (1.4% in PBS) was added to the well, and left for six minutes. 50 µl 1M Tris-HCl, pH 7.0 was added to neutralise the triethylamine, and the solution was transferred to the 8 mL culture. The culture was placed in a 37 °C incubator for one hour, and shaken once, by hand, after 30 minutes.

1 µl of the culture was combined with 100 µl 2TY, and plated out onto a LB-agar carbenicillin plate. The remainder of the culture was centrifuged to pellet the cells, and resuspended into 100 µl medium. The entire suspension was transferred and spread across a second LB-agar ampicillin plate. The plates were incubated at 37 °C overnight. The following day, the colonies on the plate containing 1 µl of cells were counted, and multiplied by 8,000 to determine the total number per 8 ml of cells. Successful panning rounds typically generated between 0.5 – 2 x 10^6 cells.

5 mL 2TY supplemented with 100 µg/ml carbenicillin (2TY carb) was added to the plate containing the full culture suspension, and a plastic spreader was used to scrape the cells into the solution. The 5 mL was transferred to a falcon tube, and a further 2 mL 2TY was used to scrape any remaining cells from the plate surface. The OD_{600} was measured of a 1:10 dilution, and the suspension was diluted into 2TY to make an 8 mL culture of OD_{600} = 0.2. The dilution was incubated at 37 °C, 230 rpm, for one hour.

0.32 µl M13K07 helper phage (titre ca. 10^{14}/ml) was added to the culture after one hour, and left to incubate at 37 °C, 90 rpm, for 30 mins. The helper phage also infect the bacteria, providing the phage-Affimer with additional components to form infectious particles. The helper phage also confers resistance to kanamycin. To select only the bacteria harbouring phage-Affimer particles and the helper phage, 16 µl of kanamycin (25 mg ml^{-1}) was added, and the culture was incubated overnight at 25 °C, 170 rpm.

The phage-infected cultures were centrifuged at 3,500 *xg* for 10 mins to pellet the infected cells, leaving the newly formed phage-Affimer particles in solution. The supernatant was retained and transferred to fresh tubes. 125 µl phage-containing supernatant was retained for the next panning round.

6.5.4. Phage purification and storage

To purify the phage, 2 ml of PEG-NaCl precipitation solution (20% (w/v) PEG 8000, 2.5 M NaCl) was added to the phage-containing supernatant, mixed, and incubated overnight at 4°C. The following day, the precipitated phage were pelleted at 4,816 *xg* for 30 mins, and the supernatant was discarded. The pellet was resuspended in 320 µl TE

buffer, transferred to a 1.5 mL Eppendorf tube, and centrifuged at 16,000 *xg* for 10 mins. The supernatant contained purified phage, which could be used directly in a subsequent panning round, or could be combined with 50% glycerol and stored at -80°C for long-term storage.

6.5.5. Panning the phage library using streptavidin-coated magnetic beads

After propagation of the phage from the first panning round, a second panning round was carried out to expose the phage to the same target, but presented in a different manner. Rather than exposing the phage to CTB-biotin captured onto streptavidin-coated plastic wells, the biotinylated target would be presented on streptavidin-coated magnetic beads. This difference in presentation should minimise the number of background binders carried through the screen by presenting a very different binding surface.

As in the first round, a colony of ER2738 *E. coli* cells was cultured overnight in 5 mL 2TY tet. 20 µl streptavidin beads (Dynabeads MyOne Streptavidin T1) were combined with 100 µl *blocking buffer* and incubated overnight at room temperature on a Stuart rotator.

The next day, the beads were centrifuged at 800 *xg* for one minute, placed onto a magnetic Eppendorf rack, and resuspended in 100 µl fresh *blocking buffer*. The magnetic rack draws the beads to the side of the tube, allowing buffer to be changed without losing the streptavidin beads. 125 µl of the phage retained from the initial propagation step, or 5 µl of the purified phage, was combined with blocking buffer to a total volume of 250 µl in Eppendorf LoBind Tubes. 25 µl of the pre-blocked streptavidin beads was added to the phage, and incubated on a Stuart rotator for one hour. Beads were separated from the phage by centrifugation and placement on the magnetic rack. The supernatant was transferred to a tube containing another 25 µl of pre-blocked streptavidin beads, and the pre-panning process was repeated.

15 µl CTB-biotin (1.5 µM) was combined with 200 µl blocking buffer, and 50 µl streptavidin beads, before being placed on a Stuart rotator for 30 minutes to bind. The beads were washed three times with 500 µl blocking buffer by removing the buffer, resuspending the beads, and then immobilising the beads to the magnetic rack, removing the buffer, and iterating the process. The supernatant containing the pre-panned phage was then transferred to the beads containing the captured CTB-biotin, and placed on a Stuart rotator for 45 minutes. After the incubation, the beads were washed manually 27 times with PBS-T.

A fresh 8 mL culture of ER2738 *E. coli* cells was set up, and the bound phage were eluted and used to infect the culture as described in *6.5.3. Phage elution and propagation*. Plates were prepared and the phage propagated and stored as described previously. 200 µl phage supernatant was retained for the following panning round.

6.5.6. Panning the phage library by competitive selection

In the third panning round, neutravidin-coated strips were used to pre-pan the phage and capture the biotinylated target. Strips were blocked as before, but six wells were blocked rather than four, and no overnight culture was required at this stage.

The phage-containing supernatant from the previous round was added to the first pre-blocked neutravidin-coated well. Four pre-panning rounds, each lasting one hour, were carried out. 10 µl CTB-biotin and 100 µl blocking buffer was added to the fifth well for immobilisation, with the sixth well retained as a negative control. To this control well, 10 µl blocking buffer was added instead. After 30 minutes, both wells were washed six times with PBS-T. 100 µl of the pre-panned phage was transferred to the fifth well containing the target (well T+), with the remaining 100 µl added to the control well (well T-). After a 45 minute incubation, both wells were washed 27 times to remove any unbound phage. To both wells, 80 µl blocking buffer, 20 µl 80% glycerol, and 20 µl 5 µM solution of unmodified CTB was added as a competitor, to remove all but the highest affinity CTB-binding Affimers. This solution was incubated overnight at room temperature. Meanwhile, an overnight culture of ER2738 *E. coli* cells was prepared.

The following day, two 5 mL cultures were prepared by diluting the overnight culture 1:15, and incubating for one hour at 37 °C, 230 rpm. Both panning wells were washed 27 times, and the phage were eluted as described in *6.5.3. Phage elution and propagation*. The eluted phage from the well T+ were transferred to one of the 5 mL cultures, whilst the eluted phage from the control well T- were added to the other culture. After a one hour incubation to allow the infection to take place, a range of volumes of the cultures were plated out onto LB-agar carbenicillin plates (Table 6.2).

Volume of bacterial culture plated out (µl)	Phage screened against CTB-biotin (T+)	Negative control (T-)
0.01	X	
0.1	X	
1	X	X
10	X	
ALL	X	

Table 6.2. The six LB-agar carbenicillin plates, and the material plated out onto each plate. Bacteria were either infected with phage eluted from the target positive (T+) well, or target negative (T-) well. The volumes stated above of each culture were plated out onto the plates, with the lowest volumes being prepared from a dilution of the culture.

Such small volumes of plated out culture allowed proliferation of single, distinct colonies on the LB-agar plates. The cultured bacteria were in such an excess compared to the phage added, that on average, any infected bacterium would be infected by a single phage particle. Each unique colony therefore represented a population of bacteria infected by a single species of phage-Affimer. Comparing the number of colonies from 1 µl T+ and T- plates gave an indication of how enriched the phage were against the particular target. If the numbers were comparable, this indicated that the screen was not successful. Ideally the number of colonies from the T+ plate should heavily outnumber the colonies from the T- plate. At this stage, the plates were ready to be analysed by phage ELISA.

The phage were propagated and stored in the advent of a fourth screen being required.

6.5.7. Panning the phage library against GM1-bound CTB

CTB is a lectin that binds with high affinity and specificity to GM1 ganglioside. The phage display protocol could therefore be modified to screen the phage library against GM1-bound unmodified CTB. GM1 plates were prepared, blocked, and washed as described in *6.5.1.2. GM1 plate* preparation. An overnight culture of ER2738 *E. coli* cells was prepared.

10 µl purified phage from the second panning round (CTB-biotin bound to streptavidin-coated magnetic beads) was added to 190 µl blocking buffer, and was pre-panned against four GM1-coated wells. 50 µl 1 µM solution of CTB was captured onto the GM1-coated surface of the fifth well, whilst the sixth well was retained as a negative control. Meanwhile, two 5 mL ER2738 *E. coli* cell cultures were prepared by diluting the overnight culture 1:15, and incubating the solution at 37°C for one hour, 230 rpm. The panning

wells were washed six times with PBS-T, before addition of the phage from the third pre-panning well, which was split between the two panning wells. After a one hour incubation, phage were eluted, and used to infect the two 5 mL ER2738 *E. coli* cell cultures. Six LB-agar carbenicillin plates were prepared, and used to plate out a range of volumes from both infected cultures (Table 6.2). Plates containing single colonies were taken forward for analysis by phage ELISA.

6.5.8. Phage ELISA

An enzyme-linked immunosorbent assay (ELISA) was carried out to validate the binding of a phage-Affimer subset to a screened target. By culturing a single colony of phage-infected bacteria, it could be assumed that a single subset of phage-Affimer would be produced. Preparing ligand-coated plates to capture either CTB-biotin, or unmodified CTB, and then presenting these single phage-Affimer populations to the captured target therefore allowed a single Affimer-target interaction to be analysed. These single subsets of phage-Affimer were thus exposed to the captured target, washed to remove any unbound material, and then detected through use of a commercially acquired antibody that recognises the major coat proteins of the phage particle. This antibody is conjugated to a horse radish peroxidase enzyme. Washing the well to remove any unbound antibody conjugate thus left a system held together by multiple interacting components (Figure 6.6). Addition of two peroxidase substrates produced a blue-coloured product in the presence of the enzyme, with the intensity of the colour being proportional to the quantity of the enzyme in the well. This process could thus be used as a high throughput method to gather preliminary data on the affinity of the isolated Affimer for its target.

200 µl aliquots of 2TY carb were transferred to a 96-well V-bottom deep well plate using a multichannel pipette. From the final panning round, 24 - 48 individual colonies were picked and used to inoculate the wells. The plate was then incubated overnight at 37°C, 1050 rpm. 200 µl 2TY was then transferred to the wells of a fresh deep well plate, which were inoculated with 25 µl of the overnight culture, before being incubated in turn for one hour at 37°C, 1050 rpm.

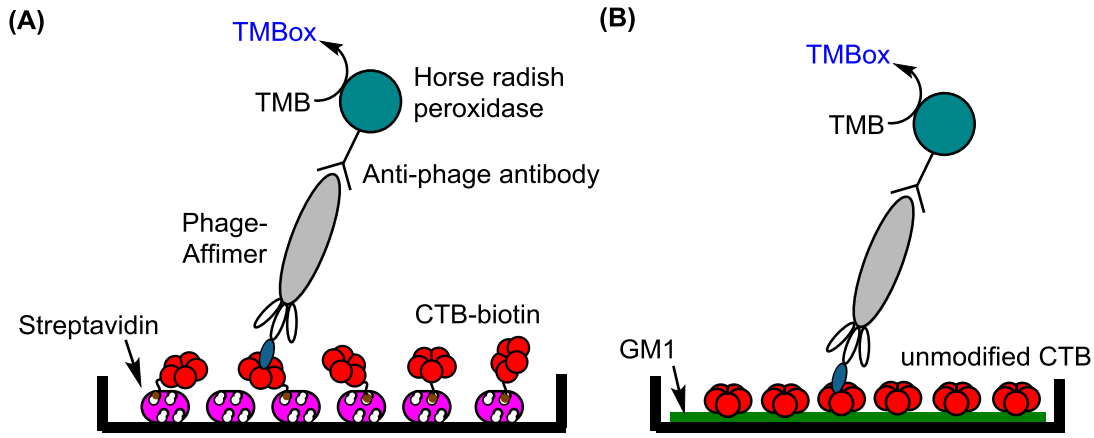

Figure 6.6. Phage ELISA schematic. **(A)** CTB-biotin is immobilised to streptavidin-coated plates, and presented to a phage-Affimer species. The bound phage is detected by anti-phage antibody, conjugated to horse radish peroxidase (HRP). Binding is detected by the addition of TMB and hydrogen peroxide, which is converted to a blue product by the peroxidase. The blue product absorbs at 620 nm and can be detected by plate reader. **(B)** Unmodified CTB is immobilised to GM1 ganglioside-coated plates, and presented to a phage-Affimer species. Detection of bound phage is facilitated through use of a peroxidase-conjugated antibody, and the peroxidase substrates TMB and hydrogen peroxide.

After one hour, 5 µl M13K07 helper phage (titre ca. 10^{14}/ml) was diluted into 5 ml 2TY carb, and 10 µl of the diluted stock was transferred into each of the wells of the one-hour culture. This culture was incubated for 30 minutes at room temperature, 450 rpm. The rpm was reduced to enable efficient infection of the cells with the helper phage, which was required in turn to supplement the phage-Affimer present in the infected cells with various complement proteins required for infectious phage-Affimer particles to escape into the surrounding medium.

Finally, kanamycin was added to the cultures by diluting the stock 20 fold into 2TY, and transferring 10 µl of the diluted antibiotic into each of the wells. As the helper phage confers kanamycin resistance to infected bacteria, this would effectively kill any *E. coli* cells that had not taken up the helper phage. This was incubated overnight at room temperature, 750 rpm. The phage-infected culture was centrifuged at 3500 *xg* for ten minutes to pellet the bacteria, leaving the Affimer-expressing phage in the supernatant. The supernatant could then be used directly in the ELISA.

Plates were prepared with either streptavidin or GM1 ganglioside (*6.5.1 Preparation of ligand-coated plates*). To half of the plate, CTB-biotin (1 µM), or unmodified CTB (1 µM), was added and allowed to bind for one hour, before being washed three times with PBS-T to remove unbound material.

40 µl of phage-containing supernatant was then transferred to the first and seventh well of the plate such that each phage was tested against the target, as well as the negative control well. 10 µl undiluted 10x Casein Blocking Buffer was added to supplement the phage. Following a one hour incubation, the plate was washed 27 times with PBS-T.

Commercially acquired Anti-Fd-Bacteriophage HRP was diluted 1000 fold in blocking buffer, and 50 µl was added to each well. After another one hour incubation, the plate was washed 12 times with PBS-T. Binding was assayed by adding 50 µl SeramunBlau solution, which contained the TMB and hydrogen peroxide. The plate was allowed to develop for approximately four minutes, before the absorbance at 620 nm was measured using a plate reader.

6.6. Biophysical Techniques

6.6.1. Isothermal Titration Calorimetry

Isothermal titration calorimetry (ITC) experiments were carried out to collect information on the thermodynamics of CTB-Affimer interactions.

6.6.1.1. An overview

Thermodynamic parameters, such as enthalpy, entropy, and Gibb's free energy dependent upon the structure of a complex, the structure of the solvent surrounding the complex, and changes in disorder within the system brought about from the binding interaction. Thermodynamic parameters can be calculated through measurement of the change in heat over the course of a binding interaction. Since a calorimeter can be used to measure heat, calorimetry can be applied to study the thermodynamics of an interaction.

An isothermal titration calorimeter functions by titrating one binding partner (ligand) into a sample cell containing the second binding partner (receptor), and measuring the change in heat produced as a result of the interaction. The device is composed several distinct units (Figure 6.7).

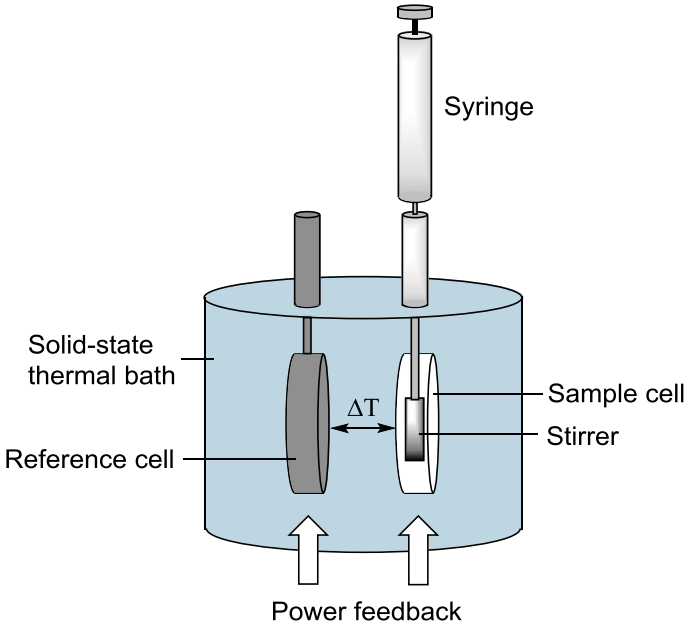

Figure 6.7. Schematic of an isothermal titration calorimeter

A solid-state thermal bath surrounds the system, and is maintained at a constant temperature, one degree cooler than the two calorimeter cells. A flat stirring syringe, containing the ligand, titrates the ligand into the sample cell harbouring a solution of the receptor, stirring to ensure the solution is thoroughly mixed. A reference cell filled with water is located next to the sample cell. The temperature in each of these cells is controlled by two heaters, which are regulated independently by a power feedback system.

The power feedback system maintains a constant temperature in both cells. If the sample cell becomes warmer even slightly than the reference cell, then the feedback system reduces the amount of power supplied to the sample cell to compensate. This power differential thus provides a physical measure of the heat released during a titration. As more ligand is titrated into the sample cell, the available receptor binding sites fill up, and the change in heat upon subsequent additions of ligand decreases. The power differential is plotted as a function of time, providing a raw ITC trace. Each peak can then be integrated, and plotted as a function of the concentration of ligand relative to the concentration of receptor (molar ratio) in a so-called Wiseman binding isotherm, which can be fitted to a binding model to derive thermodynamic parameters (Figure 6.8).[281]

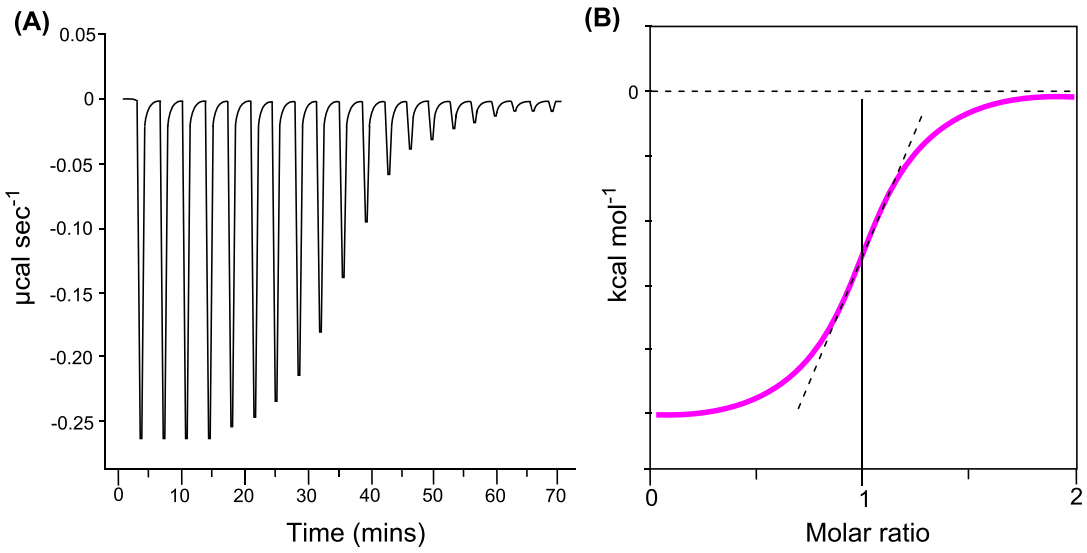

Figure 6.8. A) Raw ITC data from an exothermic binding interaction. Each peak corresponds to the heat change arising from injection of a titrant (binding protein A) into the calorimeter cell containing binding protein B. The area under each peak is proportional to the amount of heat released from the binding interaction between proteins A and B. As the start of the titration, an excess of B in the cell binds to all of the titrated protein A. As protein B becomes saturated with protein A, the heat signal begins to diminish, until only a small and constant heat change is detected corresponding to the heat of dilution. **B)** Wiseman binding isotherm obtained by integrating the area under each peak, and fitting a one site binding model to the data. The heat released per mole of titrated protein A is plotted against the molar ratio of the two binding proteins.

The molar ratio at the midpoint of where the curve inflects, provides a measure of binding stoichiometry. The scaling on the y-axis provides information on ΔH, and the slope/shape of the curve provide information on K_d. These values cannot be read directly from the graph, and are instead derived from non-linear least squares curve fitting to a suitable model.[281] ΔS cannot be determined directly from ITC data and must be derived from the measured values by using Equation 2.1.

$$\Delta S = \frac{RT \ln K_a + \Delta H}{T}$$

Equation 2.1. Equation used to calculate entropy (ΔS) using values measured directly by ITC (association constant (K_a) and enthalpy (ΔH)), the temperature of the system (T), and the gas constant (R).

To obtain the best data, certain parameters must be considered when designing experiments, such as the shape of curve, which is defined by the '*c* value'. The *c* value is calculated by the ratio of protein concentration in the calorimeter cell relative to K_d (Equation 2.2).

$$c = n[M]K_a = \frac{n[M]}{K_d}$$

Equation 2.2. The *c* value, which defines the shape of the binding isotherm, is calculated as a ratio of the dissociation constant (K_d), the concentration of protein in the ITC cell ([M]), and the stoichiometry (n).

When the *c* value is greater than 10, the shape of the binding isotherm will be sigmoidal, clearly defining the upper and lower plateaux, and therefore providing data for the heat change when there is an excess of binding sites, and when all binding sites are occupied. To obtain reliable thermodynamic information from a single experiment, *c* values of between 10 - 500 are preferable. Above this range, the transition between excess and saturation of binding sites becomes too steep, allowing for accurate determination of stoichiometry, but not for K_d. In this case, competition experiments are needed to accurately determine dissociation constants. For *c* values of lower than 10, dissociation constants can still be determined, but other thermodynamic parameters such as ΔH may be less accurate.[282]

6.6.1.2. Experimental setup

The iTC_{200} Microcalorimeter User's Manual[4] is an extremely useful tool for practical understanding of how to carry out ITC experiments, and provides detailed information on instrument navigation.

Extensive dialysis of both proteins was required to match buffers before running experiments. All ITC experiments were performed using a MicroCal ITC_{200}. Water in the reference cell was replaced at the beginning of a set of experiments, using a 1 mL Hamilton syringe. The sample cell was then washed extensively with PBS-T to ensure that no protein remained from any previous experiments. The cell was additionally washed with water, followed by the experiment buffer, to remove any bubbles remaining from the detergent used in the previous wash step, and to equilibrate the sample cell. 300 µl protein 'receptor' was gently drawn up into a 1 mL Hamilton syringe, and purged from any bubbles. The sample cell was then gently filled. The tip of the syringe was then drawn up to the ledge formed at the interface between the sample cell, and the overflow reservoir. Any excess liquid was removed up to this point, thereby ensuring that the volume was standardised across all experiments.

The titration syringe was then loaded with ligand from a microcentrifuge tube, and the fill port was closed. The titration syringe was then placed back into the tube, and the titration syringe was purged, refilled, and then transferred into the sample cell. The calorimeter was heated to 25˚C or 35 ˚C before carrying out titrations.

[4] http://www.biophysics.bioc.cam.ac.uk/files/iTC200_User_Manual_Rev_D.pdf

An initial sacrificial titration of 0.5 µl was required, before 19 x 2 µl titrations were carried out, each spaced out over 4 seconds, with a 120 second delay in between each injection. Experiments were initially carried out at 100 µM CTB, titrated into 10 µM Affimer. These concentrations were then varied, if necessary, to obtain a sigmoidal shape of curve. For each set of concentrations, a CTB titration into buffer was carried out to obtain a measure of the heat of dilution of CTB into buffer. These data could then be subtracted from the data obtained from ligand into receptor titrations to bring the baseline closer to zero, thereby facilitating curve fitting. Data were analysed and fitted with a 'one site bind' model using Origin Microcal software.

6.6.2. Affimer-lectin binding assay

An Affimer-lectin binding assay (ALBA) was developed to validate the binding of Affimers to CTB (Figure 6.9). Drawing inspiration from the phage ELISA, a plate-based assay was devised, where a GM1-bound lectin was presented to a biotinylated Affimer. After washing to remove unbound material, the Affimer could be detected by adding a streptavidin-peroxidase conjugate, which would bind to the Affimer-biotin. Addition of a peroxidase substrate would allow quantification of the amount of enzyme present in the reaction, thus providing information on the association between Affimer and lectin.

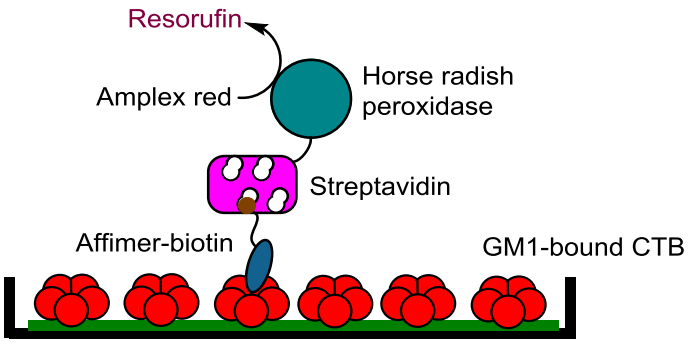

Figure 6.9. Schematic for an Affimer-lectin binding assay. A GM1-binding lectin, in this case CTB, is captured onto a GM1-coated surface. A biotinylated Affimer binding CTB is recognised by a streptavidin-peroxidase conjugate, which is quantified by addition of Amplex Red and hydrogen peroxide to form the fluorescent resorufin.

In order to carry out this assay, biotinylated Affimers were required. Affimers carrying a C-terminal cysteine were expressed, and biotinylated using biotin-PEG2-maleimide. Affimers were concentrated to 100 µM, and combined with a 20-fold molar excess of biotin-PEG2-maleimide in *phosphate buffer* supplemented with 1 mM TCEP. After an overnight incubation at room temperature, the Affimer was purified by using a PD-10 desalting column, or by dialysis into *phosphate buffer*.

50 µl GM1 ganglioside in methanol (1.3 µM) was added to wells (as required) of a Greiner Bio-one high binding black 96 well plate. The plate was then left in a lamina-flow hood until the methanol had completely evaporated. To block the plate and occupy any remaining adsorption sites, *blocking buffer* was added at a volume of 300 µl per well. The plate was covered, and incubated overnight at 37°C. Following incubation, the blocking solution was removed, and the plate was washed three times with *PBS-T*. A Combi Reagent Dispenser and standard tube dispensing cassette were used to facilitate accurate and rapid liquid transfer into the wells of the plate.

After the wash steps, 50 µl lectin (1 µM) was transferred to the appropriate wells, and left to bind for one hour at room temperature. Half the wells were deliberately left free of CTB to act as a control. The wash step was then repeated to remove any unbound CTB, and subsequently 100 µl biotinylated Affimer (250 nM) was added to each well. The Affimer was in turn allowed to bind for one hour before repeating the wash step a third time. In order to detect the presence of bound Affimer, 50 µl of a streptavidin-HRP complex (Ultra Streptavidin-HRP, Life Technologies), diluted at 1:1000 in *phosphate buffer*, was added to the wells of the plate. The one hour incubation and wash step was repeated, with an additional four washes, before one final rinse with *PBS* or *phosphate buffer*. The substrate used for peroxidase detection was a solution of Amplex Red and hydrogen peroxide in *PBS*, both at a final concentration of 5 µM. 50 µl of this substrate was added per well, and the plate was loaded into the plate reader for fluorescence detection at 585 nm.

6.6.3. Surface Plasmon Resonance

Surface plasmon resonance (SPR) was employed for studying the binding kinetics of CTB-Affimer interactions. In a traditional SPR experiment, a target protein (ligand) is immobilised on a gold chip, and a binding partner (analyte) is flowed across the ligand-coated surface. The interaction between ligand and analyte is measured by changes in the SPR.

6.6.3.1. An introduction to SPR

An SPR device consists of a glass prism mounted onto a gold sensor microchip, a light emitting diode (LED) releasing polarised light at near infrared wavelengths, and a diode array detector (DAD) (Figure 6.10).

SPR is a complex process that occurs when light stimulates thin films of conducting materials, such as gold. As the incident light passes through the glass prism,

electromagnetic waves that exist at the gold-water interface called surface plasmons become excited, resulting in resonance. The resonant coupling between the photons from the LED and surface plasmons in the gold film occurs when the light is absorbed at a specific angle. This absorption by the plasmon waves results in a 'dip' in the reflected light at a particular angle, termed the resonance angle, that is detected by the DAD.[283]

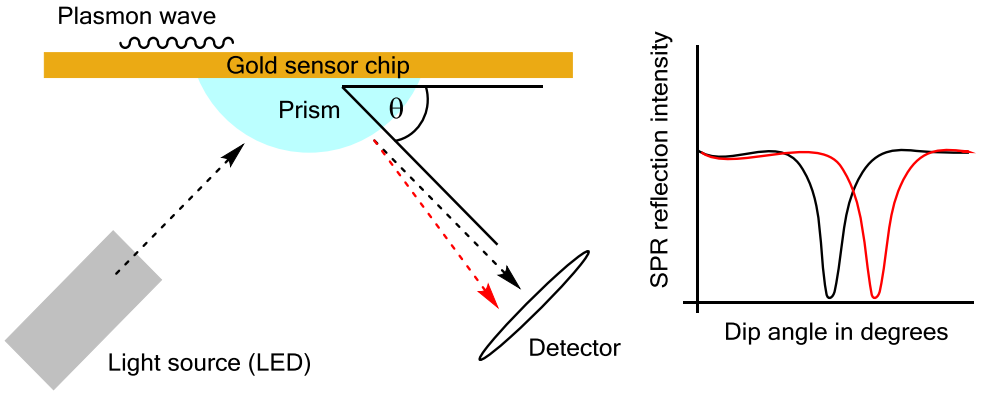

Figure 6.10. Diagram showing the setup for detection of changes to the refractive index at the surface of a gold sensor chip. An LED emits light through a prism towards a gold sensor chip. Electromagnetic plasmon waves at the surface of the gold sensor chip absorb the light at a particular incidence. The light is then reflected to a detector, which is sensitive to changes in the intensity of reflected light and the angle of the detected light. Changes in the refractive index at the surface of the chip result in changes to the incidence of the light absorbed by the surface plasmons, which is recorded by the detector, and plotted as changes in the dip angle in degrees.

Importantly, the resonance angle varies under certain conditions, including temperature, thickness of the conducting surface, and refractive index of the material on the other face of the conducting surface. Therefore, the resonance angle detected provides a measurement of the refractive index of the material distal to the incident of light in relation to the conducting film.[284] It is worth noting that SPR only detects changes to the refractive index of material that is within ~300 nm of the prism-film interface.[285] The deviation in resonance angle, and therefore refractive index, is plotted as response units (RU) in a sensorgram as a function of time, thus providing information in real-time.

Thus, dissection of the kinetic parameters governing an interaction is possible by SPR. An analyte is flowed over the microchip, where a ligand is immobilised to the conducting film (Figure 6.11). As the analyte flows over, a proportion will bind to the ligand, resulting in an increase in the refractive index close to the gold-prism interface. The refractive index will continue to increase until an equilibrium between association and dissociation is reached (R_{max}), and the trace in the sensorgram plateaus. At this point, analyte is

exchanged for buffer, and the bound analyte begins to dissociate, accompanied by a corresponding decrease in response units, until all the analyte has fully dissociated, and the trace returns to baseline. For a given change in mass concentration on a microchip surface, the change in refractive index is effectively the same for all proteins. Interestingly, this change varies slightly for other macromolecules such as lipids, nucleic acids, and glycans.[286]

By using BIAcore software, sensorgrams can be fitted with a one to one binding model, and providing the concentration of the analyte is known, values for K_d, k_{on} *and* k_{off} can be calculated.

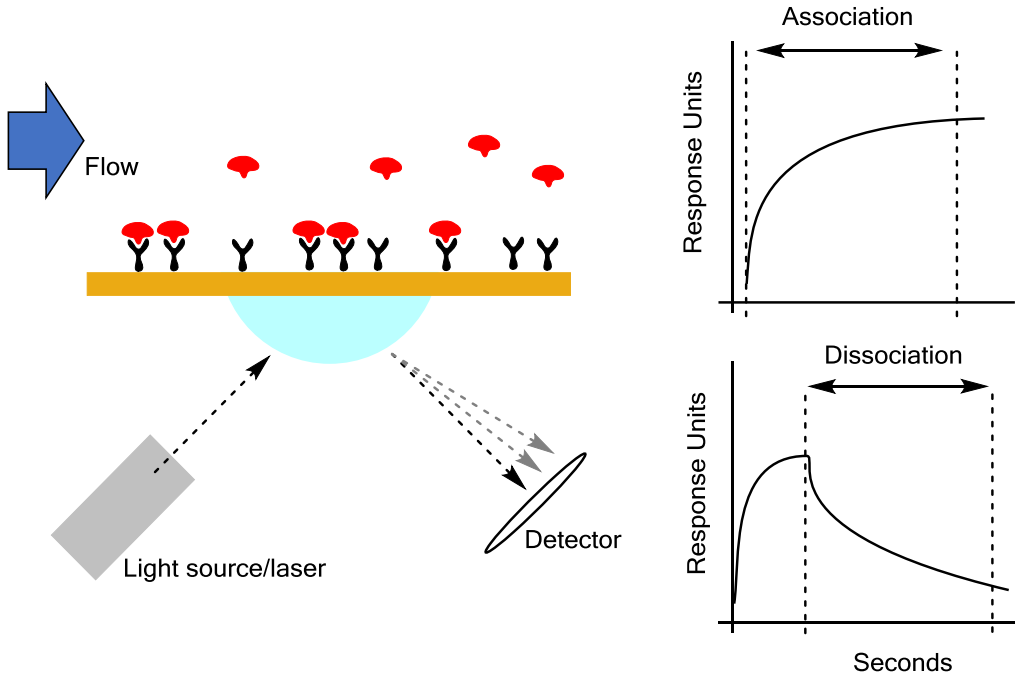

Figure 6.11. Flowing analyte over the surface of an immobilised ligand results in changes in the refractive index. As the analyte binds to the ligand, the refractive index at the surface increases, until equilibrium is reached at the surface of the sensor. When the input solution is switched back to buffer, the analyte begins to dissociate causing a reduction in the refractive index.

6.6.3.2. Derivatisation of the sensor microchip

Most commercially available microchips consist of a gold film derivatised through thiol-gold interactions with a non-crosslinked carboxymethyl dextran layer approximately 100 nm thick (Figure 6.12).

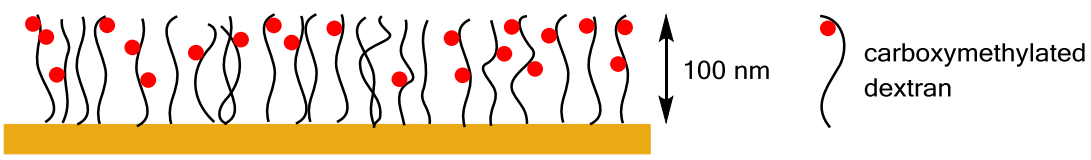

Figure 6.12. A typical gold sensor chip coated with a 100 nm carboxymethylated dextran layer.

The carboxymethyl functional groups can be modified using a range of chemistries, such as derivatisation with N-hydroxysuccinimide for the immobilisation of ligands through primary amine residues, or reductive amination for reaction with ligands containing aldehyde groups. Non-covalent capture is also possible, for instance by attaching Ni-NTA to the dextran hydrogel to trap proteins or peptides containing multiple histidine residues. A commonly used approach involves chemically conjugating streptavidin to NHS-derivatised dextran, and subsequently capturing a biotinylated ligand to the surface (Figure 6.13). This approach is employed sufficiently frequently for streptavidin-coated sensor chips to be commercially available.

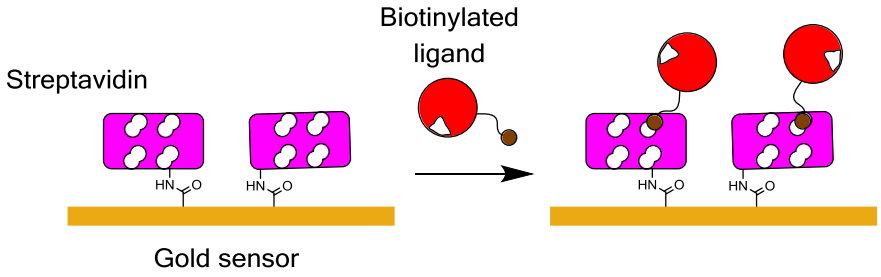

Figure 6.13. Capturing biotinylated ligands to a streptavidin-coated gold sensor chip. Streptavidin molecules are covalently coupled to the NHS ester-derivatised dextran layer through primary amines. Biotinylated ligand is then flowed over the surface, and captured by the streptavidin molecules.

In order to accurately measure kinetics, mass transfer must be efficient between the bulk (unbound analyte), and the surface (ligand-bound analyte). Failure to achieve effective mass transfer leads to differences in concentration of analyte at the surface compared to the bulk, due to the surface forming areas of analyte retention. These areas form because the analyte can only transfer across the chip when it is in an unbound state. Proceeding through an array of binding sites thus results in slower diffusion across the microchip. Analyte retention precludes accurate measurements of the binding interaction.[287] The amount of immobilised ligand was therefore kept deliberately low, and increased in small increments (50 – 100 RU) in subsequent experiments if initial injections of analyte resulted in a low signal to noise ratio.

6.6.3.3. Performing SPR experiments

Experiments were carried out using a Biacore 3000 instrument, and in all cases, biotinylated ligands were used, and immobilised to streptavidin-coated chips (Sensor Chip SA, GE Healthcare). GE Healthcare provide a helpful manual on using the BIAcore

3000 that provides information on practical aspects of using the instrument, as well as guidelines for experiment planning.[5]

Prior to use, the system was cleansed using the *Desorb* function, and was then equilibrated using filtered SPR buffer. Sensor chips were docked into the instrument, and conditioned, by applying three consecutive injections of 50 µl 1 M NaCl, 50 mM NaOH, at 50 µl min^{-1}. The sensor chips are composed of four flow cells (Fc), which can be isolated individually, targeted in pairs (Fc1 and Fc2, or Fc3 and Fc4), or can all be targeted in the same experiment (Figure 6.14).

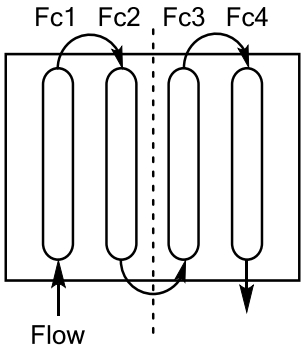

Figure 6.14. The layout of the sensor chip and direction of flow across the four flow cells (Fc).

Biotinylated ligands were diluted to 1 nM in SPR buffer, and then injected over the surface of a single flow cell (Fc2 or Fc4), at 10 µl min^{-1}. Injections were repeated, until the desired number of response units had been reached (Figure 6.15). The system was washed with SPR buffer to ensure that no biotinylated ligand remained in the tubing.

A 1 µM solution of the analyte (receptor) was then injected over the surface of the immobilised ligand, usually at 10 µl min^{-1}, although this could be slowed down, or sped up, as required. Injections were usually carried out over 300 seconds, to ensure that an equilibrium was reached. This equilibrium was assumed to have been reached once no increase in RU was seen, despite a continued flow of analyte. Dissociation was then allowed to proceed until baseline was reached. The SPR trace could then be fitted to a one to one binding model using the BIA evaluation software. An estimate of the K_d could be derived from the fitted model, and a titration range was then set up, with the lowest concentration 10-fold below the apparent K_d, and the highest concentration 10-fold above the apparent K_d. This series of analyte concentrations was then titrated across the flow cell containing the immobilised ligand, as well as the adjacent underivatised flow

[5] https://www.gelifesciences.com/gehcls_images/GELS/Related%20Content/Files/1384433006836/litdoc28938471_20161015120210.pdf

cell, to serve as a negative control for baseline subtraction. Negative control flow cell data was then subtracted from the binding data, and the curves were globally fitted using the BIA evaluation software.

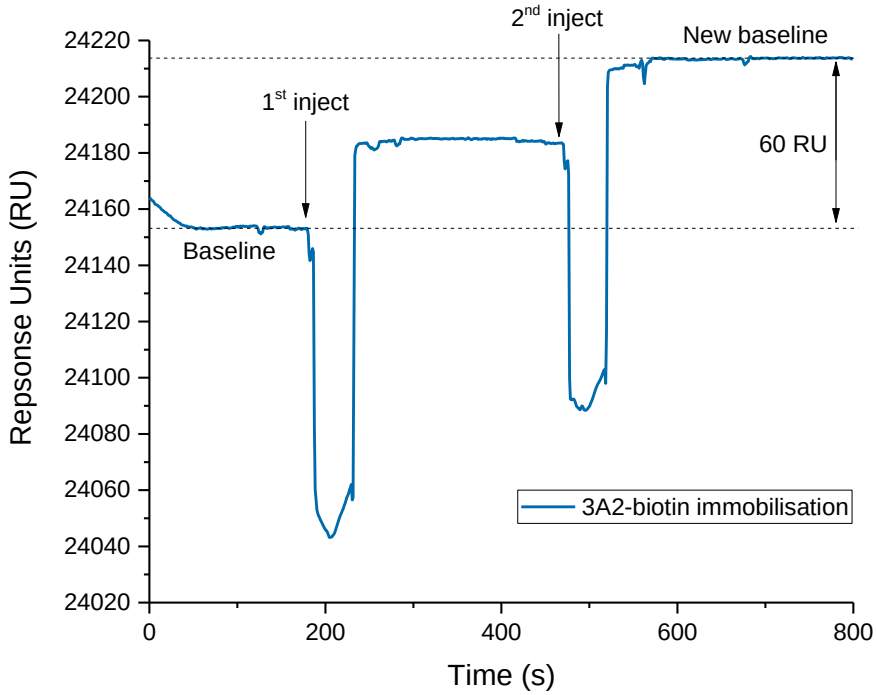

Figure 6.15. SPR trace showing the change in response units as 3A2-biotin is injected over the surface of a sensor chip. Each injection causes a decrease in the RU value, followed by a recovery to a 30 RU above baseline. To achieve a total of 60 RU ligand immobilized, a second injection was carried out.

6.7. Tissue Preparation and Analysis

6.7.1 Mammalian Cell Culture

6.7.1.1. Passage of cells

Vero cells were cultured in cell culture medium, a supplemented Dulbecco's Modified Eagle's Medium (DMEM) containing foetal bovine serum, added due to the presence of essential growth factors for the cell proliferation, and a combination of antibiotics penicillin and streptomycin, to prevent the bacterial and fungal infections. Cultures were grown in T75 cell culture flasks at 37 °C with 5% CO_2 until 90% confluency, approximately after three days of culturing. At this stage, cells were washed once with 10 mL sterile *PBS*, and combined with 3 mL TrypLE Select (Life Technologies), a trypsin-based protease solution to detach cells from the flask surface. After 5 minutes at 37 °C, flasks were placed under a light microscope to verify complete detachment. If large

numbers were seen to still be adhering to the surface, the flask was firmly tapped, and placed in the 37°C incubator for a further 3 minutes. 7 mL cell culture medium was added, neutralizing the trypsin, and the detached cells were transferred to a 15 mL falcon tube. The flask was washed twice with 10 mL PBS, and 20 mL cell culture medium was added, together with 1 mL of the resuspended cells. Cells were then returned to the incubator for culturing at 37 °C with 5% CO_2.

6.7.1.2. Cell seeding

For cell-based experiments, cells were 'seeded' onto 18 mm glass coverslips in 12-well plates. After passaging cells, the falcon tube containing the cells was retained, and used for cell seeding. A Neubauer Improved haemocytometer was used for cell counting by making a 1:10 dilution of the cells, and transferring 5 µl of the diluted sample onto the haemocytometer. A coverslip was then used to draw the cells onto the central grid by capillary action. A 5x5 grid at the centre of the haemocytometer was used for cell counting, and cells from five of the boxes were counted. This number was divided by two, and multiplied by 10^6 to calculate the number of cells per mL. For a 12-well plate, 1.2×10^5 cells per well were plated out. Cells were therefore diluted to 1.2×10^5 cells mL^{-1}, and 1 mL was transferred into the wells of a sterile 12-well plate, containing an 18 mm coverslip in each well. The plate was then incubated overnight at 37 °C with 5% CO_2 for use the following day.

6.7.1.3. Cell treatment with protein

Seeded cells in 12-well plates to be treated with protein were washed, by replacing the cell culture medium with 1 mL fresh medium. Protein solution was then added directly to the medium, and the cells were incubated for 4-6 hours at 37 °C, 5% CO_2 prior to cell fixation.

6.7.1.4. Cell fixation

Following treatment with protein, cells were exposed to a strong acid, to remove any surface-bound CTB, and then 'fixed', by adding a harsh cross-linking agent, effectively killing the cells and freezing them in a particular state.

Growth medium was removed, and the cells were washed three times with PBS. 0.5 mL cell cleansing buffer was added, and incubated at 4 °C for 6 minutes. The cleansed cells were then washed an additional three times, before addition of 4% v/v paraformaldehyde (PFA) in PBS for 30 minutes at room temperature in a fume hood. The PFA was

removed, and the cells were washed three times with PBS. Cells were then permeabilised with 0.1% Triton X-100 in PBS for one hour at room temperature in preparation for immunohistochemistry.

6.7.2. *In Vivo* Experimentation

All handling of live animals was carried out either by Dr Jessica Haigh, or Professor Jim Deuchars.

6.7.2.1. Animals

All animal experimentation was carried out under a Home Office License, and in accordance with the regulations of the UK Animals, Scientific Procedures, Act 1986. Experiments were performed on young male and female C75BL/6 adult mice, bred in house.

6.7.2.2. Intramuscular administration of protein

The tongue was targeted for intramuscular injections of protein and protein complexes, since it provided a route to deliver material into the motor neurones of the brainstem. Protein was prepared at a concentration of 50 µM in phosphate buffer, before lyophilisation for reconstitution prior to injection at a concentration of 200 µM.

Paralingual injections were carried out by heavily sedating mice with isoflurane, protruding the tongue from the mouth using forceps, and injecting 2 µl of protein material using a glass micropipette mounted onto a 10 µl Hamilton syringe. Mice were perfused after 24 – 72 hours.

6.7.2.3. Transcardial perfusion for tissue fixation

Mice were deeply anaesthetised by injection of sodium pentobarbitone (60 mg kg^{-1}) into the abdominal cavity. To ensure that the mice were fully sedated, pedal reflexes were tested. The abdomen of the animal was then dissected transversely, and a thoracotomy was carried out to reach the heart. The left ventricle of the heart was pierced, and a blunt needle was inserted and retained in position with a clip. The right atrium was then cut, and a phosphate solution (0.1 M NaH_2PO_4, pH 7.4) was applied through the needle to flush the circulatory system. Perfusion was then carried out by replacing the phosphate solution with approximately 150 mL 4% PFA.

6.7.2.4. Dissection and Tissue Preparation

The brainstem was removed by dissection of the spinal cord, opening of the skull, and separation of the meninges from the brain. The brain was then removed from the skull, ensuring not to disturb the brainstem and upper half of the spinal cord. The brain and spinal cord was then transferred into a 50 mL falcon tube with 4% PFA, and kept for 24 hours at 4°C. The PFA was then removed and replaced with PBS, and the brainstem was separated from the hind brain and spinal cord for sectioning. The brainstem could then be sectioned. All sections were taken transversely on a VT1000S vibrating microtome at 50 µm thickness. The sectioned slices were collected and transferred into PBS in a 24-well plate.

6.7.3. Immunohistochemistry

Immunohistochemistry is a technique that makes use of antibodies to visualise a molecule in a cell. Much like an ELISA, this technique relies on an antibody-target interaction to report on the presence of the target in the cell. By solubilising the plasma membrane of the cells using a detergent, an antibody against the target of interest can penetrate the cell, and bind the target protein. A second antibody, usually conjugated to a reporter such as a fluorescent molecule, is added that recognises multiple sites on the first antibody (termed polyclonal), thereby amplifying the signal.

Tissue sections, or cultured cells, were permeabilised in 1 mL solubilisation buffer for one hour at room temperature. The primary antibody (e.g. rabbit anti-CTB, chicken anti-GFP) was diluted 1:1000 in solubilisation buffer, and 0.5 mL was applied to the tissue/cells. After an overnight incubation at 4 °C, the wells were washed three times with PBS, and a 1:1000 dilution of a fluorescent secondary antibody (Alexa Flour 488 or 555) in PBS was made and 0.5 mL added to the sample. A one hour incubation at room temperature ensued, followed by three more washes with PBS. The sample was then air-dried onto a glass microscope slide, before addition of 10 µl of Vectashield Mounting Medium, and protection of the sample with a cover slip ready for visualisation. To stain the nuclei in a sample, Vectashield Mounting Medium with DAPI was used. This medium contains DAPI stain, a fluorescent stain that tightly associates to AT-rich regions of DNA in the nuclei of cells, thus facilitating visualisation of the nuclei. Microscope slides were covered with foil, and kept overnight at room temperature to dry, before being sealed with a generic nail varnish.

6.7.4. Confocal Microscopy

For confocal analysis of samples, an Axio Imager Z2 LSM880 upright confocal microscope (Zeiss) equipped with a 405 nm diode laser, Argon 458/488/514 nm, DPSS

561 nm and HeNe 633 nm lasers and a GaAsP detector. Images were captured using the Zeiss LSM Image browser software, and processed using Zen lite 2.3 software.

For wide-field analysis of samples, a Nikon Eclipse E600 microscope equipped with epifluoresence and Q-Imaging Micropublishing 5.0 camera was used. Images were captured using AcQuis image capture software.

7. Appendix

7.1. Plasmid Sequences

The genes encoding CTB, Affimer, and Synaptobrevin-CTA2 are shown in red, blue, and green, respectively.

7.1.1. pATA13

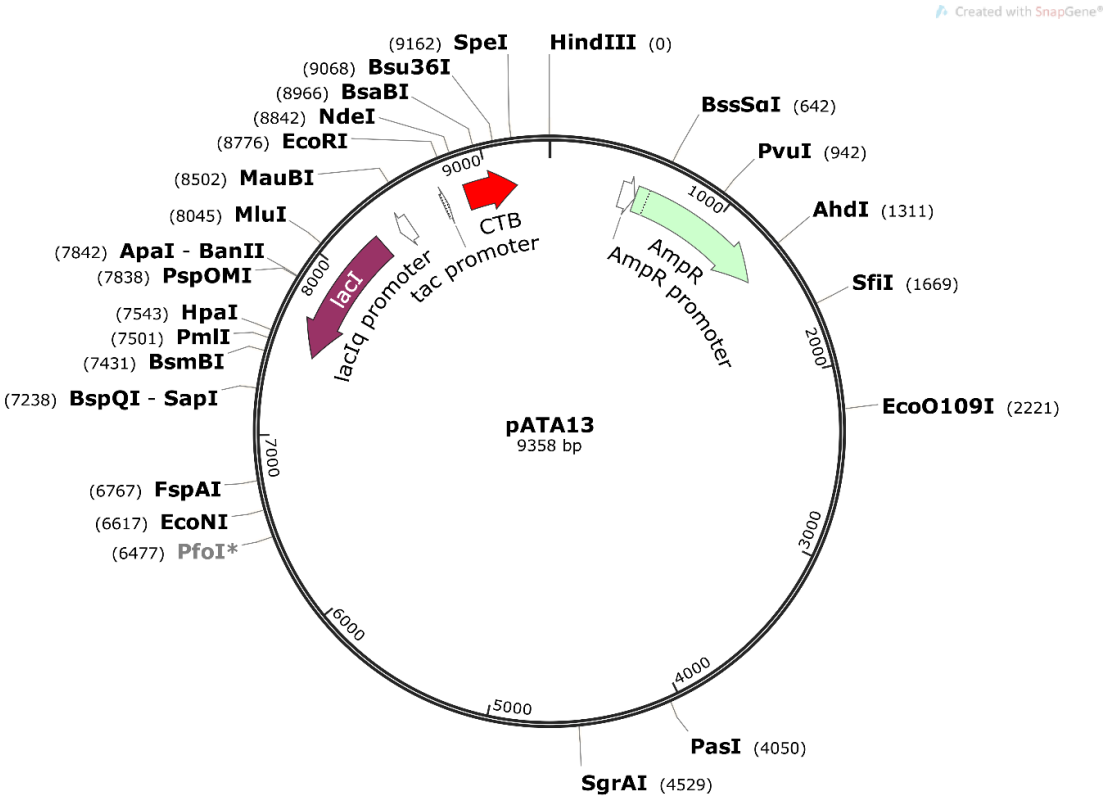

Figure 7.1. Plasmid map for pATA13.

El Tor CTB was expressed from *Vibrio sp.60* clones harbouring the pATA13 plasmid.[225]

Full sequence 5' – 3':

AGCTTGGCTGTTTTGGCGGATGAGAGAAGATTTTCAGCCTGATACAGATTAAATCAGAACGCAG
AAGCGGTCTGATAAAACAGAATTTGCCTGGCGGCAGTAGCGCGGTGGTCCCACCTGACCCCATG
CCGAACTCAGAAGTGAAACGCCGTAGCGCCGATGGTAGTGTGGGGTCTCCCCATGCGAGAGTAG
GGAACTGCCAGGCATCAAATAAAACGAAAGGCTCAGTCGAAAGACTGGGCCTTTCGTTTTATCT
GTTGTTTGTCGGTGAACGCTCTCCTGAGTAGGACAAATCCGCCGGGAGCGGATTTGAACGTTGC
GAAGCAACGGCCCGGAGGGTGGCGGGCAGGACGCCCGCCATAAACTGCCAGGCATCAAATTAAG
CAGAAGGCCATCCTGACGGATGGCCTTTTTGCGTTTCTACAAACTCTTTTGTTTATTTTTCTAA
ATACATTCAAATATGTATCCGCTCATGAGACAATAACCCTGATAAATGCTTCAATAATATTGAA
AAAGGAAGAGTATGAGTATTCAACATTTCCGTGTCGCCCTTATTCCCTTTTTTGCGGCATTTTG
CCTTCCTGTTTTTGCTCACCCAGAAACGCTGGTGAAAGTAAAAGATGCTGAAGATCAGTTGGGT

GCACGAGTGGGTTACATCGAACTGGATCTCAACAGCGGTAAGATCCTTGAGAGTTTTCGCCCCG
AAGAACGTTTTCCAATGATGAGCACTTTTAAAGTTCTGCTATGTGGCGCGGTATTATCCCGTGT
TGACGCCGGGCAAGAGCAACTCGGTCGCCGCATACACTATTCTCAGAATGACTTGGTTGAGTAC
TCACCAGTCACAGAAAAGCATCTTACGGATGGCATGACAGTAAGAGAATTATGCAGTGCTGCCA
TAACCATGAGTGATAACACTGCGGCCAACTTACTTCTGACAACGATCGGAGGACCGAAGGAGCT
AACCGCTTTTTTGCACAACATGGGGGATCATGTAACTCGCCTTGATCGTTGGGAACCGGAGCTG
AATGAAGCCATACCAAACGACGAGCGTGACACCACGATGCCTGTAGCAATGGCAACAACGTTGC
GCAAACTATTAACTGGCGAACTACTTACTCTAGCTTCCCGGCAACAATTAATAGACTGGATGGA
GGCGGATAAAGTTGCAGGACCACTTCTGCGCTCGGCCCTTCCGGCTGGCTGGTTTATTGCTGAT
AAATCTGGAGCCGGTGAGCGTGGGTCTCGCGGTATCATTGCAGCACTGGGGCCAGATGGTAAGC
CCTCCCGTATCGTAGTTATCTACACGACGGGGAGTCAGGCAACTATGGATGAACGAAATAGACA
GATCGCTGAGATAGGTGCCTCACTGATTAAGCATTGGTAACTGTCAGACCAAGTTTACTCATAT
ATACTTTAGATTGATTTCTGAAAGCGACCAGGTGCTCGGCGTGGCAAGACTCGCAGCGAACCCG
TAGAAAGCCATGCTCCAGCCGCCCGCATTGGAGAAATTCTTCAAATTCCCGTTGCACATAGCCC
GGCAATTCCTTTCCCTGCTCTGCCATAAGCGCAGCGAATGCCGGGTAATACTCGTCAACGATCT
GATAGAGAAGGGTTTGCTCGGGTCGGTGGCTCTGGTAACGACCAGTATCCCGATCCCGGCTGGC
CGTCCTGGCCGCCACATGAGGCATGTTCCGCGTCCTTGCAATACTGTGTTTACATACAGTCTAT
CGCTTAGCGGAAAGTTCTTTTACCCTCAGCCGAAATGCCTGCCGTTGCTAGACATTGCCAGCCA
GTGCCCGTCACTCCCGTACTAACTGTCACGAACCCCTGCAATAACTGTCACGCCCCCCTGCAAT
AACTGTCACGAACCCCTGCAATAACTGTCACGCCCCCAAACCTGCAAACCCAGCAGGGGCGGGG
GCTGGCGGGGTGTTGGAAAAATCCATCCATGATTATCTAAGAATAATCCACTAGGCGCGGTTAT
CAGCGCCCTTGTGGGGCGCTGCTGCCCTTGCCCAATATGCCCGGCCAGAGGCCGGATAGCTGGT
CTATTCGCTGCGCTAGGCTACACACCGCCCCACCGCTGCGCGGCAGGGGGAAAGGCGGGCAAAG
CCCGCTAAACCCCACACCAAACCCCGCAGAAATACGCTGGAGCGCTTTTAGCCGCTTTAGCGGC
CTTTCCCCCTACCCGAAGGGTGGGGGCGCGTGTGCAGCCCCGCAGGGCCTGTCTCGGTCGATCA
TTCAGCCCGGCTCATCCTTCTGGCGTGGCGGCAGACCGAACAAGGCGCGGTCGTGGTCGCGTTC
AAGGTACGCATCCATTGCCGCCATGAGCCGATCCTCCGGCCACTCGCTGCTGTTCACCTTGGCC
AAAATCATGGCCCCCACCAGCACCTTGCGCCTTGTTTCGTTCTTGCGCTCTTGCTGCTGTTCCC
TTGCCCGCTCCCGCTGAATTTCGGCATTGATTCGCGCTCGTTGTTCTTCGAGCTTGGCCAGCCG
ATCCGCCGCCTTGTTGCTCCCCTTAACCATCTTGACACCCCATTGTTAATGTGCTGTCTCGTAG
GCTATCATGGAGGCACAGCGGCGGCAATCCCGACCCTACTTTGTAGGGGAGGGCGCACTTACCG
GTTTCTCTTCGAGAAACTGGCCTAACGGCCACCCTTCGGGCGGTGCGCTCTCCGAGGGCCATTG
CATGGAGCCGAAAAGCAAAAGCAACAGCGAGGCAGCATGGCGATTTATCACCTTACGGCGAAAA
CCGGCAGCAGGTCGGGCGGCCAATCGGCCAGGGCCAAGGCCGACTACATCCAGCGCGAAGGCAA
GTATGCCCGCGACATGGATGAAGTCTTGCACGCCGAATCCGGGCACATGCCGGAGTTCGTCGAG
CGGCCCGCCGACTACTGGGATGCTGCCGACCTGTATGAACGCGCCAATGGGCGGCTGTTCAAGG
AGGTCGAATTTGCCCTGCCGGTCGAGCTGACCCTCGACCAGCAGAAGGCGCTGGCGTCCGAGTT

CGCCCAGCACCTGACCGGTGCCGAGCGCCTGCCGTATACGCTGGCCATCCATGCCGGTGGCGGC
GAGAACCCGCACTGCCACCTGATGATCTCCGAGCGGATCAATGACGGCATCGAGCGGCCCGCCG
CTCAGTGGTTCAAGCGGTACAACGGCAAGACCCCGGAGAAGGGCGGGGCACAGAAGACCGAAGC
GCTCAAGCCCAAGGCATGGCTTGAGCAGACCCGCGAGGCATGGGCCGACCATGCCAACCGGGCA
TTAGAGCGGGCTGGCCACGACGCCCGCATTGACCACAGAACACTTGAGGCGCAGGGCATCGAGC
GCCTGCCCGGTGTTCACCTGGGGCCGAACGTGGTGGAGATGGAAGGCCGGGGCATCCGCACCGA
CCGGGCAGACGTGGCCCTGAACATCGACACCGCCAACGCCCAGATCATCGACTTACAGGAATAC
CGGGAGGCAATAGACCATGAACGCAATCGACAGAGTGAAGAAATCCAGAGGCATCAACGAGTTA
GCGGAGCAGATCGAACCGCTGGCCCAGAGCATGGCGACACTGGCCGACGAAGCCCGGCAGGTCA
TGAGCCAGACCAAGCAGGCCAGCGAGGCGCAGGCGGCGGAGTGGCTGAAAGCCCAGCGCCAGAC
AGGGGCGGCATGGGTGGAGCTGGCCAAAGAGTTGCGGGAGGTAGCCGCCGAGGTGAGCAGCGCC
GCGCAGAGCGCCCGGAGCGCGTCGCGGGGGTGGCACTGGAAGCTATGGCTAACCGTGATGCTGG
CTTCCATGATGCCTACGGTGGTGCTGCTGATCGCATCGTTGCTCTTGCTCGACCTGACGCCACT
GACAACCGAGGACGGCTCGATCTGGCTGCGCTTGGTGGCCCGATGAAGAACGACAGGACTTTGC
AGGCCATAGGCCGACAGCTCAAGGCCATGGGCTGTGAGCGCTTCGATATCGGCGTCAGGGACGC
ACCCACCGGCCAGATGATGAACCGGGAATGGTCAGCCGCCGAAGTGCTCCAGAACACGCCATGG
CTCAAGCGGATGAATGCCCAGGGCAATGACGTGTATATCAGGCCCGCCGAGCAGGAGCGGCATG
GTCTGGTGCTGGTGGACGACCTCAGCGAGTTTGACCTGGATGACATGAAAGCCGAGGGCCGGGA
GCCTGCCCTGGTAGTGGAAACCAGCCCGAAGAACTATCAGGCATGGGTCAAGGTGGCCGACGCC
GCAGGCGGTGAACTTCGGGGGCAGATTGCCCGGACGCTGGCCAGCGAGTACGACGCCGACCCGG
CCAGCGCCGACAGCCGCCACTATGGCCGCTTGGCGGGCTTCACCAACCGCAAGGACAAGCACAC
CACCCGCGCCGGTTATCAGCCGTGGGTGCTGCTGCGTGAATCCAAGGGCAAGACCGCCACCGCT
GGCCCGGCGCTGGTGCAGCAGGCTGGCCAGCAGATCGAGCAGGCCCAGCGGCAGCAGGAGAAGG
CCCGCAGGCTGGCCAGCCTCGAACTGCCCGAGCGGCAGCTTAGCCGCCACCGGCGCACGGCGCT
GGACGAGTACCGCAGCGAGATGGCCGGGCTGGTCAAGCGCTTCGGTCATGACCTCAGCAAGTGC
GACTTTATCGCCGCGCAGAAGCTGGCCAGCCGGGGCCGCAGTGCCGAGGAAATCGGCAAGGCCA
TGGCCGAGGCCAGCCCAGCGCTGGCAGAGCGCAAGCCCGGCCACGAAGCGGATTACATCGAGCG
CACCGTCAGCAAGGTCATGGGTCTGCCCAGCGTCCAGCTTGCGCGGGCCGAGCTGGCACGGGCA
CCGGCACCCCGCCAGCGAGGCATGGACAGGGGCGGGCCAGATTTCAGCATGTAGTGCTTGCGTT
GGTACTCACGCCTGTTATACTATGAGTACTCACGCACAGAAGGGGGTTTTATGGAATACGAAAA
AAGCGCTTCAGGGTCGGTCTACCTGATCAAAAGTGACAAGGGCTATTGGTTGCCCGGTGGCTTT
GGTTATACGTCAAACAAGGCCGAGGCTGGCCGCTTTTCAGTCGCTGATATGGCCAGCCTTAACC
TTGACGGCTGCACCTTGTCCTTGTTCCGCGAAGACAAGCCTTTCGGCCCCGGCAAGTTTCTCGG
TGACTGATATGAAAGACCAAAAGGACAAGCAGACCGGCGACCTGCTGGCCAGCCCTGACGCTGT
ACGCCAAGCGCGATATGCCGAGCGCATGAAGGCCAAAGGGATGCGTCAGCGCAAGTTCTGGCTG
ACCGACGACGAATACGAGGCGCTGCGCGAGTGCCTGGAAGAACTCAGAGCGGCGCAGGGCGGGG
GTAGTGACCCCGCCAGCGCCTAACCACCAACTGCCTGCAAAGGAGGCAATCAATGGCTACCCAT

AAGCCTATCAATATTCTGGAGGCGTTCGCAGCAGCGCCGCCACCGCTGGACTACGTTTTGCCCA
ACATGGTGGCCGGTACGGTCGGGGCGCTGGTGTCGCCCGGTGGTGCCGGTAAATCCATGCTGGC
CCTGCAACTGGCCGCACAGATTGCAGGCGGGCCGGATCTGCTGGAGGTGGGCGAACTGCCCACC
GGCCCGGTGATCTACCTGCCCGCCGAAGACCCGCCCACCGCCATTCATCACCGCCTGCACGCCC
TTGGGGCGCACCTCAGCGCCGAGGAACGGCAAGCCGTGGCTGACGGCCTGCTGATCCAGCCGCT
GATCGGCAGCCTGCCCAACATCATGGCCCCGGAGTGGTTCGACGGCCTCAAGCGCGCCGCCGAG
GGCCGCCGCCTGATGGTGCTGGACACGCTGCGCCGGTTCCACATCGAGGAAGAAAACGCCAGCG
GCCCCATGGCCCAGGTCATCGGTCGCATGGAGGCCATCGCCGCCGATACCGGGTGCTCTATCGT
GTTCCTGCACCATGCCAGCAAGGGCGCGGCCATGATGGGCGCAGGCGACCAGCAGCAGGCCAGC
CGGGGCAGCTCGGTACTGGTCGATAACATCCGCTGGCAGTCCTACCTGTCGAGCATGACCAGCG
CCGAGGCCGAGGAATGGGGTGTGGACGACGACCAGCGCCGGTTCTTCGTCCGCTTCGGTGTGAG
CAAGGCCAACTATGGCGCACCGTTCGCTGATCGGTGGTTCAGGCGGCATGACGGCGGGGTGCTC
AAGCCCGCCGTGCTGGAGAGGCAGCGCAAGAGCAAGGGGGTGCCCCGTGGTGAAGCCTAAGAAC
AAGCACAGCCTCAGCCACGTCCGGCACGACCCGGCGCACTGTCTGGCCCCCGGCCTGTTCCGTG
CCCTCAAGCGGGGCGAGCGCAAGCGCAGCAAGCTGGACGTGACGTATGACTACGGCGACGGCAA
GCGGATCGAGTTCAGCGGCCCGGAGCCGCTGGGCGCTGATGATCTGCGCATCCTGCAAGGGCTG
GTGGCCATGGCTGGGCCTAATGGCCTAGTGCTTGGCCCGGAACCCAAGACCGAAGGCGGACGGC
AGCTCCGGCTGTTCCTGGAACCCAAGTGGGAGGCCGTCACCGCTGAATGCCATGTGGTCAAAGG
TAGCTATCGGGCGCTGGCAAAGGAAATCGGGGCAGAGGTCGATAGTGGTGGGGCGCTCAAGCAC
ATACAGGACTGCATCGAGCGCCTTTGGAAGGTATCCATCATCGCCCAGAATGGCCGCAAGCGGC
AGGGGTTTCGGCTGCTGTCGGAGTACGCCAGCGACGAGGCGGACGGGCGCCTGTACGTGGCCCT
GAACCCCTTGATCGCGCAGGCCGTCATGGGTGGCGGCCAGCATGTGCGCATCAGCATGGACGAG
GTGCGGGCGCTGGACAGCGAAACCGCCCGCCTGCTGCACCAGCGGCTGTGTGGCTGGATCGACC
CCGGCAAAACCGGCAAGGCTTCCATAGATACCTTGTGCGGCTATGTCTGGCCGTCAGAGGCCAG
TGGTTCGACCATGCGCAAGCGCCGCAAGCGGGTGCGCGAGGCGTTGCCGGAGCTGGTCGCGCTG
GGCTGGACGGTAACCGAGTTCGCGGCGGGCAAGTACGACATCACCCGGCCCAAGGCGGCAGGCT
GACCCCCCCCCACTCTATTGTAAACAAGACATTTTTATCTTTTATATTCAATGGCTTATTTTCCT
GCTAATTGGTAATACCATGAAAAATACCATGCTCAGAAAAGGCTTAACAATATTTTGAAAAATT
GCCTACTGAGCGCTGCCGCACAGCTCCATAGGCCGCTTTCCTGGCTTTGCTTCCAGATGTATGC
TCTTCTGCTCCCGAACGCCAGCAAGACGTAGCCCAGCGCGTCGGCCAGCTTGCAATTCGCGCTA
ACTTACATTAATTGCGTTGCGCTCACTGCCCGCTTTCCAGTCGGGAAACCTGTCGTGCCAGCTG
CATTAATGAATCGGCCAACGCGCGGGGAGAGGCGGTTTGCGTATTGGGCGCCAGGGTGGTTTTT
CTTTTCACCAGTGAGACGGGCAACAGCTGATTGCCCTTCACCGCCTGGCCCTGAGAGAGTTGCA
GCAAGCGGTCCACGTGGTTTGCCCCAGCAGGCGAAAATCCTGTTTGATGGTGGTTAACGGCGGG
ATATAACATGAGCTGTCTTCGGTATCGTCGTATCCCACTACCGAGATATCCGCACCAACGCGCA
GCCCGGACTCGGTAATGGCGCGCATTGCGCCCAGCGCCATCTGATCGTTGGCAACCAGCATCGC
AGTGGGAACGATGCCCTCATTCAGCATTTGCATGGTTTGTTGAAAACCGGACATGGCACTCCAG

TCGCCTTCCCGTTCCGCTATCGGCTGAATTTGATTGCGAGTGAGATATTTATGCCAGCCAGCCA
GACGCAGACGCGCCGAGACAGAACTTAATGGGCCCGCTAACAGCGCGATTTGCTGGTGACCCAA
TGCGACCAGATGCTCCACGCCCAGTCGCGTACCGTCTTCATGGGAGAAAATAATACTGTTGATG
GGTGTCTGGTCAGAGACATCAAGAAATAACGCCGGAACATTAGTGCAGGCAGCTTCCACAGCAA
TGGCATCCTGGTCATCCAGCGGATAGTTAATGATCAGCCCACTGACGCGTTGCGCGAGAAGATT
GTGCACCGCCGCTTTACAGGCTTCGACGCCGCTTCGTTCTACCATCGACACCACCACGCTGGCA
CCCAGTTGATCGGCGCGAGATTTAATCGCCGCGACAATTTGCGACGGCGCGTGCAGGGCCAGAC
TGGAGGTGGCAACGCCAATCAGCAACGACTGTTTGCCCGCCAGTTGTTGTGCCACGCGGTTGGG
AATGTAATTCAGCTCCGCCATCGCCGCTTCCACTTTTTCCCGCGTTTTCGCAGAAACGTGGCTG
GCCTGGTTCACCACGCGGGAAACGGTCTGATAAGAGACACCGGCATACTCTGCGACATCGTATA
ACGTTACTGGTTTCACATTCACCACCCTGAATTGACTCTCTTCCGGGCGCTATCATGCCATACC
GCGAAAGGTTTTGCACCATTCGATGGTGTCAACGTAAATGCCGCTTCGCCTTCGCGCGCGAATT
GCAAGCTGATCCGGGCTTATCGACTGCACGGTGCACCAATGCTTCTGGCGTCAGGCAGCCATCG
GAAGCTGTGGTATGGCTGTGCAGGTCGTAAATCACTGCATAATTCGTGTCGCTCAAGGCGCACT
CCCGTTCTGGATAATGTTTTTTGCGCCGACATCATAACGGTTCTGGCAAATATTCTGAAATGAG
CTGTTGACAATTAATCATCGGCTCGTATAATGTGTGGAATTGTGAGCGGATACAATTTCACACA
GGAAACAGAATTCGGCCCCCATAAAAAGTAAATTAAAATTTGGTGTTTTTTTTACAGTTTTACT
ATCTTCAGCATATGCACATGGAACACCTCAAAATATTACTGATTTGTGTGCAGAATACCACAAC
ACACAAATATATACGCTAAATGATAAGATATTTTCGTATACAGAATCTCTAGCTGGAAAAAGAG
AGATGGCTATCATTACTTTTAAGAATGGTGCAATTTTTCAAGTAGAAGTACCAGGTAGTCAACA
TATAGATTCACAAAAAAAAGCGATTGAAAGGATGAAGGATACCCTGAGGATTGCATATCTTACT
GAAGCTAAAGTCGAAAAGTTATGTGTATGGAATAATAAAACGCCTCATGCGATTGCCGCAATTA
GTATGGCAAACTAGTTTGCTTTAAAAGCATGTCTAATGCTAGGAACCTATATAACAACTACTGT
ACTTATACTAATGAGCCTTATGCTGCATTTGAAAAGGCGGTAGAGGATGCAATACCGATCCTTA
AACTGTAACACTATAACAGCTTCCACTACAGGGAGCTGTTATAGCAAACAGAAAAAACTAAGCT
AGGCTGGGGGGGCA

7.1.2. pBSTG

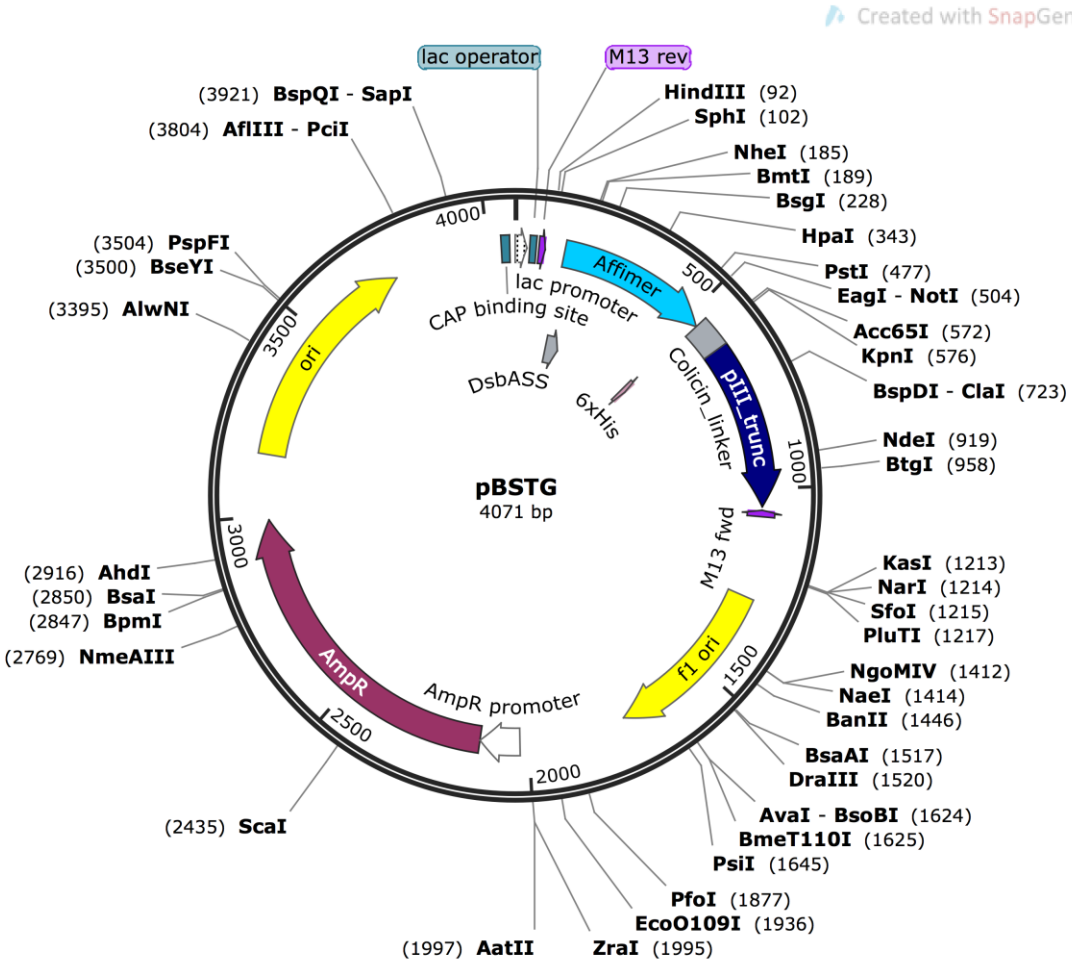

Figure 7.2. Plasmid map for pBSTG.

Affimer-pIII fusion proteins were expressed from ER2738 *E. coli* cells harbouring the pBSTG plasmid (Figure 7.2).

Full sequence 5' – 3':

TTTACACTTTATGCTTCCGGCTCGTATGTTGTGTGGAATTGTGAGCGGATAACAATTTCACACA
GGAAACAGCTATGACCATGATTACGCCAAGCTTGCATGCAAATTCTATTTCAAGGAGACAGTCA
TAATGAAAAAGATTTGGTTGGCTCTGGCTGGTCTGGTTCTGGCGTTTTCTGCGTCTGCTAGCGC
CGCTACCGGTGTTCGTGCAGTTCCGGGTAACGAAAACTCCCTGGAAATCGAAGAACTGGCTCGT
TTCGCTGTTGACGAACACAACAAAAAAGAAAACGCTCTGCTGGAATTCGTTCGTGTTGTTAAAG
CGAAAGAACAGCGTCATTGGGTTAACGTTCCGTTCCCGACCATGTACTACCTGACCCTGGAAGC
TAAAGACGGTGGTAAAAAGAAACTGTACGAAGCGAAAGTTTGGGTTAAGGGCGATGGCTTCGAT
AACGCACTGCATAACTTCAAAGAACTGCAGGAGTTCAAACCGGTTGGTGACGCTGCGGCCGCGC
ATCACCATCATCACCACTAGGGTAACGGTGGTGGTAACGGTAACTCTGGTGGTGGTTCTGGTAC
CGGCGGCTCCGGTTCCGGTGATTTTGATTATGAAAAAATGGCAAACGCTAATAAGGGGGCTATG
ACCGAAAATGCCGATGAAAACGCGCTACAGTCTGACGCTAAAGGCAAACTTGATTCTGTCGCTA

CTGATTACGGTGCTGCTATCGATGGTTTCATTGGTGACGTTTCCGGCCTTGCTAATGGTAATGG
TGCTACTGGTGATTTTGCTGGCTCTAATTCCCAAATGGCTCAAGTCGGTGACGGTGATAATTCA
CCTTTAATGAATAATTTCCGTCAATATTTACCTTCTTTGCCTCAGTCGGTTGAATGTCGCCCTT
ATGTCTTTGGCGCTGGTAAACCATATGAATTTTCTATTGATTGTGACAAAATAAACTTATTCCG
TGGTGTCTTTGCGTTTCTTTTATATGTTGCCACCTTTATGTATGTATTTTCGACGTTTGCTAAC
ATACTGCGTAATAAGGAGTCTTAATAAGAATTCACTGGCCGTCGTTTTACAACGTCGTGACTGG
GAAAACCCTGGCGTTACCCAACTTAATCGCCTTGCAGCACATCCCCCTTTCGCCAGCTGGCGTA
ATAGCGAAGAGGCCCGCACCGATCGCCCTTCCCAACAGTTGCGCAGCCTGAATGGCGAATGGCG
CCTGATGCGGTATTTTCTCCTTACGCATCTGTGCGGTATTTCACACCGCATACGTCAAAGCAAC
CATAGTACGCGCCCTGTAGCGGCGCATTAAGCGCGGCGGGTGTGGTGGTTACGCGCAGCGTGAC
CGCTACACTTGCCAGCGCCCTAGCGCCCGCTCCTTTCGCTTTCTTCCCTTCCTTTCTCGCCACG
TTCGCCGGCTTTCCCCGTCAAGCTCTAAATCGGGGGCTCCCTTTAGGGTTCCGATTTAGTGCTT
TACGGCACCTCGACCCCAAAAAACTTGATTTGGGTGATGGTTCACGTAGTGGGCCATCGCCCTG
ATAGACGGTTTTTCGCCCTTTGACGTTGGAGTCCACGTTCTTTAATAGTGGACTCTTGTTCCAA
ACTGGAACAACACTCAACCCTATCTCGGGCTATTCTTTTGATTTATAAGGGATTTTGCCGATTT
CGGCCTATTGGTTAAAAAATGAGCTGATTTAACAAAAATTTAACGCGAATTTTAACAAAATATT
AACGTTTACAATTTTATGGTGCACTCTCAGTACAATCTGCTCTGATGCCGCATAGTTAAGCCAG
CCCCGACACCCGCCAACACCCGCTGACGCGCCCTGACGGGCTTGTCTGCTCCCGGCATCCGCTT
ACAGACAAGCTGTGACCGTCTCCGGGAGCTGCATGTGTCAGAGGTTTTCACCGTCATCACCGAA
ACGCGCGAGACGAAAGGGCCTCGTGATACGCCTATTTTTATAGGTTAATGTCATGATAATAATG
GTTTCTTAGACGTCAGGTGGCACTTTTCGGGGAAATGTGCGCGGAACCCCTATTTGTTTATTTT
TCTAAATACATTCAAATATGTATCCGCTCATGAGACAATAACCCTGATAAATGCTTCAATAATA
TTGAAAAAGGAAGAGTATGAGTATTCAACATTTCCGTGTCGCCCTTATTCCCTTTTTTGCGGCA
TTTTGCCTTCCTGTTTTTGCTCACCCAGAAACGCTGGTGAAAGTAAAAGATGCTGAAGATCAGT
TGGGTGCACGAGTGGGTTACATCGAACTGGATCTCAACAGCGGTAAGATCCTTGAGAGTTTTCG
CCCCGAAGAACGTTTTCCAATGATGAGCACTTTTAAAGTTCTGCTATGTGGCGCGGTATTATCC
CGTATTGACGCCGGGCAAGAGCAACTCGGTCGCCGCATACACTATTCTCAGAATGACTTGGTTG
AGTACTCACCAGTCACAGAAAAGCATCTTACGGATGGCATGACAGTAAGAGAATTATGCAGTGC
TGCCATAACCATGAGTGATAACACTGCGGCCAACTTACTTCTGACAACGATCGGAGGACCGAAG
GAGCTAACCGCTTTTTTGCACAACATGGGGGATCATGTAACTCGCCTTGATCGTTGGGAACCGG
AGCTGAATGAAGCCATACCAAACGACGAGCGTGACACCACGATGCCTGTAGCAATGGCAACAAC
GTTGCGCAAACTATTAACTGGCGAACTACTTACTCTAGCTTCCCGGCAACAATTAATAGACTGG
ATGGAGGCGGATAAAGTTGCAGGACCACTTCTGCGCTCGGCCCTTCCGGCTGGCTGGTTTATTG
CTGATAAATCTGGAGCCGGTGAGCGTGGGTCTCGCGGTATCATTGCAGCACTGGGGCCAGATGG
TAAGCCCTCCCGTATCGTAGTTATCTACACGACGGGGAGTCAGGCAACTATGGATGAACGAAAT
AGACAGATCGCTGAGATAGGTGCCTCACTGATTAAGCATTGGTAACTGTCAGACCAAGTTTACT
CATATATACTTTAGATTGATTTAAAACTTCATTTTTAATTTAAAAGGATCTAGGTGAAGATCCT

TTTTGATAATCTCATGACCAAAATCCCTTAACGTGAGTTTTCGTTCCACTGAGCGTCAGACCCC
GTAGAAAAGATCAAAGGATCTTCTTGAGATCCTTTTTTTCTGCGCGTAATCTGCTGCTTGCAAA
CAAAAAAACCACCGCTACCAGCGGTGGTTTGTTTGCCGGATCAAGAGCTACCAACTCTTTTTCC
GAAGGTAACTGGCTTCAGCAGAGCGCAGATACCAAATACTGTCCTTCTAGTGTAGCCGTAGTTA
GGCCACCACTTCAAGAACTCTGTAGCACCGCCTACATACCTCGCTCTGCTAATCCTGTTACCAG
TGGCTGCTGCCAGTGGCGATAAGTCGTGTCTTACCGGGTTGGACTCAAGACGATAGTTACCGGA
TAAGGCGCAGCGGTCGGGCTGAACGGGGGGTTCGTGCACACAGCCCAGCTTGGAGCGAACGACC
TACACCGAACTGAGATACCTACAGCGTGAGCTATGAGAAAGCGCCACGCTTCCCGAAGGGAGAA
AGGCGGACAGGTATCCGGTAAGCGGCAGGGTCGGAACAGGAGAGCGCACGAGGGAGCTTCCAGG
GGGAAACGCCTGGTATCTTTATAGTCCTGTCGGGTTTCGCCACCTCTGACTTGAGCGTCGATTT
TTGTGATGCTCGTCAGGGGGGCGGAGCCTATGGAAAAACGCCAGCAACGCGGCCTTTTTACGGT
TCCTGGCCTTTTGCTGGCCTTTTGCTCACATGTTCTTTCCTGCGTTATCCCCTGATTCTGTGGA
TAACCGTATTACCGCCTTTGAGTGAGCTGATACCGCTCGCCGCAGCCGAACGACCGAGCGCAGC
GAGTCAGTGAGCGAGGAAGCGGAAGAGCGCCCAATACGCAAACCGCCTCTCCCCGCGCGTTGGC
CGATTCATTAATGCAGCTGGCACGACAGGTTTCCCGACTGGAAAGCGGGCAGTGAGCGCAACGC
AATTAATGTGAGTTAGCTCACTCATTAGGCACCCCAGGC

7.1.3. pET11-Affimer

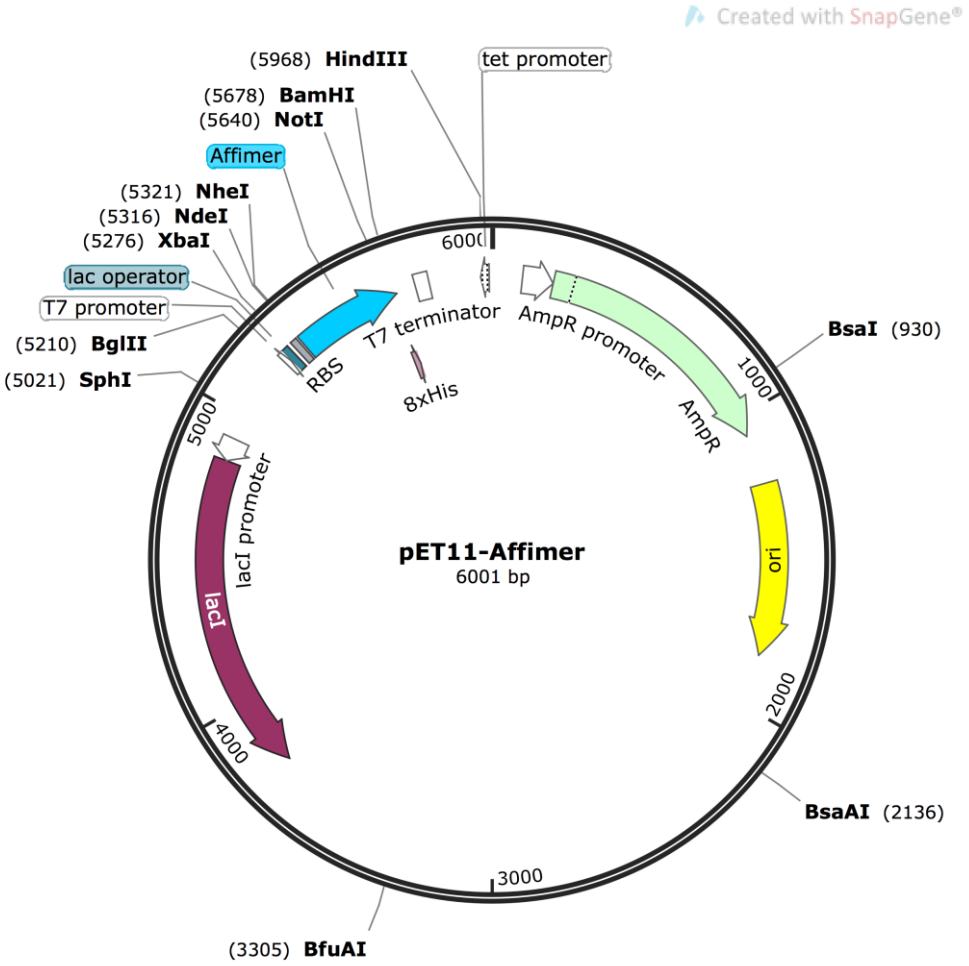

Figure 7.3. Plasmid map for pET11-Affimer.

Affimer variants were expressed from pET11-Affimer plasmid (Figure 7.3) by subcloning in between NheI and NotI restriction sites.

Full sequence 5' – 3':

TTCTTGAAGACGAAAGGGCCTCGTGATACGCCTATTTTTATAGGTTAATGTCATGATAATAATG
GTTTCTTAGACGTCAGGTGGCACTTTTCGGGGAAATGTGCGCGGAACCCCTATTTGTTTATTTT
TCTAAATACATTCAAATATGTATCCGCTCATGAGACAATAACCCTGATAAATGCTTCAATAATA
TTGAAAAAGGAAGAGTATGAGTATTCAACATTTCCGTGTCGCCCTTATTCCCTTTTTTGCGGCA
TTTTGCCTTCCTGTTTTTGCTCACCCAGAAACGCTGGTGAAAGTAAAAGATGCTGAAGATCAGT
TGGGTGCACGAGTGGGTTACATCGAACTGGATCTCAACAGCGGTAAGATCCTTGAGAGTTTTCG
CCCCGAAGAACGTTTTCCAATGATGAGCACTTTTAAAGTTCTGCTATGTGGCGCGGTATTATCC
CGTGTTGACGCCGGGCAAGAGCAACTCGGTCGCCGCATACACTATTCTCAGAATGACTTGGTTG

AGTACTCACCAGTCACAGAAAAGCATCTTACGGATGGCATGACAGTAAGAGAATTATGCAGTGC
TGCCATAACCATGAGTGATAACACTGCGGCCAACTTACTTCTGACAACGATCGGAGGACCGAAG
GAGCTAACCGCTTTTTTGCACAACATGGGGGATCATGTAACTCGCCTTGATCGTTGGGAACCGG
AGCTGAATGAAGCCATACCAAACGACGAGCGTGACACCACGATGCCTGCAGCAATGGCAACAAC
GTTGCGCAAACTATTAACTGGCGAACTACTTACTCTAGCTTCCCGGCAACAATTAATAGACTGG
ATGGAGGCGGATAAAGTTGCAGGACCACTTCTGCGCTCGGCCCTTCCGGCTGGCTGGTTTATTG
CTGATAAATCTGGAGCCGGTGAGCGTGGGTCTCGCGGTATCATTGCAGCACTGGGGCCAGATGG
TAAGCCCTCCCGTATCGTAGTTATCTACACGACGGGGAGTCAGGCAACTATGGATGAACGAAAT
AGACAGATCGCTGAGATAGGTGCCTCACTGATTAAGCATTGGTAACTGTCAGACCAAGTTTACT
CATATATACTTTAGATTGATTTAAAACTTCATTTTTAATTTAAAAGGATCTAGGTGAAGATCCT
TTTTGATAATCTCATGACCAAAATCCCTTAACGTGAGTTTTCGTTCCACTGAGCGTCAGACCCC
GTAGAAAAGATCAAAGGATCTTCTTGAGATCCTTTTTTTCTGCGCGTAATCTGCTGCTTGCAAA
CAAAAAAACCACCGCTACCAGCGGTGGTTTGTTTGCCGGATCAAGAGCTACCAACTCTTTTTCC
GAAGGTAACTGGCTTCAGCAGAGCGCAGATACCAAATACTGTCCTTCTAGTGTAGCCGTAGTTA
GGCCACCACTTCAAGAACTCTGTAGCACCGCCTACATACCTCGCTCTGCTAATCCTGTTACCAG
TGGCTGCTGCCAGTGGCGATAAGTCGTGTCTTACCGGGTTGGACTCAAGACGATAGTTACCGGA
TAAGGCGCAGCGGTCGGGCTGAACGGGGGGTTCGTGCACACAGCCCAGCTTGGAGCGAACGACC
TACACCGAACTGAGATACCTACAGCGTGAGCTATGAGAAAGCGCCACGCTTCCCGAAGGGAGAA
AGGCGGACAGGTATCCGGTAAGCGGCAGGGTCGGAACAGGAGAGCGCACGAGGGAGCTTCCAGG
GGGAAACGCCTGGTATCTTTATAGTCCTGTCGGGTTTCGCCACCTCTGACTTGAGCGTCGATTT
TTGTGATGCTCGTCAGGGGGGCGGAGCCTATGGAAAAACGCCAGCAACGCGGCCTTTTTACGGT
TCCTGGCCTTTTGCTGGCCTTTTGCTCACATGTTCTTTCCTGCGTTATCCCCTGATTCTGTGGA
TAACCGTATTACCGCCTTTGAGTGAGCTGATACCGCTCGCCGCAGCCGAACGACCGAGCGCAGC
GAGTCAGTGAGCGAGGAAGCGGAAGAGCGCCTGATGCGGTATTTTCTCCTTACGCATCTGTGCG
GTATTTCACACCGCATATATGGTGCACTCTCAGTACAATCTGCTCTGATGCCGCATAGTTAAGC
CAGTATACACTCCGCTATCGCTACGTGACTGGGTCATGGCTGCGCCCCGACACCCGCCAACACC
CGCTGACGCGCCCTGACGGGCTTGTCTGCTCCCGGCATCCGCTTACAGACAAGCTGTGACCGTC
TCCGGGAGCTGCATGTGTCAGAGGTTTTCACCGTCATCACCGAAACGCGCGAGGCAGCTGCGGT
AAAGCTCATCAGCGTGGTCGTGAAGCGATTCACAGATGTCTGCCTGTTCATCCGCGTCCAGCTC
GTTGAGTTTCTCCAGAAGCGTTAATGTCTGGCTTCTGATAAAGCGGGCCATGTTAAGGGCGGTT
TTTTCCTGTTTGGTCACTGATGCCTCCGTGTAAGGGGGATTTCTGTTCATGGGGGTAATGATAC
CGATGAAACGAGAGAGGATGCTCACGATACGGGTTACTGATGATGAACATGCCCGGTTACTGGA
ACGTTGTGAGGGTAAACAACTGGCGGTATGGATGCGGCGGGACCAGAGAAAAATCACTCAGGGT
CAATGCCAGCGCTTCGTTAATACAGATGTAGGTGTTCCACAGGGTAGCCAGCAGCATCCTGCGA
TGCAGATCCGGAACATAATGGTGCAGGGCGCTGACTTCCGCGTTTCCAGACTTTACGAAACACG
GAAACCGAAGACCATTCATGTTGTTGCTCAGGTCGCAGACGTTTTGCAGCAGCAGTCGCTTCAC
GTTCGCTCGCGTATCGGTGATTCATTCTGCTAACCAGTAAGGCAACCCCGCCAGCCTAGCCGGG

TCCTCAACGACAGGAGCACGATCATGCGCACCCGTGGCCAGGACCCAACGCTGCCCGAGATGCG
CCGCGTGCGGCTGCTGGAGATGGCGGACGCGATGGATATGTTCTGCCAAGGGTTGGTTTGCGCA
TTCACAGTTCTCCGCAAGAATTGATTGGCTCCAATTCTTGGAGTGGTGAATCCGTTAGCGAGGT
GCCGCCGGCTTCCATTCAGGTCGAGGTGGCCCGGCTCCATGCACCGCGACGCAACGCGGGGAGG
CAGACAAGGTATAGGGCGGCGCCTACAATCCATGCCAACCCGTTCCATGTGCTCGCCGAGGCGG
CATAAATCGCCGTGACGATCAGCGGTCCAGTGATCGAAGTTAGGCTGGTAAGAGCCGCGAGCGA
TCCTTGAAGCTGTCCCTGATGGTCGTCATCTACCTGCCTGGACAGCATGGCCTGCAACGCGGGC
ATCCCGATGCCGCCGGAAGCGAGAAGAATCATAATGGGGAAGGCCATCCAGCCTCGCGTCGCGA
ACGCCAGCAAGACGTAGCCCAGCGCGTCGGCCGCCATGCCGGCGATAATGGCCTGCTTCTCGCC
GAAACGTTTGGTGGCGGGACCAGTGACGAAGGCTTGAGCGAGGGCGTGCAAGATTCCGAATACC
GCAAGCGACAGGCCGATCATCGTCGCGCTCCAGCGAAAGCGGTCCTCGCCGAAAATGACCCAGA
GCGCTGCCGGCACCTGTCCTACGAGTTGCATGATAAAGAAGACAGTCATAAGTGCGGCGACGAT
AGTCATGCCCCGCGCCCACCGGAAGGAGCTGACTGGGTTGAAGGCTCTCAAGGGCATCGGTCGA
GATCCCGGTGCCTAATGAGTGAGCTAACTTACATTAATTGCGTTGCGCTCACTGCCCGCTTTCC
AGTCGGGAAACCTGTCGTGCCAGCTGCATTAATGAATCGGCCAACGCGCGGGGAGAGGCGGTTT
GCGTATTGGGCGCCAGGGTGGTTTTTCTTTTCACCAGTGAGACGGGCAACAGCTGATTGCCCTT
CACCGCCTGGCCCTGAGAGAGTTGCAGCAAGCGGTCCACGCTGGTTTGCCCCAGCAGGCGAAAA
TCCTGTTTGATGGTGGTTAACGGCGGGATATAACATGAGCTGTCTTCGGTATCGTCGTATCCCA
CTACCGAGATATCCGCACCAACGCGCAGCCCGGACTCGGTAATGGCGCGCATTGCGCCCAGCGC
CATCTGATCGTTGGCAACCAGCATCGCAGTGGGAACGATGCCCTCATTCAGCATTTGCATGGTT
TGTTGAAAACCGGACATGGCACTCCAGTCGCCTTCCCGTTCCGCTATCGGCTGAATTTGATTGC
GAGTGAGATATTTATGCCAGCCAGCCAGACGCAGACGCGCCGAGACAGAACTTAATGGGCCCGC
TAACAGCGCGATTTGCTGGTGACCCAATGCGACCAGATGCTCCACGCCCAGTCGCGTACCGTCT
TCATGGGAGAAAATAATACTGTTGATGGGTGTCTGGTCAGAGACATCAAGAAATAACGCCGGAA
CATTAGTGCAGGCAGCTTCCACAGCAATGGCATCCTGGTCATCCAGCGGATAGTTAATGATCAG
CCCACTGACGCGTTGCGCGAGAAGATTGTGCACCGCCGCTTTACAGGCTTCGACGCCGCTTCGT
TCTACCATCGACACCACCACGCTGGCACCCAGTTGATCGGCGCGAGATTTAATCGCCGCGACAA
TTTGCGACGGCGCGTGCAGGGCCAGACTGGAGGTGGCAACGCCAATCAGCAACGACTGTTTGCC
CGCCAGTTGTTGTGCCACGCGGTTGGGAATGTAATTCAGCTCCGCCATCGCCGCTTCCACTTTT
TCCCGCGTTTTCGCAGAAACGTGGCTGGCCTGGTTCACCACGCGGGAAACGGTCTGATAAGAGA
CACCGGCATACTCTGCGACATCGTATAACGTTACTGGTTTCACATTCACCACCCTGAATTGACT
CTCTTCCGGGCGCTATCATGCCATACCGCGAAAGGTTTTGCGCCATTCGATGGTGTCCGGGATC
TCGACGCTCTCCCTTATGCGACTCCTGCATTAGGAAGCAGCCCAGTAGTAGGTTGAGGCCGTTG
AGCACCGCCGCCGCAAGGAATGGTGCATGCAAGGAGATGGCGCCCAACAGTCCCCCGGCCACGG
GGCCTGCCACCATACCCACGCCGAAACAAGCGCTCATGAGCCCGAAGTGGCGAGCCCGATCTTC
CCCATCGGTGATGTCGGCGATATAGGCGCCAGCAACCGCACCTGTGGCGCCGGTGATGCCGGCC
ACGATGCGTCCGGCGTAGAGGATCGAGATCTCGATCCCGCGAAATTAATACGACTCACTATAGG

GGAATTGTGAGCGGATAACAATTCCCCTCTAGAAATAATTTTGTTTAACTTTAAGAAGGAGATA

TACATATGGCTAGCGCCGCTACCGGTGTTCGTGCAGTTCCGGGTAACGAAAACTCCCTGGAAAT

CGAAGAACTGGCTCGTTTCGCTGTTGACGAACACAACAAAAAAGAAAACGCTCTGCTGGAATTC

GTTCGTGTTGTTAAAGCGAAAGAACAAATCATCATCCACGAGAATGACGCCGACACCATGTACT

ACCTGACCCTGGAAGCTAAAGACGGTGGTAAAAAGAAACTGTACGAAGCGAAAGTTTGGGTTAA

GGGAATCATGGACGGACTGAATAAATACAACTTCAAAGAACTGCAGGAGTTCAAACCGGTTGGT

GACGCTGCGGCCGCGCATCACCATCATCACCACCATCATTGATAAGGATCCGGCTGCTAACAAA

GCCCGAAAGGAAGCTGAGTTGGCTGCTGCCACCGCTGAGCAATAACTAGCATAACCCCTTGGGG

CCTCTAAACGGGTCTTGAGGGGTTTTTTGCTGAAAGGAGGAACTATATCCGGATATCCCGCAAG

AGGCCCGGCAGTACCGGCATAACCAAGCCTATGCCTACAGCATCCAGGGTGACGGTGCCGAGGA

TGACGATGAGCGCATTGTTAGATTTCATACACGGTGCCTGACTGCGTTAGCAATTTAACTGTGA

TAAACTACCGCATTAAAGCTTATCGATGATAAGCTGTCAAACATGAGAA

7.1.4. pSAB2.2

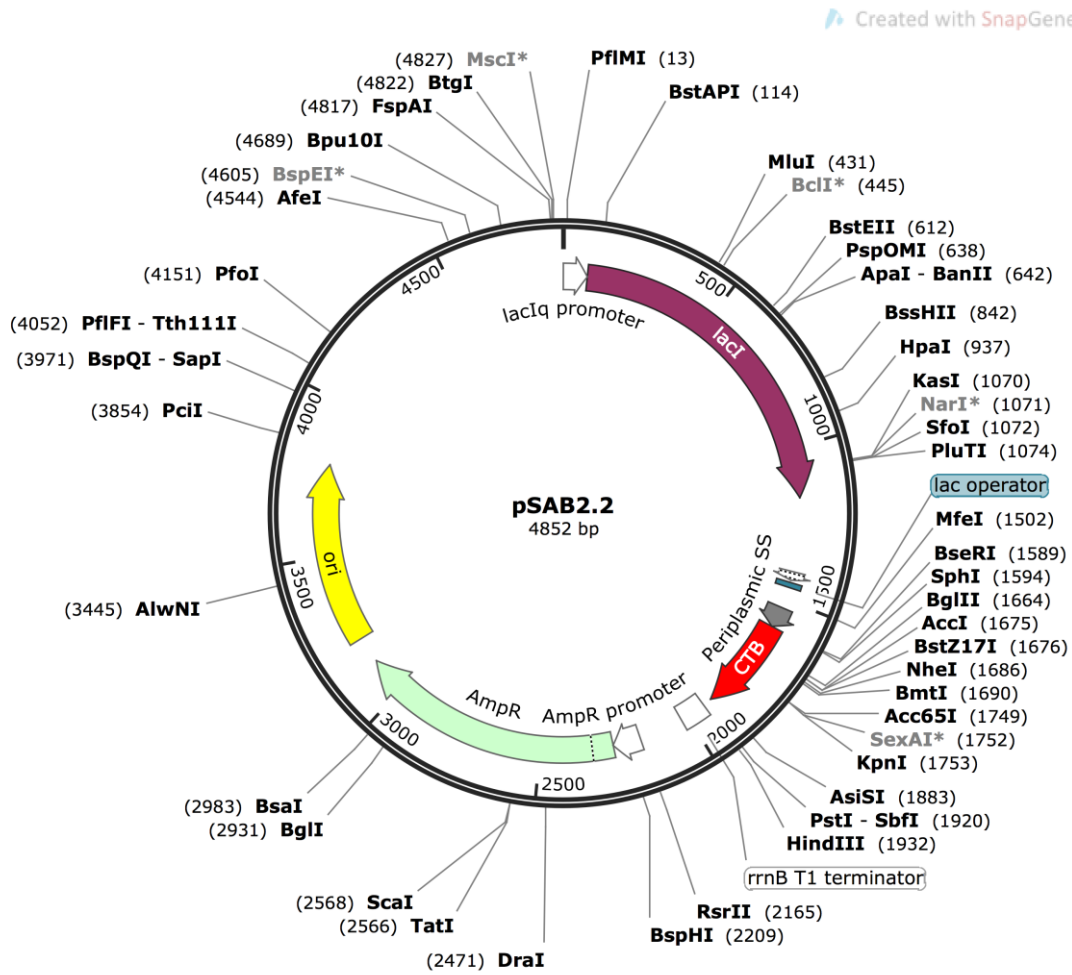

Figure 7.4. Plasmid map for pSAB2.2.

CTB variants were expressed from a plasmid based on pMal-p5x designed by Dr James Ross (Figure 7.4).

Full sequence 5' – 3':

CCGACACCATCGAATGGTGCAAAACCTTTCGCGGTATGGCATGATAGCGCCCGGAAGAGAGTCA
ATTCAGGGTGGTGAATGTGAAACCAGTAACGTTATACGATGTCGCAGAGTATGCCGGTGTCTCT
TATCAGACCGTTTCCCGCGTGGTGAACCAGGCCAGCCACGTTTCTGCGAAAACGCGGGAAAAAG
TGGAAGCGGCGATGGCGGAGCTGAATTACATTCCCAACCGCGTGGCACAACAACTGGCGGGCAA
ACAGTCGTTGCTGATTGGCGTTGCCACCTCCAGTCTGGCCCTGCACGCGCCGTCGCAAATTGTC
GCGGCGATTAAATCTCGCGCCGATCAACTGGGTGCCAGCGTGGTGGTGTCGATGGTAGAACGAA
GCGGCGTCGAAGCCTGTAAAGCGGCGGTGCACAATCTTCTCGCGCAACGCGTCAGTGGGCTGAT
CATTAACTATCCGCTGGATGACCAGGATGCCATTGCTGTGGAAGCTGCCTGCACTAATGTTCCG
GCGTTATTTCTTGATGTCTCTGACCAGACACCCATCAACAGTATTATTTTCTCCCATGAAGACG
GTACGCGACTGGGCGTGGAGCATCTGGTCGCATTGGGTCACCAGCAAATCGCGCTGTTAGCGGG

CCCATTAAGTTCTGTCTCGGCGCGTCTGCGTCTGGCTGGCTGGCATAAATATCTCACTCGCAAT
CAAATTCAGCCGATAGCGGAACGGGAAGGCGACTGGAGTGCCATGTCCGGTTTTCAACAAACCA
TGCAAATGCTGAATGAGGGCATCGTTCCCACTGCGATGCTGGTTGCCAACGATCAGATGGCGCT
GGGCGCAATGCGCGCCATTACCGAGTCCGGGCTGCGCGTTGGTGCGGATATTTCGGTAGTGGGA
TACGACGATACCGAAGACAGCTCATGTTATATCCCGCCGTTAACCACCATCAAACAGGATTTTC
GCCTGCTGGGGCAAACCAGCGTGGACCGCTTGCTGCAACTCTCTCAGGGCCAGGCGGTGAAGGG
CAATCAGCTGTTGCCCGTCTCACTGGTGAAAAGAAAAACCACCCTGGCGCCCAATACGCAAACC
GCCTCTCCCCGCGCGTTGGCCGATTCATTAATGCAGCTGGCACGACAGGTTTCCCGACTGGAAA
GCGGGCAGTGAGCGCAACGCAATTAATGTAAGTTAGCTCACTCATTAGGCACAATTCTCATGTT
TGACAGCTTATCATCGACTGCACGGTGCACCAATGCTTCTGGCGTCAGGCAGCCATCGGAAGCT
GTGGTATGGCTGTGCAGGTCGTAAATCACTGCATAATTCGTGTCGCTCAAGGCGCACTCCCGTT
CTGGATAATGTTTTTTGCGCCGACATCATAACGGTTCTGGCAAATATTCTGAAATGAGCTGTTG
ACAATTAATCATCGGCTCGTATAATGTGTGGAATTGTGAGCGGATAACAATTTCACACAGGAAA
CAGCCAGTCCGTTTAGGTGTTTTCACGAGCAATTGACCAACAAGGACCATAGATTATGAGCTTT
AAGAAAATTATCAAGGCATTTGTTATCATGGCTGCTTTGGTATCTGTTCAGGCGCATGCAGCTC
CTCAAAATATTACTGATTTGTGCGCAGAATACCACAACACACAAATATATACGCTAAATGATAA
GATCTTTTCGTATACAGAATCGCTAGCGGGAAAAAGAGAGATGGCTATCATTACTTTTAAGAAT
GGTGCAATTTTTCAAGTAGAGGTACCAGGTAGTCAACATATAGATTCACAAAAAAAAAGCGATTG
AAAGGATGAAGGATACCCTGAGGATTGCATATCTTACTGAAGCTAAAGTCGAAAAGTTATGTGT
ATGGAATAATAAAACGCCTCATGCGATCGCCGCAATTAGTATGGCAAACTAAGTTTTCCCTGCA
GGTAATTAAATAAGCTTCAAATAAAACGAAAGGCTCAGTCGAAAGACTGGGCCTTTCGTTTTAT
CTGTTGTTTGTCGGTGAACGCTCTCCTGAGTAGGACAAATCCGCCGGGAGCGGATTTGAACGTT
GCGAAGCAACGGCCCGGAGGGTGGCGGGCAGGACGCCCGCCATAAACTGCCAGGCATCAAATTA
AGCAGAAGGCCATCCTGACGGATGGCCTTTTTGCGTTTCTACAAACTCTTTCGGTCCGTTGTTT
ATTTTTCTAAATACATTCAAATATGTATCCGCTCATGAGACAATAACCCTGATAAATGCTTCAA
TAATATTGAAAAAGGAAGAGTATGAGTATTCAACATTTCCGTGTCGCCCTTATTCCCTTTTTTG
CGGCATTTTGCCTTCCTGTTTTTGCTCACCCAGAAACGCTGGTGAAAGTAAAAGATGCTGAAGA
TCAGTTGGGTGCACGAGTGGGTTACATCGAACTGGATCTCAACAGCGGTAAGATCCTTGAGAGT
TTTCGCCCCGAAGAACGTTTCCCAATGATGAGCACTTTTAAAGTTCTGCTATGTGGCGCGGTAT
TATCCCGTGTTGACGCCGGGCAAGAGCAACTCGGTCGCCGCATACACTATTCTCAGAATGACTT
GGTTGAGTACTCACCAGTCACAGAAAAGCATCTTACGGATGGCATGACAGTAAGAGAATTATGC
AGTGCTGCCATAACCATGAGTGATAACACTGCGGCCAACTTACTTCTGACAACGATCGGAGGAC
CGAAGGAGCTAACCGCTTTTTTGCACAACATGGGGGATCATGTAACTCGCCTTGATCGTTGGGA
ACCGGAGCTGAATGAAGCCATACCAAACGACGAGCGTGACACCACGATGCCTGTAGCAATGGCA
ACAACGTTGCGCAAACTATTAACTGGCGAACTACTTACTCTAGCTTCCCGGCAACAATTAATAG
ACTGGATGGAGGCGGATAAAGTTGCAGGACCACTTCTGCGCTCGGCCCTTCCGGCTGGCTGGTT
TATTGCTGATAAATCTGGAGCCGGTGAGCGTGGGTCTCGCGGTATCATTGCAGCACTGGGGCCA

GATGGTAAGCCCTCCCGTATCGTAGTTATCTACACGACGGGGAGTCAGGCAACTATGGATGAAC
GAAATAGACAGATCGCTGAGATAGGTGCCTCACTGATTAAGCATTGGTAACTGTCAGACCAAGT
TTACTCATATATACTTTAGATTGATTTCCTTAGGACTGAGCGTCAACCCCGTAGAAAAGATCAA
AGGATCTTCTTGAGATCCTTTTTTTCTGCGCGTAATCTGCTGCTTGCAAACAAAAAAACCACCG
CTACCAGCGGTGGTTTGTTTGCCGGATCAAGAGCTACCAACTCTTTTTCCGAAGGTAACTGGCT
TCAGCAGAGCGCAGATACCAAATACTGTCCTTCTAGTGTAGCCGTAGTTAGGCCACCACTTCAA
GAACTCTGTAGCACCGCCTACATACCTCGCTCTGCTAATCCTGTTACCAGTGGCTGCTGCCAGT
GGCGATAAGTCGTGTCTTACCGGGTTGGACTCAAGACGATAGTTACCGGATAAGGCGCAGCGGT
CGGGCTGAACGGGGGGTTCGTGCACACAGCCCAGCTTGGAGCGAACGACCTACACCGAACTGAG
ATACCTACAGCGTGAGCTATGAGAAAGCGCCACGCTTCCCGAAGGGAGAAAGGCGGACAGGTAT
CCGGTAAGCGGCAGGGTCGGAACAGGAGAGCGCACGAGGGAGCTTCCAGGGGGAAACGCCTGGT
ATCTTTATAGTCCTGTCGGGTTTCGCCACCTCTGACTTGAGCGTCGATTTTTGTGATGCTCGTC
AGGGGGGCGGAGCCTATGGAAAAACGCCAGCAACGCGGCCTTTTTACGGTTCCTGGCCTTTTGC
TGGCCTTTTGCTCACATGTTCTTTCCTGCGTTATCCCCTGATTCTGTGGATAACCGTATTACCG
CCTTTGAGTGAGCTGATACCGCTCGCCGCAGCCGAACGACCGAGCGCAGCGAGTCAGTGAGCGA
GGAAGCGGAAGAGCGCCTGATGCGGTATTTTCTCCTTACGCATCTGTGCGGTATTTCACACCGC
ATATAAGGTGCACTGTGACTGGGTCATGGCTGCGCCCCGACACCCGCCAACACCCGCTGACGCG
CCCTGACGGGCTTGTCTGCTCCCGGCATCCGCTTACAGACAAGCTGTGACCGTCTCCGGGAGCT
GCATGTGTCAGAGGTTTTCACCGTCATCACCGAAACGCGCGAGGCAGCTGCGGTAAAGCTCATC
AGCGTGGTCGTGCAGCGATTCACAGATGTCTGCCTGTTCATCCGCGTCCAGCTCGTTGAGTTTC
TCCAGAAGCGTTAATGTCTGGCTTCTGATAAAGCGGGCCATGTTAAGGGCGGTTTTTTCCTGTT
TGGTCACTGATGCCTCCGTGTAAGGGGGATTTCTGTTCATGGGGGTAATGATACCGATGAAACG
AGAGAGGATGCTCACGATACGGGTTACTGATGATGAACATGCCCGGTTACTGGAACGTTGTGAG
GGTAAACAACTGGCGGTATGGATGCGGCGGGACCAGAGAAAAATCACTCAGGGTCAATGCCAGC
GCTTCGTTAATACAGATGTAGGTGTTCCACAGGGTAGCCAGCAGCATCCTGCGATGCAGATCCG
GAACATAATGGTGCAGGGCGCTGACTTCCGCGTTTCCAGACTTTACGAAACACGGAAACCGAAG
ACCATTCATGTTGTTGCTCAGGTCGCAGACGTTTTGCAGCAGCAGTCGCTTCACGTTCGCTCGC
GTATCGGTGATTCATTCTGCTAACCAGTAAGGCAACCCCGCCAGCCTAGCCGGGTCCTCAACGA
CAGGAGCACGATCATGCGCACCCGTGGCCAGGACCCAACGCTGCCCGAAATT

7.1.5. pNIC-Affimer-GFP

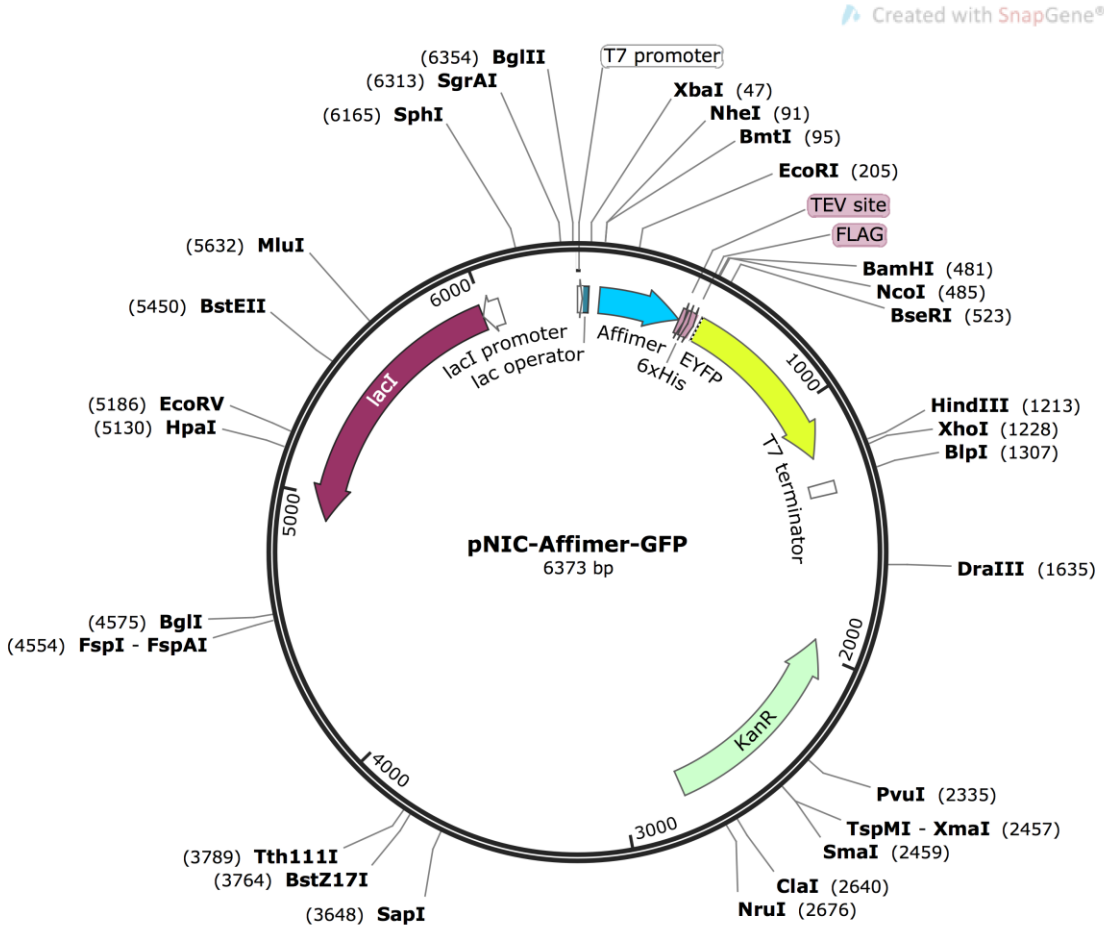

Figure 7.5. Plasmid map for pNIC-Affimer-GFP.

The Affimer CDS was introduced by ligation-independent cloning into pNIC-CTHF. eGFP was then ligated into pNIC-CTHF in between restriction sites BamHI and HindIII. The stop codon was then removed by mutagenesis to produce pNIC-Affimer-GFP (Figure 7.5).

Full sequence 5' – 3':

TAATACGACTCACTATAGGGGAATTGTGAGCGGATAACAATTCCCCTCTAGAAATAATTTTGTT
TAACCTTAAGAAGGAGATATACTATGGCTAGCGCCGCTACCGGTGTTCGTGCAGTTCCGGGTAA
CGAAAACTCCCTGGAAATCGAAGAACTGGCTCGTTTCGCTGTTGACGAACACAACAAAAAAGAA
AACGCTCTGCTGGAATTCGTTCGTGTTGTTAAAGCGAAAGAACAGCAGCATGAACGTTCTCATT
GGGTTGACACCATGTACTACCTGACCCTGGAAGCTAAAGACGGTGGTAAAAAGAAACTGTACGA
AGCGAAAGTTTGGGTTAAGCATAACCAGTTCTTCGATTATTTCATTAACTTCAAAGAACTGCAG
GAGTTCAAACCGGTTGGTGACGCTGCGGCCGCAGAGAACCTCTACTTCCAATCGCACCATCATC
ACCACCATGATTACAAGGATGACGACGATAAGGGATCCATGGGCAAAGTGAGCAAGGGCGAGGA
GCTGTTCACCGGGGTGGTGCCCATCCTGGTCGAGCTGGACGGCGACGTAAACGGCCACAAGTTC

AGCGTGTCCGGCGAGGGCGAGGGCGATGCCACCTACGGCAAGCTGACCCTGAAGTTCATCTGCA
CCACCGGCAAGCTGCCCGTGCCCTGGCCCACCCTCGTGACCACCTTCGGCTACGGCCTGCAGTG
CTTCGCCCGCTACCCCGACCACATGAAGCAGCACGACTTCTTCAAGTCCGCCATGCCCGAAGGC
TACGTCCAGGAGCGCACCATCTTCTTCAAGGACGACGGCAACTACAAGACCCGCGCCGAGGTGA
AGTTCGAGGGCGACACCCTGGTGAACCGCATCGAGCTGAAGGGCATCGACTTCAAGGAGGACGG
CAACATCCTGGGGCACAAGCTGGAGTACAACTACAACAGCCACAACGTCTATATCATGGCCGAC
AAGCAGAAGAACGGCATCAAGGTGAACTTCAAGATCCGCCACAACATCGAGGACGGCAGCGTGC
AGCTCGCCGACCACTACCAGCAGAACACCCCCATCGGCGACGGCCCCGTGCTGCTGCCCGACAA
CCACTACCTGAGCACCCAGTCCGCCCTGAGCAAAGACCCCAACGAGAAGCGCGATCACATGGTC
CTGCTGGAGTTCGTGACCGCCGCCGGGATCACTCTCGGCATGGACGAGCTGTACAAGTAGAAGC
TTGCGGCCGCACTCGAGCACCACCACCACCACCACTGAGATCCGGCTGCTAACAAAGCCCGAAA
GGAAGCTGAGTTGGCTGCTGCCACCGCTGAGCAATAACTAGCATAACCCCTTGGGGCCTCTAAA
CGGGTCTTGAGGGGTTTTTTGCTGAAAGGAGGAACTATATCCGGATTGGCGAATGGGACGCGCC
CTGTAGCGGCGCATTAAGCGCGGCGGGTGTGGTGGTTACGCGCAGCGTGACCGCTACACTTGCC
AGCGCCCTAGCGCCCGCTCCTTTCGCTTTCTTCCCTTCCTTTCTCGCCACGTTCGCCGGCTTTC
CCCGTCAAGCTCTAAATCGGGGGCTCCCTTTAGGGTTCCGATTTAGTGCTTTACGGCACCTCGA
CCCCAAAAAACTTGATTAGGGTGATGGTTCACGTAGTGGGCCATCGCCCTGATAGACGGTTTTT
CGCCCTTTGACGTTGGAGTCCACGTTCTTTAATAGTGGACTCTTGTTCCAAACTGGAACAACAC
TCAACCCTATCTCGGTCTATTCTTTTGATTTATAAGGGATTTTGCCGATTTCGGCCTATTGGTT
AAAAAATGAGCTGATTTAACAAAAATTTAACGCGAATTTTAACAAAATATTAACGTTTACAATT
TCAGGTGGCACTTTTCGGGGAAATGTGCGCGGAACCCCTATTTGTTTATTTTTCTAAATACATT
CAAATATGTATCCGCTCATGAATTAATTCTTAGAAAAACTCATCGAGCATCAAATGAAACTGCA
ATTTATTCATATCAGGATTATCAATACCATATTTTTGAAAAAGCCGTTTCTGTAATGAAGGAGA
AAACTCACCGAGGCAGTTCCATAGGATGGCAAGATCCTGGTATCGGTCTGCGATTCCGACTCGT
CCAACATCAATACAACCTATTAATTTCCCCTCGTCAAAAATAAGGTTATCAAGTGAGAAATCAC
CATGAGTGACGACTGAATCCGGTGAGAATGGCAAAAGTTTATGCATTTCTTTCCAGACTTGTTC
AACAGGCCAGCCATTACGCTCGTCATCAAAATCACTCGCATCAACCAAACCGTTATTCATTCGT
GATTGCGCCTGAGCGAGACGAAATACGCGATCGCTGTTAAAAGGACAATTACAAACAGGAATCG
AATGCAACCGGCGCAGGAACACTGCCAGCGCATCAACAATATTTTCACCTGAATCAGGATATTC
TTCTAATACCTGGAATGCTGTTTTCCCGGGGATCGCAGTGGTGAGTAACCATGCATCATCAGGA
GTACGGATAAAATGCTTGATGGTCGGAAGAGGCATAAATTCCGTCAGCCAGTTTAGTCTGACCA
TCTCATCTGTAACATCATTGGCAACGCTACCTTTGCCATGTTTCAGAAACAACTCTGGCGCATC
GGGCTTCCCATACAATCGATAGATTGTCGCACCTGATTGCCCGACATTATCGCGAGCCCATTTA
TACCCATATAAATCAGCATCCATGTTGGAATTTAATCGCGGCCTAGAGCAAGACGTTTCCCGTT
GAATATGGCTCATAACACCCCTTGTATTACTGTTTATGTAAGCAGACAGTTTTATTGTTCATGA
CCAAAATCCCTTAACGTGAGTTTTCGTTCCACTGAGCGTCAGACCCCGTAGAAAAGATCAAAGG
ATCTTCTTGAGATCCTTTTTTTCTGCGCGTAATCTGCTGCTTGCAAACAAAAAAACCACCGCTA

CCAGCGGTGGTTTGTTTGCCGGATCAAGAGCTACCAACTCTTTTTCCGAAGGTAACTGGCTTCA
GCAGAGCGCAGATACCAAATACTGTCCTTCTAGTGTAGCCGTAGTTAGGCCACCACTTCAAGAA
CTCTGTAGCACCGCCTACATACCTCGCTCTGCTAATCCTGTTACCAGTGGCTGCTGCCAGTGGC
GATAAGTCGTGTCTTACCGGGTTGGACTCAAGACGATAGTTACCGGATAAGGCGCAGCGGTCGG
GCTGAACGGGGGGTTCGTGCACACAGCCCAGCTTGGAGCGAACGACCTACACCGAACTGAGATA
CCTACAGCGTGAGCTATGAGAAAGCGCCACGCTTCCCGAAGGGAGAAAGGCGGACAGGTATCCG
GTAAGCGGCAGGGTCGGAACAGGAGAGCGCACGAGGGAGCTTCCAGGGGGAAACGCCTGGTATC
TTTATAGTCCTGTCGGGTTTCGCCACCTCTGACTTGAGCGTCGATTTTTGTGATGCTCGTCAGG
GGGGCGGAGCCTATGGAAAAACGCCAGCAACGCGGCCTTTTTACGGTTCCTGGCCTTTTGCTGG
CCTTTTGCTCACATGTTCTTTCCTGCGTTATCCCCTGATTCTGTGGATAACCGTATTACCGCCT
TTGAGTGAGCTGATACCGCTCGCCGCAGCCGAACGACCGAGCGCAGCGAGTCAGTGAGCGAGGA
AGCGGAAGAGCGCCTGATGCGGTATTTTCTCCTTACGCATCTGTGCGGTATTTCACACCGCATA
TATGGTGCACTCTCAGTACAATCTGCTCTGATGCCGCATAGTTAAGCCAGTATACACTCCGCTA
TCGCTACGTGACTGGGTCATGGCTGCGCCCCGACACCCGCCAACACCCGCTGACGCGCCCTGAC
GGGCTTGTCTGCTCCCGGCATCCGCTTACAGACAAGCTGTGACCGTCTCCGGGAGCTGCATGTG
TCAGAGGTTTTCACCGTCATCACCGAAACGCGCGAGGCAGCTGCGGTAAAGCTCATCAGCGTGG
TCGTGAAGCGATTCACAGATGTCTGCCTGTTCATCCGCGTCCAGCTCGTTGAGTTTCTCCAGAA
GCGTTAATGTCTGGCTTCTGATAAAGCGGGCCATGTTAAGGGCGGTTTTTTCCTGTTTGGTCAC
TGATGCCTCCGTGTAAGGGGGATTTCTGTTCATGGGGGTAATGATACCGATGAAACGAGAGAGG
ATGCTCACGATACGGGTTACTGATGATGAACATGCCCGGTTACTGGAACGTTGTGAGGGTAAAC
AACTGGCGGTATGGATGCGGCGGGACCAGAGAAAAATCACTCAGGGTCAATGCCAGCGCTTCGT
TAATACAGATGTAGGTGTTCCACAGGGTAGCCAGCAGCATCCTGCGATGCAGATCCGGAACATA
ATGGTGCAGGGCGCTGACTTCCGCGTTTCCAGACTTTACGAAACACGGAAACCGAAGACCATTC
ATGTTGTTGCTCAGGTCGCAGACGTTTTGCAGCAGCAGTCGCTTCACGTTCGCTCGCGTATCGG
TGATTCATTCTGCTAACCAGTAAGGCAACCCCGCCAGCCTAGCCGGGTCCTCAACGACAGGAGC
ACGATCATGCGCACCCGTGGGGCCGCCATGCCGGCGATAATGGCCTGCTTCTCGCCGAAACGTT
TGGTGGCGGGACCAGTGACGAAGGCTTGAGCGAGGGCGTGCAAGATTCCGAATACCGCAAGCGA
CAGGCCGATCATCGTCGCGCTCCAGCGAAAGCGGTCCTCGCCGAAAATGACCCAGAGCGCTGCC
GGCACCTGTCCTACGAGTTGCATGATAAAGAAGACAGTCATAAGTGCGGCGACGATAGTCATGC
CCCGCGCCCACCGGAAGGAGCTGACTGGGTTGAAGGCTCTCAAGGGCATCGGTCGAGATCCCGG
TGCCTAATGAGTGAGCTAACTTACATTAATTGCGTTGCGCTCACTGCCCGCTTTCCAGTCGGGA
AACCTGTCGTGCCAGCTGCATTAATGAATCGGCCAACGCGCGGGGAGAGGCGGTTTGCGTATTG
GGCGCCAGGGTGGTTTTTCTTTTCACCAGTGAGACGGGCAACAGCTGATTGCCCTTCACCGCCT
GGCCCTGAGAGAGTTGCAGCAAGCGGTCCACGCTGGTTTGCCCCAGCAGGCGAAAATCCTGTTT
GATGGTGGTTAACGGCGGGATATAACATGAGCTGTCTTCGGTATCGTCGTATCCCACTACCGAG
ATATCCGCACCAACGCGCAGCCCGGACTCGGTAATGGCGCGCATTGCGCCCAGCGCCATCTGAT
CGTTGGCAACCAGCATCGCAGTGGGAACGATGCCCTCATTCAGCATTTGCATGGTTTGTTGAAA

ACCGGACATGGCACTCCAGTCGCCTTCCCGTTCCGCTATCGGCTGAATTTGATTGCGAGTGAGA
TATTTATGCCAGCCAGCCAGACGCAGACGCGCCGAGACAGAACTTAATGGGCCCGCTAACAGCG
CGATTTGCTGGTGACCCAATGCGACCAGATGCTCCACGCCCAGTCGCGTACCGTCTTCATGGGA
GAAAATAATACTGTTGATGGGTGTCTGGTCAGAGACATCAAGAAATAACGCCGGAACATTAGTG
CAGGCAGCTTCCACAGCAATGGCATCCTGGTCATCCAGCGGATAGTTAATGATCAGCCCACTGA
CGCGTTGCGCGAGAAGATTGTGCACCGCCGCTTTACAGGCTTCGACGCCGCTTCGTTCTACCAT
CGACACCACCACGCTGGCACCCAGTTGATCGGCGCGAGATTTAATCGCCGCGACAATTTGCGAC
GGCGCGTGCAGGGCCAGACTGGAGGTGGCAACGCCAATCAGCAACGACTGTTTGCCCGCCAGTT
GTTGTGCCACGCGGTTGGGAATGTAATTCAGCTCCGCCATCGCCGCTTCCACTTTTTCCCGCGT
TTTCGCAGAAACGTGGCTGGCCTGGTTCACCACGCGGGAAACGGTCTGATAAGAGACACCGGCA
TACTCTGCGACATCGTATAACGTTACTGGTTTCACATTCACCACCCTGAATTGACTCTCTTCCG
GGCGCTATCATGCCATACCGCGAAAGGTTTTGCGCCATTCGATGGTGTCCGGGATCTCGACGCT
CTCCCTTATGCGACTCCTGCATTAGGAAGCAGCCCAGTAGTAGGTTGAGGCCGTTGAGCACCGC
CGCCGCAAGGAATGGTGCATGCAAGGAGATGGCGCCCAACAGTCCCCCGGCCACGGGGCCTGCC
ACCATACCCACGCCGAAACAAGCGCTCATGAGCCCGAAGTGGCGAGCCCGATCTTCCCCATCGG
TGATGTCGGCGATATAGGCGCCAGCAACCGCACCTGTGGCGCCGGTGATGCCGGCCACGATGCG
TCCGGCGTAGAGGATCGAGATCTCGATCCCGCGAAAT

7.1.6. pNIC-CTHF

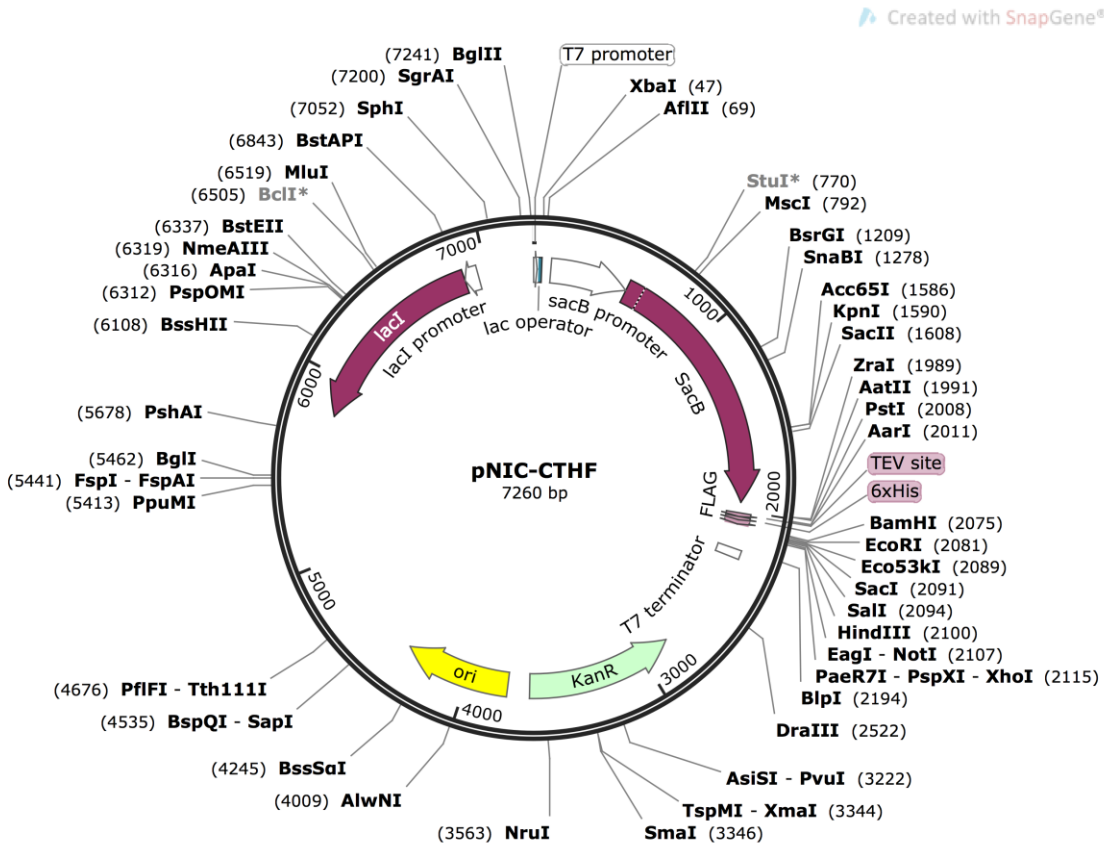

Figure 7.6. Plasmid map for pNIC-CTHF.

Full sequence 5' – 3':

TAATACGACTCACTATAGGGGAATTGTGAGCGGATAACAATTCCCCTCTAGAAATAATTTTGTT
TAACCTTAAGAAGGAGATATACTATGCAGGTCGTTCACTATTATTTAGTGAAATGAGATATTAT
GATATTTTCTGAATTGTGATTAAAAAGGCAACTTTATGCCCATGCAACAGAAACTATAAAAAAT
ACAGAGAATGAAAAGAAACAGATAGATTTTTTAGTTCTTTAGGCCCGTAGTCTGCAAATCCTTT
TATGATTTTCTATCAAACAAAAGAGGAAAATAGACCAGTTGCAATCCAAACGAGAGTCTAATAG
AATGAGGTCGAAAAGTAAATCGCGCGGGTTTGTTACTGATAAAGCAGGCAAGACCTAAAATGTG
TAAAGGGCAAAGTGTATACTTTGGCGTCACCCCTTACATATTTTAGGTCTTTTTTTATTGTGCG
TAACTAACTTGCCATCTTCAAACAGGAGGGCTGGAAGAAGCAGACCGCTAACACAGTACATAAA
AAAGGAGACATGAACGATGAACATCAAAAAGTTTGCAAAACAAGCAACAGTATTAACCTTTACT
ACCGCACTGCTGGCAGGAGGCGCAACTCAAGCGTTTGCGAAAGAAACGAACCAAAAGCCATATA
AGGAAACATACGGCATTTCCCATATTACACGCCATGATATGCTGCAAATCCCTGAACAGCAAAA
AAATGAAAAATATAAAGTTCCTGAGTTCGATTCGTCCACAATTAAAAATATCTCTTCTGCAAAA
GGCCTGGACGTTTGGGACAGCTGGCCATTACAAAACACTGACGGCACTGTCGCAAACTATCACG
GCTACCACATCGTCTTTGCATTAGCCGGAGATCCTAAAAATGCGGATGACACATCGATTTACAT
GTTCTATCAAAAAGTCGGCGAAACTTCTATTGACAGCTGGAAAAACGCTGGCCGCGTCTTTAAA
GACAGCGACAAATTCGATGCAAATGATTCTATCCTAAAAGACCAAACACAAGAATGGTCAGGTT

CAGCCACATTTACATCTGACGGAAAAATCCGTTTATTCTACACTGATTTCTCCGGTAAACATTA
CGGCAAACAAACACTGACAACTGCACAAGTTAACGTATCAGCATCAGACAGCTCTTTGAACATC
AACGGTGTAGAGGATTATAAATCAATCTTTGACGGTGACGGAAAAACGTATCAAAATGTACAGC
AGTTCATCGATGAAGGCAACTACAGCTCAGGCGACAACCATACGCTGAGAGATCCTCACTACGT
AGAAGATAAAGGCCACAAATACTTAGTATTTGAAGCAAACACTGGAACTGAAGATGGCTACCAA
GGCGAAGAATCTTTATTTAACAAAGCATACTATGGCAAAAGCACATCATTCTTCCGTCAAGAAA
GTCAAAAACTTCTGCAAAGCGATAAAAAACGCACGGCTGAGTTAGCAAACGGCGCTCTCGGTAT
GATTGAGCTAAACGATGATTACACACTGAAAAAAGTGATGAAACCGCTGATTGCATCTAACACA
GTAACAGATGAAATTGAACGCGCGAACGTCTTTAAAATGAACGGCAAATGGTACCTGTTCACTG
ACTCCCGCGGATCAAAAATGACGATTGACGGCATTACGTCTAACGATATTTACATGCTTGGTTA
TGTTTCTAATTCTTTAACTGGCCCATACAAGCCGCTGAACAAAACTGGCCTTGTGTTAAAAATG
GATCTTGATCCTAACGATGTAACCTTTACTTACTCACACTTCGCTGTACCTCAAGCGAAAGGAA
ACAATGTCGTGATTACAAGCTATATGACAAACAGAGGATTCTACGCAGACAAACAATCAACGTT
TGCGCCTAGCTTCCTGCTGAACATCAAAGGCAAGAAAACATCTGTTGTCAAAGACAGCATCCTT
GAACAAGGACAATTAACAGTTAACAAATAAAAACGCAAAAGAAAATGCCGATATCCTATTGGCA
TTGACGTCAGGTGGCACACCTGCAGAGAACCTCTACTTCCAATCGCACCATCATCACCACCATG
ATTACAAGGATGACGACGATAAGTGAGGATCCGAATTCGAGCTCCGTCGACAAGCTTGCGGCCG
CACTCGAGCACCACCACCACCACCACTGAGATCCGGCTGCTAACAAAGCCCGAAAGGAAGCTGA
GTTGGCTGCTGCCACCGCTGAGCAATAACTAGCATAACCCCTTGGGGCCTCTAAACGGGTCTTG
AGGGGTTTTTTGCTGAAAGGAGGAACTATATCCGGATTGGCGAATGGGACGCGCCCTGTAGCGG
CGCATTAAGCGCGGCGGGTGTGGTGGTTACGCGCAGCGTGACCGCTACACTTGCCAGCGCCCTA
GCGCCCGCTCCTTTCGCTTTCTTCCCTTCCTTTCTCGCCACGTTCGCCGGCTTTCCCCGTCAAG
CTCTAAATCGGGGGCTCCCTTTAGGGTTCCGATTTAGTGCTTTACGGCACCTCGACCCCAAAAA
ACTTGATTAGGGTGATGGTTCACGTAGTGGGCCATCGCCCTGATAGACGGTTTTTCGCCCTTTG
ACGTTGGAGTCCACGTTCTTTAATAGTGGACTCTTGTTCCAAACTGGAACAACACTCAACCCTA
TCTCGGTCTATTCTTTTGATTTATAAGGGATTTTGCCGATTTCGGCCTATTGGTTAAAAAATGA
GCTGATTTAACAAAAATTTAACGCGAATTTTAACAAAATATTAACGTTTACAATTTCAGGTGGC
ACTTTTCGGGGAAATGTGCGCGGAACCCCTATTTGTTTATTTTTCTAAATACATTCAAATATGT
ATCCGCTCATGAATTAATTCTTAGAAAAACTCATCGAGCATCAAATGAAACTGCAATTTATTCA
TATCAGGATTATCAATACCATATTTTTGAAAAAGCCGTTTCTGTAATGAAGGAGAAAACTCACC
GAGGCAGTTCCATAGGATGGCAAGATCCTGGTATCGGTCTGCGATTCCGACTCGTCCAACATCA
ATACAACCTATTAATTTCCCCTCGTCAAAAATAAGGTTATCAAGTGAGAAATCACCATGAGTGA
CGACTGAATCCGGTGAGAATGGCAAAAGTTTATGCATTTCTTTCCAGACTTGTTCAACAGGCCA
GCCATTACGCTCGTCATCAAAATCACTCGCATCAACCAAACCGTTATTCATTCGTGATTGCGCC
TGAGCGAGACGAAATACGCGATCGCTGTTAAAAGGACAATTACAAACAGGAATCGAATGCAACC
GGCGCAGGAACACTGCCAGCGCATCAACAATATTTTCACCTGAATCAGGATATTCTTCTAATAC
CTGGAATGCTGTTTTCCCGGGGATCGCAGTGGTGAGTAACCATGCATCATCAGGAGTACGGATA

AAATGCTTGATGGTCGGAAGAGGCATAAATTCCGTCAGCCAGTTTAGTCTGACCATCTCATCTG
TAACATCATTGGCAACGCTACCTTTGCCATGTTTCAGAAACAACTCTGGCGCATCGGGCTTCCC
ATACAATCGATAGATTGTCGCACCTGATTGCCCGACATTATCGCGAGCCCATTTATACCCATAT
AAATCAGCATCCATGTTGGAATTTAATCGCGGCCTAGAGCAAGACGTTTCCCGTTGAATATGGC
TCATAACACCCCTTGTATTACTGTTTATGTAAGCAGACAGTTTTATTGTTCATGACCAAAATCC
CTTAACGTGAGTTTTCGTTCCACTGAGCGTCAGACCCCGTAGAAAAGATCAAAGGATCTTCTTG
AGATCCTTTTTTTCTGCGCGTAATCTGCTGCTTGCAAACAAAAAAACCACCGCTACCAGCGGTG
GTTTGTTTGCCGGATCAAGAGCTACCAACTCTTTTTCCGAAGGTAACTGGCTTCAGCAGAGCGC
AGATACCAAATACTGTCCTTCTAGTGTAGCCGTAGTTAGGCCACCACTTCAAGAACTCTGTAGC
ACCGCCTACATACCTCGCTCTGCTAATCCTGTTACCAGTGGCTGCTGCCAGTGGCGATAAGTCG
TGTCTTACCGGGTTGGACTCAAGACGATAGTTACCGGATAAGGCGCAGCGGTCGGGCTGAACGG
GGGGTTCGTGCACACAGCCCAGCTTGGAGCGAACGACCTACACCGAACTGAGATACCTACAGCG
TGAGCTATGAGAAAGCGCCACGCTTCCCGAAGGGAGAAAGGCGGACAGGTATCCGGTAAGCGGC
AGGGTCGGAACAGGAGAGCGCACGAGGGAGCTTCCAGGGGGAAACGCCTGGTATCTTTATAGTC
CTGTCGGGTTTCGCCACCTCTGACTTGAGCGTCGATTTTTGTGATGCTCGTCAGGGGGGCGGAG
CCTATGGAAAAACGCCAGCAACGCGGCCTTTTTACGGTTCCTGGCCTTTTGCTGGCCTTTTGCT
CACATGTTCTTTCCTGCGTTATCCCCTGATTCTGTGGATAACCGTATTACCGCCTTTGAGTGAG
CTGATACCGCTCGCCGCAGCCGAACGACCGAGCGCAGCGAGTCAGTGAGCGAGGAAGCGGAAGA
GCGCCTGATGCGGTATTTTCTCCTTACGCATCTGTGCGGTATTTCACACCGCATATATGGTGCA
CTCTCAGTACAATCTGCTCTGATGCCGCATAGTTAAGCCAGTATACACTCCGCTATCGCTACGT
GACTGGGTCATGGCTGCGCCCCGACACCCGCCAACACCCGCTGACGCGCCCTGACGGGCTTGTC
TGCTCCCGGCATCCGCTTACAGACAAGCTGTGACCGTCTCCGGGAGCTGCATGTGTCAGAGGTT
TTCACCGTCATCACCGAAACGCGCGAGGCAGCTGCGGTAAAGCTCATCAGCGTGGTCGTGAAGC
GATTCACAGATGTCTGCCTGTTCATCCGCGTCCAGCTCGTTGAGTTTCTCCAGAAGCGTTAATG
TCTGGCTTCTGATAAAGCGGGCCATGTTAAGGGCGGTTTTTTCCTGTTTGGTCACTGATGCCTC
CGTGTAAGGGGGATTTCTGTTCATGGGGGTAATGATACCGATGAAACGAGAGAGGATGCTCACG
ATACGGGTTACTGATGATGAACATGCCCGGTTACTGGAACGTTGTGAGGGTAAACAACTGGCGG
TATGGATGCGGCGGGACCAGAGAAAAATCACTCAGGGTCAATGCCAGCGCTTCGTTAATACAGA
TGTAGGTGTTCCACAGGGTAGCCAGCAGCATCCTGCGATGCAGATCCGGAACATAATGGTGCAG
GGCGCTGACTTCCGCGTTTCCAGACTTTACGAAACACGGAAACCGAAGACCATTCATGTTGTTG
CTCAGGTCGCAGACGTTTTGCAGCAGCAGTCGCTTCACGTTCGCTCGCGTATCGGTGATTCATT
CTGCTAACCAGTAAGGCAACCCCGCCAGCCTAGCCGGGTCCTCAACGACAGGAGCACGATCATG
CGCACCCGTGGGGCCGCCATGCCGGCGATAATGGCCTGCTTCTCGCCGAAACGTTTGGTGGCGG
GACCAGTGACGAAGGCTTGAGCGAGGGCGTGCAAGATTCCGAATACCGCAAGCGACAGGCCGAT
CATCGTCGCGCTCCAGCGAAAGCGGTCCTCGCCGAAAATGACCCAGAGCGCTGCCGGCACCTGT
CCTACGAGTTGCATGATAAAGAAGACAGTCATAAGTGCGGCGACGATAGTCATGCCCCGCGCCC
ACCGGAAGGAGCTGACTGGGTTGAAGGCTCTCAAGGGCATCGGTCGAGATCCCGGTGCCTAATG

AGTGAGCTAACTTACATTAATTGCGTTGCGCTCACTGCCCGCTTTCCAGTCGGGAAACCTGTCG
TGCCAGCTGCATTAATGAATCGGCCAACGCGCGGGGAGAGGCGGTTTGCGTATTGGGCGCCAGG
GTGGTTTTTCTTTTCACCAGTGAGACGGGCAACAGCTGATTGCCCTTCACCGCCTGGCCCTGAG
AGAGTTGCAGCAAGCGGTCCACGCTGGTTTGCCCCAGCAGGCGAAAATCCTGTTTGATGGTGGT
TAACGGCGGGATATAACATGAGCTGTCTTCGGTATCGTCGTATCCCACTACCGAGATATCCGCA
CCAACGCGCAGCCCGGACTCGGTAATGGCGCGCATTGCGCCCAGCGCCATCTGATCGTTGGCAA
CCAGCATCGCAGTGGGAACGATGCCCTCATTCAGCATTTGCATGGTTTGTTGAAAACCGGACAT
GGCACTCCAGTCGCCTTCCCGTTCCGCTATCGGCTGAATTTGATTGCGAGTGAGATATTTATGC
CAGCCAGCCAGACGCAGACGCGCCGAGACAGAACTTAATGGGCCCGCTAACAGCGCGATTTGCT
GGTGACCCAATGCGACCAGATGCTCCACGCCCAGTCGCGTACCGTCTTCATGGGAGAAAATAAT
ACTGTTGATGGGTGTCTGGTCAGAGACATCAAGAAATAACGCCGGAACATTAGTGCAGGCAGCT
TCCACAGCAATGGCATCCTGGTCATCCAGCGGATAGTTAATGATCAGCCCACTGACGCGTTGCG
CGAGAAGATTGTGCACCGCCGCTTTACAGGCTTCGACGCCGCTTCGTTCTACCATCGACACCAC
CACGCTGGCACCCAGTTGATCGGCGCGAGATTTAATCGCCGCGACAATTTGCGACGGCGCGTGC
AGGGCCAGACTGGAGGTGGCAACGCCAATCAGCAACGACTGTTTGCCCGCCAGTTGTTGTGCCA
CGCGGTTGGGAATGTAATTCAGCTCCGCCATCGCCGCTTCCACTTTTTCCCGCGTTTTCGCAGA
AACGTGGCTGGCCTGGTTCACCACGCGGGAAACGGTCTGATAAGAGACACCGGCATACTCTGCG
ACATCGTATAACGTTACTGGTTTCACATTCACCACCCTGAATTGACTCTCTTCCGGGCGCTATC
ATGCCATACCGCGAAAGGTTTTGCGCCATTCGATGGTGTCCGGGATCTCGACGCTCTCCCTTAT
GCGACTCCTGCATTAGGAAGCAGCCCAGTAGTAGGTTGAGGCCGTTGAGCACCGCCGCCGCAAG
GAATGGTGCATGCAAGGAGATGGCGCCCAACAGTCCCCCGGCCACGGGGCCTGCCACCATACCC
ACGCCGAAACAAGCGCTCATGAGCCCGAAGTGGCGAGCCCGATCTTCCCCATCGGTGATGTCGG
CGATATAGGCGCCAGCAACCGCACCTGTGGCGCCGGTGATGCCGGCCACGATGCGTCCGGCGTA
GAGGATCGAGATCTCGATCCCGCGAAAT

7.1.7. pSAB-Syb-AB5

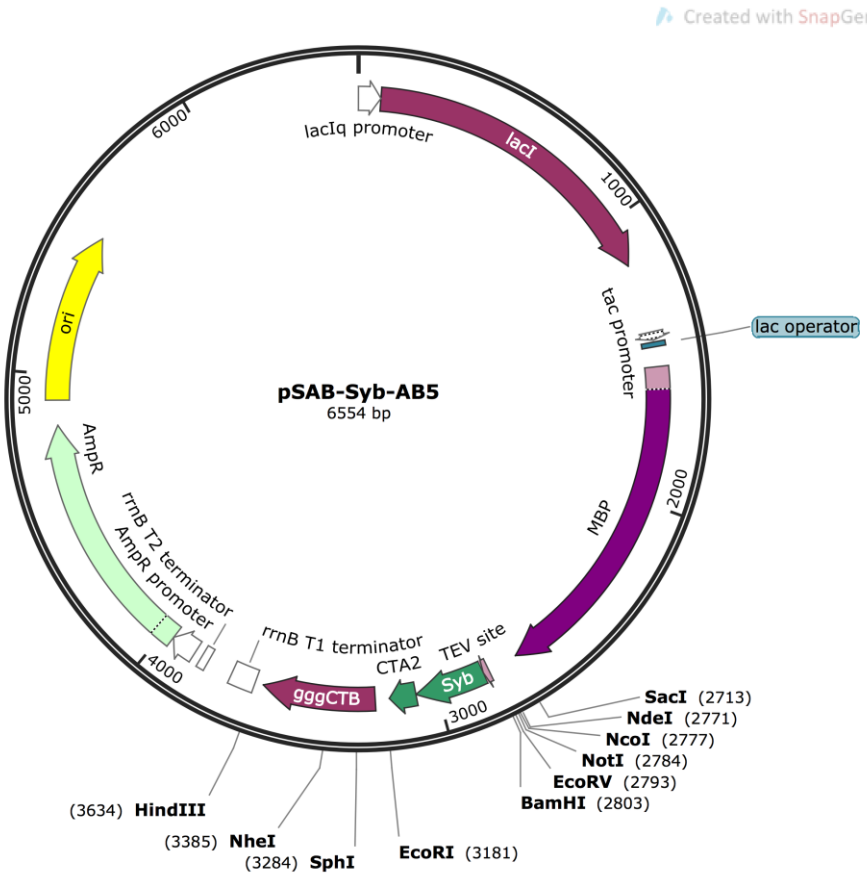

Figure 7.7. Plasmid map for pSAB-Syb-AB$_5$.

MBP-Syb-AB$_5$ was expressed from BL21-Gold cells harbouring the pSAB-Syb-AB$_5$ plasmid (Figure 7.7).

Full sequence 5' – 3':

CCGACACCATCGAATGGTGCAAAACCTTTCGCGGTATGGCATGATAGCGCCCGGAAGAGAGTCA
ATTCAGGGTGGTGAATGTGAAACCAGTAACGTTATACGATGTCGCAGAGTATGCCGGTGTCTCT
TATCAGACCGTTTCCCGCGTGGTGAACCAGGCCAGCCACGTTTCTGCGAAAACGCGGGAAAAAG
TGGAAGCGGCGATGGCGGAGCTGAATTACATTCCCAACCGCGTGGCACAACAACTGGCGGGCAA
ACAGTCGTTGCTGATTGGCGTTGCCACCTCCAGTCTGGCCCTGCACGCGCCGTCGCAAATTGTC
GCGGCGATTAAATCTCGCGCCGATCAACTGGGTGCCAGCGTGGTGGTGTCGATGGTAGAACGAA
GCGGCGTCGAAGCCTGTAAAGCGGCGGTGCACAATCTTCTCGCGCAACGCGTCAGTGGGCTGAT
CATTAACTATCCGCTGGATGACCAGGATGCCATTGCTGTGGAAGCTGCCTGCACTAATGTTCCG
GCGTTATTTCTTGATGTCTCTGACCAGACACCCATCAACAGTATTATTTTCTCCCATGAAGACG
GTACGCGACTGGGCGTGGAGCATCTGGTCGCATTGGGTCACCAGCAAATCGCGCTGTTAGCGGG
CCCATTAAGTTCTGTCTCGGCGCGTCTGCGTCTGGCTGGCTGGCATAAATATCTCACTCGCAAT
CAAATTCAGCCGATAGCGGAACGGGAAGGCGACTGGAGTGCCATGTCCGGTTTTCAACAAACCA
TGCAAATGCTGAATGAGGGCATCGTTCCCACTGCGATGCTGGTTGCCAACGATCAGATGGCGCT

GGGCGCAATGCGCGCCATTACCGAGTCCGGGCTGCGCGTTGGTGCGGATATTTCGGTAGTGGGA
TACGACGATACCGAAGACAGCTCATGTTATATCCCGCCGTTAACCACCATCAAACAGGATTTTC
GCCTGCTGGGGCAAACCAGCGTGGACCGCTTGCTGCAACTCTCTCAGGGCCAGGCGGTGAAGGG
CAATCAGCTGTTGCCCGTCTCACTGGTGAAAAGAAAAACCACCCTGGCGCCCAATACGCAAACC
GCCTCTCCCCGCGCGTTGGCCGATTCATTAATGCAGCTGGCACGACAGGTTTCCCGACTGGAAA
GCGGGCAGTGAGCGCAACGCAATTAATGTAAGTTAGCTCACTCATTAGGCACAATTCTCATGTT
TGACAGCTTATCATCGACTGCACGGTGCACCAATGCTTCTGGCGTCAGGCAGCCATCGGAAGCT
GTGGTATGGCTGTGCAGGTCGTAAATCACTGCATAATTCGTGTCGCTCAAGGCGCACTCCCGTT
CTGGATAATGTTTTTTGCGCCGACATCATAACGGTTCTGGCAAATATTCTGAAATGAGCTGTTG
ACAATTAATCATCGGCTCGTATAATGTGTGGAATTGTGAGCGGATAACAATTTCACACAGGAAA
CAGCCAGTCCGTTTAGGTGTTTTCACGAGCAATTGACCAACAAGGACCATAGATTATGAAAATA
AAAACAGGTGCACGCATCCTCGCATTATCCGCATTAACGACGATGATGTTTTCCGCCTCGGCTC
TCGCCAAAATCGAAGAAGGTAAACTGGTAATCTGGATTAACGGCGATAAAGGCTATAACGGTCT
CGCTGAAGTCGGTAAGAAATTCGAGAAAGATACCGGAATTAAAGTCACCGTTGAGCATCCGGAT
AAACTGGAAGAGAAATTCCCACAGGTTGCGGCAACTGGCGATGGCCCTGACATTATCTTCTGGG
CACACGACCGCTTTGGTGGCTACGCTCAATCTGGCCTGTTGGCTGAAATCACCCCGGACAAAGC
GTTCCAGGACAAGCTGTATCCGTTTACCTGGGATGCCGTACGTTACAACGGCAAGCTGATTGCT
TACCCGATCGCTGTTGAAGCGTTATCGCTGATTTATAACAAAGATCTGCTGCCGAACCCGCCAA
AAACCTGGGAAGAGATCCCGGCGCTGGATAAAGAACTGAAAGCGAAAGGTAAGAGCGCGCTGAT
GTTCAACCTGCAAGAACCGTACTTCACCTGGCCGCTGATTGCTGCTGACGGGGGTTATGCGTTC
AAGTATGAAAACGGCAAGTACGACATTAAAGACGTGGGCGTGGATAACGCTGGCGCGAAAGCGG
GTCTGACCTTCCTGGTTGACCTGATTAAAAACAAACACATGAATGCAGACACCGATTACTCCAT
CGCAGAAGCTGCCTTTAATAAAGGCGAAACAGCGATGACCATCAACGGCCCGTGGGCATGGTCC
AACATCGACACCAGCAAAGTGAATTATGGTGTAACGGTACTGCCGACCTTCAAGGGTCAACCAT
CCAAACCGTTCGTTGGCGTGCTGAGCGCAGGTATTAACGCCGCCAGTCCGAACAAAGAGCTGGC
AAAAGAGTTCCTCGAAAACTATCTGCTGACTGATGAAGGTCTGGAAGCGGTTAATAAAGACAAA
CCGCTGGGTGCCGTAGCGCTGAAGTCTTACGAGGAAGAGTTGGTGAAAGATCCGCGTATTGCCG
CCACTATGGAAAACGCCCAGAAAGGTGAAATCATGCCGAACATCCCGCAGATGTCCGCTTTCTG
GTATGCCGTGCGTACTGCGGTGATCAACGCCGCCAGCGGTCGTCAGACTGTCGATGAAGCCCTG
AAAGACGCGCAGACTAATTCGAGCTCGAACAACAACAACAATAACAATAACAACAACCTCGGGA
TCGAGGGAAGGATTTCACATATGTCCATGGGCGGCCGCGATATCGTCGACGGATCCGAAAACCT
GTACTTTCAGAGCGCGACCGCGGCGACCGTGCCGCCGGCGGCGCCGGCGGGTGAAGGTGGTCCG
CCGGCGCCGCCGCCGAACCTGACCAGCAACCGCCGCCTGCAGCAGACCCAGGCGCAGGTGGATG
AAGTGGTGGATATTATGCGCGTGAACGTGGATAAAGTGCTGGAACGCGATCAGAAACTGAGCGA
ACTGGATGATCGCGCGGATGCGCTGCAGGCGGGCGCGAGCCAGTTTGAAACCAGCGCGGCGAAA
CTGGGTGGCAACAACAACTCCTCTAAGGTGAAGCGTCAGATATTTTCAGGCTATCAATCTGATA
TTGATACCCACAACCGTATCAAGGATGAATTATGACCTCGAGGTGAATTCACGAGCAATTGACC

AACAAGGACCATAGATTATGAGCTTTAAGAAAATTATCAAGGCATTTGTTATCATGGCTGCTTT
GGTATCTGTTCAGGCGCATGCAGGCGGTGGCACCCCTCAAAATATTACTGATTTGTGCGCAGAA
TACCACAACACACAAATATATACGCTAAATGATAAGATCTTTTCGTATACAGAATCGCTAGCGG
GAAAAAGAGAGATGGCTATCATTACTTTTAAGAATGGTGCAATTTTTCAAGTAGAGGTACCAGG
TAGTCAACATATAGATTCACAAAAAAAAGCGATTGAAAGGATGAAGGATACCCTGAGGATTGCA
TATCTTACTGAAGCTAAAGTCGAAAAGTTATGTGTATGGAATAATAAAACGCCTCATGCGATCG
CCGCAATTAGTATGGCAAACTAATGAGTTTTCCCTGCAGGTAATTAAATAAGCTTCAAATAAAA
CGAAAGGCTCAGTCGAAAGACTGGGCCTTTCGTTTTATCTGTTGTTTGTCGGTGAACGCTCTCC
TGAGTAGGACAAATCCGCCGGGAGCGGATTTGAACGTTGCGAAGCAACGGCCCGGAGGGTGGCG
GGCAGGACGCCCGCCATAAACTGCCAGGCATCAAATTAAGCAGAAGGCCATCCTGACGGATGGC
CTTTTTGCGTTTCTACAAACTCTTTCGGTCCGTTGTTTATTTTTCTAAATACATTCAAATATGT
ATCCGCTCATGAGACAATAACCCTGATAAATGCTTCAATAATATTGAAAAAGGAAGAGTATGAG
TATTCAACATTTCCGTGTCGCCCTTATTCCCTTTTTTGCGGCATTTTGCCTTCCTGTTTTTGCT
CACCCAGAAACGCTGGTGAAAGTAAAAGATGCTGAAGATCAGTTGGGTGCACGAGTGGGTTACA
TCGAACTGGATCTCAACAGCGGTAAGATCCTTGAGAGTTTTCGCCCCGAAGAACGTTTCCCAAT
GATGAGCACTTTTAAAGTTCTGCTATGTGGCGCGGTATTATCCCGTGTTGACGCCGGGCAAGAG
CAACTCGGTCGCCGCATACACTATTCTCAGAATGACTTGGTTGAGTACTCACCAGTCACAGAAA
AGCATCTTACGGATGGCATGACAGTAAGAGAATTATGCAGTGCTGCCATAACCATGAGTGATAA
CACTGCGGCCAACTTACTTCTGACAACGATCGGAGGACCGAAGGAGCTAACCGCTTTTTTGCAC
AACATGGGGGATCATGTAACTCGCCTTGATCGTTGGGAACCGGAGCTGAATGAAGCCATACCAA
ACGACGAGCGTGACACCACGATGCCTGTAGCAATGGCAACAACGTTGCGCAAACTATTAACTGG
CGAACTACTTACTCTAGCTTCCCGGCAACAATTAATAGACTGGATGGAGGCGGATAAAGTTGCA
GGACCACTTCTGCGCTCGGCCCTTCCGGCTGGCTGGTTTATTGCTGATAAATCTGGAGCCGGTG
AGCGTGGGTCTCGCGGTATCATTGCAGCACTGGGGCCAGATGGTAAGCCCTCCCGTATCGTAGT
TATCTACACGACGGGGAGTCAGGCAACTATGGATGAACGAAATAGACAGATCGCTGAGATAGGT
GCCTCACTGATTAAGCATTGGTAACTGTCAGACCAAGTTTACTCATATATACTTTAGATTGATT
TCCTTAGGACTGAGCGTCAACCCCGTAGAAAAGATCAAAGGATCTTCTTGAGATCCTTTTTTTC
TGCGCGTAATCTGCTGCTTGCAAACAAAAAAACCACCGCTACCAGCGGTGGTTTGTTTGCCGGA
TCAAGAGCTACCAACTCTTTTTCCGAAGGTAACTGGCTTCAGCAGAGCGCAGATACCAAATACT
GTCCTTCTAGTGTAGCCGTAGTTAGGCCACCACTTCAAGAACTCTGTAGCACCGCCTACATACC
TCGCTCTGCTAATCCTGTTACCAGTGGCTGCTGCCAGTGGCGATAAGTCGTGTCTTACCGGGTT
GGACTCAAGACGATAGTTACCGGATAAGGCGCAGCGGTCGGGCTGAACGGGGGGTTCGTGCACA
CAGCCCAGCTTGGAGCGAACGACCTACACCGAACTGAGATACCTACAGCGTGAGCTATGAGAAA
GCGCCACGCTTCCCGAAGGGAGAAAGGCGGACAGGTATCCGGTAAGCGGCAGGGTCGGAACAGG
AGAGCGCACGAGGGAGCTTCCAGGGGGAAACGCCTGGTATCTTTATAGTCCTGTCGGGTTTCGC
CACCTCTGACTTGAGCGTCGATTTTTGTGATGCTCGTCAGGGGGGCGGAGCCTATGGAAAAACG
CCAGCAACGCGGCCTTTTTACGGTTCCTGGCCTTTTGCTGGCCTTTTGCTCACATGTTCTTTCC

TGCGTTATCCCCTGATTCTGTGGATAACCGTATTACCGCCTTTGAGTGAGCTGATACCGCTCGC
CGCAGCCGAACGACCGAGCGCAGCGAGTCAGTGAGCGAGGAAGCGGAAGAGCGCCTGATGCGGT
ATTTTCTCCTTACGCATCTGTGCGGTATTTCACACCGCATATAAGGTGCACTGTGACTGGGTCA
TGGCTGCGCCCCGACACCCGCCAACACCCGCTGACGCGCCCTGACGGGCTTGTCTGCTCCCGGC
ATCCGCTTACAGACAAGCTGTGACCGTCTCCGGGAGCTGCATGTGTCAGAGGTTTTCACCGTCA
TCACCGAAACGCGCGAGGCAGCTGCGGTAAAGCTCATCAGCGTGGTCGTGCAGCGATTCACAGA
TGTCTGCCTGTTCATCCGCGTCCAGCTCGTTGAGTTTCTCCAGAAGCGTTAATGTCTGGCTTCT
GATAAAGCGGGCCATGTTAAGGGCGGTTTTTTCCTGTTTGGTCACTGATGCCTCCGTGTAAGGG
GGATTTCTGTTCATGGGGGTAATGATACCGATGAAACGAGAGAGGATGCTCACGATACGGGTTA
CTGATGATGAACATGCCCGGTTACTGGAACGTTGTGAGGGTAAACAACTGGCGGTATGGATGCG
GCGGGACCAGAGAAAAATCACTCAGGGTCAATGCCAGCGCTTCGTTAATACAGATGTAGGTGTT
CCACAGGGTAGCCAGCAGCATCCTGCGATGCAGATCCGGAACATAATGGTGCAGGGCGCTGACT
TCCGCGTTTCCAGACTTTACGAAACACGGAAACCGAAGACCATTCATGTTGTTGCTCAGGTCGC
AGACGTTTTGCAGCAGCAGTCGCTTCACGTTCGCTCGCGTATCGGTGATTCATTCTGCTAACCA
GTAAGGCAACCCCGCCAGCCTAGCCGGGTCCTCAACGACAGGAGCACGATCATGCGCACCCGTG
GCCAGGACCCAACGCTGCCCGAAATT

7.1.8. Primer Library

Primer name	Primer sequence
pNIC_Adhiron_FWD	TTAAGAAGGAGATATACTATGGGTGGTAACGAAAACTCCCTGGAAATC
pNIC_Adhiron_REV	GATTGGAAGTAGAGGTTCTCTGCGTCACCAACCGGTTTGAACTCC
pET11-Adhiron_forward	TTC TGG CGT TTT CTG CGT CTG C
pET11-Adhiron_rev	TAC CCT AGT GGT GAT GAT GGT GAT GC
pDHis_Cys_C-term_rev	TTA CTA ATG CGG CCG CAC AAG CGT CAC CAA CCG GTT TG
CTB_H13R_fwd	GCG TAT ATA TTT GTG TGT TGC GGT ATT CTG CGC ACA AAT C
CTB_H13R_rev	GAT TTG TGC GCA GAA TAC CGC AAC ACA CAA ATA TAT ACG C
CTB_F25L_rev	AGCGATTCTGTATACGATAAGATCTTATCATTTAGCGTATATATTTGTG
CTB_F25L_fwd	CACAAATATATACGCTAAATGATAAGATCTTATCGTATACAGAATCGCT
CTB_N44S_rev	CTTGAAAAATTGCACCACTCTTAAAAGTAATGATAGCCATCTCTCTTTTTC
CTB_N44S_fwd	GAAAAAGAGAGATGGCTATCATTACTTTTAAGAGTGGTGCAATTTTTCAAG
CTB_A80T_rev	TACACATAACTTTTCGACTTTAGTTTCAGTAAGATATGCAATCCTCA
CTB_A80T_fwd	TGAGGATTGCATATCTTACTGAAACTAAAGTCGAAAAGTTATGTGTA
CTB_E83D_rev	GTTTTATTATTCCATACACATAACTTATCGACTTTAGCTTCAGTAAGATATGC
CTB_E83D_fwd	GCATATCTTACTGAAGCTAAAGTCGATAAGTTATGTGTATGGAATAATAAAAC
CTB_A103E_rev	GCAGGGAAAACTTAGTTTTCCATACTAATTGCGGCGA
CTB_A103E_fwd	TCGCCGCAATTAGTATGGAAAACTAAGTTTTCCCTGC
CTHF-Ad_fwd	TTA AGA AGG AGA TAT ACT ATG GCT AGC GCC GCT ACC
CTHF-Ad_rev	GAT TGG AAG TAG AGG TTC TCT GCG GCC GCA GCG TCA CCA AC
eGFP-BamHI_fwd	GCA GAA GAA CGG ATC CAT GGG CAA AGT GAG CAA GG
eGFP-HindIII_rev	GTT CTT CTG CAA GCT TCT ACT TGT ACA GCT CGT CC
Del_tga-AdGFP-fwd	GGA TGA CGA CGA TAA GGG ATC CAT GGG CAA AG
Del_tga-AdGFP-rev	CTT TGC CCA TGG ATC CCT TAT CGT CGT CAT CC
NheI_Ad-CTHF_fwd	AGG AGA TAT ACT ATG GCT AGC
NcoI_Ad-CTHF_rev	AGC CAT CCA TGG ATC CCT TAT CGT CGT CAT CCT TG

Table 7.1. Table of primers, showing their names and DNA sequences. Additional information on each primer is provided in Table 7.2.

Primer name	Additional Info
M13-26 Rev	For sequencing Affimer CDS from pBSTG phagemid
pNIC_Adhiron_FWD	For subcloning truncated Affimer constructs into pNIC-CTHF by ligation independent cloning to give a diglycine stretch at the N-terminus, with C-term His tag/Flag tag, preceded by a TEV protease site
pNIC_Adhiron_REV	
pET11-Adhiron_forward	For subcloning Affimer CDS from pBSTG into pET11c with a C-terminal polyhistidine tag. Affimer CDS is amplified by PCR to produce a linear fragment to be ligated into digested pET11c using restriction sites NheI and NotI
pET11-Adhiron_rev	
pDHis_Cys_C-term_rev	For subcloning Affimer CDS from pBSTG into pET11c with a C-terminal cysteine followed by a polyhistidine tag (NheI and NotI)
CTB_H13R_fwd	For introducing various mutations into the CTB gene in pSAB2.2 by Quikchange site-directed mutagenesis
CTB_H13R_rev	
CTB_F25L_rev	
CTB_F25L_fwd	
CTB_N44S_rev	
CTB_N44S_fwd	
CTB_A80T_rev	
CTB_A80T_fwd	
CTB_E83D_rev	
CTB_E83D_fwd	
CTB_A103E_rev	
CTB_A103E_fwd	
CTHF-Ad_fwd	Primers for subcloning full-length Affimer into pNIC-CTHF by ligation independent cloning
CTHF-Ad_rev	
eGFP-BamHI_fwd	For producing a linear fragment of eGFP DNA with flanking BamHI and HindIII restriction sites. Digested DNA can be ligated into pNIC-CTHF-Affimer similarly digested.
eGFP-HindIII_rev	
Del_tga-AdGFP-fwd	For removing the stop codon in between the Affimer CDS and subcloned GFP by SDM (Quikchange)
Del_tga-AdGFP-rev	
NheI_Ad-CTHF_fwd	For subcloning Affimers into pNIC-CTHF-Affimer-GFP using the restriction sites NheI and NcoI
NcoI_Ad-CTHF_rev	

Table 7.2. Additional cloning information for the primer sequences provided in Table 7.1.

7.2. Protein Sequences

7.2.1. CTB/LTB protein sequences

Protein sequences for LTBh, LTBh T80A, El Tor CTB, and CTB A80T. Highlighted in light green is residue T80.

```
LTBh (H74-114)      APQSITELCS  EYHNTQIYTI  NDKILSYTES  MAGKREMVII
LTBh T80A           APQSITELCS  EYHNTQIYTI  NDKILSYTES  MAGKREMVII
CTB (El Tor)        TPQNITDLCA  EYHNTQIYTL  NDKIFSYTES  LAGKREMAII
CTB A80T            TPQNITDLCA  EYHNTQIYTL  NDKIFSYTES  LAGKREMAII

LTBh (H74-114)      TFKSGATFQV  EVPGSQHIDS  QKKAIERMKD  TLRITYLTET
LTBh T80A           TFKSGATFQV  EVPGSQHIDS  QKKAIERMKD  TLRITYLTEA
CTB (El Tor)        TFKNGAIFQV  EVPGSQHIDS  QKKAIERMKD  TLRIAYLTEA
CTB A80T            TFKNGAIFQV  EVPGSQHIDS  QKKAIERMKD  TLRIAYLTET

LTBh (H74-114)      KIDKLCVWNN  KTPNSIAAIS  MEN
LTBh T80A           KIDKLCVWNN  KTPNSIAAIS  MEN
CTB (El Tor)        KVEKLCVWNN  KTPHAIAAIS  MAN
CTB A80T            KVEKLCVWNN  KTPHAIAAIS  MAN
```

7.2.2. Syb-AB_5 protein sequences

Primary sequence for MBP is shown in purple, amino acids 3 – 84 of synaptobrevin from *Rattus norvegicus*, and the truncated CTA2 subunit are shown in dark green, with a six residue linker (black) separating the two sequences.

```
MKIKTGARIL ALSALTTMMF SASALAKIEE GKLVIWINGD KGYNGLAEVG KKFEKDTGIK
VTVEHPDKLE EKFPQVAATG DGPDIIFWAH DRFGGYAQSG LLAEITPDKA FQDKLYPFTW
DAVRYNGKLI AYPIAVEALS LIYNKDLLPN PPKTWEEIPA LDKELKAKGK SALMFNLQEP
YFTWPLIAAD GGYAFKYENG KYDIKDVGVD NAGAKAGLTF LVDLIKNKHM NADTDYSIAE
AAFNKGETAM TINGPWAWSN IDTSKVNYGV TVLPTFKGQP SKPFVGVLSA GINAASPNKE
LAKEFLENYL LTDEGLEAVN KDKPLGAVAL KSYEEELVKD PRIAATMENA QKGEIMPNIP
QMSAFWYAVR TAVINAASGR QTVDEALKDA QTNSSSNNNN NNNNNNLGIE GRISHMSMGG
RDIVDGSENL YFQSATAATV PPAAPAGEGG PPAPPPNLTS NRRLQQTQAQ VDEVVDIMRV
NVDKVLERDQ KLSELDDRAD ALQAGASQFE TSAAKLGGNN NSSKVKRQIF SGYQSDIDTH
NRIKDEL
```

7.2.3. Affimer protein sequences

Binding loop sequences are shown in red.

7.2.3.1 Affimer 3A2 protein sequences

Affimer 3A2

```
GVGASAATGV RAVPGNENSL EIEELARFAV DEHNKKENAL LEFVRVVKAK EQQHERSHWV
DTMYYLTLEA KDGGKKKLYE AKVWVKHNQF FDYFINFKEL QEFKPVGDAA AAHHHHHHHH
```

Affimer 3A2-cys

```
GVGASAATGV RAVPGNENSL EIEELARFAV DEHNKKENAL LEFVRVVKAK EQQHERSHWV
DTMYYLTLEA KDGGKKKLYE AKVWVKHNQF FDYFINFKEL QEFKPVGDAC AAAHHHHHHH
H
```

Affimer 3A2-cys-KDEL

GVGASAATGV RAVPGNENSL EIEELARFAV DEHNKKENAL LEFVRVVKAK EQQHERSHWV DTMYYLTLEA KDGGKKKLYE AKVWVKHNQF FDYFINFKEL QEFKPVGDAC AAAHHHHHHH HKDEL

7.2.3.2. 3C6-Cys protein sequences

Affimer 3C6

ASAATGVRAV PGNENSLEIE ELARFAVDEH NKKENALLEF VRVVKAKEQM DLNAGLPRTM YYLTLEAKDG GKKKLYEAKV WVKQGLKKLK FTNFKELQEF KPVGDAAAAH HHHHHHH

Affimer 3C6-cys

ASAATGVRAV PGNENSLEIE ELARFAVDEH NKKENALLEF VRVVKAKEQM DLNAGLPRTM YYLTLEAKDG GKKKLYEAKV WVKQGLKKLK FTNFKELQEF KPVGDACAAA HHHHHHHH

Affimer 3C6-cys-KDEL

ASAATGVRAV PGNENSLEIE ELARFAVDEH NKKENALLEF VRVVKAKEQM DLNAGLPRTM YYLTLEAKDG GKKKLYEAKV WVKQGLKKLK FTNFKELQEF KPVGDACAAA HHHHHHHHKD EL

7.2.3.3. Sequence of binding loops of Affimers from Screen 3

	Variable loop 1									Variable loop 2									
3A2	Q	H	E	R	S	H	W	V	D	H	N	Q	F	F	D	Y	F	I	
3B1	P	D	M	G	T	V	K	Q	H	S	F	K	T	I	G	K	L	F	
3B2	S	P	L	H	V	D	M	S	Q	A	L	Y	M	G	S	W	H	V	R
3B3	V	D	E	A	E	Y	T	Q	S	N	R	L	L	H	K	Y	F	P	
3B11	P	P	D	S	T	E	Q	Q	R	K	W	P	G	K	F	N	K	Y	
3C6	M	D	L	N	A	G	L	P	R	Q	G	L	K	K	L	K	F	T	
3D3	E	F	S	S	S	R	R	V	K	G	L	S	T	I	G	K	I	L	
3D7	P	L	E	T	T	A	G	H	K	S	Y	F	R	S	R	K	E	L	
3E7	V	W	D	L	H	F	H	K	G	S	K	F	P	A	K	L	P	W	
3E12	V	D	Q	K	P	P	A	R	M	K	N	F	W	F	P	S	Q	N	
3F4	W	T	E	H	G	Q	I	V	E	R	N	A	I	R	A	M	A	F	
3F5	Q	Q	P	P	R	Q	F	N	E	Y	M	R	K	L	P	N	L	F	
3F6	A	S	A	A	A	A	V	Y	S	V	P	K	I	F	Q	K	K	F	
3F7	W	S	Q	P	M	G	F	P	E	K	N	L	L	K	A	F	G	M	
3F8	T	L	Y	P	S	S	G	Q	H	Y	P	F	P	Q	S	L	R	I	
3F10	Q	D	Q	T	S	N	L	A	P	G	P	K	F	F	N	N	M	R	
3G2	V	N	F	V	G	P	S	Q	G	G	A	K	V	Y	Q	Y	F	K	
3H4	Q	N	T	D	Q	R	V	E	R	S	W	K	Y	I	G	N	K	W	
3H11	S	E	L	H	-	V	T	G	F	N	G	R	F	L	K	F	F	P	

Figure 7.8. Primary sequences of the binding loops of Affimers sequenced in screen 3.

	Amino Acid				
Acidic	D	E			
Hydrophobic	A	G	I	L	V
Amido	N	Q			
Aromatic	F	W	Y		
Basic	R	H	K		
Hydroxyl	S	T			
Proline	P				
Sulfur	C	M			

Figure 7.9. Table of amino acids colour-coded according to their sidechain.

7.2.2.4. Various figures

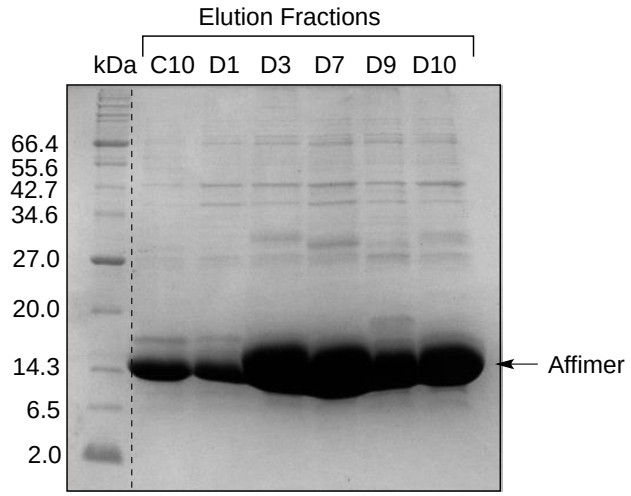

Figure 7.10. SDS-PAGE analysis of Affimers from screen 3 (C10 – D10).

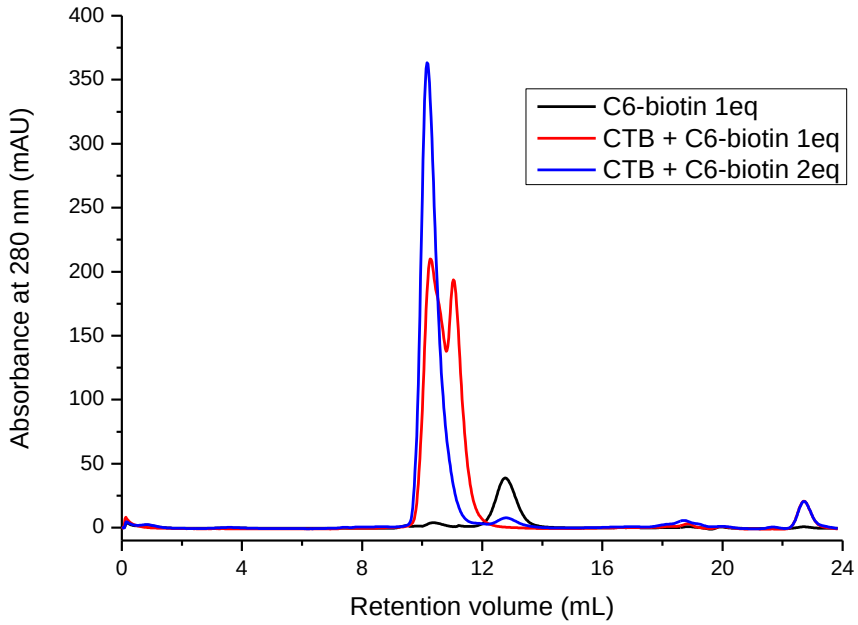

Figure 7.11. Overlay of chromatograms generated following analysis of C6-biotin:CTB complex formation.

Complex formation was assessed using one or two equivalents of C6-biotin with CTB. One equivalent of C6-biotin in the absence of CTB was also analysed by size exclusion chromatography as a control (black).

7.3. Isothermal Titration Calorimetry

7.3.1. Titration of CTB into Affimer 3C6

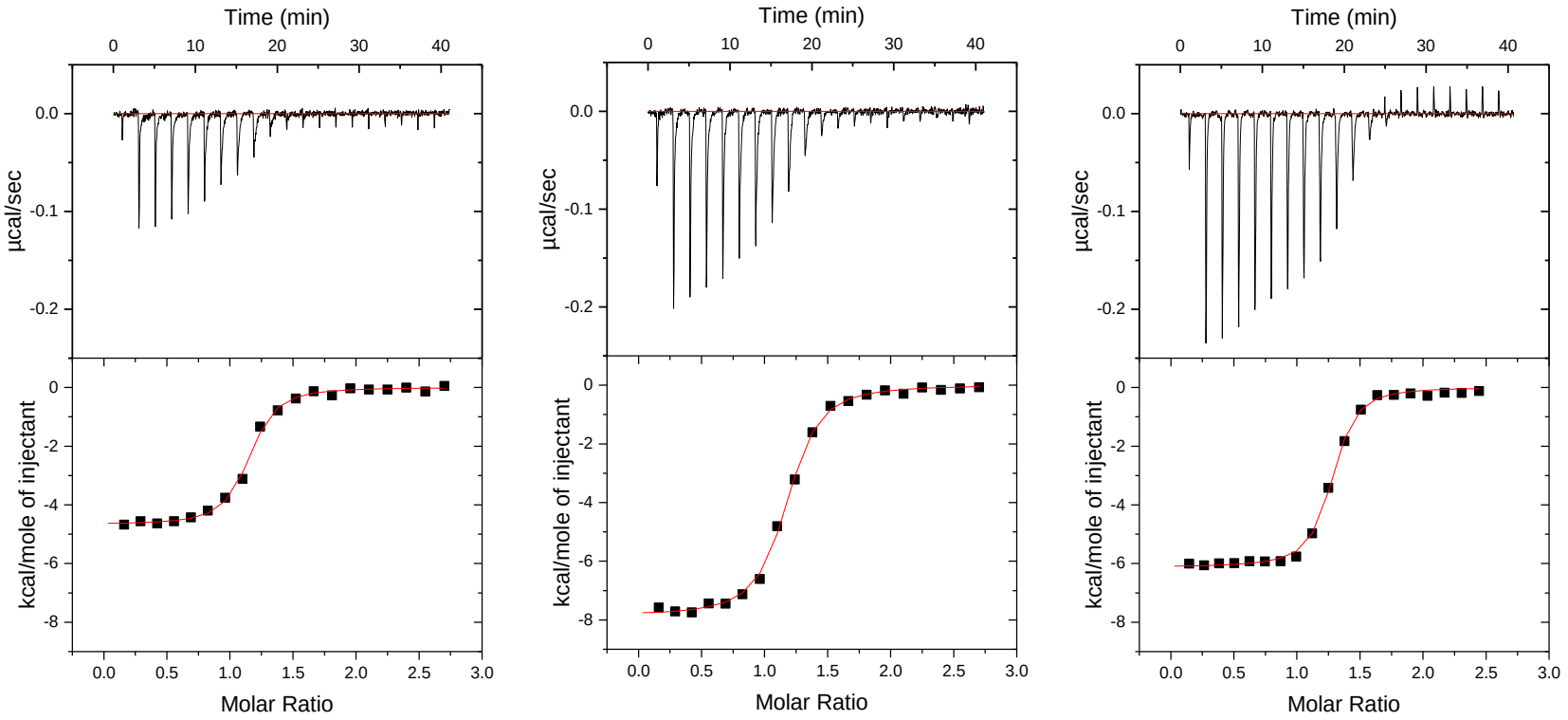

Figure 7.12. Binding isotherms generated following the titration of CTB into Affimer 3C6. Left – Titration of 100 µM CTB into 10 µM 3C6 at 25°C. Middle – Titration of 100 µM CTB into 10 µM 3C6 at 35°C Right – Titration of 200 µM CTB into 20 µM 3C6 at 35°C.

7.3.2. Titration of CTB into Affimer 3A2

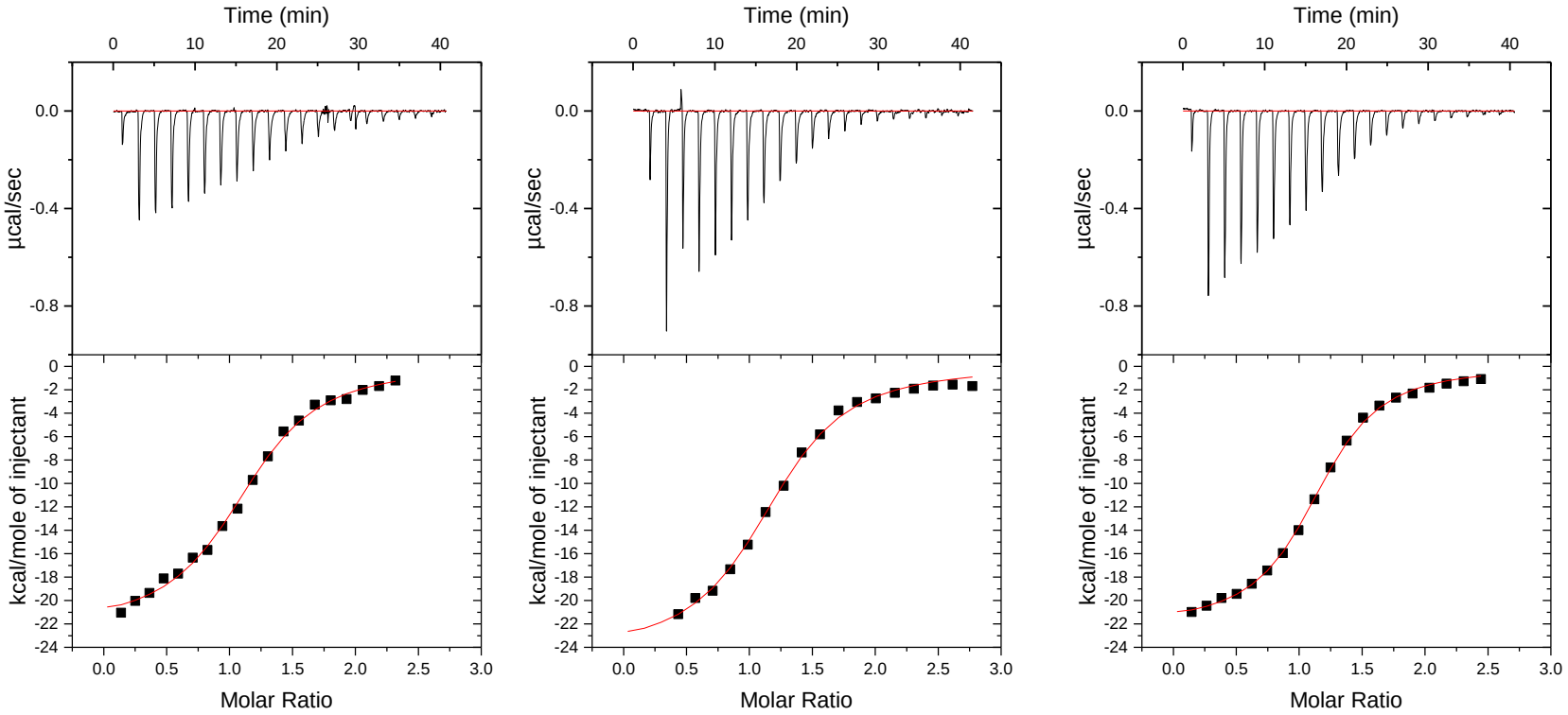

Figure 7.13. Binding isotherms generated following the titration of 150 µM CTB into 15 µM Affimer 3A2 at 35°C.

8. References

[1] B. Leader, Q. J. Baca, D. E. Golan, *Nat. Rev. Drug Discov.* **2008**, *7*, 21–39.

[2] D. M. Ecker, S. D. Jones, H. L. Levine, *MAbs* **2015**, *7*, 9–14.

[3] "Top 5 Highest-Selling Drugs of 2016," can be found under http://www.ajpb.com/news/top-5-highestselling-drugs-of-2016, **n.d.**

[4] D. B. Thompson, R. Villaseñor, B. M. Dorr, M. Zerial, D. R. Liu, *Chem. Biol.* **2012**, *19*, 831–843.

[5] S. Miersch, S. S. Sidhu, *F1000Research* **2016**, *5*, 1947.

[6] X. Fan, W. Y. Jin, J. Lu, J. Wang, Y. T. Wang, *Nat. Neurosci.* **2014**, *17*, 471–80.

[7] M. C. Morris, J. Depollier, J. Mery, F. Heitz, G. Divita, *Nat. Biotechnol.* **2001**, *19*, 1173–1176.

[8] A. Lalatsa, A. G. Schatzlein, I. F. Uchegbu, *Mol. Pharm.* **2014**, *11*, 1081–93.

[9] N. J. Abbott, *J. Inherit. Metab. Dis.* **2013**, *36*, 437–449.

[10] W. A. Banks, *Nat. Rev. Drug Discov.* **2016**, *15*, 275–292.

[11] W. A. Banks, S. A. Farr, W. Butt, V. B. Kumar, M. W. Franko, J. E. Morley, *J. Pharmacol. Exp. Ther.* **2001**, *297*, 1113–21.

[12] J. Hardy, D. J. Selkoe, *Science* **2002**, *297*, 353–6.

[13] V. B. Kumar, S. A. Farr, J. F. Flood, V. Kamlesh, M. Franko, W. A. Banks, J. E. Morley, *Peptides* **2000**, *21*, 1769–1775.

[14] J. Georgieva, D. Hoekstra, I. Zuhorn, *Pharmaceutics* **2014**, *6*, 557–583.

[15] Z. M. Qian, H. Li, H. Sun, K. Ho, *Pharmacol. Rev.* **2002**, *54*, 561–87.

[16] P. Aisen, *Ann. Neurol.* **1992**, *32 Suppl*, S62-8.

[17] N. J. Abbott, L. Rönnbäck, E. Hansson, *Nat. Rev. Neurosci.* **2006**, *7*, 41–53.

[18] K. Ulbrich, T. Hekmatara, E. Herbert, J. Kreuter, *Eur. J. Pharm. Biopharm.* **2009**, *71*, 251–256.

[19] Z. Pang, W. Lu, H. Gao, K. Hu, J. Chen, C. Zhang, X. Gao, X. Jiang, C. Zhu, *J. Control. Release* **2008**, *128*, 120–127.

[20] H. Bao, X. Jin, L. Li, F. Lv, T. Liu, *J. Mater. Sci. Mater. Med.* **2012**, *23*, 1891–1901.

[21] Y. Aktaş, M. Yemisci, K. Andrieux, R. N. Gürsoy, M. J. Alonso, E. Fernandez-Megia, R. Novoa-Carballal, E. Quiñoá, R. Riguera, M. F. Sargon, et al., *Bioconjug. Chem.* **2005**, *16*, 1503–1511.

[22] S. Gosk, C. Vermehren, G. Storm, T. Moos, *J. Cereb. Blood Flow Metab.* **2004**, *24*, 1193–1204.

[23] R. J. Boado, H. Tsukamoto, W. M. Pardridge, *J. Pharm. Sci.* **1998**, *87*, 1308–1315.

[24] B. Zhang, X. Sun, H. Mei, Y. Wang, Z. Liao, J. Chen, Q. Zhang, Y. Hu, Z. Pang, X. Jiang, *Biomaterials* **2013**, *34*, 9171–9182.

[25] M. Mousazadeh, A. Palizban, R. Salehi, M. Salehi, *J. Drug Target.* **2007**, *15*, 226–230.

[26] H. R. Kim, S. Gil, K. Andrieux, V. Nicolas, M. Appel, H. Chacun, D. Desmaële, F. Taran, D. Georgin, P. Couvreur, *Cell. Mol. Life Sci.* **2007**, *64*, 356–364.

[27] B. Liou, A. Kazimierczuk, M. Zhang, C. R. Scott, R. S. Hegde, G. a. Grabowski, *J. Biol. Chem.* **2006**, *281*, 4242–4253.

[28] Y. Shaaltiel, D. Bartfeld, S. Hashmueli, G. Baum, E. Brill-Almon, G. Galili, O. Dym, S. a. Boldin-Adamsky, I. Silman, J. L. Sussman, et al., *Plant Biotechnol. J.* **2007**, *5*, 579–590.

[29] B. J. Spencer, I. M. Verma, *Proc. Natl. Acad. Sci. U. S. A.* **2007**, *104*, 7594–9.

[30] B. Engelhardt, R. M. Ransohoff, *Trends Immunol.* **2012**, *33*, 579–589.

[31] B. Engelhardt, *J. Neural Transm.* **2006**, *113*, 477–485.

[32] N. Doshi, A. J. Swiston, J. B. Gilbert, M. L. Alcaraz, R. E. Cohen, M. F. Rubner, S. Mitragotri, *Adv. Mater.* **2011**, *23*, H105–H109.

[33] N. L. Klyachko, R. Polak, M. J. Haney, Y. Zhao, R. J. Gomes Neto, M. C. Hill, A. V. Kabanov, R. E. Cohen, M. F. Rubner, E. V. Batrakova, *Biomaterials* **2017**, *140*, 79–87.

[34] D. L. Sellers, J. M. Bergen, R. N. Johnson, H. Back, J. M. Ravits, P. J. Horner, S. H. Pun, *Proc. Natl. Acad. Sci. U. S. A.* **2016**, *113*, 2514–2519.

[35] Y. Fujinaga, *J. Biochem.* **2006**, *140*, 155–160.

[36] K. A. Sheikh, T. J. Deerinck, M. H. Ellisman, J. W. Griffin, *Brain* **1999**, *122 (Pt 3)*, 449–60.

[37] K. Ogawa-Goto, N. Funamoto, Y. Ohta, T. Abe, K. Nagashima, *J. Neurochem.* **1992**, *59*, 1844–9.

[38] R. W. Ledeen, G. Wu, Z. H. Lu, D. Kozireski-Chuback, Y. Fang, *Ann. N. Y. Acad. Sci.* **1998**, *845*, 161–175.

[39] B. Hazes, R. J. Read, *Biochemistry* **1997**, *36*, 11051–4.

[40] M. R. Popoff, B. Poulain, *Toxins (Basel).* **2010**, *2*, 683–737.

[41] L. L. Simpson, *Pharmacol. Rev.* **1981**, *33*.

[42] G. Schiavo, M. Matteoli, C. Montecucco, *Physiol. Rev.* **2000**, *80*, 717–66.

[43] S. S. Arnon, R. Schechter, T. V. Inglesby, D. A. Henderson, J. G. Bartlett, M. S. Ascher, E. Eitzen, A. D. Fine, J. Hauer, M. Layton, et al., *JAMA* **2001**, *285*, 1059.

[44] T. J. Smith, J. Lou, I. N. Geren, C. M. Forsyth, R. Tsai, S. L. LaPorte, W. H. Tepp, M. Bradshaw, E. A. Johnson, L. A. Smith, et al., *Infect. Immun.* **2005**, *73*, 5450–5457.

[45] D. Dressler, F. A. Saberi, E. R. Barbosa, *Arq. Neuropsiquiatr.* **2005**, *63*, 180–185.

[46] R. P.-A. Berntsson, L. Peng, M. Dong, P. Stenmark, *Nat. Commun.* **2013**, *4*, 2058.

[47] P. Stenmark, J. Dupuy, A. Imamura, M. Kiso, R. C. Stevens, *PLoS Pathog.* **2008**, *4*, e1000129.

[48] M. R. Baldwin, J.-J. P. Kim, J. T. Barbieri, *Nat. Struct. Mol. Biol.* **2007**, *14*, 9–10.

[49] F. L. Yeh, M. Dong, J. Yao, W. H. Tepp, G. Lin, E. A. Johnson, E. R. Chapman, *PLoS Pathog.* **2010**, *6*, e1001207.

[50] L. L. Simpson, *J. Pharmacol. Exp. Ther.* **1983**, *225*, 546–52.

[51] J. E. Keller, F. Cai, E. A. Neale, *Biochemistry* **2004**, *43*, 526–532.

[52] A. Fischer, C. Garcia-Rodriguez, I. Geren, J. Lou, J. D. Marks, T. Nakagawa, M. Montal, *J. Biol. Chem.* **2008**, *283*, 3997–4003.

[53] L. K. Koriazova, M. Montal, *Nat. Struct. Biol.* **2003**, *10*, 13–18.

[54] C. Montecucco, J. Molgó, *Curr. Opin. Pharmacol.* **2005**, *5*, 274–279.

[55] G. Masuyer, J. Conrad, P. Stenmark, *EMBO Rep.* **2017**, *18*, 1306–1317.

[56] M. Pirazzini, F. Bordin, O. Rossetto, C. C. Shone, T. Binz, C. Montecucco, *FEBS Lett.* **2013**, *587*, 150–155.

[57] S. Bade, A. Rummel, C. Reisinger, T. Karnath, G. Ahnert-Hilger, H. Bigalke, T. Binz, *J. Neurochem.* **2004**, *91*, 1461–1472.

[58] M. Pirazzini, D. A. Tehran, O. Leka, G. Zanetti, O. Rossetto, C. Montecucco, *Biochim. Biophys. Acta - Biomembr.* **2016**, *1858*, 467–474.

[59] Y. A. Chen, R. H. Scheller, *Nat. Rev. Mol. Cell Biol.* **2001**, *2*, 98–106.

[60] H. Niemann, J. Blasi, R. Jahn, *Trends Cell Biol.* **1994**, *4*, 179–85.

[61] T. Söllner, S. W. Whiteheart, M. Brunner, H. Erdjument-Bromage, S. Geromanos, P. Tempst, J. E. Rothman, *Nature* **1993**, *362*, 318–324.

[62] D. Fasshauer, R. B. Sutton, A. T. Brunger, R. Jahn, *Proc. Natl. Acad. Sci. U. S. A.* **1998**, *95*, 15781–6.

[63] T. Weimbs, S. H. Low, S. J. Chapin, K. E. Mostov, P. Bucher, K. Hofmann, *Proc. Natl. Acad. Sci. U. S. A.* **1997**, *94*, 3046–51.

[64] J. M. Cánaves, M. Montal, *J. Biol. Chem.* **1998**, *273*, 34214–21.

[65] M. A. Poirier, W. Xiao, J. C. Macosko, C. Chan, Y.-K. Shin, M. K. Bennett, *Nat. Struct. Biol.* **1998**, *5*, 765–769.

[66] W. S. Trimble, D. M. Cowan, R. H. Scheller, *Proc. Natl. Acad. Sci. U. S. A.* **1988**, *85*, 4538–42.

[67] M. K. Bennett, N. Calakos, R. H. Scheller, *Science* **1992**, *257*, 255–9.

[68] I. Fernandez, J. Ubach, I. Dulubova, X. Zhang, T. C. Südhof, J. Rizo, *Cell* **1998**, *94*, 841–9.

[69] G. A. Oyler, G. A. Higgins, R. A. Hart, E. Battenberg, M. Billingsley, F. E. Bloom,

M. C. Wilson, *J. Cell Biol.* **1989**, *109*, 3039–52.

[70] S. R. Lane, Y. Liu, *J. Neurochem.* **1997**, *69*, 1864–9.

[71] S. Gonzalo, M. E. Linder, *Mol. Biol. Cell* **1998**, *9*, 585–97.

[72] R. C. Lin, R. H. Scheller, *Neuron* **1997**, *19*, 1087–1094.

[73] G. van den Bogaart, M. G. Holt, G. Bunt, D. Riedel, F. S. Wouters, R. Jahn, *Nat. Struct. Mol. Biol.* **2010**, *17*, 358–364.

[74] R. Sinha, S. Ahmed, R. Jahn, J. Klingauf, *Proc. Natl. Acad. Sci. U. S. A.* **2011**, *108*, 14318–23.

[75] L. L. Simpson, *Annu. Rev. Pharmacol. Toxicol.* **2004**, *44*, 167–193.

[76] V. V Vaidyanathan, K. I. Yoshino, M. Jahnz, C. Dörries, S. Bade, S. Nauenburg, H. Niemann, T. Binz, *J. Neurochem.* **1999**, *72*, 327–337.

[77] R. Jahn, T. Lang, T. C. Südhof, *Cell* **2003**, *112*, 519–33.

[78] J. Mellanby, P. A. Thompson, N. Hampden, *Naunyn. Schmiedebergs. Arch. Pharmacol.* **1973**, *276*, 303–310.

[79] A. Carruthers, J. Carruthers, *Dermatologic Surg.* **1998**, *24*, 1168–1171.

[80] A. B. Scott, *Dermatol. Clin.* **2004**, *22*, 131–3, v.

[81] W. S. Sim, *Korean J. Pain* **2011**, *24*, 1.

[82] M. Ho, L.-H. Chang, M. Pires-Alves, B. Thyagarajan, J. E. Bloom, Z. Gu, K. K. Aberle, S. A. Teymorian, Y. Bannai, S. C. Johnson, et al., *Protein Eng. Des. Sel.* **2011**, *24*, 247–253.

[83] B. Davletov, M. Bajohrs, T. Binz, *Trends Neurosci.* **2005**, *28*, 446–452.

[84] K. Turton, J. A. Chaddock, K. R. Acharya, *Trends Biochem. Sci.* **2002**, *27*, 552–8.

[85] A. Rummel, S. Mahrhold, H. Bigalke, T. Binz, *Mol. Microbiol.* **2004**, *51*, 631–43.

[86] U. Eisel, W. Jarausch, K. Goretzki, A. Henschen, J. Engels, U. Weller, M. Hudel, E. Habermann, H. Niemann, *EMBO J.* **1986**, *5*, 2495–502.

[87] G. Lalli, S. Bohnert, K. Deinhardt, C. Verastegui, G. Schiavo, *Trends Microbiol.* **2003**, *11*, 431–7.

[88] C. Chen, Z. Fu, J.-J. P. Kim, J. T. Barbieri, M. R. Baldwin, *J. Biol. Chem.* **2009**, *284*, 26569–26577.

[89] P. Munro, H. Kojima, J.-L. Dupont, J.-L. Bossu, B. Poulain, P. Boquet, *Biochem. Biophys. Res. Commun.* **2001**, *289*, 623–629.

[90] J. B. Cabot, A. Mennone, N. Bogan, J. Carroll, C. Evinger, J. T. Erichsen, *Neuroscience* **1991**, *40*, 805–23.

[91] C. Evinger, J. T. Erichsen, *Brain Res.* **1986**, *380*, 383–8.

[92] M. E. Schwab, K. Suda, H. Thoenen, *J. Cell Biol.* **1979**, *82*, 798–810.

[93] C. Montecucco, G. Schiavo, *Mol. Microbiol.* **1994**, *13*, 1–8.

[94] C. Verderio, S. Coco, A. Bacci, O. Rossetto, P. De Camilli, C. Montecucco, M. Matteoli, *J. Neurosci.* **1999**, *19*, 6723–32.

[95] E. Link, L. Edelmann, J. H. Chou, T. Binz, S. Yamasaki, U. Eisel, M. Baumert, T. C. Südhof, H. Niemann, R. Jahn, *Biochem. Biophys. Res. Commun.* **1992**, *189*, 1017–23.

[96] M. E. Pichichero, *Hum. Vaccin. Immunother.* **2013**, *9*, 2505–23.

[97] C. Pan, P. Sun, B. Liu, H. Liang, Z. Peng, Y. Dong, D. Wang, X. Liu, B. Wang, M. Zeng, et al., *MBio* **2016**, *7*, e00443-16.

[98] J. W. Francis, E. Bastia, C. C. Matthews, D. a. Parks, M. a. Schwarzschild, R. H. Brown, P. S. Fishman, *Brain Res.* **2004**, *1011*, 7–13.

[99] K. Dobrenis, a Joseph, M. C. Rattazzi, *Proc. Natl. Acad. Sci. U. S. A.* **1992**, *89*, 2297–2301.

[100] S. A. Townsend, G. D. Evrony, F. X. Gu, M. P. Schulz, R. H. Brown, R. Langer, *Biomaterials* **2007**, *28*, 5176–5184.

[101] E. L. Bearer, X. O. Breakefield, D. Schuback, T. S. Reese, J. H. LaVail, *Proc. Natl. Acad. Sci. U. S. A.* **2000**, *97*, 8146–50.

[102] J. K. Liu, Q. Teng, M. Garrity-Moses, T. Federici, D. Tanase, M. J. Imperiale, N. M. Boulis, *Neurobiol. Dis.* **2005**, *19*, 407–418.

[103] J. V. Georgieva, R. P. Brinkhuis, K. Stojanov, C. A. G. M. Weijers, H. Zuilhof, F. P. J. T. Rutjes, D. Hoekstra, J. C. M. van Hest, I. S. Zuhorn, *Angew. Chemie Int. Ed.* **2012**, *51*, 8339–8342.

[104] Y. Zhang, W. Zhang, A. H. Johnston, T. A. Newman, I. Pyykkö, J. Zou, *Int. J. Nanomedicine* **2012**, *7*, 1015–22.

[105] I.-K. Park, J. Lasiene, S.-H. Chou, P. J. Horner, S. H. Pun, *J. Gene Med.* **2007**, *9*, 691–702.

[106] E. A. Merritt, W. G. Hol, *Curr. Opin. Struct. Biol.* **1995**, *5*, 165–171.

[107] S. Mukhopadhyay, A. D. Linstedt, *J. Mol. Med. (Berl).* **2013**, *91*, 1131–41.

[108] T. Beddoe, A. W. Paton, J. Le Nours, J. Rossjohn, J. C. Paton, *Trends Biochem. Sci.* **2010**, *35*, 411–418.

[109] E. A. Merritt, W. G. Hol, *Curr. Opin. Struct. Biol.* **1995**, *5*, 165–71.

[110] T. K. Sixma, P. E. Stein, W. G. J. Hol, R. J. Read, *Biochemistry* **1993**, *32*, 191–198.

[111] W. N. Burnette, *Behring Inst. Mitt.* **1997**, 434–41.

[112] M. Tamura, K. Nogimori, S. Murai, M. Yajima, K. Ito, T. Katada, M. Ui, S. Ishii, *Biochemistry* **1982**, *21*, 5516–5522.

[113] W. N. Burnette, *Structure* **1994**, *2*, 151–8.

[114] K. Sandvig, B. van Deurs, *Gene Ther.* **2005**, *12*, 865–872.

[115] B. D. Spangler, *Microbiol. Rev.* **1992**, *56*, 622–47.

[116] J. Holmgren, P. Fredman, M. Lindblad, A. M. Svennerholm, L. Svennerholm, *Infect. Immun.* **1982**, *38*, 424–33.

[117] S. Fukuta, J. L. Magnani, E. M. Twiddy, R. K. Holmes, V. Ginsburg, *Infect. Immun.* **1988**, *56*, 1748–53.

[118] M. E. Fraser, M. Fujinaga, M. M. Cherney, A. R. Melton-Celsa, E. M. Twiddy, A. D. O'Brien, M. N. G. James, *J. Biol. Chem.* **2004**, *279*, 27511–7.

[119] P. E. Stein, A. Boodhoo, G. D. Armstrong, S. A. Cockle, M. H. Klein, R. J. Read, *Structure* **1994**, *2*, 45–57.

[120] F. van den Akker, S. Sarfaty, E. M. Twiddy, T. D. Connell, R. K. Holmes, W. G. Hol, *Structure* **1996**, *4*, 665–678.

[121] R. G. Zhang, D. L. Scott, M. L. Westbrook, S. Nance, B. D. Spangler, G. G. Shipley, E. M. Westbrook, *J. Mol. Biol.* **1995**, *251*, 563–573.

[122] C. Chen, A. Przedpelski, W. H. Tepp, S. Pellett, E. A. Johnson, J. T. Barbieri, *MBio* **2015**, *6*, 4–11.

[123] N. M. Ng, D. R. Littler, A. W. Paton, J. Le Nours, J. Rossjohn, J. C. Paton, T. Beddoe, *Structure* **2013**, *21*, 2003–2013.

[124] W. Y. Chung, R. Carter, T. Hardy, M. Sack, T. R. Hirst, R. F. L. James, *J. Biol. Chem.* **2006**, *281*, 39465–39470.

[125] B. Mudrak, M. J. Kuehn, *Toxins (Basel).* **2010**, *2*, 1445–1470.

[126] K. T. Hamorsky, J. C. Kouokam, L. J. Bennett, K. J. Baldauf, H. Kajiura, K. Fujiyama, N. Matoba, *PLoS Negl. Trop. Dis.* **2013**, *7*, e2046.

[127] J. M. Wild, *J. Comp. Neurol.* **1990**, *298*, 157–171.

[128] P. J. Dederen, A. A. Gribnau, M. H. Curfs, *Histochem. J.* **1994**, *26*, 856–62.

[129] M. Hirakawa, J. T. McCabe, M. Kawata, *Cell Tissue Res.* **1992**, *267*, 419–27.

[130] J. P. Craig, *Nature* **1965**, *207*, 614–6.

[131] R. L. Richards, J. Moss, C. R. Alving, P. H. Fishman, R. O. Brady, *Proc. Natl. Acad. Sci. U. S. A.* **1979**, *76*, 1673–6.

[132] J. J. Mekalanos, D. J. Swartz, G. D. N. Pearson, N. Harford, F. Groyne, M. de Wilde, *Nature* **1983**, *306*, 551–557.

[133] C. Y. Lai, *J. Biol. Chem.* **1977**, *252*, 7249–56.

[134] S. J. Hardy, J. Holmgren, S. Johansson, J. Sanchez, T. R. Hirst, *Proc. Natl. Acad. Sci.* **1988**, *85*, 7109–7113.

[135] S. J. Streatfield, M. Sandkvist, T. K. Sixma, M. Bagdasarian, W. G. Hol, T. R. Hirst, *Proc. Natl. Acad. Sci. U. S. A.* **1992**, *89*, 12140–4.

[136] C. F. Schierle, M. Berkmen, D. Huber, C. Kumamoto, D. Boyd, J. Beckwith, *J. Bacteriol.* **2003**, *185*, 5706–13.

[137] H. Hofstras, B. Witholt, **1984**, *259*, 15182–15187.

[138] T. R. Hirst, J. Holmgren, *Proc. Natl. Acad. Sci. U. S. A.* **1987**, *84*, 7418–7422.

[139] L. W. Ruddock, J. J. Coen, C. Cheesman, R. B. Freedman, T. R. Hirst, *J. Biol. Chem.* **1996**, *271*, 19118–23.

[140] B. T. Hovey, C. L. M. J. Verlinde, E. A. Merritt, W. G. J. Hol, *J. Mol. Biol.* **1999**, *285*, 1169–1178.

[141] J. K. Tinker, J. L. Erbe, W. G. J. Hol, R. K. Holmes, *Infect. Immun.* **2003**, *71*, 4093–101.

[142] T. R. Hirst, J. Sanchez, J. B. Kaper, S. J. Hardy, J. Holmgren, *Proc. Natl. Acad. Sci. U. S. A.* **1984**, *81*, 7752–6.

[143] Y. Takeda, T. Honda, S. Taga, T. Miwatani, *Infect. Immun.* **1981**, *34*, 341–6.

[144] E. A. Merritt, S. Sarfaty, F. Van Den Akker, C. L'Hoir, J. A. Martial, W. G. J. Hol, *Protein Sci.* **1994**, *3*, 166–175.

[145] J. K. Tinker, J. L. Erbe, W. G. J. Hol, R. K. Holmes, *Infect. Immun.* **2003**, *71*, 4093–4101.

[146] W. B. Turnbull, B. L. Precious, S. W. Homans, *J. Am. Chem. Soc.* **2004**, *126*, 1047–1054.

[147] C. A. Bewley, S. Shahzad-Ul-Hussan, *Biopolymers* **2013**, *99*, 796–806.

[148] E. A. Merritt, S. Sarfaty, F. van den Akker, C. L'Hoir, J. A. Martial, W. G. Hol, *Protein Sci.* **1994**, *3*, 166–75.

[149] T. R. Branson, T. E. McAllister, J. Garcia-Hartjes, M. A. Fascione, J. F. Ross, S. L. Warriner, T. Wennekes, H. Zuilhof, W. B. Turnbull, *Angew. Chemie - Int. Ed.* **2014**, *53*, 8323–8327.

[150] M. G. Jobling, R. K. Holmes, *Infect. Immun.* **2002**, *70*, 1260–1271.

[151] W. I. Lencer, B. Tsai, *Trends Biochem. Sci.* **2003**, *28*, 639–645.

[152] T. L. Williams, a. T. a Jenkins, *J. Am. Chem. Soc.* **2008**, *130*, 6438–6443.

[153] A. Schön, E. Freire, *Biochemistry* **1989**, *28*, 5019–24.

[154] N. C. Worstell, P. Krishnan, J. D. Weatherston, H.-J. Wu, *PLoS One* **2016**, *11*, e0153265.

[155] H. Lin, E. N. Kitova, J. S. Klassen, *J. Am. Soc. Mass Spectrom.* **2014**, *25*, 104–110.

[156] T. R. Branson, T. E. McAllister, J. Garcia-Hartjes, M. A. Fascione, J. F. Ross, S. L. Warriner, T. Wennekes, H. Zuilhof, W. B. Turnbull, *Angew. Chemie Int. Ed.* **2014**, *53*, 8323–8327.

[157] J. Garcia-Hartjes, S. Bernardi, C. A. G. M. Weijers, T. Wennekes, M. Gilbert, F. Sansone, A. Casnati, H. Zuilhof, *Org. Biomol. Chem.* **2013**, *11*, 4340–4349.

[158] W. Y. Chung, M. Sack, R. Carter, H. Spiegel, R. Fischer, T. R. Hirst, N. A.

Williams, R. F. L. James, *J. Immunol. Methods* **2008**, *339*, 115–123.

[159] C. C. Grant, R. J. Messer, W. Cieplak, Jr, *Infect. Immun.* **1994**, *62*, 4270–8.

[160] W. I. Lencer, C. Constable, S. Moe, M. G. Jobling, H. M. Webb, S. Ruston, J. L. Madara, T. R. Hirst, R. K. Holmes, *J. Cell Biol.* **1995**, *131*, 951–62.

[161] B. Tsai, C. Rodighiero, W. I. Lencer, T. A. Rapoport, *Cell* **2001**, *104*, 937–948.

[162] A. H. Pande, P. Scaglione, M. Taylor, K. N. Nemec, S. Tuthill, D. Moe, R. K. Holmes, S. A. Tatulian, K. Teter, *J. Mol. Biol.* **2007**, *374*, 1114–28.

[163] A. Winkeler, D. Gödderz, V. Herzog, A. Schmitz, *FEBS Lett.* **2003**, *554*, 439–442.

[164] W. I. Lencer, *Am J Physiol Gastrointest Liver Physiol* **2001**, *280*, G781-786.

[165] B. D. Spangler, *Microbiol. Rev.* **1992**, *56*, 622–47.

[166] W. T. Norton, S. E. Poduslo, *New York* **1971**, *12*, 84–90.

[167] R. a McIlhinney, S. J. Bacon, a D. Smith, *J. Neurosci. Methods* **1988**, *22*, 189–194.

[168] I. J. Llewellyn-Smith, J. B. Minson, A. P. Wright, A. J. Hodgson, *J. Comp. Neurol.* **1990**, *294*, 179–191.

[169] N. Zhou, Z. Hao, X. Zhao, S. Maharjan, S. Zhu, Y. Song, B. Yang, L. Lu, *Nanoscale* **2015**, *7*, 15635–15642.

[170] S. K. Chakraborty, J. A. J. Fitzpatrick, J. A. Phillippi, S. Andreko, A. S. Waggoner, M. P. Bruchez, B. Ballou, *Nano Lett.* **2007**, *7*, 2618–2626.

[171] C. W.-H. Wu, O. Vasalatiy, N. Liu, H. Wu, S. Cheal, D.-Y. Chen, A. P. Koretsky, G. L. Griffiths, R. B. H. Tootell, L. G. Ungerleider, *Neuron* **2011**, *70*, 229–243.

[172] J. M. Alisky, C. I. van de Wetering, B. L. Davidson, *Exp. Neurol.* **2002**, *178*, 139–146.

[173] R. Vazquez-Lombardi, T. G. Phan, C. Zimmermann, D. Lowe, L. Jermutus, D. Christ, *Drug Discov. Today* **2015**, *20*, 1271–1283.

[174] I. M. Tomlinson, *Nat. Biotechnol.* **2004**, *22*, 521–522.

[175] N. K. Mehta, J. R. Cochran, Wiley-VCH Verlag GmbH & Co. KGaA, **2017**, pp. 161–188.

[176] P. Chames, M. Van Regenmortel, E. Weiss, D. Baty, *Br. J. Pharmacol.* **2009**, *157*, 220–33.

[177] D. E. Steinmeyer, E. L. McCormick, *Drug Discov. Today* **2008**, *13*, 613–8.

[178] T. Wakayama, Y. Kato, R. Utsumi, A. Tsuji, S. Iseki, *Acta Histochem. Cytochem.* **2006**, *39*, 79–87.

[179] C. E. Z. Chan, A. H. Y. Chan, A. P. C. Lim, B. J. Hanson, *J. Immunol. Methods* **2011**, *373*, 79–88.

[180] C. E. Z. Chan, A. P. C. Lim, P. A. MacAry, B. J. Hanson, *Int. Immunol.* **2014**, *26*, 649–657.

[181] K. Škrlec, B. Štrukelj, A. Berlec, *Trends Biotechnol.* **2015**, DOI 10.1016/j.tibtech.2015.03.012.

[182] J. Löfblom, J. Feldwisch, V. Tolmachev, J. Carlsson, S. Ståhl, F. Y. Frejd, *FEBS Lett.* **2010**, *584*, 2670–80.

[183] A. Skerra, *Curr. Opin. Biotechnol.* **2007**, *18*, 295–304.

[184] R. Monika, *Electr. Eng.* **2013**.

[185] A. Skerra, *Curr. Opin. Biotechnol.* **2007**, *18*, 295–304.

[186] T. Hey, E. Fiedler, R. Rudolph, M. Fiedler, *Trends Biotechnol.* **2005**, *23*, 514–522.

[187] P.-Å. Nygren, *FEBS J.* **2008**, *275*, 2668–2676.

[188] B. Zuraw, U. Yasothan, P. Kirkpatrick, *Nat. Rev. Drug Discov.* **2010**, *9*, 189–90.

[189] M. S. Dennis, A. Herzka, R. A. Lazarus, *J. Biol. Chem.* **1995**, *270*, 25411–25417.

[190] F. Y. Frejd, K.-T. Kim, *Exp. Mol. Med.* **2017**, *49*, e306.

[191] A. Knappik, L. Ge, A. Honegger, P. Pack, M. Fischer, G. Wellnhofer, A. Hoess, J. Wölle, A. Plückthun, B. Virnekäs, *J. Mol. Biol.* **2000**, *296*, 57–86.

[192] R. S. Komor, P. A. Romero, C. B. Xie, F. H. Arnold, *Protein Eng. Des. Sel.* **2012**, *25*, 827–33.

[193] C. Tiede, A. A. S. Tang, S. E. Deacon, U. Mandal, J. E. Nettleship, R. L. Owen, S. E. George, D. J. Harrison, R. J. Owens, D. C. Tomlinson, et al., *Protein Eng. Des. Sel.* **2014**, *27*, 145–55.

[194] S. Arai, K. Abe, Y. Emori, Springer, Boston, MA, **1996**, pp. 73–78.

[195] C. Tiede, R. Bedford, S. J. Heseltine, G. Smith, I. Wijetunga, R. Ross, D. AlQallaf, A. P. Roberts, A. Balls, A. Curd, et al., *Elife* **2017**, *6*, DOI 10.7554/eLife.24903.

[196] R. Sharma, S. E. Deacon, D. Nowak, S. E. George, M. P. Szymonik, A. A. S. Tang, D. C. Tomlinson, A. G. Davies, M. J. McPherson, C. Wälti, *Biosens. Bioelectron.* **2016**, *80*, 607–613.

[197] G. Smith, *Science (80-.).* **1985**, *228*, 1315–1317.

[198] L. Riechmann, P. Holliger, *Cell* **1997**, *90*, 351–360.

[199] L. W. Deng, P. Malik, R. N. Perham, *Virology* **1999**, *253*, 271–7.

[200] J. Lubkowski, F. Hennecke, A. Plückthun, A. Wlodawer, *Structure* **1999**, *7*, 711–22.

[201] J. Vieira, J. Messing, *Recombinant DNA Part D*, Elsevier, **1987**.

[202] M. Russel, P. Model, *Cell* **1982**, *28*, 177–84.

[203] C. H. M. Papavoine, B. E. C. Christiaans, R. H. A. Folmer, R. N. H. Konings, C. W. Hilbers, *J. Mol. Biol.* **1998**, *282*, 401–419.

[204] S. S. Sidhu, *Phage Display in Biotechnology and Drug Discovery*, CRC Press/Taylor & Francis, **2005**.

[205] G. Å. Løset, N. Roos, B. Bogen, I. Sandlie, *PLoS One* **2011**, *6*, e17433.

[206] T. Clackson, H. B. Lowman, *Phage Display: A Practical Approach*, OUP Oxford, **2004**.

[207] M. Russel, P. Model, *J. Virol.* **1989**, *63*, 3284–95.

[208] D. Steiner, P. Forrer, M. T. Stumpp, A. Plückthun, *Nat. Biotechnol.* **2006**, *24*, 823–31.

[209] C. W. Gray, R. S. Brown, D. A. Marvin, *J. Mol. Biol.* **1981**, *146*, 621–627.

[210] M. A. Gonzalez Porras, P. N. Durfee, A. M. Gregory, G. C. Sieck, C. J. Brinker, C. B. Mantilla, *J. Neurosci. Methods* **2016**, *273*, 160–174.

[211] C. P. Guimaraes, M. D. Witte, C. S. Theile, G. Bozkurt, L. Kundrat, A. E. M. Blom, H. L. Ploegh, *Nat. Protoc.* **2013**, *8*, 1787–99.

[212] A. T. Aman, S. Fraser, E. A. Merritt, C. Rodigherio, M. Kenny, M. Ahn, W. G. Hol, N. A. Williams, W. I. Lencer, T. R. Hirst, *Proc. Natl. Acad. Sci. U. S. A.* **2001**, *98*, 8536–41.

[213] R. Leece, T. R. Hirst, *J. Gen. Microbiol.* **1992**, *138*, 719–724.

[214] E. A. Merritt, S. Sarfaty, M. G. Jobling, T. Chang, R. K. Holmes, T. R. Hirst, W. G. Hol, *Protein Sci.* **1997**, *6*, 1516–1528.

[215] E. A. Merritt, P. Kuhn, S. Sarfaty, J. L. Erbe, R. K. Holmes, W. G. Hol, *J. Mol. Biol.* **1998**, *282*, 1043–59.

[216] J. Chen, W. Zeng, R. Offord, K. Rose, *Bioconjug. Chem.* **2003**, *14*, 614–618.

[217] A. Dirksen, T. M. Hackeng, P. E. Dawson, *Angew. Chemie - Int. Ed.* **2006**, *45*, 7581–7584.

[218] K. Rose, J. Chen, M. Dragovic, W. Zeng, D. Jeannerat, P. Kamalaprija, U. Burger, *Bioconjug. Chem.* **1999**, *10*, 1038–1043.

[219] W. A. Hendrickson, A. Pähler, J. L. Smith, Y. Satow, E. A. Merritt, R. P. Phizackerley, *Proc. Natl. Acad. Sci. U. S. A.* **1989**, *86*, 2190–4.

[220] N. M. Green, *Advances in Protein Chemistry Volume 29*, Elsevier, **1975**.

[221] A.-M. Svennerholm, J. Holmgren, *Curr. Microbiol.* **1978**, *1*, 19–23.

[222] J. A. Mertz, J. A. McCann, W. D. Picking, *Biochem. Biophys. Res. Commun.* **1996**, *226*, 140–144.

[223] M. Bäckström, V. Shahabi, S. Johansson, S. Teneberg, A. Kjellberg, H. Miller-Podraza, J. Holmgren, M. Lebens, *Mol. Microbiol.* **1997**, *24*, 489–97.

[224] P. K. Mandal, T. R. Branson, E. D. Hayes, J. F. Ross, J. A. Gavín, A. H. Daranas, W. B. Turnbull, *Angew. Chemie - Int. Ed.* **2012**, *51*, 5143–5146.

[225] M. Sandkvist, T. R. Hirst, M. Bagdasarian ', *J. Bacteriol.* **1987**, *169*, 4570–4576.

[226] E. Angov, *Biotechnol. J.* **2011**, *6*, 650–9.

[227] A. K. Bronowska, *Thermodyn. - Interact. Stud. - Solids, Liq. Gases* **2011**, 1–49.

[228] R. A. Copeland, D. L. Pompliano, T. D. Meek, *Nat. Rev. Drug Discov.* **2006**, *5*,

730–739.

[229] J. M. Williams, T. Inoue, L. Banks, B. Tsai, *Mol. Biol. Cell* **2013**, *24*, 785–795.

[230] J. K. Tinker, J. L. Erbe, R. K. Holmes, *Infect. Immun.* **2005**, *73*, 3627–3635.

[231] L. de Haan, T. R. Hirst, *Mol. Membr. Biol.* **2004**, *21*, 77–92.

[232] T. Matsudaira, Y. Uchida, K. Tanabe, S. Kon, T. Watanabe, T. Taguchi, H. Arai, *PLoS One* **2013**, *8*, e69145.

[233] Y. Fujinaga, A. A. Wolf, C. Rodighiero, H. Wheeler, B. Tsai, L. Allen, M. G. Jobling, T. Rapoport, R. K. Holmes, W. I. Lencer, *Mol. Biol. Cell* **2003**, *14*, 4783–93.

[234] M. G. Jobling, R. K. Holmes, *Mol. Microbiol.* **1991**, *5*, 1755–1767.

[235] Y. Feng, A. P. Jadhav, C. Rodighiero, Y. Fujinaga, T. Kirchhausen, W. I. Lencer, *EMBO Rep.* **2004**, *5*, 596–601.

[236] I. V Majoul, P. I. H. Bastiaens, H.-D. Ssling, **n.d.**

[237] M. J. Lewis, D. J. Sweet, H. R. Pelham, *Cell* **1990**, *61*, 1359–63.

[238] N. L. B. Wernick, D. J.-F. Chinnapen, J. A. Cho, W. I. Lencer, *Toxins (Basel).* **2010**, *2*, 310–25.

[239] V. K. Chaudhary, Y. Jinno, D. FitzGerald, I. Pastan, *Proc. Natl. Acad. Sci. U. S. A.* **1990**, *87*, 308–12.

[240] R. M. Clegg, *Curr. Opin. Biotechnol.* **1995**, *6*, 103–110.

[241] P. G. Wu, L. Brand, *Anal. Biochem.* **1994**, *218*, 1–13.

[242] M. Hirakawa, J. T. McCabe, M. Kawata, *Cell Tissue Res.* **1992**, *267*, 419–427.

[243] P. J. Gatti, W. C. Coleman, M. Shirahata, T. A. Johnson, V. J. Massari, *Exp Brain Res* **1996**, *110*, 175–182.

[244] L. A. Verkruyse, S. L. Hofmann, *J. Biol. Chem.* **1996**, *271*, 15831–6.

[245] J. Vesa, E. Hellsten, L. A. Verkruyse, L. A. Camp, J. Rapola, P. Santavuori, S. L. Hofmann, L. Peltonen, *Nature* **1995**, *376*, 584–587.

[246] "Mouse : Decision tree for blood sampling | NC3Rs," can be found under https://www.nc3rs.org.uk/mouse-decision-tree-blood-sampling, **n.d.**

[247] F. Darios, D. Niranjan, E. Ferrari, F. Zhang, M. Soloviev, A. Rummel, H. Bigalke, J. Suckling, Y. Ushkaryov, N. Naumenko, et al., *Proc. Natl. Acad. Sci.* **2010**, *107*, 18197–18201.

[248] E. Ferrari, M. Soloviev, D. Niranjan, J. Arsenault, C. Gu, Y. Vallis, J. O'Brien, B. Davletov, *Bioconjug. Chem.* **2012**, *23*, 479–484.

[249] N. Mahant, P. D. Clouston, I. T. Lorentz, *J. Clin. Neurosci.* **2000**, *7*, 389–394.

[250] K. R. Bell, F. Williams, *Phys. Med. Rehabil. Clin. N. Am.* **2003**, *14*, 821–35.

[251] S. Chen, *Toxins (Basel).* **2012**, *4*, 913–39.

[252] R. G. Glogau, *Clin. J. Pain.* **2002.**, *18*, S191-7.

[253] Z.-S. Thant, E.-K. Tan, *Med. Sci. Monit.* **2003**, *9*, RA40-8.

[254] T. Hayashi, H. McMahon, S. Yamasaki, T. Binz, Y. Hata, T. C. Südhof, H. Niemann, *EMBO J.* **1994**, *13*, 5051–61.

[255] D. Fasshauer, W. Antonin, V. Subramaniam, R. Jahn, *Nat. Struct. Biol.* **2002**, *9*, 144–151.

[256] A. Yersin, H. Hirling, P. Steiner, S. Magnin, R. Regazzi, B. Hüni, P. Huguenot, P. De los Rios, G. Dietler, S. Catsicas, et al., *Proc. Natl. Acad. Sci. U. S. A.* **2003**, *100*, 8736–41.

[257] R. J. Barnard, A. Morgan, R. D. Burgoyne, *J. Cell Biol.* **1997**, *139*, 875–83.

[258] B. Lu, *PeerJ* **2015**, *3*, e1065.

[259] G. Schiavo, G. Stenbeck, J. E. Rothman, T. H. Söllner, *Proc. Natl. Acad. Sci. U. S. A.* **1997**, *94*, 997–1001.

[260] Dirk Fasshauer, William K. Eliason, and Axel T. Brünger, Reinhard Jahn, **1998**, DOI 10.1021/BI980542H.

[261] E. Ferrari, C. Gu, D. Niranjan, L. Restani, C. Rasetti-Escargueil, I. Obara, S. M. Geranton, J. Arsenault, T. A. Goetze, C. B. Harper, et al., *Bioconjug. Chem.* **2013**, *24*, 1750–1759.

[262] A. S. Mangione, I. Obara, M. Maiarú, S. M. Geranton, C. Tassorelli, E. Ferrari, C. Leese, B. Davletov, S. P. Hunt, *Pain* **2016**, *157*, 1045–55.

[263] P. Harvey, B. Gong, A. J. Rossomando, E. Frank, *Proc. Natl. Acad. Sci. U. S. A.* **2010**, *107*, 11585–90.

[264] A. M. Slovic, J. D. Lear, W. F. DeGrado, *J. Pept. Res.* **2005**, *65*, 312–321.

[265] V. N. Malashkevich, R. A. Kammerer, V. P. Efimov, T. Schulthess, J. Engel, *Science (80-.).* **n.d.**, *274*, 761–765.

[266] B. Sauer, N. Henderson, *Proc. Natl. Acad. Sci. U. S. A.* **1988**, *85*, 5166–70.

[267] D. R. Beers, B.-K. Ho, L. Siklós, M. E. Alexianu, D. R. Mosier, A. H. Mohamed, Y. Otsuka, M. E. Kozovska, R. E. McAlhany, R. G. Smith, et al., *J. Neurochem.* **2008**, *79*, 499–509.

[268] W. Maetzler, C. Nitsch, K. Bendfeldt, P. Racay, F. Vollenweider, B. Schwaller, **n.d.**, DOI 10.1016/j.expneurol.2003.10.014.

[269] R. G. Miller, J. H. Petajan, W. W. Bryan, C. Armon, R. J. Barohn, J. C. Goodpasture, R. J. Hoagland, G. J. Parry, M. A. Ross, S. C. Stromatt, *Ann. Neurol.* **1996**, *39*, 256–260.

[270] A. Henriques, C. Pitzer, A. Schneider, *Front. Neurosci.* **2010**, *4*, 32.

[271] S. Watanabe, T. Hayakawa, K. Wakasugi, K. Yamanaka, *Cell Death Dis.* **2014**, *5*, e1497.

[272] G. Haase, C. Rabouille, *Front. Neurosci.* **2015**, *9*, 448.

[273] J.-H. Ryou, Y.-K. Sohn, D.-E. Hwang, W.-Y. Park, N. Kim, W.-D. Heo, M.-Y. Kim,

H.-S. Kim, *Biotechnol. Bioeng.* **2016**, *113*, 1639–1646.

[274] J.-H. Ryou, Y.-K. Sohn, D.-E. Hwang, H.-S. Kim, *Biochem. Biophys. Res. Commun.* **2015**, *464*, 1282–1289.

[275] K. Sudo, K. Niikura, K. Iwaki, S. Kohyama, K. Fujiwara, N. Doi, *J. Control. Release* **2017**, *255*, 1–11.

[276] J. M. Alisky, C. I. van de Wetering, B. L. Davidson, *Exp. Neurol.* **2002**, *178*, 139–146.

[277] K. Sandvig, B. van Deurs, *FEBS Lett.* **2002**, *529*, 49–53.

[278] C. B. Louise, T. G. Obrig, *Infect. Immun.* **1992**, *60*, 1536–43.

[279] S. Ashkenazi, T. G. Cleary, *J. Clin. Microbiol.* **1989**, *27*, 1145–50.

[280] W. A. Kibbe, *Nucleic Acids Res.* **2007**, *35*, W43-6.

[281] T. Wiseman, S. Williston, J. F. Brandts, L. N. Lin, *Anal. Biochem.* **1989**, *179*, 131–7.

[282] W. B. Turnbull, A. H. Daranas, *J. Am. Chem. Soc.* **2003**, *125*, 14859–14866.

[283] U. Jönsson, L. Fägerstam, B. Ivarsson, B. Johnsson, R. Karlsson, K. Lundh, S. Löfås, B. Persson, H. Roos, I. Rönnberg, *Biotechniques* **1991**, *11*, 620–7.

[284] C. Hahnefeld, S. Drewianka, F. W. Herberg, *Methods Mol. Med.* **2004**, *94*, 299–320.

[285] L. R. Baker, *Opt. Acta Int. J. Opt.* **1983**, *30*, 257–257.

[286] E. Stenberg, B. Persson, H. Roos, C. Urbaniczky, *J. Colloid Interface Sci.* **1991**, *143*, 513–526.

[287] P. Schuck, H. Zhao, *Methods Mol. Biol.* **2010**, *627*, 15–54.